united nations
educational, scientific
and cultural
organization

international atomic
energy agency

the
abdus salam
international centre for theoretical physics

SMR/1108 - 17

COURSE ON "MEDITERRANEAN SEA(S) CIRCULATION & ECOSYSTEM FUNCTIONING" 2 - 20 November 1998

Trieste, Italy

"The Flow and Hydrology in the Strait of Gibraltor and the Gulf of Cadiz"

J. OCHOA DE LA TORRE
CICESE
Ensenasda, Mexico

Pergamon

Prog. Oceanog. Vol. 33, pp. 201-248, 1994

0079 - 6611/94 $26.00

0079-6611(94)00004-2

Exchange through the Strait of Gibraltar

HARRY L. BRYDEN[1], JULIO CANDELA[2] and THOMAS H. KINDER[3]

[1]*James Rennell Centre for Ocean Circulation, Chilworth Research Centre, Chilworth, Southampton SO1 7NS, UK*
[2]*Department of Physical Oceanography, Woods Hole Oceanographic Institution, Woods Hole, Massachusetts 02543, USA*
[3]*United States Naval Academy, Annapolis, Maryland 21402, USA*

Abstract – To measure the exchange between the Atlantic and Mediterranean through the Strait of Gibraltar, an array of current meter moorings was deployed for a year in the Strait during 1985-86. A novel aspect of these measurements is the inclusion of conductivity as well as temperature and pressure sensors on each current meter so that the salinity of the flows could be monitored continuously. These salinity measurements determine the water mass characteristics of the flows crossing the sill; they allow definition of the 37psu isohaline as the interface between inflowing fresher Atlantic water and outflowing saltier Mediterranean water; and they enable time series to be developed for the depth of this interface, for the upper layer inflow, and for the lower layer outflow.

From these measurements, the time-averaged outflow of Mediterranean water is estimated to be -0.68Sv (1Sv = 1 x $10^6 m^3 s^{-1}$) and the outflow salinity transport, defined to be the outflow times the salinity excess above a basic Atlantic water salinity of 36.1psu, is estimated to be -1.50 x $10^3 m^3 s^{-1}$ (1Sv x 1psu = 1 x $10^3 m^3 s^{-1}$) equivalent to a net evaporation over the Mediterranean basin of 52cm y^{-1}. Extrapolated measurements of the inflow from current meters generally deployed below 100m depth yield an estimate for the time-averaged inflow of 0.93Sv, which is believed to be unrealistically high in view of the better measured outflow and net evaporation. Thus, a more realistic estimate of the inflow is 0.72Sv, equal to the sum of the outflow and net evaporation as required by the mass budget for the Mediterranean Sea. Such estimates of the exchange are smaller by almost a factor of 2 than previous values for the exchange by LACOMBE and RICHEZ (1982).

The exchange across the Gibraltar sill is found to be due in nearly equal parts to the mean currents and to the tidal fluctuations. The mean currents are smaller than had been expected reaching a peak value of only about -60cm s^{-1} in the deep outflow over the sill. The tidal exchange is due to a strong correlation over the tidal period between the depth of the interface and the strength of the inflowing currents. For the M_2-tide at the sill, the amplitude of the interface depth is 51m and the amplitude of the tidal currents is 1.2m s^{-1}; furthermore, the inflow and interface depth have similar phases. As a consequence, the upper layer is deep on the inflowing tide so that a large slug of Atlantic water crosses the sill into the Mediterranean; on the outflowing tide, the interface is shallow so that a large slug of Mediterranean water crosses the sill into the Atlantic. Similar processes occur for the S_2, O_1 and K_1 tides, though the amplitudes are smaller. In this manner, tidal oscillations lead to a time-averaged exchange of water masses across the Gibraltar sill.

The inflow and outflow, defined to be the instantaneous transports above and below the 37psu isohaline interface, exhibit M_2-tidal amplitudes of 2.3Sv and 1.3Sv respectively. Thus, the tides are large enough to reverse the mean upper layer inflow and lower layer outflow. Daily averaged inflow and outflow transports exhibit low-frequency fluctuations with standard deviations of 0.37Sv and 0.22Sv respectively. Such low frequency fluctuations have been shown previously to be associated with barotropic flows through the Strait of Gibraltar compensating for sea level variations over the Mediterranean due to atmospheric pressure fluctuations (CANDELA, WINANT and BRYDEN, 1989). Finally, from these measurements there appear to be little fortnightly or annual period fluctuations in the exchange through the Strait of Gibraltar.

CONTENTS

1. INTRODUCTION

Observing and modelling the exchange between the Atlantic and Mediterranean basins through the Strait of Gibraltar stimulated many of the early advances in oceanography (DEACON, 1971). The perpetual inflowing surface currents through the Strait of Gibraltar combined with river inputs and even surface waters flowing through the Bosporus into the Mediterranean basin raised the mystery of how the water budget could be maintained when evaporation was clearly not large enough to balance all the inflows. MARSIGLI's (1681) remarkable laboratory experiment demonstrating the two-layer exchange between two basins of different densities combined with his field observations in the Bosporus of a subsurface countercurrent established that the water budget of the Mediterranean must be maintained by a subsurface outflow through the Strait of Gibraltar. Confirmation of this subsurface outflow awaited nearly two centuries until CARPENTER and JEFFREYS (1870), as part of Mediterranean field work in preparation for the upcoming *Challenger* expedition, established the existence of a deep outflow by deploying a drogue at 300m depth from a small boat south of the rock of Gibraltar and observing the boat to drift westward against the wind and the surface currents. This outflow of Mediterranean water over the Gibraltar sill not only aspirates the deep waters of the Mediterranean basin (STOMMEL, BRYDEN and MANGELSDORF, 1973; KINDER and BRYDEN, 1990) but also provides a source of high salinity waters for the intermediate and deep water circulation of the North Atlantic (REID, 1979; PRICE and BARINGER, 1994).

Although NIELSEN (1912) is often cited for first determining the inflow and outflow through the Strait of Gibraltar by applying the Knudsen relations, BUCHANAN (1877) actually applied mass and salt conservation statements for the Mediterranean basin to early values for the salinities of the upper inflow of Atlantic water and of the lower outflow of Mediterranean water derived from specific gravity determinations in the Strait. Combining the salinity values with estimates of the net evaporation (evaporation minus precipitation and river runoff, E-P-R) over the Mediterranean basin, BUCHANAN made surprisingly accurate estimates for the inflow and outflow transports. For the next 100 years, a succession of scientists have made different estimates of the exchange through the Strait using 'improved' values for the net evaporation and for the salinities of Atlantic and Mediterranean waters in the Strait of Gibraltar (Table 1).

LACOMBE (1961) summarised early measurements of the currents in the Strait and concluded that the widely cited inflow transport value of 1.75Sv ($1Sv = 1 \times 10^6 m^3 s^{-1}$) by SCHOTT (1915) had little basis in measurement. From analysis of historical current measurements over periods shorter

than a day (particularly an estimate by his colleague Lizeray using measurements in 1910), LACOMBE suggested that the inflow and outflow transports were likely to be about 1.0Sv. During a series of cruises in the Strait beginning in 1958 and extending through the 1960s in an international field programme called Projet Gibraltar, LACOMBE (1971, and for a more accessible summary see LACOMBE and RICHEZ, 1982) made the first direct current measurements to determine the tidally averaged inflow of Atlantic water and outflow of Mediterranean water across the Gibraotar sill. These current measurements consisted primarily of current meter lowerings from an anchored ship and the major problem was to take a series of measurements at each depth over a tidal period so that the substantial tidal currents could be averaged out to determine the mean inflow and outflow. The resulting estimates of about 1.2Sv for both the inflow and outflow have been the standard values for the exchange between the Atlantic and Mediterranean basin across the Gibraltar sill for the past 20 years.

TABLE 1. Estimates of net evaporation over the Mediterranean basin, outflow salinity transport, salinity difference between the inflow and outflow transport.

Source	Net Evaporation ($cm\ y^{-1}$)	Outflow Salinity Transport ($x10^3 m^3 s^{-1}$)	Salinity Difference S_M-S_A (psu)	Outflow Transport (Sv)
BUCHANAN 1877	55	1.61	2.60	0.62
NIELSEN 1912	117	3.38	1.91	1.78
SCHOTT 1915	131	3.78	2.31	1.64
SVERDRUP, JOHNSON and FLEMING 1942	87	2.52	1.51	1.68
WÜST 1952	96	2.76		
CARTER 1956	47	1.38	1.50	0.91
TIXERONT 1970	56	1.61		
LACOMBE and TCHERNIA 1972	69	2.00	1.71	1.15
BETHOUX 1979	95	2.75	1.72	1.60
LACOMBE and RICHEZ 1982	75	2.01	1.75	1.15
BRYDEN, CANDELA and KINDER (this paper)	52	1.50	2.20	0.68

The values attributed to NEILSON, SCHOTT, SVERDRUP *et al*, WÜST, CARTER, TIXERONT, and LACOMBE and TCHERNIA are adaptations from Table 2 of HOPKINS (1978). The BRYDEN, CANDELA and KINDER values are those described in this paper from the 1985-86 Gibraltar Experiment measurements.

In the mid 1980s, a group of oceanographers organised an international field programme in the Strait of Gibraltar, called the Gibraltar Experiment, with an overall hypothesis that the amount of exchange between the Atlantic and Mediterranean was determined by the physical configuration of the Strait of Gibraltar, that is by the width and depth of the Strait (BRYDEN and KINDER, 1986). The principal goals of the Gibraltar Experiment were to develop realistic models for the exchange through a strait, to measure the amount of exchange across the Gibraltar sill, and to develop a long-term monitoring strategy to make long time series measurements of the exchange. The field programme and some of the early results of the Gibraltar Experiment are described by KINDER and BRYDEN (1987, 1988).

During the Gibraltar Experiment field programme, remarkable progress was made in developing hydraulic control models for two-layer flow through a strait and sill region like Gibraltar (BRYDEN and KINDER, 1991a). BRYDEN and STOMMEL (1984) put forward an initial model with a single control point at the sill that stimulated ARMI (1986) to publish the results from his 1975 PhD thesis

on two-layer flow over obstacles which demonstrated there are in fact two control points of critical flow. ARMI and FARMER (1985) reanalysed the 1960s measurements in the Strait of Gibraltar to suggest that the two control points appeared to be at the sill section and at the narrowest section. Then ARMI and FARMER (1986) and FARMER and ARMI (1986) formulated and solved the maximal exchange problem of steady, two-layer flow through a strait and sill region like Gibraltar for a given density contrast between Mediterranean and Atlantic waters. Furthermore, in analysis of their own observations in the Strait, ARMI and FARMER (1988) found confirmation of the hydraulic control concepts during a three-week shipboard survey of the exchange processes. DALZIEL (1990, 1991, 1992) refined the formulation, re-solved the Gibraltar problem, and studied rotational effects as well as parabolic configurations for the cross-sections of the Strait. BORMANS and GARRETT (1989a,b) also solved the maximal two-layer Gibraltar exchange and studied rotational and frictional effects as well as triangular configurations for the cross-sections; but they stressed the differences between maximal and submaximal exchange solutions and argued that the Gibraltar exchange switches between maximal and submaximal states over the course of a year (BORMANS, GARRETT and THOMPSON, 1986; GARRETT, BORMANS and THOMPSON, 1990). Finally, BRYDEN and KINDER (1991b) solved the steady, two-layer flow using triangular cross-sections, summarised the other models, and emphasized how the maximal exchange solution determined not only the size of the exchange but also the salinity difference between the Mediterranean and Atlantic waters for a given net evaporation over the Mediterranean basin. For a net evaporation of 60cm y^{-1}, BRYDEN and KINDER found that the predicted maximal exchange through the Strait of Gibraltar consists of 0.92Sv Atlantic water inflow, 0.88Sv Mediterranean water outflow with a salinity difference of 1.98psu.

The second goal of the Gibraltar Experiment to measure the exchange through the Strait was also carried out through an extensive programme of moored current meter measurements (PILLSBURY, BARSTOW, BOTTERO, MILLEIRO, MOORE, PITTOCK, ROOT, SIMPKINS, STILL and BRYDEN (1987). Preliminary estimates of the observed exchange from these current meter measurements have so far been presented in a series of limited papers at conferences (BRYDEN, BRADY and PILLSBURY, 1989; BRYDEN and PILLSBURY, 1990; BRYDEN, 1993). The principal purposes of this present paper are to describe these current measurements at the Gibraltar sill during 1985-86, to present various methods for estimating the mean exchange across the sill and to show that the different methods yield consistent estimates for the inflow of Atlantic water and outflow of Mediterranean water through the Strait of Gibraltar, and to investigate the temporal variability of the exchange over time-scales ranging from semi-diurnal tides to the seasonal cycle.

2. DATA AND METHODS

An array of 8 moorings was set in the Strait of Gibraltar during October 1985 (Fig. 1a) from the Spanish naval vessel *Tofino* as part of the Gibraltar Experiment (BRYDEN and KINDER, 1986). This array with 3 moorings across the sill section of smallest cross-sectional area (Fig. 1b, moorings 1, 2, 3) and with 6 moorings along the central axis of the Strait (Fig. 1c, moorings 4, 8, 2, 5, 6, 7) was scheduled for a 6-month deployment and then for replacement to provide a year-long time series of the inflow and outflow through the Strait of Gibraltar. To reduce drag in the high current environment of the Strait, the mooring line was faired above 230m nominal depth and large buoyancy spheres rather than vertically distributed buoyancy were utilized at the tops of the moorings. Two novel techniques were used: new S4 electromagnetic current meters were deployed at the tops of moorings 1, 2, 3, 5 for their first operational use; and all of the current meters measured conductivity as well as current speed and direction, temperature and pressure so that time series of salinity could be obtained.

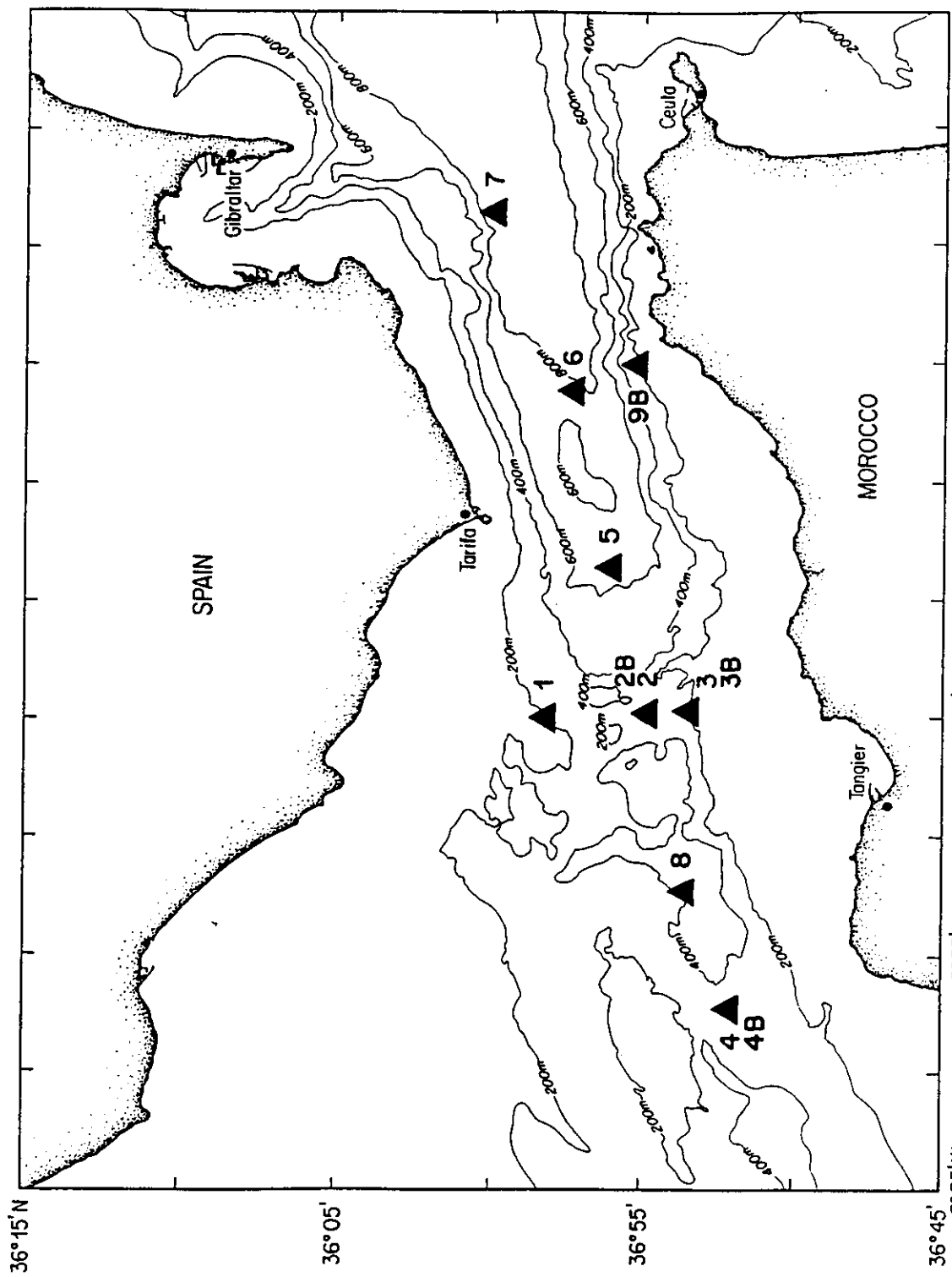

FIG. 1a. Configuration of moorings deployed in the Strait of Gibraltar during 1985-86. Moorings 1 through 8 were deployed for the period October 1985 to May 1986 and moorings 2B, 3B, 4B and 9B were deployed for the period May 1986 to October 1986. Moorings 1, 2 and 3 were deployed across the sill section, that is the section with minimum cross-sectional area, and moorings 2 and 2B were deployed at the sill, that is the location of greatest depth on the sill section.

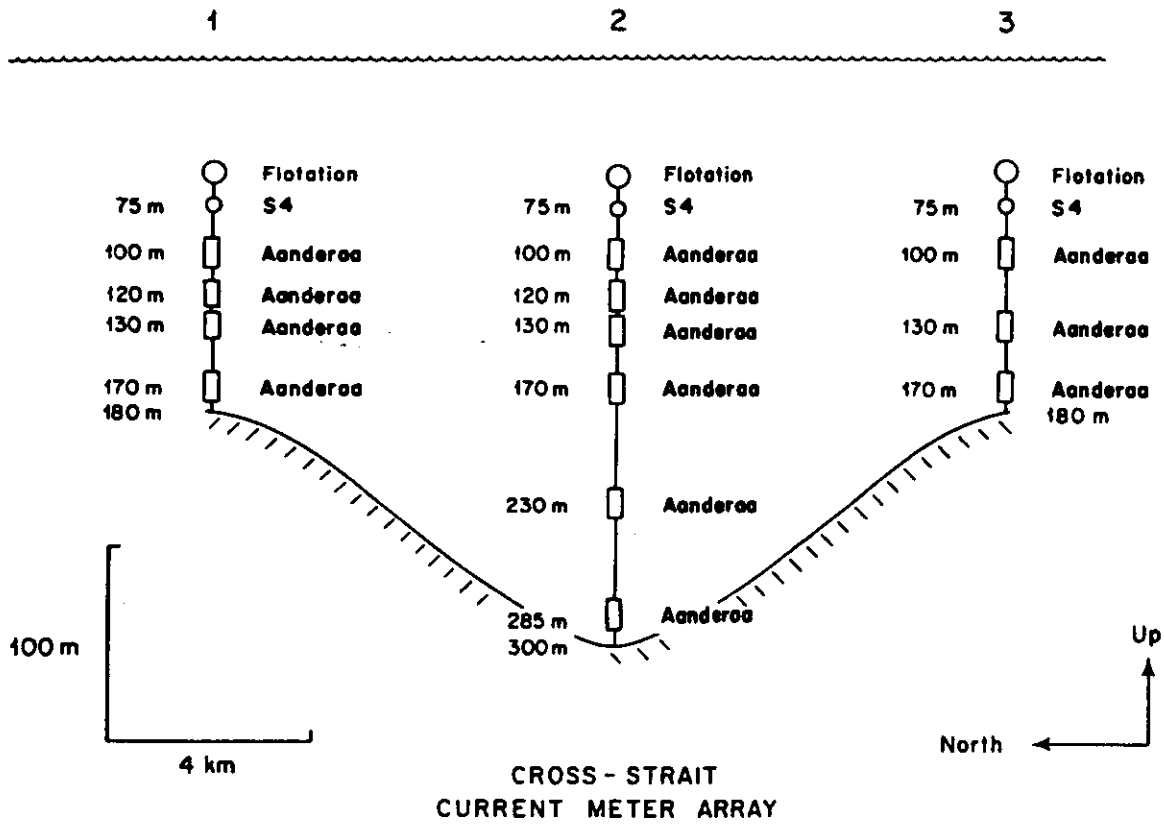

FIG. 1b. Design configuration for the moored current meters deployed across the sill section during October 1985.

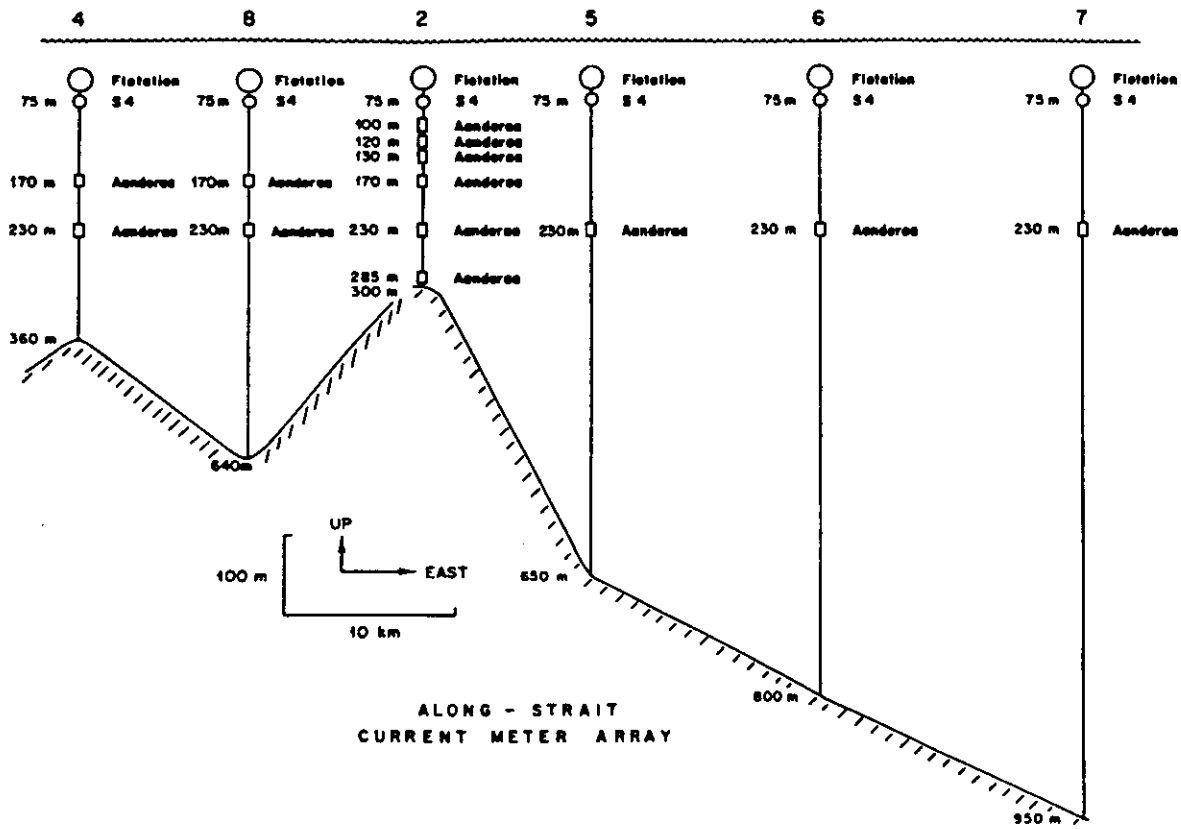

FIG. 1c. Design configuration for the moored current meters deployed along the axis of the strait during October 1985.

There were several technical problems in this first deployment. First, the S4 current meters were improperly programmed for too high a sampling rate so that the instruments ran out of power during the first 36 hours in the water. Secondly, moorings 2, 4, 5, 6, 7, 8 all broke apart at various times during the deployment period so that complete 6-month records were not obtained at these sites. The problem appears to have been that the wire below 230m depth on these moorings was bare, not covered with fairing because of the lengthy time required for fairing installation during deployment and not jacketed because of the effort to keep the wire diameter as small as possible to reduce drag. Although the wire was galvanized, we believe that the currents caused high frequency vibration, or strumming, in the mooring wire which gradually flaked off the galvanizing material. Once the galvanizing material was gone, a battery action was set up and the wire corroded rapidly until it parted. Moroccan and Spanish fishermen recovered the upper parts of moorings 2, 4, 7 and 8 and returned the equipment to the Spanish Navy. At the end of the initial 6-month deployment period, moorings 1 and 3 were recovered intact and the bottom portions of moorings 2 and 5 were also recovered aboard US naval vessel *Lynch*.

The data from the first deployment then consists of complete 6-month records from moorings 1 and 3 on the northern and southern sides of the sill section, one-month records from mooring 2 on the sill and from mooring 4 at the Spartel sill, a 4-month record from mooring 8 in Tangier Basin, and 5-month records from mooring 7 at the eastern entrance of the Strait (Fig.2).

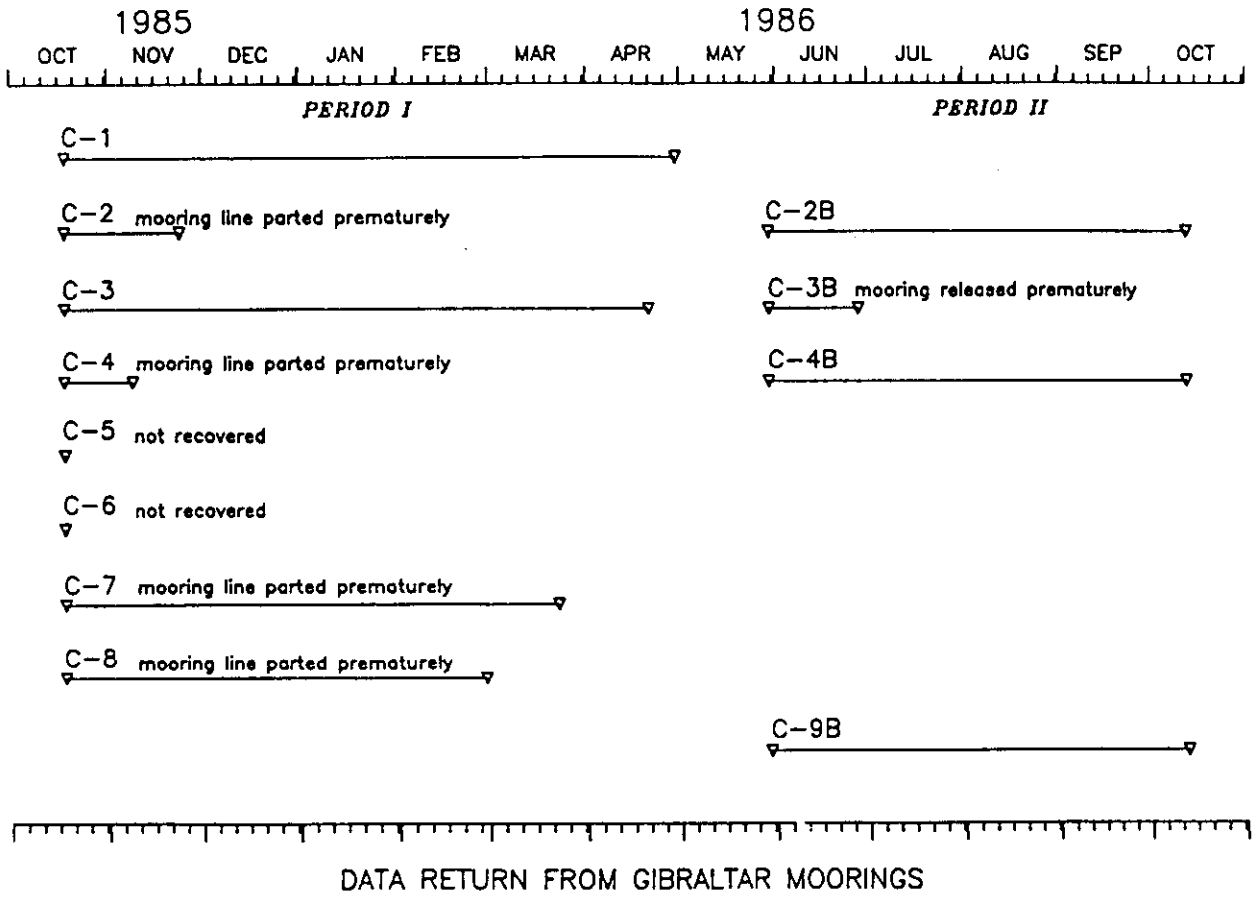

Fig.2. Maximum data length for each mooring deployed during the Gibraltar Experiment.

After the magnitude of the corrosion problem became apparent during the recovery cruise, the array for the second 6-month deployment was redesigned with thicker, jacketed wire throughout each mooring. Fairing was not used on the second deployment because it would not fit over the thicker wire. Because of the limited number of recovered current meters from the first setting, only 4 moorings were redeployed in the Strait from Spanish Naval Vessel *Malaspina*, moorings 2B, 3B, 4B and 9B (Fig.1a). To provide additional measurements, this array was coordinated with the deployment of two Doppler Acoustic profiling current meter (DAPCM) moorings by Dr Neal Pettigrew on the northern side of the sill section (near the location of mooring 1) and on the northern side of the narrowest cross-section (across the Strait from mooring 9). Unfortunately, these 2 DAPCMs did not return any usable data. In mid-October 1986, these moorings were recovered aboard US naval vessel *Lynch*. Of the 4 moorings during the second deployment, only mooring 3B parted prematurely after a month, where the tension bar on the uppermost S4 current meter broke. Each of the other 3 moorings, however, suffered extreme vibration so that some of the current meter sensors failed during their deployment period.

The data from the second deployment then consists of 5-month records at mooring 2B on the sill, mooring 4B at the Spartel sill, and mooring 9B on the southern side of the narrowest cross-section, and one-month records at mooring 3B on the southern side of the sill (Fig.2).

In all, there are 31 current meter records on 10 moorings in the Strait of Gibraltar during the period October 1985 to October 1986. The maximum data length for each mooring is shown in Fig.2 and the time-averaged east and north currents, temperature and salinity and principal axis direction of the current fluctuations for each record are given in Table 2. Current speed and direction, pressure, temperature, and conductivity were measured on each instrument at 30-minute intervals. Presure, temperature and conductivity values are then put into the algorithm given by FOFONOFF and MILLARD (1983) to determine salinity at 30-minute intervals. The data are more fully described by PILLSBURY *et al* (1987).

Because conductivity drifts slowly with time due to cell contamination, each basic salinity time series is corrected for any drift by using the fact that Mediterranean water in the Strait has a maximum salinity of 38.4 to 38.5psu. For each basic salinity time series, the maximum salinity observed over successive four-day intervals was fitted with a least-squares technique to a second order polynomial in time. At each point in the salinity series, the difference between this fit and 38.4psu was subtracted from the salinity. The resulting corrected salinity time series then have a maximum salinity of about 38.4psu which remains relatively constant over the entire data period. As an example of the correction process, the basic and corrected salinity time series are shown in Fig.3 for the current meter at 254m depth on mooring 2.

The character of the current meter data is most easily shown by the time series from mooring 2 at the sill during October-November 1985 (Fig.4). Because the Strait of Gibraltar is oriented in a westsouthwest-eastnortheast direction, the measured currents have been rotated into a coordinate system with the along-strait direction 13° north of east and the cross-strait direction 13° west of north. This rotation was selected by averaging the principal axis directions for all 9 moorings (Table 1) and it is consonant with the general orientation of the Strait. The most striking feature of the along-strait currents (Fig.4a) is the large semidiurnal tidal signal. CANDELA, WINANT and RUIZ (1990) determined that the M_2 tidal currents have an amplitude of 112cm s^{-1} at 123m depth on mooring 2, decreasing to 79cm s^{-1} at 254m depth and that the S_2 tidal currents have an amplitude of 40cm s^{-1} at 123m decreasing to 28cm s^{-1} at 254m. The beating of the M_2 and S_2 tidal signals can be seen in the fortnightly cycle of the amplitude of the semidiurnal tidal currents (Fig.4a). The tidal currents have a similar phase throughout the water column but with a tendency for earlier phase towards the bottom. In the deeper part of the water column, there is a strong mean outflow (negative

TABLE 2. Record-length averaged currents, temperature, salinity and pressure for 31 current meters moored in the Strait of Gibraltar during the period October 1985 to October 1986. Values in parentheses indicate sensor failure during the deployment period so that the averages are over periods shorter than the indicated data length. For the exact time periods of individual sensors, refer to PILLSBURY *et al* (1987).

Mooring	Minimum Pressure (dbars)	Data Length (days)	East Current (cm s^{-1})	Northward Current (cm s^{-1})	Principal Axis Direction (°T)	Temperature (°C)	Salinity (psu)	Pressure (dbars)
1	144	194	-12.58	-9.25	98	13.39	37.93	147
	158	194	-16.69	-8.51	98	13.26	38.01	166
	169	194	-17.70	-10.19	100	13.22	38.03	172
	217	194	-11.21	2.36	107	13.14	(38.23)	218
2	124	32	-3.35	-9.27	78	14.29	36.94	127
	144	32	-14.06	-8.19	78	13.94	37.18	149
	155	32	-22.69	-14.76	75	13.83	37.33	158
	192	32				13.34	37.86	196
	256	32	-46.35	-27.98	61	13.03	38.26	261
	309	32	-26.63	-28.67	49	12.96	38.35	312
2B	91	82	-14.03	-1.94	81	14.43	36.63	102
	113	137	(-1.64)	(0.24)	76	13.92	36.95	123
	136	137	(-26.56)	(-13.37)	74	13.55	37.41	151
	183	137	(-47.27)	(-19.36)	70	13.20	37.91	192
	239	137	(-56.94)	(-21.25)	64	12.98	38.28	247
	302	137	-38.94	-25.51	50	12.95	38.33	306
3	111	182	8.61	10.26	82	14.83	36.85	113
	135	182	-4.66	4.12	80	14.29	37.21	143
	181	182	-22.69	-9.68	69	13.56	37.78	182
3B	103	26	13.20	9.54	86	14.54	36.54	106
	128	23	9.14	6.73	82	14.15	36.87	133
	173	29	-6.55	-2.28	75	13.59	37.52	175
4	68	22	23.96	8.52	73	15.79	36.29	70
4B	(~220)	10	-40.70	-10.20	66	13.13		
	298	7	-85.28	-34.41	60	13.06	38.19	301
	(~340)	136	-86.43	-18.18	65			
7	54	159	53.86	6.83	79	14.43	37.15	(62)
	194	159	-19.70	-10.71	64	13.15	38.29	201
8	28	132	35.76	8.08	75	16.08		36
9B	58	138	(57.70)	(7.87)	76	15.04	36.06	64
	160	138	24.80	16.52	75	13.51	37.79	162

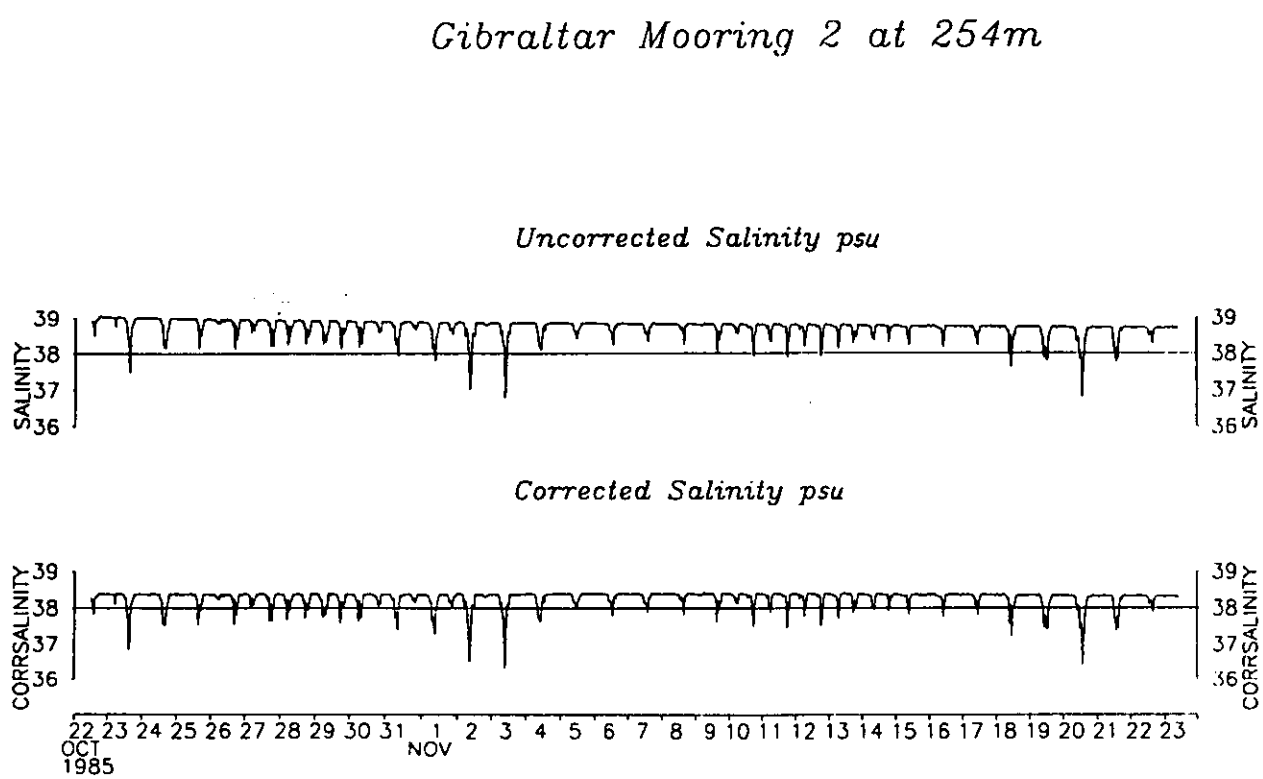

FIG.3. Salinities measured on mooring 2 at 254m depth during October-November 1985. Note the bias toward high (unrealistic) salinities and the slow drift toward fresher values. Such bias and drift are typical for moored conductivity time series. A corrected salinity record was created for each current meter time series by eliminating the bias and drift based on a maximum salinity of 38.4psu.

along-strait current) of order 40cm s^{-1}, but the tidal oscillations are still large enough to reverse the mean outflow during a portion of each day, even at 306m depth, only 15m above the bottom. The cross-strait velocities (Fig.4b) exhibit tidal oscillations of order 10cm s^{-1} and the corrected salinity time series (Fig.4c) also exhibit strong semidiurnal oscillations[1]. In the deeper part of the water column, the variations away from the maximum value of 38.4psu are small, indicating that the current meter is nearly always in the Mediterranean Water. Higher in the water column, there is an increasing number of salinity spikes toward lower salinity, that indicate the instrument is occasionally in Atlantic water. At 123m depth, at the top of the mooring, the spikes appear to be reversed: toward higher salinity from a base at about 36.1psu. This reversal indicates that the uppermost instrument spends the majority of its time in Atlantic water, but often is in Mediterranean water.

All salinity time series on each mooring are used to derive time series for the depths of the 37, 37.5 and 38psu isohalines. The depth interval between these isohalines defines the interfacial region that separates Atlantic Water with salinities less than 37psu in the upper water from Mediterranean Water with salinities greater than 38psu in the deeper water. At each 30-minute sampling interval, the salinities and pressures measured by all instruments on one mooring are interpolated/

[1]The oscillations in salinity are not due to mooring motion. The uppermost current meter on mooring 2 had a maximum downward dip of 28m from its minimum pressure of 123m. Such a small dip in such strong currents is due to the relatively short vertical extent of the mooring. We will show shortly that the interface between Atlantic and Mediterranean water oscillates vertically by 51m over semidiurnal periods at the sill.

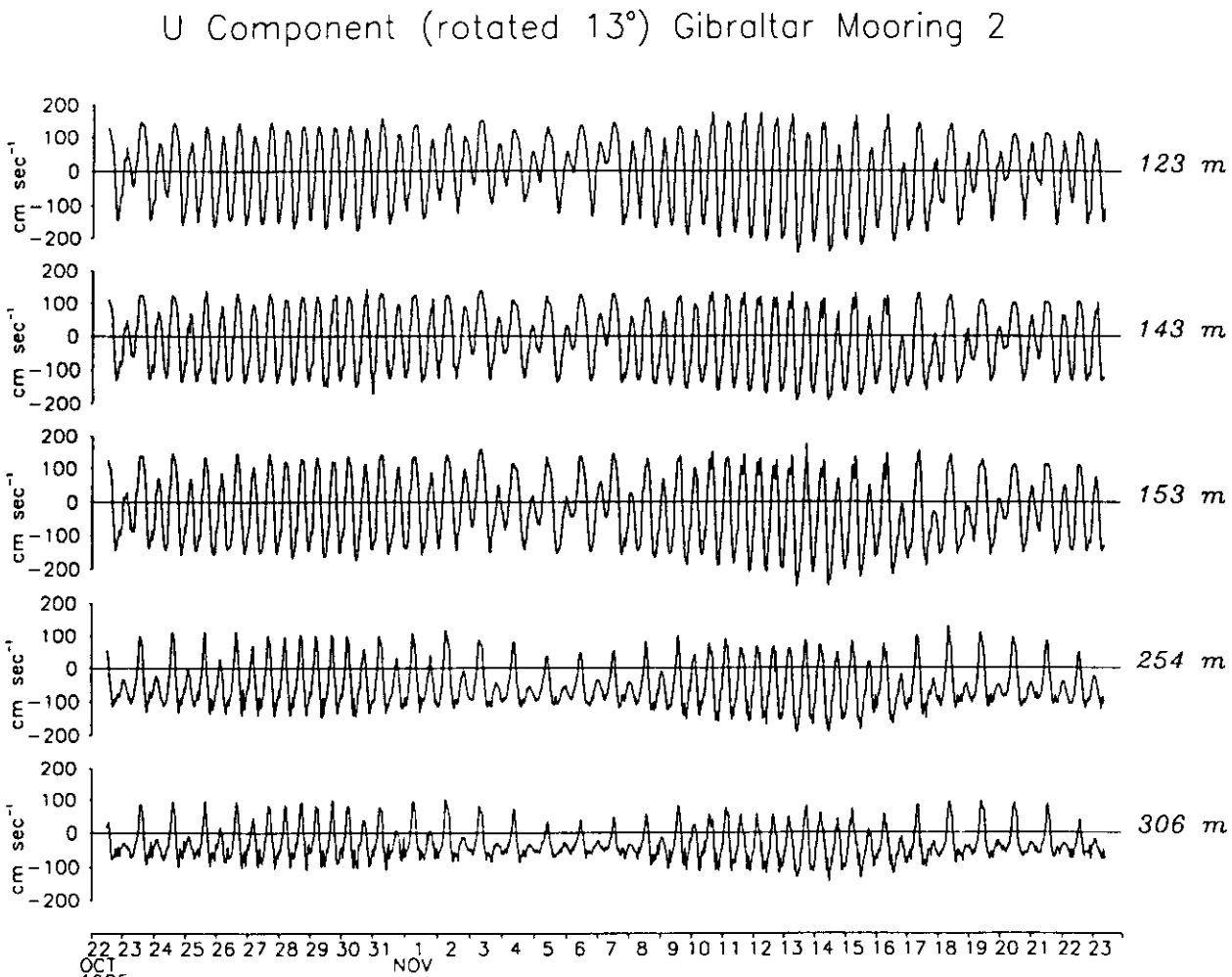

FIG.4. Time series of along-strait (a, above) and cross-strait (b, overleaf) velocities and corrected salinities (c, overleaf) on mooring 2 during October-November 1985. Along-strait direction is defined to be 77°T based on the average principal axis orientation of the current fluctuations and on the physical orientation of the Strait of Gibraltar. Cross-strait direction is then defined to be 347°T.

extrapolated to find the pressures of the 37, 37.5 and 38psu isohalines. If all instruments measure salinities less than 37psu, so that the interfacial region is deeper than the deepest instrument, or greater than 38psu, so that the interfacial region is shallower than the shallowest instrument, there is a gap where no isohaline depths are initially calculated. The time series of the interpolated/extrapolated depths of the 37, 37.5 and 38psu isohalines are shown at the sill for mooring 2 in Fig.5a. Because gappy time series are difficult to deal with, the gaps in isohaline depths are filled by determining the average vertical salinity gradient at the edges of each gap. This vertical salinity gradient is then used to extrapolate upwards or downwards from the salinity time series on the current meter closest to the interfacial region during the time period of the gap. If the pressure of an isohaline is extrapolated to a value less than 0dbar (the sea surface), the isohaline depth is set to 0. The time series of isohaline depths at the sill on mooring 2 with the gaps filled by this procedure is shown in Fig.5b.

FIG.4b

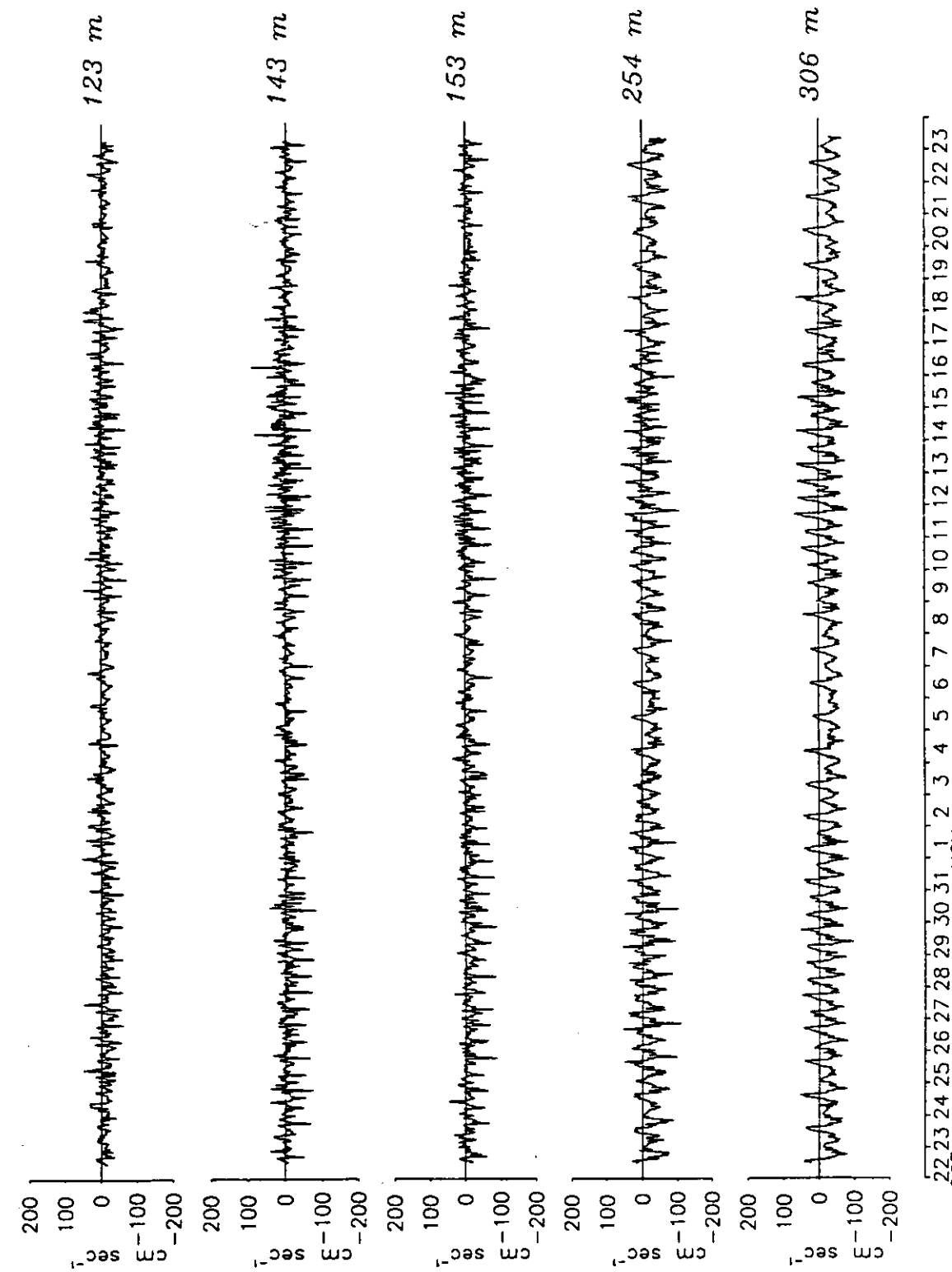
V Component (rotated 13°) Gibraltar Mooring 2
123 m
143 m
153 m
254 m
306 m
200
100
0
−100
−200
cm sec⁻¹
22 23 24 25 26 27 28 29 30 31 1 2 3 4 5 6 7 8 9 10 11 12 13 14 15 16 17 18 19 20 21 22 23
OCT
NOV
1985

FIG 4c

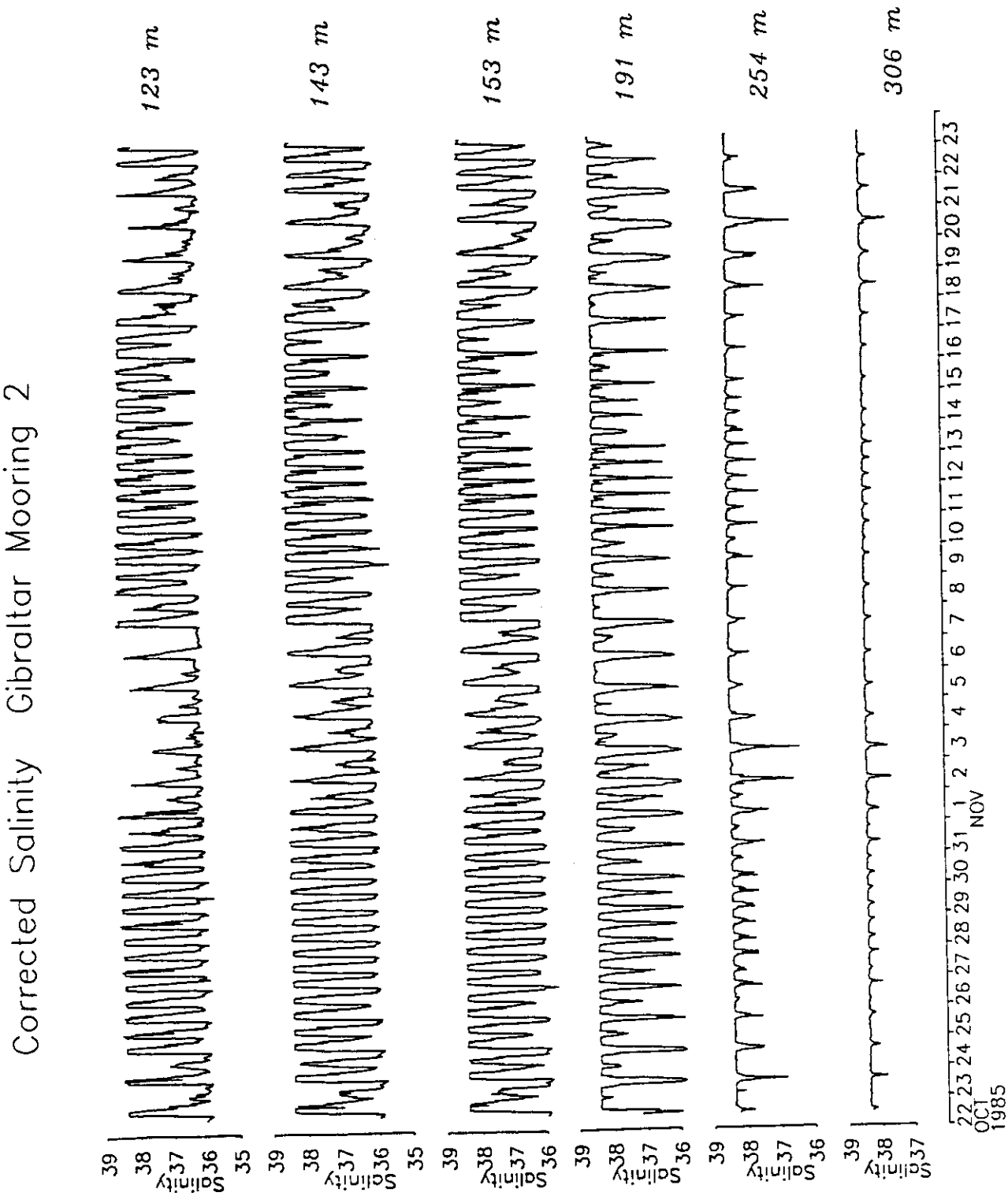
Corrected Salinity Gibraltar Mooring 2
123 m
143 m
153 m
191 m
254 m
306 m
Salinity
39
38
37
36
35
22 23 24 25 26 27 28 29 30 31 1 2 3 4 5 6 7 8 9 10 11 12 13 14 15 16 17 18 19 20 21 22 23
OCT
NOV
1985

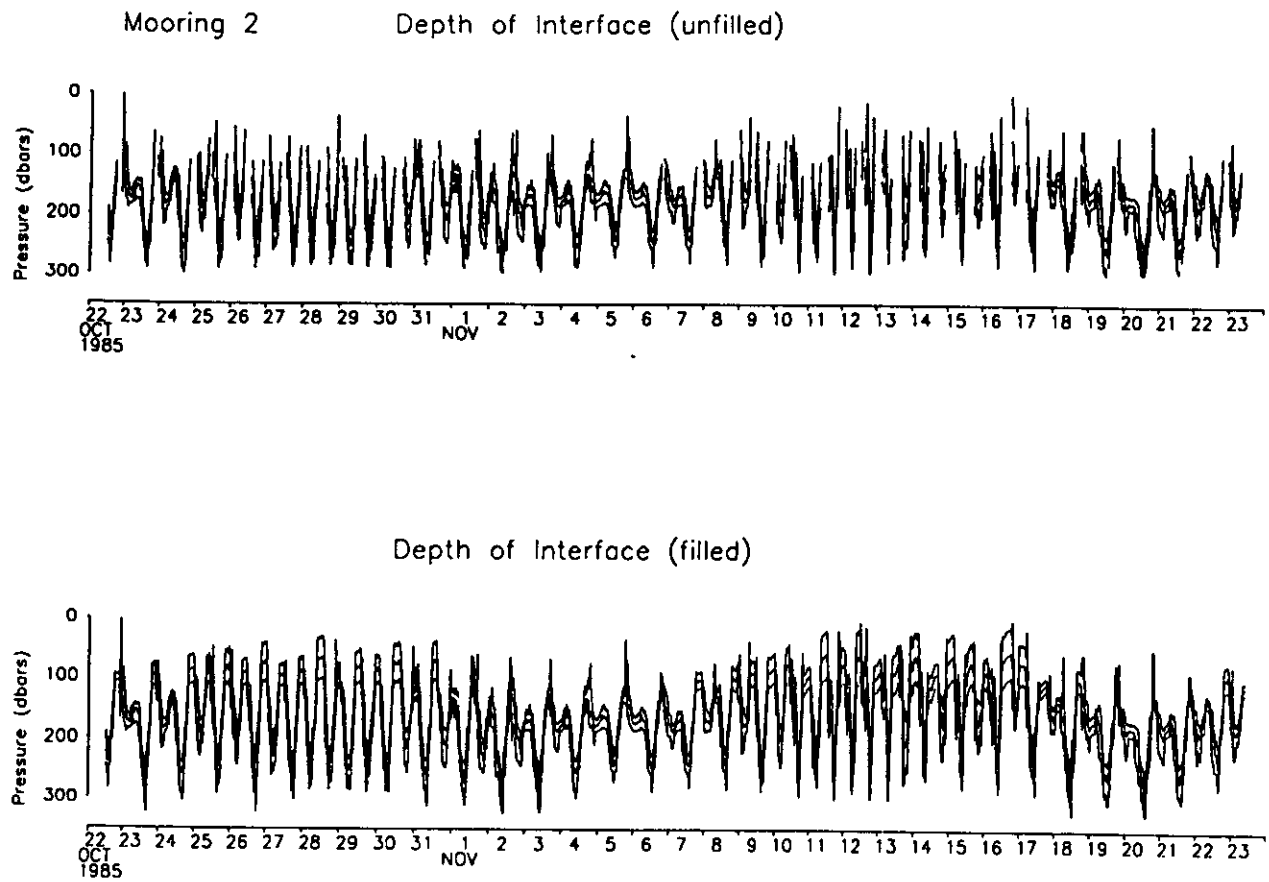

FIG.5. Depths of the 37, 37.5 and 38psu isohalines on mooring 2 during October-November 1985. The upper, unfilled time series are the result of interpolating salinity and pressure time series from the 6 current meters on mooring 2. The lower, filled time series are the result of the combined temporal interpolation-vertical extrapolation technique designed by Esther Brady to create uniform time series.

3. TRANSPORT DEFINITIONS

Traditional estimates of the mean transports through the Strait of Gibraltar have been expressed as average values of the inflow and outflow at nominal salinity values. Generally, a typical salinity difference, $\Delta S = S_M - S_A$ where S_M and S_A are the nominal Mediterranean and Atlantic salinities, of about 2psu between the outflowing and inflowing waters is assumed and is combined with a value for the net evaporation, E, over the Mediterranean basin to yield the outflow and inflow transports, Q_M and Q_A of Mediterranean and Atlantic waters:[1]

[1]The definition of sign of the outflow can be confusing. While we will call Q_M the outflow, Q_M will generally be negative as the Mediterranean water typically flows westward.

$$Q_M = -\frac{S_A}{\Delta S} E \qquad Q_A = \frac{S_M}{\Delta S} E. \tag{1}$$

Such estimates have typically varied between 1 and 2 x $10^6 m^3 s^{-1}$ principally depending on the estimate of E (Table 1). Of course, the inflow and outflow do not occur at constant salinity, so that with measurements of the flow over the Gibraltar sill it is important to define both the inflow and outflow transports *and* their associated salinities.

In concept, the quantity that remains constant throughout the Strait of Gibraltar is the outflow salinity transport, $Q_M(\Delta S)$. Rearranging the mass and salt conservation equations for the Mediterranean basin:

$$\begin{aligned} Q_A + Q_M &= E \\ Q_A S_A + Q_M S_M &= 0 \end{aligned} \tag{2}$$

we find that the outflow salinity transport is proportional to the product of the net evaporation and the Atlantic water salinity:

$$Q_M(\Delta S) = -E\, S_A, \tag{3}$$

which is effectively constant since the Atlantic water salinity varies by only about 1% through the Strait. Thus, while mixing and entrainment in the Strait may change the salinity difference between the inflowing and outflowing waters and the size of the inflow and outflow transports, the outflow salinity transport remains constant. From the observations, one needs to define not only the inflow and outflow transports but also the outflow salinity transport. In return, the observed outflow salinity transport provides a direct estimate of the net evaporation over the Mediterranean basin.

To estimate the inflow and outflow transports and the outflow salinity transport, we will use the measurements on moorings 1, 2, 2B, 3 and 3B deployed across the sill section from Punta Alboassa in Morocco to Punta Paloma in Spain. This section has the minimum cross-sectional area (3.16 x $10^6 m^2$) of any section across the Strait of Gibraltar and its deepest point of 284m is at the sill of the Strait of Gibraltar. Due to the configuration of the sill section, as described by BRYDEN and KINDER (1991b) for their hydraulic model analysis, the direction of along-strait currents for mooring 1 is taken to be 98°T for the transport estimates and the along-strait direction for all other moorings is 77°T. Because 17 of the 21 current records from the moorings on the sill section were deployed below the mean depth of the interface between the Atlantic and Mediterranean waters, these measurements are best suited for determining the transport of the outflowing Mediterranean water. Hence, in the following analyses, the estimates of outflow transport are considered to be generally more reliable than the inflow transport estimates.

There appear to be two reasonable ways to estimate the mean inflow and outflow transports across the Gibraltar sill. The first is to integrate the time-averaged along-strait velocities for all current meters vertically from the bottom up to the depth of zero velocity and then laterally across the sill section to determine the outflow:

$$\bar{Q}_M = \int dy \int_{Bottom}^{z(\bar{u}=0)} \bar{u}(z)\, dz \tag{4a}$$

and then similarly to integrate vertically from the depth of zero velocity up to the sea surface to determine the inflow:

$$\bar{Q}_A = \int dy \int_{z(\bar{u}=0)}^{0} \tilde{u}\,(z)\,dz \tag{4b}$$

The second method is to find the depth of the interface, h(t) between Mediterranean and Atlantic waters at each instant of time; to integrate the along-strait velocities vertically from the bottom up to the depth of the interface to determine the instantaneous outflow; and to integrate the velocities vertically from the interface depth up to the sea surface to determine the instantaneous inflow:

$$Q_M(t) = \int dy \int_{Bottom}^{h(t)} u\,(z,t)\,dz \tag{5a}$$

$$Q_A(t) = \int dy \int_{h(t)}^{0} u\,(z,t)\,dz \tag{5b}$$

Then the mean inflow and outflow transports can be estimated by time-averaging these instantaneous transports.

We will describe the results of each of these methods for determining the exchange between the Atlantic and Mediterranean basins across the Gibraltar sill. While the two approaches appear initially to yield radically different results, careful definition and determination of the outflow salinity transport for each approach and of the contribution to the exchange by the tidal oscillations demonstrate that the two approaches yield consistent results for the exchange. Generally, we conclude that the second approach of determining instantaneous transports provides more insight into the nature of the exchange across the Gibraltar sill.

4. TRANSPORT ESTIMATES FROM MEAN CURRENTS

The first method for estimating the mean inflow and outflow transports starts with the profile of time-averaged currents at each mooring (Fig.6). Because moorings 1, 2B and 3 offer the longest measurement periods at the northern, central and southern mooring sites on the sill cross-section, we will determine the time-averaged transports from these moorings[1]. From interpolation or extrapolation of the mean velocity profiles, we determine that the depth of zero mean inflow-outflow velocity slopes downward from 84m at mooring 1 on the northern side of the sill-section to 120m at mooring 2B on the sill to 134m at mooring 3 on the southern side[2].

To determine an average outflow, we integrate vertically the interpolated time-averaged velocity profile at each mooring, $\bar{u}_i(z)$, and then sum the 3 mooring contributions

$$Q_M = \sum_{i=1}^{3} \int_{Bottom}^{z(\bar{u}=0)} \bar{u}_i(z) L_i(z) dz = -0.385 Sv, \tag{6a}$$

where $L_i(z)$ is the effective cross-sectional width at each depth for each mooring determined from the digitized cross-section bathymetry described by BRYDEN and KINDER (1991b), to estimate the average outflow to be .385Sv. Likewise, to determine an average inflow, we extrapolate the time-averaged velocity profile at each mooring up to the sea surface, vertically integrate, and sum over the 3 moorings as before to estimate the average inflow to be

[1]Measurements on moorings 1 and 3 extended from October 1985 to April 1986, while the measurements on mooring 2B extended from May to October 1986. It will be argued later that there is no significant difference in mean transports for these two periods.

[2]For comparison, the month-long measurements on Mooring 2 and 3B yield depths of zero mean inflow-outflow equal to 115m at mooring 2 and 157m at mooring 3B.

$$Q_A = \sum_{i=1}^{3} \int_{z(\bar{u}=0)}^{0} \bar{u}_i(z) L_i(z) dz = +0.505 \text{Sv}. \quad (6b)$$

Such average values for the inflow and outflow are surprisingly low. For example, the outflow estimate, which should be considered more reliable due to the preponderance of current meters in the deeper waters, is a factor of 3 smaller than the classic value of 1.2Sv determined by LACOMBE and RICHEZ (1982) from shipboard measurements during the 1960s.

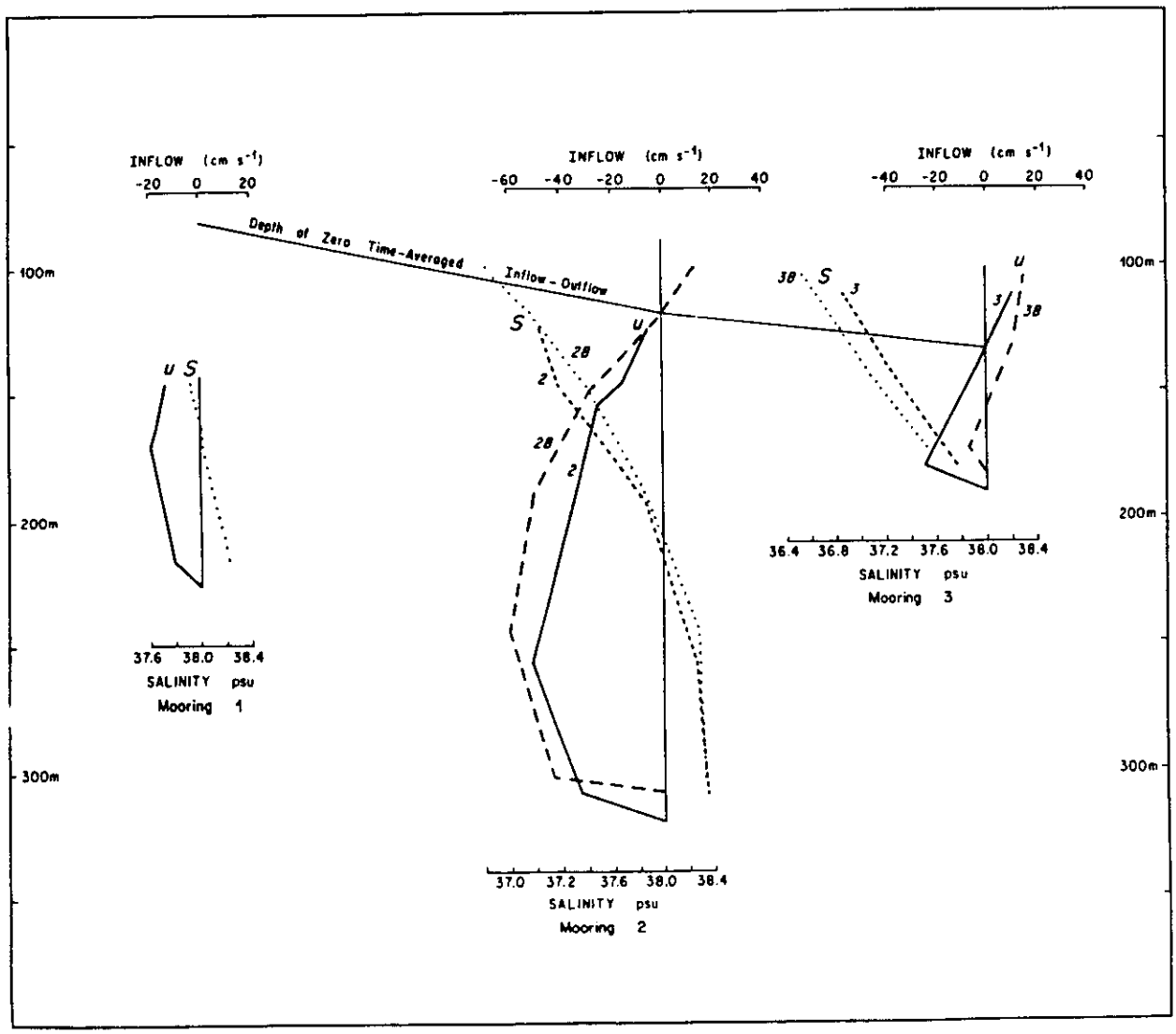

FIG.6. Vertical profiles of record-length averaged along-strait currents ($\bar{u}$) and salinities ($\bar{S}$) for each of the moorings deployed on the sill section. Also indicated is a schematic of the depth of an interface defined to be the location where the average along-strait velocity is zero, i.e. it switches from outflow below to inflow above.

5. CONTRIBUTION OF THE TIDES TO THE MEAN EXCHANGE

The reason that these estimates of the average inflow and outflow are so small is that they do not include all of the exchange between the Atlantic and Mediterranean across the Gibraltar sill. We argued above that the outflow salinity transport must be determined in order to properly quantify the exchange. To determine the outflow salinity transport from the time-averaged statistics at each mooring, we must calculate:

$$\text{Outflow Salinity Transport} = \sum_{i=1}^{3} \int_{\text{Bottom}}^{0} [\bar{u}_i(z)\,(\bar{S}_i(z) - 36.1\text{psu}) + \overline{u'S'}]\, L_i(z)dz = 1.56 \times 10^3 \text{m}^3\text{s}^{-1} \quad (7)$$

where $\overline{u'S'}$ represents an eddy salinity flux due to the correlation between the fluctuations in inflow-outflow velocity and in salinity measured at each current meter. In this estimate, we have subtracted a basic Atlantic water salinity value of 36.1psu in order to minimize the effect of the small imbalance between the mean inflow and outflow transports[1].

Now, the eddy salinity flux dominates the magnitude of the outflow salinity transport. For example at mooring 2B (Fig.7), the outflow salinity transport due to the mean flow is confined to the deep regions of the sill below 175m depth. The eddy salinity flux contribution, on the other hand, is large in the depth range where the interface betwen Atlantic and Mediterranean waters normally resides. The relative contributions to the outflow salinity transport by the mean flow and by the temporal variability are estimated as follows. First, the average salinities of the average outflow and inflow can be determined to be 37.9psu and 36.7psu respectively from

$$S_M = 36.1\text{psu} + \frac{\sum_{i=1}^{3} \int_{\text{Bottom}}^{z_i(\bar{u}=0)} \bar{u}_i(z)(\bar{S}_i(z) - 36.1\text{psu})L_i(z)dz}{\sum_{i=1}^{3} \int_{\text{Bottom}}^{z_i(\bar{u}=0)} \bar{u}_i(z)L_i(z)dz} = 37.9\text{psu}$$

$$S_A = 36.1\text{psu} + \frac{\sum_{i=1}^{3} \int_{z_i(\bar{u}=0)}^{0} \bar{u}_i(z)(\bar{S}_i(z) - 36.1\text{psu})_i(z)dz}{\sum_{i=1}^{3} \int_{z_i(\bar{u}=0)}^{0} \bar{u}_i(z)L_i(z)dz} = 36.7\text{psu}$$

Effectively then, the mean outflow of -0.385Sv occurs at a salinity difference of 1.2psu for an outflow salinity transport of only $-0.46 \times 10^3 \text{m}^3\text{s}^{-1}$. The eddy salinity flux,

$$\sum_{i=1}^{3} \int_{\text{Bottom}}^{0} \overline{u'S'}(z)L_i(z)dz = -1.10 \times 10^3 \text{m}^3\text{s}^{-1} \quad (8)$$

on the other hand, contributes more than twice as much outflow salinity transport so that the total outflow salinity transport is $-1.56 \times 10^3 \text{m}^3\text{s}^{-1}$. Dividing this outflow salinity transport by the Atlantic water salinity of 36.1psu then yields a net average evaporation over the Mediterranean basin of 54cm y^{-1}.

[1]The imbalance of $0.12 \times 10^6 \text{m}^3\text{s}^{-1}$ appears to be too large to represent realistically the net evaporation over the Mediterranean basin since it would equal a net evaporation of 150cm y^{-1} that is a factor of 3 larger than our final estimate of the net evaporation determined from the estimate of outflow salinity transport. The imbalance most likely reflects error in the less reliable estimate of the inflow transport.

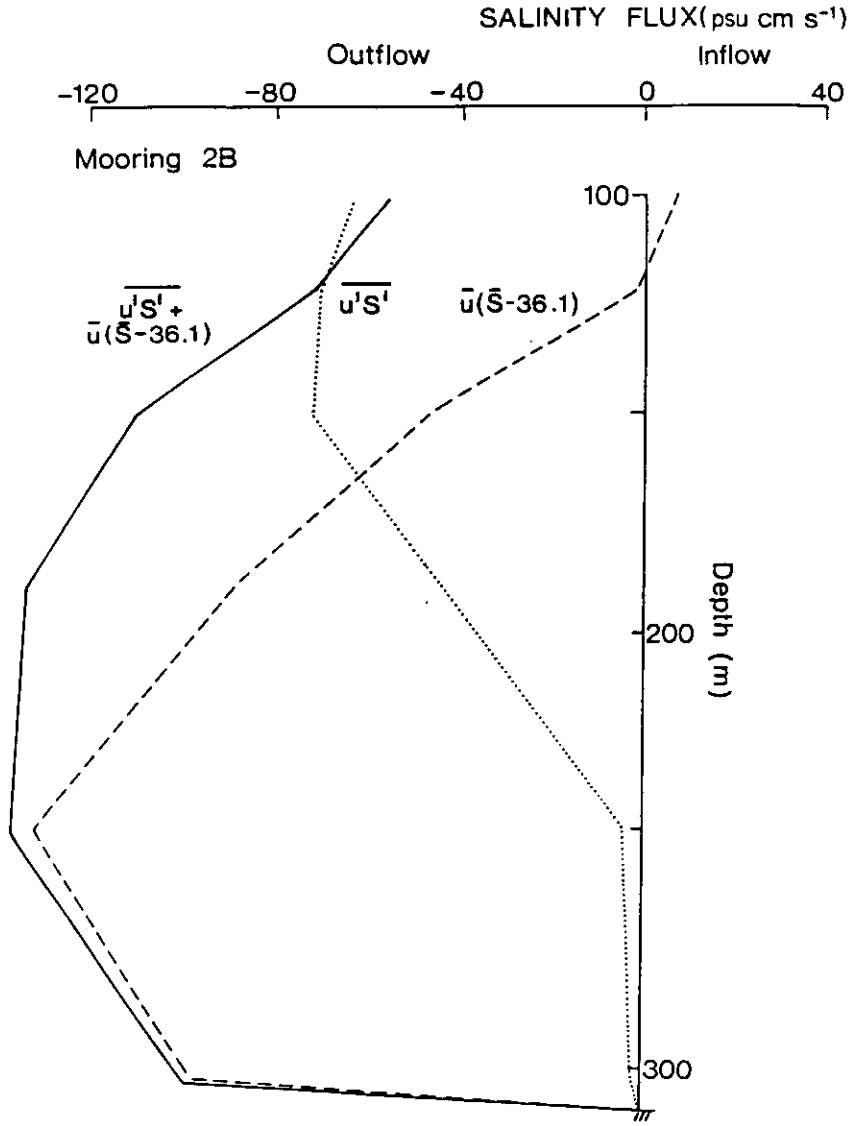

FIG.7. Vertical profile of the time-averaged outflow salinity transport on mooring 2B at the sill. The salinity transport is separated into a contribution due to the mean flow and mean salinity profile, $\overline{u}(\overline{S}-36.1)$, and an average contribution due to temporal (principally tidal) fluctuations in the currents and salinity, $\overline{u'S'}$. The mean flow contribution occurs principally in the deep regions of the sill where there is a strong outflow of salty Mediterranean water, while the contribution from the fluctuations is large in the 100 to 150m depth range where the interface oscillates up and down over the tidal period.

There is a substantial eddy salinity flux at nearly every current meter due to a significant correlation between high salinity and strong outflow velocity, particularly for those current meters in the depth range of the interface between Atlantic and Mediterranean waters. For example, Fig.8a shows the scatter plot between inflow-outflow velocity and salinity measured for 6 months at 110m depth on mooring 3. At every instrument, higher salinity is associated with outflow velocity and lower salinity with inflow velocity and most of this correlation is due to tidal fluctuations. For example, for the 110m record on mooring 3 (Fig.8a), the correlation coefficient between inflow velocity and salinity is -.79 and the resulting eddy salinity flux, $\overline{u'S'}$, is -48.3psu cm s^{-1}. Tidal analysis (Table 3) indicates that the M_2 tidal fluctuations contribute 29.3psu cm s^{-1}, or 61%, of this outflow salinity flux while the S_2, O_1, K_1, N_2, K_2 and M_4 tides contribute an additional 22%. Thus, these tides are responsible for 83% of the eddy salinity flux in this record.

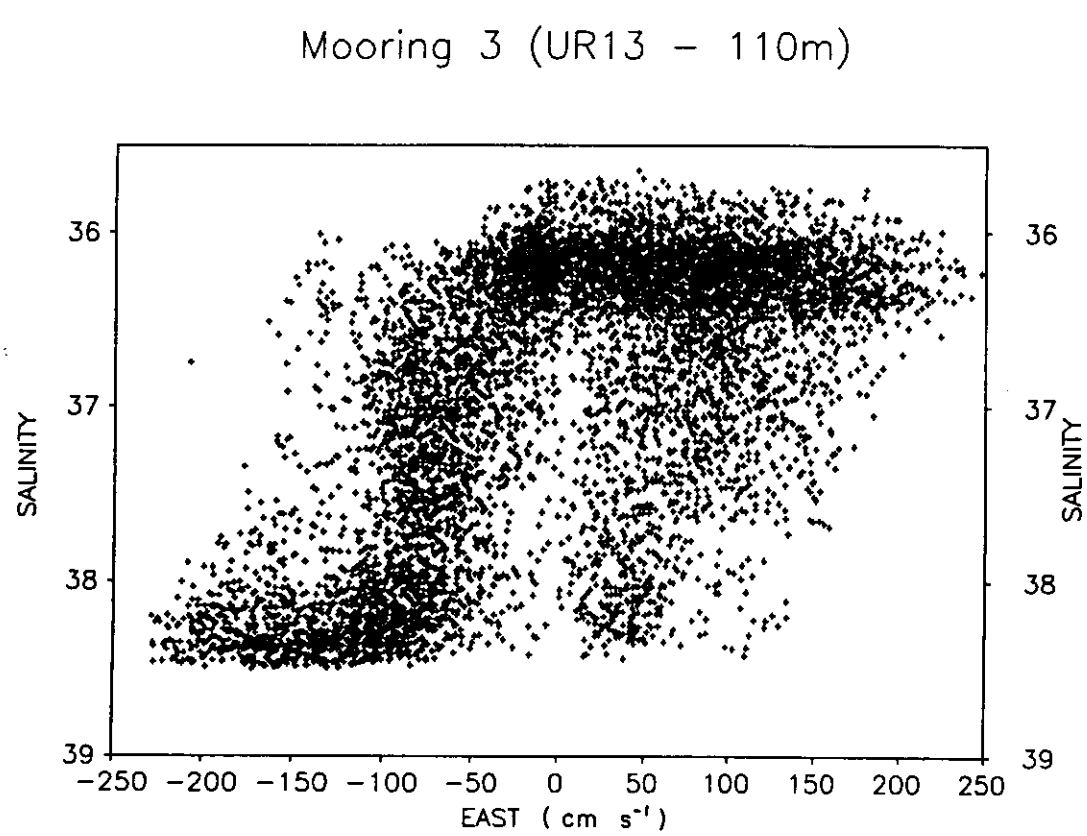

FIG.8a. Scatter plot of along-strait (77°T) velocity versus salinity for the six-month current meter record at 110m depth on mooring 3.

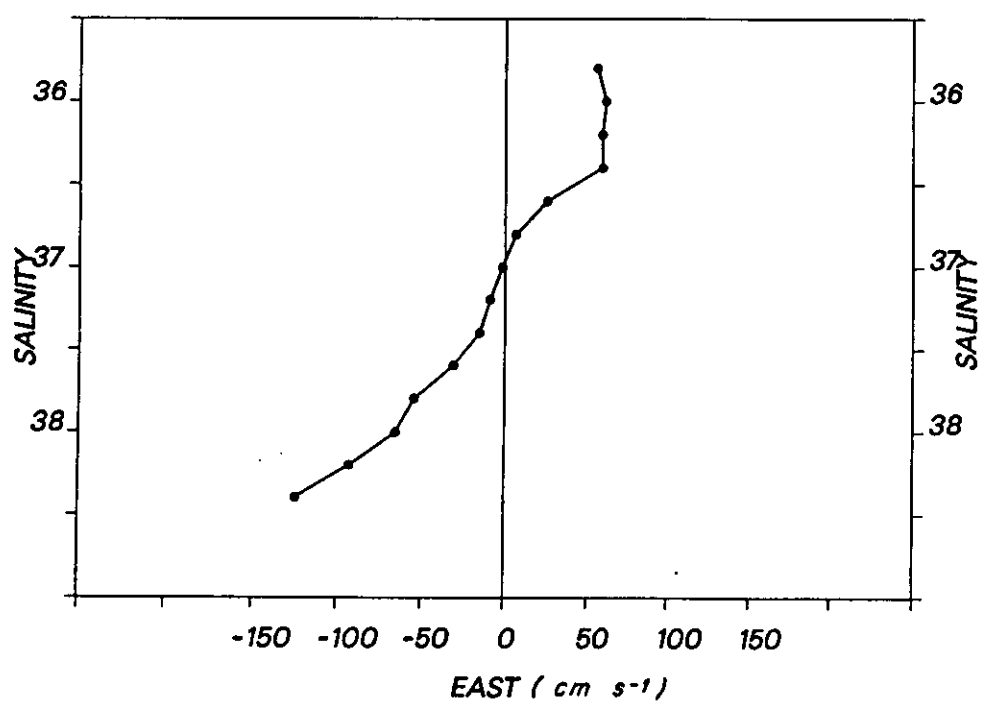

FIG.8b. Average along-strait velocity for salinity bins of 0.2psu. The salinity where the average velocity changes from inflow to outflow is used to define the salinity of the interface between Mediterranean and Atlantic waters. R13 refers to the rotation of currents by 13° counterclockwise from east.

TABLE 3. Tidal amplitudes and phases for six-month record on mooring 3 at 110m depth.

Tidal Constituent		Inflow Velocity - u Amp ($cm\ s^{-1}$)	Phase (°)	Salinity - S Amp (10^{-2}psu)	Phase (°)	Salinity Flux $uS\cos(\Delta\phi)/2$ (psu $cm\ s^{-1}$)
M_2	(12.42 hours)	117	146	76	15	-29.3
S_2	(12.00 hours)	39	174	24	46	-2.9
O_1	(25.82 hours)	29	355	22	185	-3.2
K_1	(23.93 hours)	26	69	20	252	-2.5
N_2	(12.66 hours)	24	129	16	358	-1.2
K_2	(11.97 hours)	12	173	12	46	-0.4
M_4	(6.21 hours)	10	216	13	358	-0.5

In terms of the depth of the interface between Mediterranean and Atlantic waters, the eddy salinity flux can be explained as a correlation between the depth of the interface and the strength of the inflow velocity. When the salinity at a particular instrument is high, the interface is at relatively shallow depth; when the salinity is low, the interface is relatively deep. Thus, there is strong outflow when the salinity is high and the interface is shallow, resulting in a strong outflow of a thick layer of Mediterranean water. And there is strong inflow when the salinity is low and the interface is deep resulting in a strong inflow of a thick layer of Atlantic water. We can make an estimate of this effective exchange of Atlantic and Mediterranean waters across the Gibraltar sill by determining the covariance between the velocity at the interface and the depth of the interface, h_i where h_i is the depth of the 37psu isohaline at each mooring:

$$\text{Exchange due to Temporal Fluctuations} = \sum_{i=1}^{3} \overline{u'h'_i} L_i(z=\overline{h}_i) = 0.41\,\text{Sv} \qquad (9)$$

where L_i is the effective width of the cross-section for each mooring at the depth of the mean interface (Table 4). This exchange is equally both an inflow and an outflow; that is, it effectively increases the inflow by 0.41Sv for a total Atlantic layer inflow of 0.91Sv and it increases the outflow by -0.41Sv to a total Mediterranean layer outflow of -0.79Sv. With reference to these estimates of the time-averaged exchange due to the combination of the time-averaged currents and the eddy fluxes, we conclude that the total exchange is due approximately half to the temporal fluctuations and half to the time-averaged flow.

From a calculation similar to that for the outflow salinity flux, it is principally the M_2 semidiurnal tide that accomplishes the eddy exchange across the Gibraltar sill. LAVIOLETTE and LACOMBE (1988) had suggested that the M_2 tide could contribute to the outflow, but they were unable to quantify the contribution based on their synoptic measurements. Tidal analyses for the depth of the interface taken to be the 37psu isohaline and for current at or near the interface depth indicate that the inflow velocity and interface depth are close to being in phase for the dominant M_2 tidal variability. The velocity does peak at each mooring before the interface achieves its greatest depth but the phase difference is only 35° at mooring 1, 36° at mooring 2B and 51° at mooring 3. It is straightforward to calculate that these M_2 fluctuations accomplish 0.25Sv, or 62%, of the eddy exchange (Table 5). Thus, we can understand the principal process of eddy exchange across the sill as follows. On each M_2 semidiurnal cycle, when the inflowing tide is a maximum, the interface is deeper than average and a bolus of Atlantic water crosses the sill into the Mediterranean. On the

outflowing tide, the interface is shallower than average and a bolus of Mediterranean water crosses the sill into the Atlantic. While there is no average tidal current at each depth, the tides do transport water types effectively across the sill. Although the M_2 fluctuations contribute the bulk of the exchange due to the temporal variations, tidal analyses of the interface depth and currents measured near the interface (Table 5) indicate that the S_2, O_1, and K_1 tides also contribute .029, .022 and .019Sv respectively to the exchange across the sill as well. The total exchange accomplished by these four principal tidal components is 0.32Sv, or nearly half of the total exchange across the sill.

TABLE 4. Eddy exchange across the Gibraltar sill. Moorings 1, 2B and 3 were deployed on the north side, at the sill, and on the south side of the sill section. Variances and covariances for u, the along-strait velocity, and h_{37}, the depth of the 37psu isohaline that marks the interface between Atlantic and Mediterranean waters, indicate strong positive correlation coefficients, C, between strong inflow and deep interface. At mooring 1, u is taken to be the extrapolated velocity at 75m depth; at mooring 2B, u is the measured velocity at 112m depth; at mooring 3, u is the measured velocity at 110m depth. The effective cross-sectional width for mooring 1 is the distance from the 82m isobath at the northern boundary of the sill section to a point halfway between moorings 1 and 2B. The width for mooring 2B is the distance between the points halfway between moorings 1 and 2B and moorings 2B and 3. The width for mooring 3 is the distance from the point halfway between moorings 2B and 3 and the 123m isobath at the southern boundary of the sill section.

Mooring	$\overline{u'h'}_{37}$ (m^2s^{-1})	$\overline{u'^2}$ (m^2s^{-2})	$\overline{h'^2}_{37}$ (m^2)	$C_{\overline{u'h'}_{37}}$	$\overline{h_{37}}$ (m)	Cross-Sectional width (km)
1	28.5	1.297	2402	0.51	82	6.7
2B	37.8	0.968	2607	0.75	131	4.3
3	31.3	0.750	3374	0.62	123	1.8

We label the above values of the exchange (inflow = 0.91Sv, outflow = -0.79Sv, outflow salinity transport = $-1.56 \times 10^3 m^3 s^{-1}$) as statistical estimates because they utilise the longest current meter records at moorings 1, 2B and 3 without regard to possible seasonal variations in the exchange that could affect the combination of October-to-April measurements on moorings 1 and 3 with the May-to-August measurements on mooring 2B. In addition, the above statistical estimates of the inflow and outflow transports do not take into account the slight asymmetry of upward or downward displacements of the interface on the transports as a result of the decrease in width of the sill section with increasing depth. To take into account such hypsometric effects, the interface depth, inflow and outflow need to be defined continuously in time, as carried out in the following sections.

6. TEMPORALLY VARYING ESTIMATES OF THE EXCHANGE

The second method for determining the inflow and outflow through the Strait of Gibraltar based on Eq.5 includes making time series estimates of the upper layer mass transport (ULT), lower layer mass transport (LLT), and outflow salinity transport (OST). It requires a definition of the depth of the interface between inflowing Atlantic water and outflowing Mediterranean water at each instant of time and then vertical integration of the lower layer flow from the bottom up to the interface and of the upper layer flow from the interface up to the sea surface according to Eq.5. Outflow salinity transport (OST following Eq.3) can also be estimated at each instant of time with a method similar to that used for the mean exchange:

TABLE 5. Principal tidal contributions to the sill exchange. As in Table 4, u is the along-strait velocity and h_{37} is the depth of the 37psu isohaline. Tidal analyses for the long records on moorings 1, 2B and 3 yield amplitude and phase for the principal M_2, S_2, O_1 and K_1 tides. The contribution of each tidal constituent to the exchange is determined from the cospectrum $\overline{u'h'_{37}}$ at the particular frequency of the tide. The cospectrum can be compared directly to the covariances, $\overline{u'h'_{37}}$, in Table 4 to determine the fraction of exchange accounted for by each tidal component.

	u		h_{37}		$\overline{u'h'_{37}}$
	AMP ($m\ s^{-1}$)	PH (°)	AMP (m)	PH (°)	$0.5\ Uh_{37}\cos(\Delta PH)$ (m^2s^{-1})
Mooring 1					
M_2	1.09	136	33.4	171	15.0
S_2	.41	156	8.3	210	1.0
O_1	.28	21	14.1	46	1.8
K_1	.27	96	15.3	127	1.8
					19.6 Total
Mooring 2B					
M_2	1.24	152	51.4	188	25.8
S_2	.63	190	15.7	222	4.2
O_1	.25	11	12.0	33	1.4
K_1	.18	88	10.8	100	1.0
					32.4 Total
Mooring 3					
M_2	1.18	146	61.8	197	23.0
S_2	.39	174	16.9	228	2.4
O_1	.29	354	15.8	22	2.0
K_1	.26	69	13.6	91	1.6
					29.0 Total

$$OST = Q_M(S_M - S_A) = \int dy \int_{Bottom}^{0} u(z,t)\,(S(z,t) - 36.1psu)dz \qquad (10)$$

Definition of the interface at each instant of time, h(t), is a critical step for making time series estimates of the inflow and outflow.

It is not possible to define the interface based on a depth of zero velocity between inflow and outflow at each instant of time. The tidal currents are strong and barotropic in character, that is the tidal velocities are nearly in phase vertically and they are larger than the mean inflow or outflow at all depths (Fig.3). Thus, for much of each tidal cycle, the flow throughout the water column is directed either eastward into the Mediterranean or westward out toward the Atlantic and there is no depth where the velocity is zero.

Conceptually, the interface is a water mass boundary between fresher (S = 36.1psu) Atlantic water and saltier (S = 38.4psu) Mediterranean water. For this reason, we prefer to define the interface in terms of a particular isohaline marking the water mass boundary. Initially, we found the depths of the 37, 37.5 and 38 psu isohalines (e.g. Fig.5) at each mooring since these isohalines determine a transition region between pure Atlantic water and pure Mediterranean water. In order to pick a single isohaline to define the interface, scatter plots of velocity versus salinity are made for each current meter record on the sill section within the interfacial region above 140m depth (e.g.

Fig.8a); average along-strait velocity is then calculated in salinity bins of 0.2psu (e.g. Fig.8b); and the salinity where the average along-strait velocity switches from inflow to outflow is identified. For all current meter records, the salinity of this zero-crossing varies only from 36.6 to 37.4psu. Thus, the 37psu isohaline is taken to define the interface. Such definition is consistent with the traditional choice by LACOMBE and RICHEZ (1982).

The depth of the interface, that is the depth of the 37psu isohaline, oscillates vertically at the sill with a standard deviation value of 47m for mooring 2B. The M_2-tide is the dominant contributor to the variability in the Strait (CANDELA, WINANT and RUIZ, 1990) and M_2-tidal fluctuations in the interface depth have an amplitude of 51m at mooring 2B. On the sill, the interface achieves its shallowest depth at a phase of 8° with respect to Greenwich, or about 100 minutes before high water at the sill which has a phase of about 57° (CANDELA, WINANT and RUIZ, 1990). Rather than compensate for the surface tidal pressure then, these tidal fluctuations in interface depth enhance the deep pressure signals, though the added baroclinic pressure signal due to the depth variations of the interface is only about 9 millibars or 16% of the sea level pressure amplitude of 55 millibars for the M_2 tide (CANDELA, WINANT and RUIZ, 1990).

With this definition of the depth of the interface, the estimates of upper layer transport, lower layer transport and outflow salinity transport are made at 30 minute intervals according to Eqs 5 and 10. The upper layer transport is of Atlantic water and the lower layer transport is of Mediterranean water since we have defined the interface as a water mass boundary. It is important to note that the Atlantic water transport does not have to be positive, i.e. an inflow, at all times, nor does the Mediterranean water transport have to be an outflow at all times. In fact, there are times in the tidal cycle when the Atlantic water flows out of the Mediterranean and times when Mediterranean water flows back into the Mediterranean.

To estimate transports at each 30 minute interval, along-strait velocity is linearly interpolated or extrapolated vertically at each mooring to values at 5m depth intervals from the bottom to the sea surface. A filter is put on the extrapolated velocities such that velocities in excess of ±400cm s^{-1} are set to ±400cm s^{-1}. Salinity is also interpolated or extrapolated vertically at each mooring to values at 5m depths. For the situation when the interface is above the shallowest instrument on the mooring, a salinity of 37psu at the depth of the interface is used along with the salinity measurements on the mooring to extrapolate salinity up to the sea surface. A filter is put on extrapolated salinities such that salinities less than 35.8psu are set equal to 35.8psu and salinities greater than 38.5psu are set equal to 38.5psu. Examination of CTD data sets during the Gibraltar Experiment (BRAY, 1986; KINDER, BURNS and BROOME, 1986; KINDER, BURNS and WILCOX, 1987; SHULL and BRAY, 1989) suggests that 35.8psu and 38.5psu are reasonable extreme values for the Atlantic water and Mediterranean water salinities on the sill section. We examined the individual profiles on moorings 1, 2, 2B and 3 for situations when the velocities were ±400cm s^{-1} or when the salinities were 35.8psu and found that nearly all extreme values are in the upper waters above 50m depth where there are no direct measurements. For this reason, the estimates of upper layer transport must be considered to be the most uncertain of the transport estimates and it is essential to subtract a reference Atlantic water salinity in estimating the outflow salinity transport.

The optimal period for estimating the exchange through the Strait of Gibraltar with these measurements is the 32-day period during October-November 1985 when 16 current meter records on three moorings 1, 2 and 3, across the sill section are available. After mooring 2 parted prematurely in November 1985, there is a further five-month period through April 1986 when the 7 current meters on moorings 1 and 3 provide reasonable estimates on the temporal variability in the exchange across the sill. To obtain a longer record of the exchange, the 6 current meters on mooring 2B are used to estimate the exchange for an additional 3 months from May to August 1986.

We estimate upper layer transport, lower layer transport and outflow salinity transport for each of these time periods, taking some care to ensure that the estimates of the exchange are consistent for the three periods so that the low frequency variability over a 9 month period can be assessed.

7. EXCHANGE DURING OCTOBER-NOVEMBER PERIOD OF BEST SPATIAL COVERAGE

First, estimates of the exchange are made for the optimal 32-day period when moorings 1, 2 and 3 provide measurements of the flow across the sill. We estimate upper layer transport, lower layer transport and outflow salinity transport at 30-minute intervals (Fig.9) by vertically integrating the profiles of along-strait velocity, u, and salinity, S, at each mooring using the effective cross-sectional width at each depth for each mooring, $L_i(z)$, defined above:

$$ULT(t) = \sum_{i=1}^{3} \int_{h(t)}^{0} u_i(z,t)L_i(z)dz$$

$$LLT(t) = \sum_{i=1}^{3} \int_{Bottom}^{h(t)} u_i(z,t)L_i(z)dz \qquad (11)$$

$$OST(t) = \sum_{i=1}^{3} \int_{Bottom}^{0} u_i(z,t)(S_i(z,t) - 36.1psu)L_i(z)dz$$

From these 32-day time series of transports, the time-averaged upper layer transport of Atlantic water is 0.93Sv directed into the Mediterranean; the time-averaged lower layer transport of Mediterranean water is -0.68Sv directed out over the sill into the Atlantic; and the time-averaged outflow salinity transport is $-1.50 \times 10^3 m^3 s^{-1}$. Such time averages agree reasonably well with the estimates of the mean exchange based purely on the statistics of the current meter records as described above[1]. Such agreement provides some confirmation that the procedures of interface determination and vertical extrapolation and filtering have not altered the basic character of the exchange through the Strait.

These time series estimates of transports through the Strait of Gibraltar exhibit strong semidiurnal tidal fluctuations: the M_2-tidal fluctuations in upper layer transport have an amplitude of 2.3Sv with a phase of 151° and in lower layer transport have an amplitude of 1.3Sv with a phase of 144°. Thus, the tidal fluctuations are indeed large enough to reverse the inflow of Atlantic water in the upper layer and the outflow of Mediterranean water in the lower layer. To estimate the uncertainty in the time-averaged inflow of Atlantic water and outflow of Mediterranean water, we determine the standard error of the upper layer and lower layer transports based on an assumption of independent estimates of these transports every semidiurnal tidal period. With 61 semidiurnal

[1]The data are somewhat different between these estimates and the earlier statistical estimates. Here moorings 1, 2 and 3 are used for the October-November 1985 time period while in the statistical estimates moorings 1 and 3 were used for their full record length October 1985 to April 1986 and mooring 2B for its full record length May to October 1986.

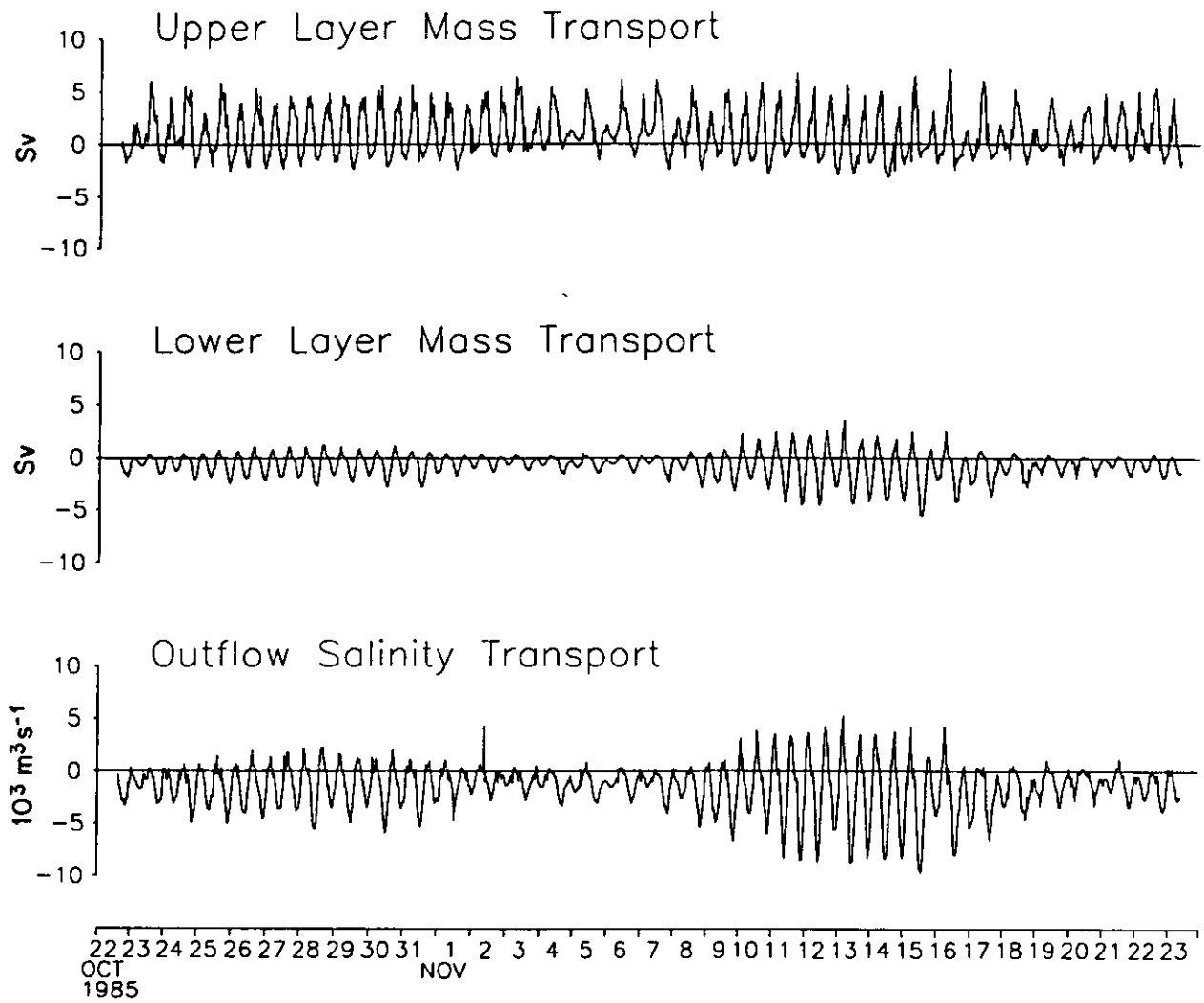

FIG.9. Time series of 30-minute values of upper layer mass transport, lower layer mass transport and outflow salinity transport during October-November 1985 when moorings 1, 2 and 3 were all measuring the sill exchange. At each instant of time the upper layer mass transport is the integral of the along-strait velocity from the depth of the 37psu isohaline up to the sea surface and across the strait. The lower layer transport is similarly the integral of along-strait velocity from the bottom up to the depth of the 37psu isohaline and across the strait. The outflow salinity transport is the integral of along-strait velocity times the salinity anomaly above the basic Atlantic water salinity of 36.1psu from the bottom to the sea surface and across the sill section.

tidal periods in the 32 day measurement period, the standard error in the mean Atlantic water inflow is ±0.27Sv, the standard error in Mediterranean outflow is ±0.15Sv, and the standard error in outflow salinity transport is $\pm 0.27 \times 10^3 m^3 s^{-1}$.

There may also be bias errors in these estimates of the exchange, particularly for the upper layer transports since they are based primarily on extrapolations of measurements made below the interface. In making these estimates, we particularly worried about the reliability of the upper layer transport of Atlantic wter, and we admit to a certain satisfaction that the time-averaged inflow does balance the time-averaged outflow within its standard error. On the basis of mass and salt

conservation requirements for the Mediterranean basin, the inflow and outflow should balance within about 0.05Sv. Because of the uncertainty in upper layer transport estimates, we do not attribute the sum of the time-averaged inflow and outflow to be a reliable estimate of the net evaporation over the Mediterranean basin. Instead, we would argue that this sum is due to the uncertainty in determination of the upper layer Atlantic water inflow.

Using these Gibraltar measurements, we can estimate of the net evaporation over the Mediterranean basin from the outflow salinity transport according to Eq.3. By dividing the time-averaged outflow salinity transport of $1.50 \times 10^3 m^3 s^{-1}$ by the Atlantic water salinity of 36.1psu, a direct estimate of 52cm y^{-1} is made for the net evaporation over the Mediterranean basin (surface area = $2.52 \times 10^{12} m^2$). Again, the lack of direct measurements in the upper layer casts some uncertainty on this estimate of outflow salinity transport. To decrease the uncertainty, we had first subtracted the basic Atlantic water salinity of 36.1psu before carrying out the salinity transport calculations so that, even if there were an error in upper layer mass transport of 1Sv, it would only be multiplied by a salinity anomaly of order 0.1psu and the resulting error in outflow salinity transport would be only of order $0.1 \times 10^3 m^3 s^{-1}$. The second check on the salinity transport involves estimating the outflow salinity transport separately for the lower layer and for the upper layer. We expect the lower layer outflow of high salinity Mediterranean water to contribute most of the salinity flux and it does contribute $-1.33 \times 10^3 m^3 s^{-1}$ to the total outflow salinity transport of $-1.5 \times 10^3 m^3 s^{-1}$. The upper layer contributes only $-0.17 \times 10^3 m^3 s^{-1}$ to the salt transport and we argue that this is a reasonable contribution given that correlations between strong outflow velocity and high salinity above the 37psu isohaline surely do add to the outflow salinity transport. We would estimate, however, that the upper layer contribution to the outflow salinity transport might have a bias error as large as a factor of 2, so that the total outflow salinity transport could be as large as $-1.67 \times 10^3 m^3 s^{-1}$, equivalent to a net evaporation of 58cm y^{-1}.

Overall for the 32-day period of measurements on moorings 1, 2 and 3, we estimate the time-averaged outflow of Mediterranean water over the Gibraltar sill to be -0.682Sv ±0.15Sv. We estimate that the time averaged outflow salinity transport is $-1.50 \times 10^3 m^3 s^{-1}$, but it may be as large as $-1.67 \times 10^3 m^3 s^{-1}$ due to uncertainty in the upper layer contribution, and the mean value has a standard error of $\pm 0.27 \times 10^3 m^3 s^{-1}$. Thus, our estimate for the net evaporation over the Mediterranean basin based on measurements of the exchange through the Strait of Gibraltar lies between 52 and 58cm y^{-1}, with a standard error uncertainty of ±9cm y^{-1}. Based on this estimate of the net evaporation, we would calculate that the mean inflow of Atlantic water should be 0.042 ± 0.01Sv larger than the absolute value of the mean outflow of Mediterranean water, and hence our best estimate for the mean inflow is +0.724Sv ±0.16Sv. This 'best' estimate of the mean inflow is indirect, but it does lie within the uncertainty of the direct estimate of the time-averaged Atlantic water inflow transport of 0.93 ±0.27Sv described above.

These are the first estimates of the Gibraltar exchange that utilize more than one mooring or one site to measure the inflow and the outflow across the sill. In an attempt to assess the usefulness of multiple moorings, calculations of the exchange across the Gibraltar sill are made on the basis of each mooring by itself, assigning the entire cross-sectional width of the sill section to the current and salinity profiles obtained from the individual moorings 1, 2, 2B and 3 (Table 6). Current and salinity profiles on moorings 1 and 3 are extrapolated downward to depths as great as 285m, the sill depth of the Strait, as well as upward to the sea surface for these calculations. The estimates of lower layer outflow of Mediterranean water for moorings 1 and 3 are substantially smaller than the estimate based on mooring 2 which is quite close to the mean value of -0.68Sv derived from all three moorings above. Such a result indicates that it is essential to make direct current measurements in the deep parts of the sill section below 200m depth for an accurate estimate of

the outflow of Mediterranean water. Because the deep regions of the sill section are quite confined (the width between the 200m isobaths on the sill section is only 6.9km), a single mooring at or near the sill can provide reasonable measurements of the Mediterranean outflow. Similar results and implications are found for estimating the outflow salinity transport by comparing the values obtained for the three moorings: it is essential to make direct current and salinity measurements in the deep part of the sill section in order to estimate accurately the outflow salinity flux. For the upper layer transport, the estimates of the inflow of Atlantic water using only mooring 2 or mooring 2B at the sill are much larger than the mean inflow of 0.92Sv derived from all three moorings above. This result appears to be due to the facts that the interface depth at mooring 1 and over the relatively broad region north of mooring 1 is substantially shallower than the interface depth at the sill, so that there is less area of the upper layer inflow than would be estimated from mooring 2 alone, and that the currents in the northern part of the Strait are somewhat smaller than those at the sill. The upper layer transport derived from mooring 3 alone is quite a good estimate of the inflow of Atlantic water, but this appears to be fortuitous due to a combination of smaller currents and deeper interface than are typical of the sill cross-section. In summary, we conclude that a single mooring at or near the sill measuring the currents particularly below 150m depth down to the sill depth of 285m can provide an accurate estimate of the lower layer outflow of Mediterranean water across the sill but that several moorings across the sill section are needed to measure the upper layer inflow of Atlantic water because of cross-strait variations in the interface depth and in the size of the currents.

TABLE 6. Estimates of Gibraltar exchange from single moorings. Upper and lower layer transports are defined to be the vertically and horizontally (cross-strait) integrated flows above and below the 37psu isohaline defined by the instantaneous salinity and pressure measurements on the particular mooring. Velocity measurements on each mooring are linearly interpolated and extrapolated vertically to the bottom (285m depth) and to the sea surface at each instant of time. The cross-strait distance at each depth is the distance between the isobaths on the sill cross-section.

	Upper Layer Mass Transport (Sv)	Lower Layer Mass Transport (Sv)	Outflow Salinity Transport ($10^3 m^3 s^{-1}$)	Period
Mooring 1	.69	-.40	-.95	Oct-Nov 85
Mooring 2	1.35	-.78	-1.68	Oct-Nov 85
Mooring 3	.94	-.61	-1.21	Oct-Nov 85
Mooring 1	.52	-.45	-.96	Oct 85 - May 86
Mooring 3	1.22	-.65	-1.34	Oct 85 - Apr 86
Mooring 2B	1.44	-.80	-1.68	May-Aug 86

8. NINE-MONTH TIME SERIES OF THE EXCHANGE

To extend the estimates of exchange through the Strait of Gibraltar to as long a time period as possible, we utilise the measurements on moorings 1 and 3 to estimate the exchange for the period October 1985 to April 1986 and the measurements on mooring 2B for the period May to August 19086. All 7 current meters on moorings 1 and 3 made continuous measurements during the entire 6-month deployment period from October 22 1985 to April 21 1986. The temporal gap in moorings from late April to late May 1986 was planned as part of the Gibraltar Experiment in order to allow WESSON and GREGG (1994) to carry out an extensive series of tethered microstructure profiles without fears of snagging a mooring with the tether (BRYDEN and KINDER, 1986). The current meters on mooring 2B, deployed on May 29, gradually failed over the 5-month lifetime of the mooring due to vibration so that the current meter at 112m depth ceased measuring currents after 31 days, the 181m instrument ceased after 41 days, the 90m and 135m instruments ceased after 82 days, and the 233m instrument ceased after 92 days. We judged that reliable transport estimates could be made only for the first 82 day period from 29 May to 19 August 1986 when at least 4 instruments provided current measurements. The interface time series, however, is continuous for the entire 137-day deployment period as vibration did not adversely affect the temperature, conductivity and pressure measurements.

To ensure that upper layer, lower layer and outflow salinity transports are consistently determined for the three time periods (October-November using moorings 1, 2 and 3; November-April using moorings 1 and 3; and May-August using mooring 2B), regression for daily-averaged transport estimates ULT, LLT and OST during the October-November time period are carried out to derive linear fits of the transports using mooring 1 and 3 (denoted with a subscript 13) and using mooring 2 (denoted with a subscript 2) to the optimal transports derived from moorings 1, 2 and 3 (denoted with a subscript 123):

$$\begin{aligned} \mathrm{Trans}_{123} &= A^{*}\mathrm{Trans}_{13} + B \\ &\text{and} \\ \mathrm{Trans}_{123} &= C^{*}\,\mathrm{Trans}_{2} + D \end{aligned} \qquad (12)$$

where each set of regressions (12) is carried out 3 times, for Trans = ULT, for Trans = LLT and for Trans = OST, to determine the coefficients A, B, C and D (Table 7). Then the resulting regression coefficients are applied to derive scaled transport estimates using moorings 1 and 3 for the period October to April and using mooring 2B for the period May to August:

$$\begin{aligned} \mathrm{Trans}_{13}\mathrm{Scaled} &= A^{*}\mathrm{Trans}_{13} + B \\ &\text{and} \\ \mathrm{Trans}_{2B}\mathrm{Scaled} &= C^{*}\mathrm{Trans}_{2B} + D. \end{aligned} \qquad (13)$$

The basis for such scaled transport estimates is CANDELA, WINANT and BRYDEN's (1989) result that the low-frequency currents vary consistently together primarily as a nearly uniform fluctuation in along-strait current at all depths and locations on the sill section. In their analysis, a single empirical orthogonal function (EOF) accounted for more than 80% of the low-frequency variance in along-strait currents in the Strait and the form of this primary EOF was nearly barotropic on the sill section. Here, we present the low-frequency along-strait currents on mooring 3 (Fig.10a) to illustrate the pronounced vertical correlation throughout the water column; the along-strait currents at about 140m depth on moorings 1 and 3 (Fig.10b) to illustrate the pronounced lateral correlation across the sill section; and along-strait currents on moorings 8, 3 and 7 (Fig.10c) to illustrate the pronounced lateral correlation along the axis of the Strait. Correlation coefficients are

typically 0.8 and higher. Thus, the low-frequency variations observed in any current meter record on the sill are indicative of the variations in flow throughout the Strait. The resulting 9-month time series of scaled transports through the Strait (Fig.11) then should represent consistent estimates of the Atlantic water inflow, Mediterranean outflow and outflow salinity transport for describing the low frequency variability in the exchange between the Atlantic and Mediterranean basins.

TABLE 7. Consistent transport estimates. Variables ULT, LLT and OST refer to upper layer transport, lower layer transport, and outflow salinity transport respectively. Regressions for each variable are carried out on daily-averaged values for the October-November time period. The transports determined using Moorings 1, 2, 3 are considered to be the standard and the linear regressions are used to determine how to scale transports using only moorings 1 and 3 or only mooring 2 to make them consistent with the transports using all 3 moorings.

Regression:	$Trans_{123}$ =	$A \times Trans_{13} + B$	for October-November time period using daily averaged values
	Trans	A	B
	ULT	1.180	.005
	LLT	1.033	-.124
	OST	1.035	-.278
Regression:	$Trans_{123}$ =	$C \times Trans_{2} + D$	for October-November time period using daily averaged values
	Trans	C	D
	ULT	0.490	.282
	LLT	0.696	-.136
	OST	0.709	-.306
Then	$Trans_{13}$ Scaled =	$A \times Trans_{13} + B$	for October-April time period
	$Trans_{2B}$ Scaled =	$C \times Trans_{2B} + D$	for May-August time period

From these long time series of consistent transports, the 9-month average Atlantic water inflow is 0.935Sv; the average Mediterranean water outflow is -0.718Sv; and the average outflow salinity transport is $-1.54 \times 10^3 m^3 s^{-1}$. Thus, these 9-month averages are similar to the 32-day averages for the October-November period of best instrument coverage. It is worth noting that the similarity of the averages cannot be attributed purely to the regression techniques, since the regression coefficients are based only on October-November measurements. Currents could have been stronger or weaker in the later periods, so that the transports could have been higher or lower.

While there is little difference in the 32-day and 9-month averaged transports, there is substantial low frequency variability in the daily averaged transports (Fig.11). The daily values of lower layer transport always represent an outflow of Mediterranean water, but the outflow varies from a minimum of -0.33Sv to a maximum of -1.62Sv, with a standard deviation of 0.22Sv. On the other hand, the daily values of upper layer transport actually change sign so that for a short period in late February the Atlantic water appears to flow back out toward the Atlantic. For the most part, upper layer transports represent Atlantic water flowing into the Mediterranean with a maximum daily averaged inflow estimated to be 2.09Sv, a minimum (reverse) flow of -0.60Sv, and a standard deviation of 0.37Sv. The outflow salinity transport is always of one sign, but it does vary from a maximum of $-2.90 \times 10^3 m^3 s^{-1}$ to a minimum of $-0.61 \times 10^3 m^3 s^{-1}$ with a standard deviation of $0.40 \times 10^3 m^3 s^{-1}$.

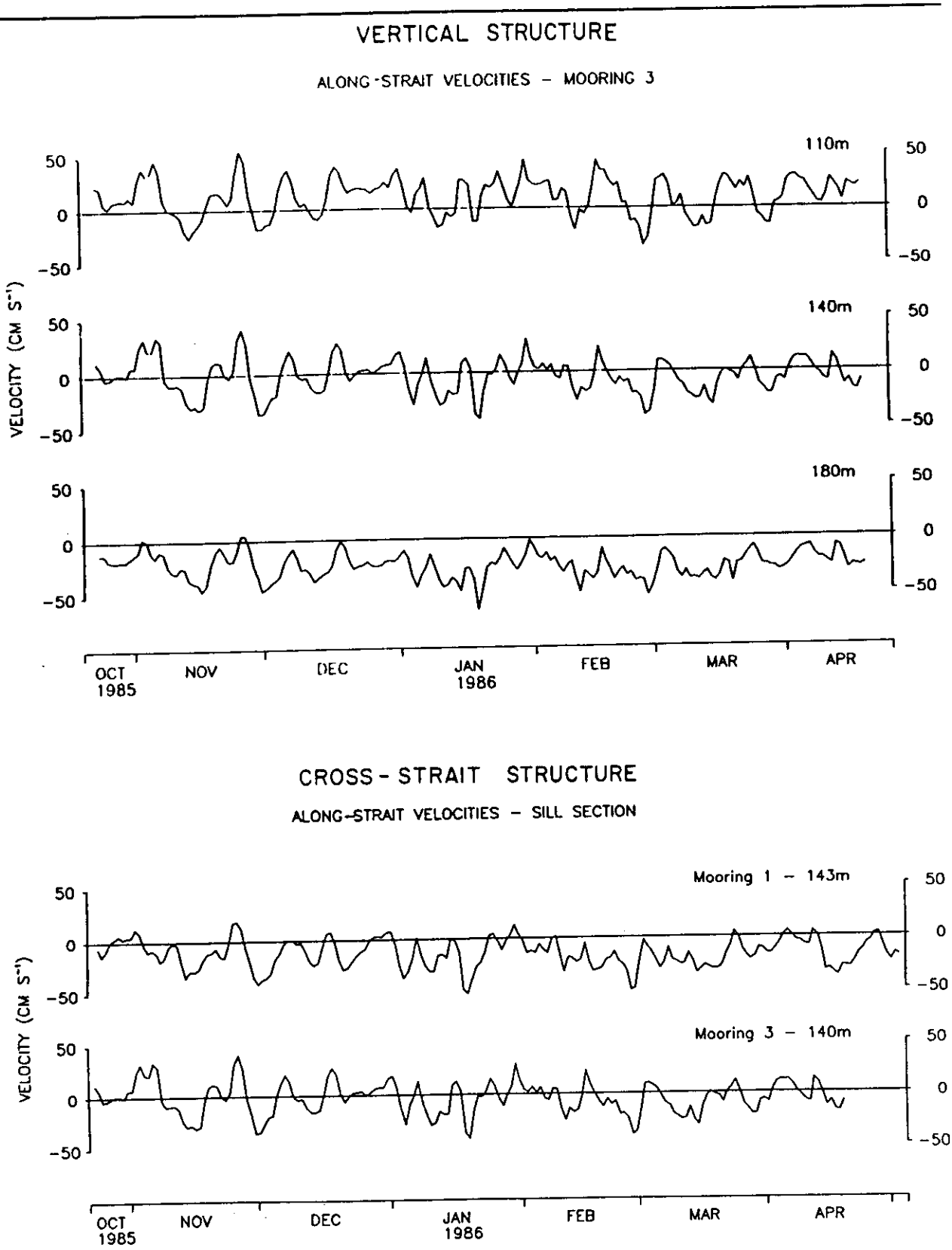

FIG. 10. Spatial structure in along-strait currents. (a) Daily averaged along-strait velocities at 110, 140 and 180m depths on moorings 3 exhibit strong vertical correlations. (b) Daily averaged along-strait velocities at about 140m depth on moorings 1 and 3 on the northern and southern sides of the Strait exhibit strong cross-strait correlation. (c, overleaf) Daily averaged along-strait velocities in the upper waters on moorings 8, 3 and 7 along the axis of the Strait exhibit strong along-strait correlations.

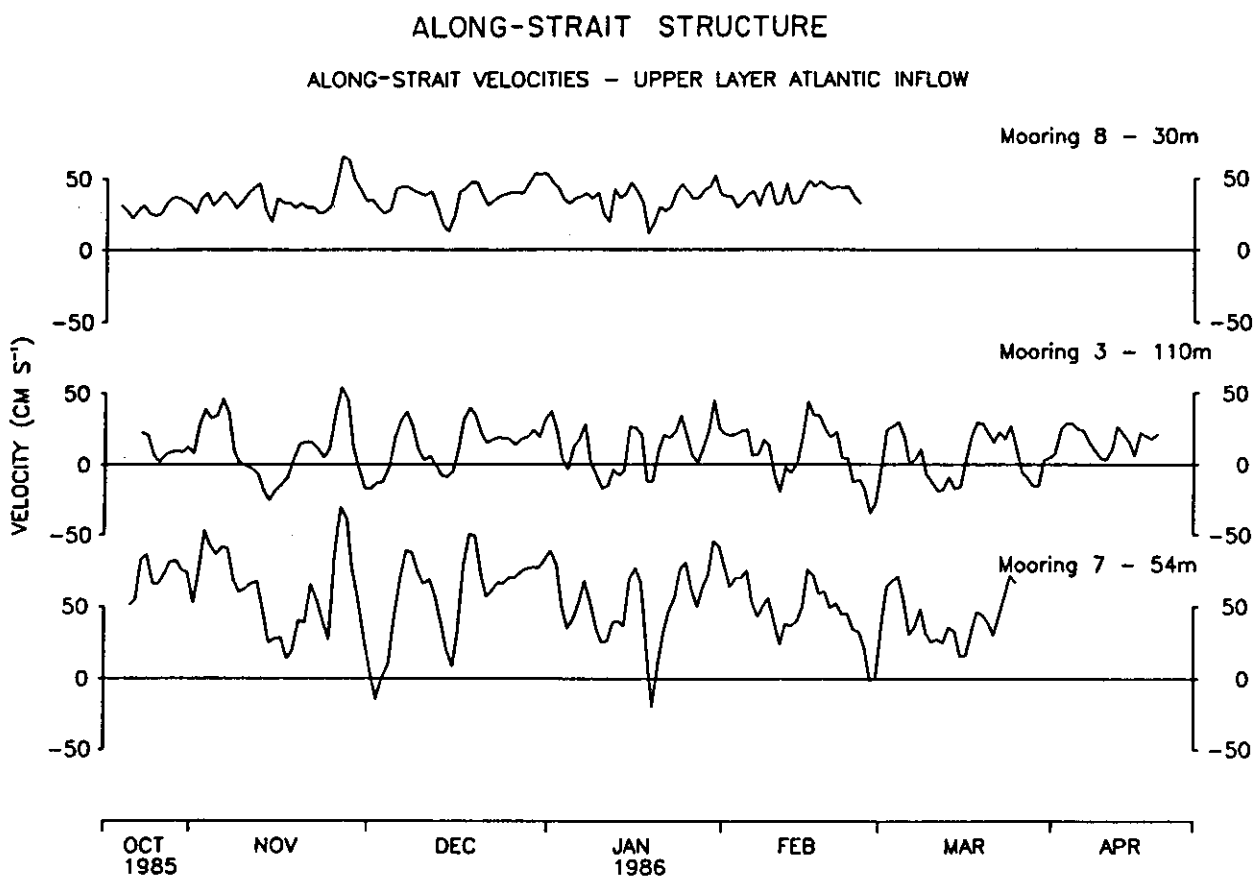

FIG.10C

The temporal variability in transports appears to have a dominant period of about 15 days. In particular, there are peaks in the autocorrelation function for the outflow transport at lags of 15, 36 and 49 days. Also, autospectra of inflow transport and outflow transport estimates using mooring 1 and 3 for the period October to April and using mooring 2B for the period May to August exhibit a band of high energy at periods of 15 to 22 days. Square-integral time scales (integral of the square of the autocorrelation function) are estimated to be 2.9 days for ULT and 4.8 days for LLT. With these integral time scales and with the estimated standard deviations in ULT and LLT over the 259-day period of measurements, the standard error due to the low-frequency temporal variability in the mean inflow is 0.04Sv and the standard error in the mean outflow is 0.03Sv. While these standard errors are small, it is important to remember that there is larger real uncertainty in the mean transport estimates due to spatial sampling problems, particularly due to the lack of adequate instrumentation in the upper layer above 90m depth.

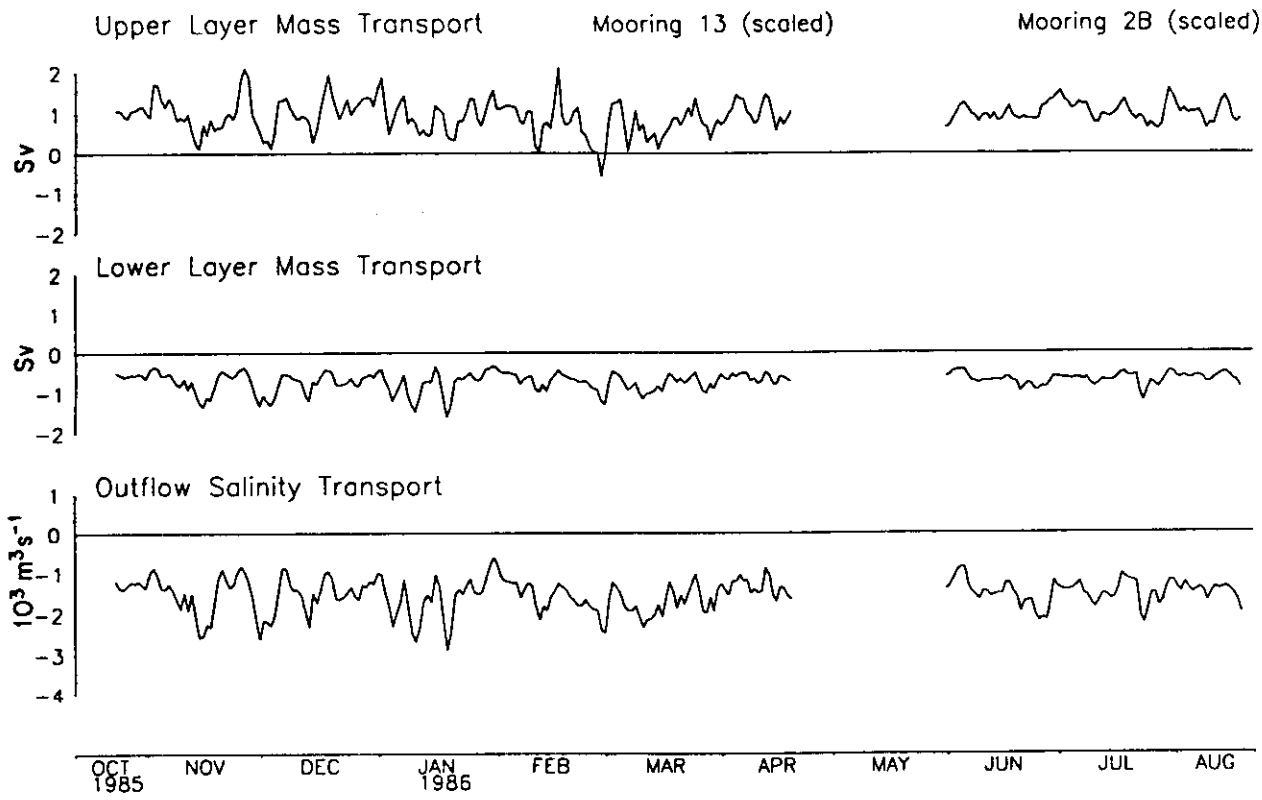

FIG.11. Time series of daily averaged upper layer mass transport, lower layer mass transport and outflow salinity transport from October 1985 to August 1986. Transports are defined as for Fig.9. Transport estimates from mooring 1 and 3 (October 1985 - April 1986) and from mooring 2B (May-August 1986) are scaled so that they are consonant with the optimal values derived from moorings 1, 2 and 3 during October-November 1985 according to the regressions in Table 7.

9. CROSS-STRAIT SLOPE OF THE INTERFACE

In the Strait of Gibraltar, there is a well known cross-strait slope to the interface between the upper inflowing Atlantic water and the lower outflowing Mediterranean water with the interface banked up against the European continental slope. These current meter measurements with accompanying salinity time series provide unprecedented information on the character of the interface and its fluctuations. Previous measurements of the interface have relied on time series hydrographic stations over one to two days to resolve the amplitude of the tidal fluctuations (e.g. LACOMBE and RICHEZ, 1982). The tidal fluctuations in the depth of the interface have already been described as part of the demonstration on how the correlation between interface depth and inflow velocity at tidal periods contributes to the exchange across the sill. Here, the time-averaged cross-strait slope of the interface and its relation to the vertical shear in along-strait currents are described.

The time-averaged depths of the 37psu isohaline during October-November 1985 are 98.7 at

mooring 1 on the northern side of the sill section, 135m at mooring 2 on the sill and 134.0 at mooring 3 on the southern side. From these averages and from the bathymetry of the sill cross-section as described by BRYDEN and KINDER (1991b), we calculate that the upper layer flow above the 37psu isohaline occupies on average 2.01 x $10^6 m^2$, or 64% of the total sill cross-sectional area of 3.16 x $10^6 m^2$, while the lower layer flow occupies 1.15 x $10^6 m^2$ or 36% of the sill area. Dividing the mean upper and lower layer transports by these areas yields area-averaged, or 'typical', velocities of 36cm s^{-1} for the inflowing Atlantic water and -59cm s^{-1} for the outflowing Mediterranean water.

For the longer 6-month period from October to April when moorings 1 and 3 recorded data, the time-averaged depths of the 37psu isohaline are slightly shallower: 82.3m at mooring 1 and 123.9m at mooring 3. For this longer period, the average cross-strait slope of the interface is 4.6 x 10^{-3}, or a 42m change in depth across the 9km distance between moorings 1 and 3. Geostrophically, this cross-strait slope of the interface should be balanced by the vertical shear in the along-strait currents between inflow above and outflow below. In modelling the flow through the Strait of Gibraltar as a two-layer exchange (e.g. BORMANS and GARRETT, 1989a), a reduced gravity model is generally used with the geostrophic balance in the form:

$$g' h_y = f(u_1 - u_2) \qquad (14)$$

where $g' = g(\rho_2 - \rho_1)/\rho_2$, ρ is the density, h_y is the cross-strait slope of the interface, f is the Coriolis parameter, u is the along-strait velocity, 1 denotes the upper layer and 2 denotes the lower layer. For the observed interface slope and the difference between the 'typical' upper and lower layer velocities, we calculate a g' equal to 1.77cm s^{-2} and a density difference of 1.86 x 10^{-3}gm cm^{-3} between the upper Atlantic water and lower Mediterranean water. Such a density difference is similar to the observed density difference between Mediterranean water and Atlantic water as used in two-layer models (e.g. FARMER and ARMI, 1986).

More direct geostrophic comparisons can be carried out by comparing the time-averaged cross-strait density difference between moorings 1 and 3 on the northern and southern sides of the sill section with the vertical differences in along-strait velocity at moorings 2 and 2B in the central sill region (Table 8). Density differences are best estimated for the depth interval between 140 and 180m where each of moorings 1 and 3 had three current meters (Table 2). The observed cross-strait density gradients of 0.4 to 0.8 x 10^{-9}g cm^{-4} imply geostrophically vertical shears in along-strait velocity of 0.4 to 0.9 x $10^{-2} s^{-1}$ (Table 8a). These vertical shears are then integrated using the trapezoidal rule for the depth intervals between the current meters on moorings 2 and 2B, where the observed vertical differences in velocity of order 20cm s^{-1} over approximately 30m depth seem well matched to the geostrophically predicted velocity differences (Table 8b). While these comparisons are favourable, there are several cautionary aspects that prevent precise conclusions. First, the observed vertical shears in velocity at mooring 1 are much smaller than those at moorings 2, 2B and 3, indicating cross-strait variability in the vertical shears. Also, the comparisons in Table 8 represent point estimates of the vertical shear, but cross-strait averages of the geostrophic shear. Furthermore, the geostrophic estimates are based on time-averaged density differences over the period from October to April, while the observed velocity difference at mooring 2 is an average over the October-November time period and the differences at mooring 2B are averages over the May-August time period. Hence the observed and predicted velocity differences are for different time periods. Despite these cautionary notes, there is reasonable agreement between the observed and geostrophically predicted velocity differences which are each of order 20cm s^{-1} over a 30m depth interval in the interface region at the Gibraltar sill.

A second type of geostrophic comparison is to correlate the temporal fluctuations in the daily averaged vertical shear of along-strait current at moorings 1 and 3 and the daily-averaged cross-

strait difference in interface depth between moorings 1 and 3 for the six-month time period from October to April. The time series of the vertical shear at mooring 3 and of the difference in depth of the 37.5psu isohaline (Fig.12) are significantly correlated with a correlation coefficient of 0.55. (The 37.5psu isohaline is chosen here to represent the interface because it is better resolved by the distribution of instruments on mooring 1.) The vertical shear at mooring 1, however, is smaller than, and negatively correlated (although not significantly) with, either the shear at mooring 3 or the interface depth difference time series. It may be that during periods of large interface slope the Atlantic water inflow becomes effectively separated from the northern boundary so that the shear at mooring 1 reflects the smaller shear within the Mediterranean water rather than the stronger shear between Atlantic and Mediterranean waters. For the central and southern parts of the sill, the correlation between the observed shear and the slope of the interface on low-frequency time scales has the sign expected from geostrophic arguments such that larger interface slopes are correlated with stronger vertical shears in the along-strait currents. The standard deviation of the interface slope is 55% as large as the mean slope, and the standard deviation of the vertical shear on mooring 3 is 48% as large as the mean shear. Thus the interface slope and vertical shear exhibit low-frequency fluctuations that are about half as large as the mean slope and mean shear. This low-frequency variability appears to be dominated by fortnightly fluctuations, as will be shown next.

TABLE 8. Thermal wind shear and geostrophic comparison. (a) The cross-strait density gradient, $\partial\rho/\partial y$, determined from temperature, salinity and pressure time series on moorings 1 and 3 is evaluated at 140, 160 and 180dbar and the implied thermal wind shear in along-strait velocity, $\partial u/\partial z$ is estimated. (b) Geostrophic comparisons are carried out between the observed current differences on moorings 2 and 2B and the geostrophically predicted current differences from the thermal wind shears in (a) for the specific depth intervals of the instruments.

(a) Cross-strait density gradient and thermal wind shear in inflow-outflow velocity

	Mooring 1		Mooring 3		$\frac{\partial\bar{\rho}}{\partial y} = \frac{\Delta\sigma_\theta(1\text{-}3)}{8.99\text{km}}$	$x\, g/\rho_o f(=1.11$ $x10^7 cm^4 g^{-1} s^{-1})$	$\frac{\partial\bar{u}}{\partial z}$
Pressure	$\bar{S}$(psu)	$\bar{\sigma}_\theta(10^{-3}gcm^{-3})$	S(psu)	$\sigma_\theta(10^{-3}gcm^{-3})$	$(x10^{-9}gcm^{-4})$		$(x10^{-2}s^{-1})$
140dbar	37.906	28.563	37.178	27.802	.847		.943
160dbar	37.986	28.634	37.457	28.098	.596		.664
180dbar	38.046	28.747	37.743	28.400	.387		.431
					Cross-Strait Density Gradient		Vertical Shear

(b) Geostrophic comparison

	Time-Averaged along-strait velocity difference $\Delta u(cm\ s^{-1})$	
	Observed	Geostrophically predicted
Mooring 2		
127-158 dbar	19.5	26.5
Mooring 2B		
123-153 dbar	22.8	27.5
153-191 dbar	24.5	20.6
123-191 dbar	47.3	48.1

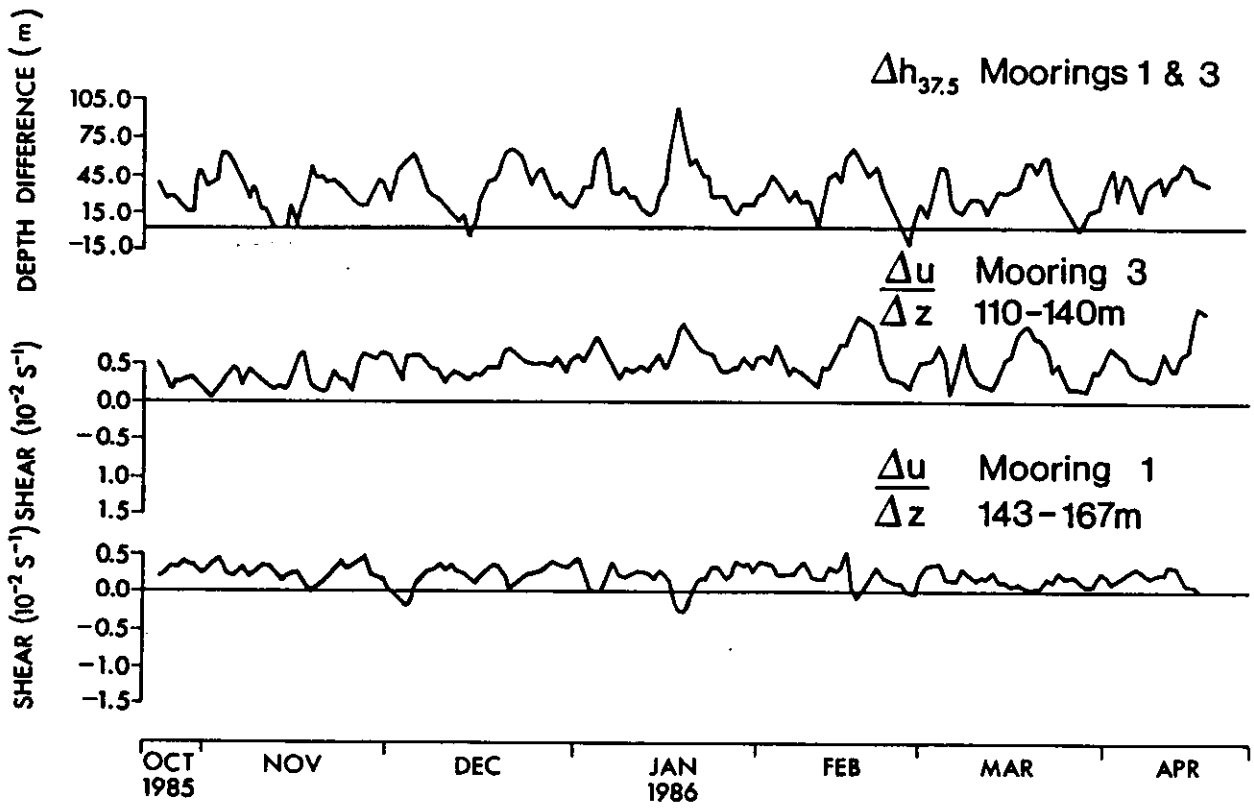

FIG.12. Comparison of the daily-averaged cross-strait difference in depth of the 37.5psu isohaline between moorings 1 and 3, $\Delta h_{37.5}$, and the observed vertical shears in along-strait currents on moorings 3 and 1. The thermal wind relation implies that the series should be correlated for geostrophic fluctuations. There is good correlation of the interface depth difference with vertical shear on mooring 3 but poor correlation with shear on mooring 1.

10. FORTNIGHTLY VARIATIONS

A common question is whether there are fluctuations in the exchange across a sill at fortnightly period. Any observed fortnightly signal in the exchange might then be related to the spring-neap cycle in semidiurnal tidal forcing. For example, GEYER and CANNON (1982) observed a maximum exchange across the sill in Puget Sound near neap tides and argued that it was due to less tidal mixing during the neap period of smaller amplitude tidal currents. Here in the Strait of Gibraltar, the regular oscillations in outflow transport at about 15-day period (Fig.11) are suggestive of a fortnightly cycle. Indeed, tidal analyses of the 180-day time series of ULT and LLT derived from moorings 1 and 3 yield fortnightly amplitudes of 0.103 Sv in the inflow transport and of 0.083 Sv in the outflow transport with phases relative to Greenwich of 257° and 227° respectively. These phases imply that positive transports (directed eastward toward the Mediterranean) occur in both the upper layer and lower layer 2 to 3 days after the time when the sun and moon are 90° out of phase. Thus, there is maximum inflow of Atlantic water but minimum outflow of Mediterranean water just after neap tides, while there is minimum inflow and maximum outflow just after spring tides.

These fortnightly variations in transport are associated primarily with fluctuations in along-strait currents in the central and southern parts of the sill. From the long records above 200m depth on the sill at mooring 2B and on the southern side of the sill section at mooring 3, the amplitudes of the fortnightly current signals increase vertically from 5 to 20cm s^{-1} with phases of 220° to 310° and with larger amplitudes at shallower depths (Table 9). In contrast, at mooring 1 on the northern side of the sill section the fortnightly current variations are less than 5cm s^{-1}. The depth of the interface between upper layer Atlantic water inflow and lower layer Mediterranean water outflow similarly exhibits a fortnightly cycle in the central and southern regions but effectively no fortnightly cycle in the northern part of the sill at mooring 1 (Fig.13). The amplitude of the fortnightly signal in interface depth is 19.5m at mooring 3, 15.3m at mooring 2B, and 1.5m at mooring 1, with phases of 220°, 228° and 233° respectively; that is, the interface is deeper just after neap tides when the inflowing along-strait currents achieve maximum amplitude. Similar to the analysis of semidiurnal tidal fluxes presented above, this coherence between maximum inflow and deepest interface over the fortnightly cycle in the central and southern regions effectively contributes both a mean inflow and a mean outflow to the total exchange across the sill. In contrast to the semidiurnal tidal fluxes, however, this fortnightly cycle in exchange is small, of order 0.003Sv, due to the combination of relatively small interface and current signals and the confinement of the fortnightly signals to the central and southern portions of the sill. The major fortnightly cycle in the Strait is a nearly unidirectional current fluctuation of order 10cm s^{-1} at all depths that is directed into the Mediterranean just after neap tides.

TABLE 9. Amplitude and phase of the fortnightly (M_{sf}) cycles in upper layer transport (ULT), lower layer transport (LLT), interface depths from the long records on moorings 1, 2B and 3, cross-strait difference in interface depth between moorings 1 and 3 (h_1-h_3), and currents for the long records on moorings 1, 2B and 3.

		Amplitude		Phase	
Transport		(Sv)			
ULT		.103	±.065	256°	±37°
LLT		.083	±.049	227°	±34°
Interface Depth		(m)			
h_1		1.5	±4.4	233°	±175°
h_{2B}		15.3	±3.1	228°	±12°
h_3		19.5	±3.5	220°	±10°
h_1-h_3		18.3	±3.1	217°	±10°
Current		(cm s^{-1})			
Mooring 1	U_{140}	4.3	±2.9	7°	±39°
	U_{156}	4.3	±2.4	13°	±33°
	U_{167}	3.9	±1.4	13°	±30°
	U_{215}	2.1	±1.2	20°	±33°
Mooring 2B	U_{90}	15.0	±5.3	234°	±20°
	U_{112}	18.0	±3.9	245°	±12°
	U_{135}	14.3	±3.3	270°	±13°
	U_{181}	9.7	±2.3	306°	±18°
	U_{233}	7.2	±2.5	353°	±18°
	U_{299}	5.0	±2.7	87°	±34°
Mooring 3	U_{110}	16.8	±2.9	222°	±10°
	U_{140}	11.4	±2.8	223°	±14°
	U_{180}	5.0	±2.1	230°	±25°

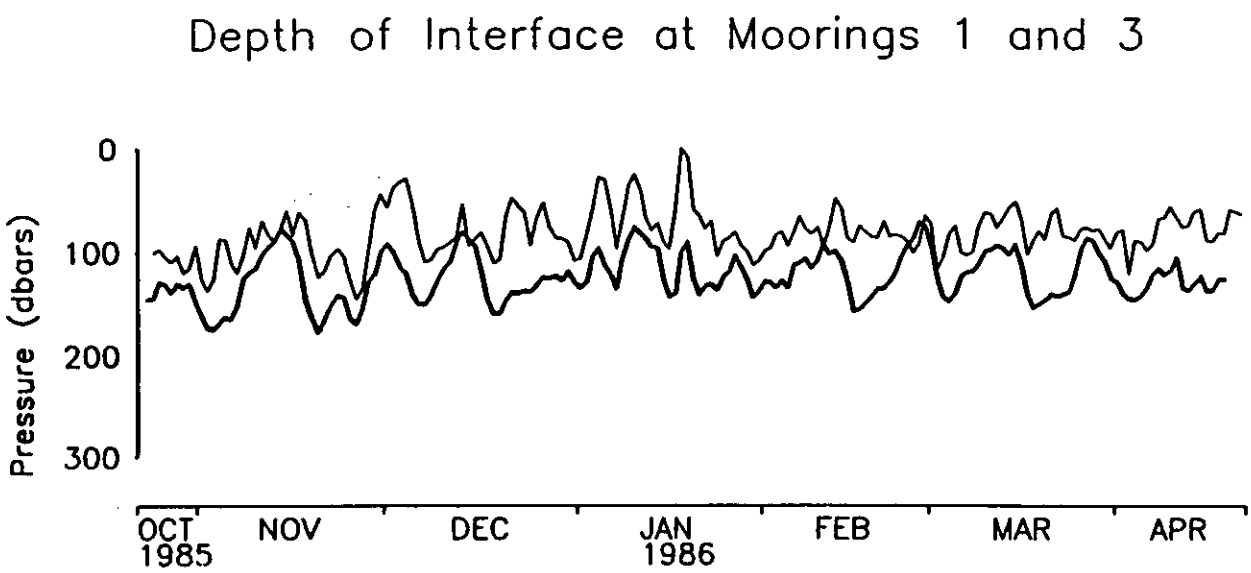

FIG. 13. Daily averaged depths of the interface defined by the 37psu isohaline on mooring 1 and on mooring 3. Note the greater depth of the interface on mooring 3 on the southern side of the sill section and the strong oscillations in mooring 3 interface depth with a period of about 14 days.

Because the fortnightly cycle in interface depth in the central and southern regions of the sill is not matched by a fortnightly cycle in interface depth in the northern region of the sill, there is a distinct fortnightly variation in the slope of the interface across the sill section. Since the interface slopes downward toward the south in the mean, the slope is largest just after neap tides. Tidal analysis of the difference between the depths of the 37psu isohaline at mooring 3 and at mooring 1 indicates that the fortnightly amplitude of the interface depth difference is 18.3m, nearly all of it due to the fortnightly cycle of amplitude 19.5m at mooring 3. Since the mean depths of the 37psu isohaline are 82.3m at mooring 1 and 123.9m at mooring 3, the fortnightly cycle in interface slope has an amplitude that is 44% of the time-averaged slope. These fortnightly variations in interface slope across the sill seciton, which are correlated with the variations in vertical shear in along-strait currents (Fig. 12), account for about 70% of the total low-frequency variability in interface slope.

It is common to try to relate this fortnightly cycle in interface slope to a fortnightly signal in exchange, defined to be the difference ULT-LLT or the sum of the inflow and the outflow. In this vein, stronger interface slopes are often taken to indicate both stronger eastward inflow and stronger westward outflow leading to larger values of the exchange. At the Gibraltar sill, however, the available current meter records indicate that the increased shear at neap tides is the result of added eastward or inflow velocity at all depths at neap tides, with the added inflow being larger at shallower depths. Thus, the observed fortnightly cycle in shear does not appear to relate to stronger exchange, i.e. stronger inflow and stronger outflow. In fact, the fortnightly signal in the exchange, ULT-LLT, is only 0.003Sv, much smaller than the fortnightly cycle in either inflow or outflow. Rather, the observed fortnightly cycle in shear represents stronger inflow in the surface layer and weaker outflow in the lower layer near neap tides.

In conclusion, there is a fortnightly cycle in observed along-strait currents with stronger eastward flow at all depths near neap tides so that the upper layer transport achieves a maximum eastward inflow and the lower layer transport achieves a minimum westward outflow just after neap tides. The amplitudes of the fortnightly cycles in upper layer transport and lower layer transport are about 12% as large as the mean inflow and outflow. There is also a fortnightly cycle in the slope of the interface across the Strait of Gibraltar with stronger slopes occurring near neap tides. The stronger interface slopes do accompany stronger vertical shears in along-strait currents, but the current shears are due to larger fortnightly amplitudes in observed currents at shallower depths. Thus, there appears to be little fortnightly cycle in the size of the exchange across the sill despite the substantial fortnightly cycle in interface slope.

11. ANNUAL SIGNALS

With data sets that are a little less than a year in duration, it is risky to estimate the size of the annual cycle for any variable. There is, however, much interest in whether or not the exchange through the Strait of Gibraltar exhibits changes through the year. The interest principally derives from work by GARRETT and collaborators who first showed that the sea level difference across the Strait, and hence by dynamical implication the geostrophic surface inflow, exhibits a seasonal cycle such that inflow currents are strongest in the spring (BORMANS, GARRETT and THOMPSON, 1986). Further stimulation for determining annual cycles is provided by GARRETT, BORMANS and THOMPSON's (1990) argument that the nature of the exchange across the sill switches from maximal to submaximal during the course of a year. They suggest that the flow is maximal for the period after February-March when the Mediterranean reservoir of intermediate and deep water has just refilled due to wintertime water formation, but that the flow switches to a submaximal state later in the year after the supply of newly formed water has drained out over the sill. To provide more grist for Garrett's mill, we make the following estimates of the annual cycles in inflow, outflow and interface depth from the time series measurements on the sill during the period from October 1985 to October 1986.

The scaled upper and lower layer transports for the period October 1985 to August 1986 (Fig.11) and the depth of the interface at mooring 3 for the period October 1985 to April 1986 (Fig.14) are least square fitted to sine and cosine functions, $A \sin \omega t + B \cos \omega t$ where ω is the annual frequency and t is year-day, to determine the coefficients A and B. While the time series for the depth of the interface could have been extended using the interface depth from mooring 2B, we decided that, because moorings 3 and 2B were deployed at different locations on the sill section, there could be a discrete jump in the mean depth of the interface between the two series. The alternative of removing the means separately for each of the two pieces would also compromise any estimate of the annual signal since there would then be zero difference between the 6 month period when mooring 3 was deployed and for the following 5 month period when mooring 2B was deployed, thereby suppressing any real annual signal. Hence, we use only the 6-month time series of interface depth at mooring 3 in fitting the annual cycle. Because of the scaling described above to make the upper and lower layer transports consistent for the measurement periods of moorings 1 and 3 and of mooring 2B, the complete transport time series are used. The least squares estimates of A and B are then transformed into estimates of amplitude and phase for each annual signal.

The upper layer transport exhibits an annual cycle with an amplitude of 0.12Sv and a phase such that maximum inflow occurs on year-day 261 (18 September). The lower layer transport has an annual cycle amplitude of 0.03Sv and maximum outflow occurs on year-day 23 (23 January). The depth of the interface has an annual cycle amplitude of 18m and minimum depth is achieved on year-

day 40 (9 February). With less than a year of data, estimates of error bars on these amplitudes and phases would be meaningless. Thus, the yearly cycle in outflow appears to be small. The inflow, which is poorly resolved due to the lack of instruments in the upper layer, has a larger signal but its maximum is in September, nearly 180° out of phase with the maximum surface currents inferred by BORMANS, GARRETT and THOMPSON (1986) from long-term sea level measurements. The annual cycle in interface depth appears to be the most robust of these estimates: one can almost 'see' the February minimum above the low-frequency variability in the year-long time series that includes mooring 2B (Fig.14); and minimum depth in mid winter corresponds with GARRETT, BORMANS and THOMPSON's (1990) arguments for a wintertime shallowing of the interface due to wintertime renewal of the Mediterranean reservoir. In summary, these estimates of annual cycles in inflow, outflow and interface depth indicate that maximum outflow, minimum inflow and shallowest interface depth occur in mid to late winter, between 23 January and 18 March. But it is important to remember that these estimates are based on only one year of measurements and hence have great uncertainty.

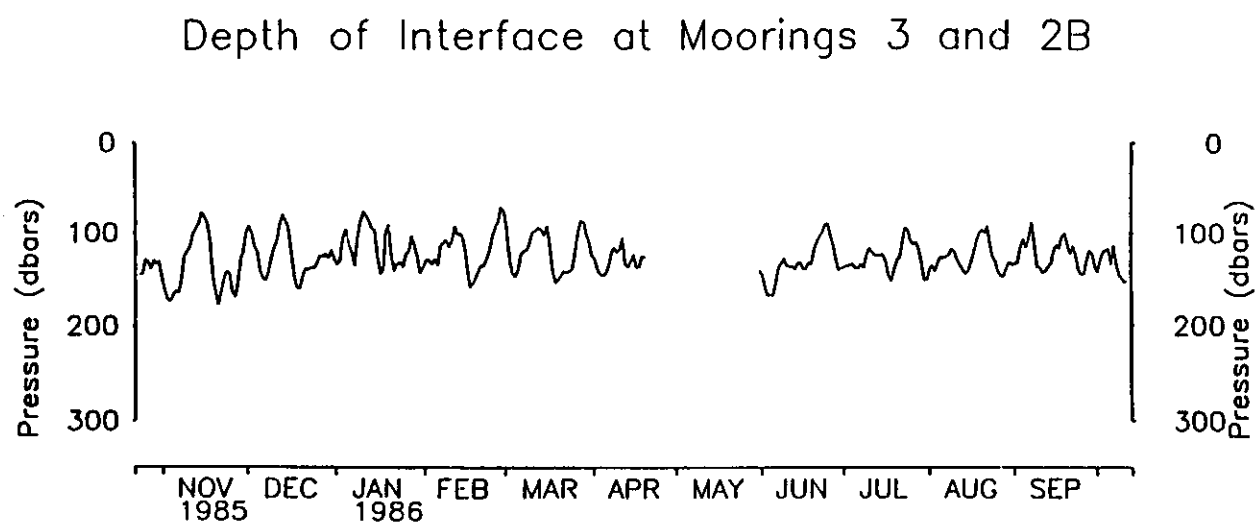

FIG.14. Daily averaged depth of the interface defined by the 37psu isohaline on mooring 3 from October 1985 to April 1986 and on mooring 2B from May to October 1986.

12. DISCUSSION

It is difficult to overemphasize the importance of time series salinity measurements for defining the exchange across the Gibraltar sill. At the outset of this analysis, we were naive enough to think that the mean exchange could be determined simply by time-averaging the current meter measurements and integrating the average currents vertically and horizontally across the strait. Such a procedure produced our first estimate of the outflow over the sill of only 0.38Sv, a factor of 3 smaller than LACOMBE and RICHEZ's (1982) standard value of 1.2Sv and a factor of 2 smaller than the time-averaged outflow of Mediterranean water found here. Without salinity time series, we would be forced to accept this low value for the outflow. The shock of such a low outflow transport, however, forced a reconsideration of what is meant by outflow and by exchange; and the importance of the salinity measurements for defining the water mass characteristics of the flow at every instant of time became clear.

The salinity measurements allow us to estimate the relative contributions of the mean currents and of the time-varying (principally tidal) fluctuations in effecting the exchange across the sill in a statistical sense. In fact, the fluctuations account for half of the total exchange due to the correlation between strong outflow and high salinity at every instrument. Secondly, the salinity measurements enable us to determine continuously the depth of various isohalines, to define a particular isohaline, the 37psu isohaline, as the interface between Atlantic and Mediterranean waters, and then to understand the mechanism of the time dependent exchange process in which strong outflow is associated with shallow interface over the tidal cycle so that a large bolus of Mediterranean water crosses the sill on the outflowing tide while a large bolus of Atlantic water crosses the sill on the inflowing tide. Thirdly, the definition of the interface as a water mass boundary allows the development of time series for the upper layer transport of Atlantic water and for the lower layer transport of Mediterranean water so that the tidal and low-frequency fluctuations in the inflow and outflow can be assessed. Finally, the salinity measurements allow a determination of the outflow salinity transport which is essentially a direct estimate of the net evaporation over the Mediterranean basin.

The estimate of net evaporation over the Mediterranean basin of 52cm y^{-1} derived from these measurements at the Gibraltar sill appears to be inherently more accurate than previous estimates of net evaporation, that have ranged from 47 to 131cm y^{-1} (Table 1), derived from bulk formula, rainfall determined from coastal stations, and river runoff. Bulk formula methods are notorious for the arguments over their uncertainties and biases. Rainfall is hopeless to measure at sea with all the spray, and coastal station rainfall measurement is subject to local topographic effects. In contrast, the measurements of current and salinity at the Gibraltar sill effectively provide a spatial integration of the air-sea fluxes over the entire Mediterranean basin. BUNKER, CHARNOCK and GOLDSMITH (1982) were the first to utilise the Gibraltar exchange to constrain traditional bulk formula parameterizations of air-sea exchange over the Mediterranean basin. GARRETT, OUTERBRIDGE and THOMPSON (1993) have recently re-examined the bulk formula estimates of air-sea heat and freshwater exchange in the light of the new direct estimates of net evaporation of 52cm y^{-1} reported here and of net heat gain of about 5Wm^{-2} carried out with these same measurements by MACDONALD, CANDELA and BRYDEN (1994) to identify where traditional parameterizations are in error. They conclude that the measured exchanges across the Gibraltar sill indicate that bulk formula estimates of evaporation are accurate so that the problem in net heat flux from bulk formula must lie with incoming radiation values that are too high. HARZALLAH, CADET and CREPON (1993) have recently used a global atmospheric model to determine the divergence in water vapour flux over the Mediterranean basin. Their resulting estimate for the freshwater flow through the Strait of Gibraltar of 30 x $10^6 m^3 s^{-1}$ is equivalent to a net evaporation of only 37cm y^{-1} or to an outflow salinity transport of only 1.1 x $10^3 m^3 s^{-1}$, but there may be substantial uncertainties in the atmospheric freshwater balance due to the coarse resolution of the Mediterranean basin in the global model. Thus, the measurements of exchange across the Gibraltar sill provide values for the net air-sea heat exchange and for net evaporation over the Mediterranean basin that are more accurate than traditional bulk formula estimates or those based on atmospheric flux divergence; and the heat and freshwater transports across the Gibraltar sill may in fact be useful for diagnosing problems in the alternative methods.

The observed outflow and inflow transports across the Gibraltar sill reported here of 0.7Sv are smaller than the values of about 1.2Sv reported by LACOMBE and RICHEZ (1982). We would not attribute the difference to long-term variability without carefully considering other differences. LACOMBE and RICHEZ's estimates were based on daily averaged currents measured by lowering current meters from a ship anchored at station A4, west of the sill, and there were no salinity values

attached to the currents. West of the sill, the outflowing Mediterranean water quickly loses its high salinity signature (PRICE, O'NEIL-BARINGER, LUECK, JOHNSON, AMBAR, PARRILLA, CANTOS, KENNELLY and SANFORD (1993) and its transport must increase accordingly so that the outflow salinity transport remains constant. If the effective salinity contrast between Mediterranean and Atlantic waters at A4 were only 1.3psu rather than the 2.2psu found here at the sill, the two sets of transport would be essentially equivalent. In fact, RICHEZ and GASCARD (personal communication) did estimate the average salinities for the inflow and outflow over 12 tidal cycles during May and June 1961 to determine that the salinity difference at A4 between the inflow and outflow was 1.56psu ($S_M = 37.81$, $S_A = 36.25$) but this was during a period of strong outflow ($Q_M = 1.33$Sv) so that their outflow salinity transport still matched the $2.0 \times 10^3 m^3 s^{-1}$ value in LACOMBE and RICHEZ (1982). Thus, we would ascribe much of the difference between the new transports of 0.7Sv and LACOMBE and RICHEZ's transports of 1.2Sv as being due to different salinities in the measured outflows as a result of mixing west of the sill. For future Gibraltar measurement or monitoring programmes, it is essential to determine not only the outflow but also the effective salinity of the outflow in order to assess long-term changes in the exchange.

It is useful to compare the observed exchange with the theoretically predicted maximum exchange from hydraulic control modelling (Table 10). In summarizing the developments of hydraulic control models applied to the Strait of Gibraltar, BRYDEN and KINDER (1991b) tabulated the theoretically predicted inflow, outflow and salinity difference as a function of ent evaporation over the Mediterranean basin. From the above analysis of the Gibraltar measurements, there are two primary estimates of the observed exchange: the outflow of Mediterranean water of -0.68Sv and the outflow salinity transport of $-1.50 \times 10^3 m^3 s^{-1}$, that is equivalent to a net evaporation of 52cm y^{-1}. The analysis also provides secondary estimates of the inflow, equal to the outflow plus the evaporation, of 0.72Sv, and of the salinity difference of 2.20psu determined by dividing the outflow salinity transport by the outflow transport. Interpolation of BRYDEN and KINDER's (1991b) tabulated predictions to a net evaporation of 52cm y^{-1} yields a predicted outflow of -0.84Sv, a predicted inflow of 0.88Sv and a predicted salinity difference of 1.80psu. Thus, the observed flows are about 20% smaller than the theoretically predicted maximum exchange through the Strait of Gibraltar.

At first, agreement between the observed exchange and the theoretically predicted exchange within 20% may seem reasonably successful. Furthermore, the observed exchange is satisfyingly less than the predicted maximum exchange, perhaps lending support to GARRETT, BORMANS and THOMPSON's (1990) argument that the Gibraltar exchange is sometimes submaximal. There is, however, a marked difference beween the modes of exchange in the models and in the observations. In the models, the two-layer flow is steady and it achieves critical composite Froude number of 1 at the sill and at the narrowest section. As noted by FARMER and ARMI (1986), the lower layer outflow essentially achieves critical Froude number at the sill in the hydraulic control models. In the observations, only half of the total exchange is carried by the time-averaged flows and the remaining half is effected by the tidal fluctuations. Froude number calculations reveal that the Froude number for the 'typical' time-averaged flows at the sill is about 0.25, substantially subcritical. For the instantaneous tidal currents, the Froude number at the sill is generally subcritical but achieves supercritical values about 10% of the time, mostly on the outflowing tide (Fig.15). Surprisingly, despite strong outflow velocities on the outflowing tide, the lower layer Froude number is nearly always less than 1 because the interface rises on the outflowing tide making the lower layer very thick so that $U_2^2/g'h_2$ remains less than 1. Surprisingly then, the supercritical Froude numbers on the outflowing tide are principally due to the thinness of the upper layer flow, so that $U_1^2/g'h_1$ is greater than 1.

TABLE 10. Comparison between observed and predicted exchanges. The observed outflow salinity transport of $-1.50 \times 10^3 m^3 s^{-1}$ divided by the Atlantic water salinity of 36.1 psu and by the surface area of the Mediterranean basin of $2.52 \times 10^{12} m^2$ provides the value for the observed net evaporation of 52cm y^{-1}. The predicted outflow, inflow and salinity difference are derived by interpolation of BRYDEN and KINDER's (1991b) Table 1 for the maximal exchange as a function of net evaporation to a value for the net evaporation of 52cm y^{-1}.

	Net Evaporation $e(cm\,y^{-1})$	Outflow $Q_M(x10^6 m^3 s^{-1})$	Inflow $Q_A(x10^6 m^3 s^{-1})$	Salinity Difference $\Delta S(psu)$
Observed	52	-.68	.72	2.20
Predicted for e =	52	-.84	.88	1.80

Such difference in the modes of exchange between the models and observations suggests that the models must incorporate time-dependent processes in order to properly predict the exchange across the Gibraltar sill. FARMER and ARMI (1986) modelled the time-dependent problem as a succession of steady states with varying barotropic net flow to represent the tidal currents. They argued that steady-state conditions would be valid if the time it takes for an interfacial wave to travel between the control points at the sill and the narrowest section were less than a quarter tidal period, a condition not really valid for the Gibraltar situation where interfacial wave typically take 6 hours to travel from the sill to the narrowest section (WATSON and ROBINSON, 1990). Averaging over the series of steady states, FARMER and ARMI (1986) noted that the exchange always increases due to the fluctuations and the exchange more than doubles for tidal current amplitudes as large as the steady maximal exchange flows.

Recently, HELFRICH (1994) has combined theoretical and laboratory models to solve the time dependent exchange through a strait as a function of the tidal forcing and of the length of the strait. There are only two nondimensional parameters: the ratio of the tidal flow to the steady maximal exchange; and the ratio of the period of the tidal forcing to the time it takes an interfacial wave to propagate between the two control points at the sill and manowest section. He shows that the time dependent exchange for parameters applicable to the Strait of Gibraltar is substantially less than the doubling determined by FARMER and ARMI (1986), who effectively assumed the second parameter to be infinite. For Gibraltar parameters, HELFRICH (1994) suggests that the exchange predicted by the time-dependent model should be approximately 20% more than the steady, maximal exchange; but he also notes that mixing in the interfacial region between the inflow and outflow reduces the time-dependent exchange of pure Atlantic and Mediterranean waters by about 20%. Thus, the theoretically predicted exchange for a hydraulic control model including realistic tidal forcing and interfacial mixing is within 5% of the steady maximal exchange, yielding an outflow of Mediterranean water of 0.80Sv which is still about 15% larger than the measured outflow of 0.68Sv. Friction and rotation which are still not included in the model may yet account for the difference between the measured and predicted exchanges.

In terms of designing an observational strategy for long-term measurements of the exchange through the Strait of Gibraltar, the above analysis indicates that a single mooring at the sill with 4 to 8 current meters combining current, temperature, conductivity and pressure measurements can monitor the outflow of Mediterranean water and the outflow salinity transport, two basic measures of the exchange. On the other hand, monitoring the upper layer inflow is more difficult. With present current measuring technology, it is not clear how to measure directly the inflow, as surface moorings are unlikely to survive the high currents and high density shipping and fishing activities in the Strait and bottom-mounted, upward-looking Doppler current profilers cannot yet measure remotely the salinity of the flows.

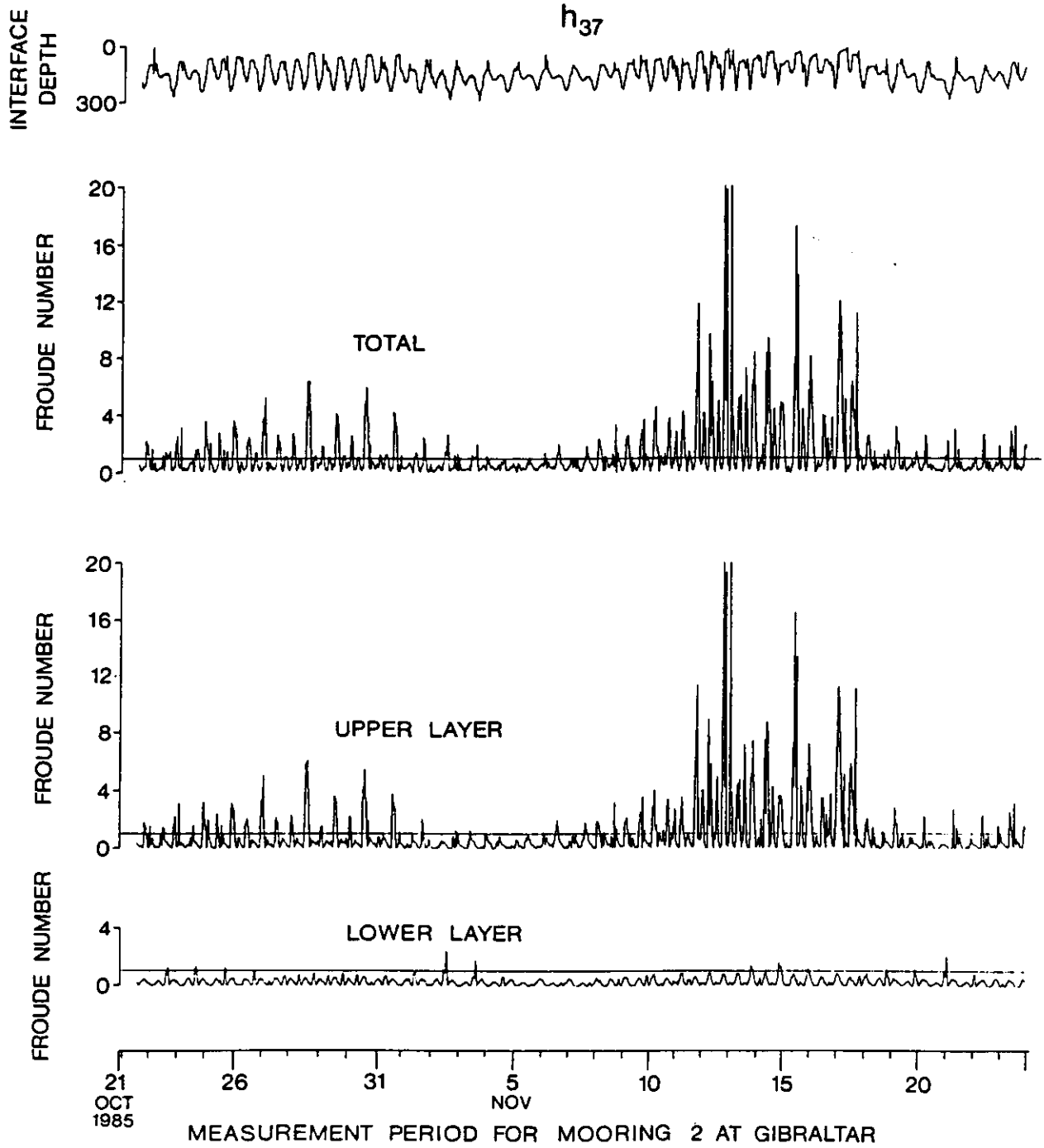

FIG.15. Froude numbers for the flow on mooring 2 at the Gibraltar sill during October-November 1985. The upper and lower layer Froude numbers are defined to be $U_1^2/g'H_1$ and $U_2^2/g'H_2$ where H_1 is the depth for the 37psu isohaline, H_2=284-H_1, U_1 is the along-strait velocity at depth = H_1+284/2, and g' is taken to be 2cm s^{-2}. Note that the lower layer Froude number is nearly always less than the critical value of 1 and that the upper layer Froude number reaches supercritical values above 1 for a short period on nearly every tidal cycle except during neap tides around 5 November. The total Froude number is the sum of the upper and lower layer Froude numbers. The depth of the 37psu isohaline is shown at the top in order to illustrate that supercritical Froude numbers are achieved principally when the interface is shallow.

An added complication is the horizontal variation in the strength of the inflow currents implied by these measurements across the 30km width of the sill section at the surface. Hence, direct measurement of the upper layer inflow remains a research question that needs to be addressed with a field experiment consisting of several conventional subsurface moorings and several bottom-mounted Doppler moorings deployed across the sill section in order to use the conventional moorings to define the interface depth and salinity of the flows and the Doppler instruments to measure the currents up to the surface. Simultaneous pressure gauge or sea level measurements on the northern and southern sides of the sill section would provide time series of pressure difference across the strait that should be related geostrophically to low-frequency variations in the surface currents. Determining how such pressure difference variations combined with measured interface depth variations are related to variations in upper layer inflow transport would be an important result from such an experiment that should allow previous and future pressure difference measurements to be used to define the long-term variations in the inflow.

Thus, our choice at present for an efficient monitoring strategy for the Strait of Gibraltar would be to combine the single conventional current meter mooring at the sill measuring outflow, outflow salinity transport, and depth of the interface with shallow pressure gauges on the northern and southern sides of the sill section to provide an index on the strength of the inflow. At some time, a larger experiment should be carried out to define how this index of the inflow is related quantitatively to the inflow transport.

Eight years after the field work ended, it is worthwhile to state a summary of the progress made in achieving the three goals of the Gibraltar Experiment (BRYDEN and KINDER, 1986):

(1) to understand how the dynamical constraints for flow through a narrow and shallow strait act to control the amount of exchange between the Atlantic and Mediterranean;

(2) to measure the exchange through the Strait and its temporal variations over tidal to seasonal time scales; and

(3) to define a measurement strategy for long-term monitoring of the exchange.

First, the exciting developments in hydraulic control models of the two-layer flow through the Strait of Gibraltar by Armi and Farmer, Bormans and Garrett, Dalziel, and Helfrich have clearly increased understanding on how the physical configuration of the strait and the nonlinear dynamics of the flows do constrain the maximal exchange possible through a strait and sill region. Progress is still needed in extending hydraulic control theory to accommodate mixing, friction and rotation in a fully time dependent model of the exchange through the Strait of Gibraltar. Secondly, while the year-long measurements of the exchange had multiple technical difficulties, high quality measurements of the exchange across the sill were made for 31 days and consistent analysis allows a nine-month time series of the exchange to be developed. While these measurements do serve to quantify how important the tidal fluctuations are to effecting the exchange across the sill, longer term measurements are still needed to define the seasonal and interannual variability in the exchange. Finally, a long-term strategy is put forward to monitor cost-effectively the outflow of Mediterranean water into the Atlantic and the net evaporation over the Mediterranean basin and to provide an index for the inflow of Atlantic water into the Mediterranean. Such monitoring is essential for determining whether the exchange switches between maximal and submaximal on seasonal or interannual time scales. True monitoring of the inflow must await more extensive field measurements of the upper layer inflow to define how the variations in the inflow transport are related to measurements of pressure difference and interface depth. Thus, while there is need for future work in all three areas, substantial progress has been made on each of the broad goals set out for the Gibraltar experiment a decade ago.

13. ACKNOWLEDGEMENTS

These year-long current meter measurements in the Strait of Gibraltar were carried out through the support of the Office of Naval Research and the Instituto Hidrografico de la Marina. The Oregon State University Buoy Group under the personal direction of Dale Pillsbury had principal responsibility for the current meter operations and it is always a pleasure to acknowledge Robert Still's meticulous preparations for work at sea. Capitans José Fernandez Lopez, Celso Milleiro, and Antonio Ruiz Cañavate organised the current meter operations in Spain. Commander Mohamed Tanari helped with recovery operations in Morocco. The officers and crews aboard BIO *Malaspina* and *Tofiño* and USNS *Lynch* enthusiastically helped whenever necessary in mooring operations in the Strait. Ahmed Kribeche of the Moroccan National Society for the Study of the Strait (SNED), José Luis Almazán of the Spanish Society for the Study of the Strait of Gibraltar (SECEG) and Captain John Chubb of the Naval Oceanography Command Center, Rota, were instrumental in arranging logistical help and diplomatic permission for these measurements. We especially thank Dennis Conlon for his help in establishing the scientific and technical management of the Gibraltar Experiment and for his wisdom and flair in managing the finances for the overall Gibraltar Experiment and particularly for the current measurement programme. Succeeding Dr Conlon at the Office of Naval Research, Alan Brandt enabled the results of the Gibraltar Experiment to be published without premature pressure to switch into new programme areas.

Many people helped with the analysis of the current meter records including Gregory Johnson, Alison Macdonald, Francisco Morales, Ann Spencer and Perfecto Villanueva. In particular, Joseph Bottero developed the new processing routines for salinity time series; Juan Rico did much of the tidal analysis; and Esther Brady devised the combined temporal interpolation-vertical extrapolation procedure to determine continuously the depth of the interface. We thank Henri Lacombe and Bruce Warren for providing early references on the flows through the Strait of Gibraltar. Veta Green and Louise Fuger tirelessly prepared numerous versions of this work over the past three years. This is Contribution 8525 of Woods Hole Oceanographic Institution.

In working on these Gibraltar measurements, we not only benefited from discussions with Laurence Armi, Myriam Bormans, Nancy Bray, Stuart Dalziel, David Farmer, Christopher Garrett, Michael Gregg, Karl Helfrich, Gregorio Parrilla, Neal Pettigrew, Claude Richez, Henry Stommel, Gary Watson and Clinton Winant, but we also thoroughly enjoyed our scientific and personal interactions with them throughout the course of the Gibraltar Experiment. Let's do it again.

14. REFERENCES

ARMI, L. (1986) The hydraulics of two flowing layers with different densities. *Journal of Fluid Mechanics*, **163**, 27-58.

ARMI, L. and D.M. FARMER (1985) The internal hydraulics of the Strait of Gibraltar and associated sills and narrows. *Oceanologica Acta*, **8**, 37-46.

ARMI, L. and D.M. FARMER (1986) Maximal two-layer exchange through a contraction with barotropic net flow. *Journal of Fluid Mechanics*, **164**, 27-51.

ARMI, L. and D.M. FARMER (1988) The flow of Mediterranean Water through the Strait of Gibraltar (also: FARMER, D.M. and L. ARMI. The flow of Atlantic Water through the Strait of Gibraltar). *Progress in Oceanography*, **21**, 1-105.

BETHOUX, J.P. (1979) Budgets of the Mediterranean Sea. Their dependence on the local climate and on the characteristics of the Atlantic waters. *Oceanologica Acta*, **2**, 157-163.

BORMANS, M. and C. GARRETT (1989a) The effect of rotation on the surface inflow through the Strait of Gibraltar. *Journal of Physical Oceanography*, **19**, 1535-1542.

BORMANS, M. and C. GARRETT (1989b) The effects of nonrectangular cross section, friction, and barotropic fluctuations on the exchange through the Strait of Gibraltar. *Journal of Physical Oceanography*, **19**, 1543-1557.

BORMANS, M., C. GARRETT and K.R. THOMPSON (1986) Seasonal variability of the surface inflow through the Strait of Gibraltar. *Oceanologica Acta*, **9**, 403-414.

BRAY, N.A. (1986) Gibraltar Experiment CTD Data Report: March-April 1986, USNS *Lynch*. Scripps Institution of Oceanography References Series 86-21, 212pp.

BRYDEN, H.L. (1993) Sill exchange to and from enclosed seas. *Symposium, "Mediterranean Sea 2000", September 1991*. N.F.R. DELLA CROCE, editor, Istituto Scienze Ambientali Marine, Santa Margherita Ligure, 17-36.

BRYDEN, H.L. and T.H. KINDER (1986) Gibraltar Experiment. A plan for dynamic and kinematic investigations of Strait mixing, exchange and turbulence. *Woods Hole Oceanographic Institution Technical Report* **WHOI-86-29**, 83pp.

BRYDEN, H.L. and T.H. KINDER (1991a) Recent progress in strait dynamics. *Reviews of Geophysics*, Supplement, 617-631.

BRYDEN, H.L. and T.H. KINDER (1991b) Steady two-layer exchange through the Strait of Gibraltar. *Deep-Sea Research*, **38** (Supplement 1), S445-S463.

BRYDEN, H.L. and R.D. PILLSBURY (1990) Measurement of flow through the Strait of Gibraltar. *Advances in Water Resources*, **12**(2), 64-69.

BRYDEN, H.L. and H.M. STOMMEL (1984) Limiting processes that determine basic features of the circulation in the Mediterranean Sea. *Oceanologica Acta*, 7(3), 289-296.

BRYDEN, H.L., E.C. BRADY and R.D. PILLSBURY (1989) Flow through the Strait of Gibraltar. In: *Seminario Sobre la Oceanografía Fisca del Estrecho de Gibraltar, Madrid, 24-28 Octubre 1988*, J.P. ALMAZAN, H. BRYDEN, T. KINDER and G. PARRILLA, editors, SECEG, Madrid, 166-194.

BUCHANAN, J.Y. (1877) On the distribution of salt in the ocean. *Journal of the Royal Geographical Society*,**47**, 72-86.

BUNKER, A.F., H. CHARNOCK and R.A. GOLDSMITH (1982) A note on the heat balance of the Mediterranean and Red Seas. *Journal of Marine Research*, **40** (Supplement), 73-84.

CANDELA, J., C.D. WINANT and H.L. BRYDEN (1989) Meteorologically forced subinertial flows through the Strait of Gibraltar. *Journal of Geophysical Research*, **94**, 12667-12674.

CANDELA, J., C. WINANT and A. RUIZ (1990) Tides in the Strait of Gibraltar. *Journal of Geophysical Research*, **95**, 7313-7335.

CARPENTER, W.B. and J.G. JEFFREYS (1870) Report on deep-sea researches carried on during the months of July, August, and September 1870 in HM surveying-ship *Porcupine*. *Proceedings of the Royal Society, London*, **19**, 146-221.

CARTER, D.B. (1956) The water balance of the Mediterranean and Black Seas. *Climatology*, Drexel Institute of Technology, Laboratory of Climatology, **9**, 123-175.

DALZIEL, S.B. (1990) Rotating two-layer sill flows. In: *The Physical Oceanography of Sea Straits*, L.J. PRATT, editor, Kluwer, Boston, 343-371.

DALZIEL, S.B. (1991) Two-layer hydraulics: A functional approach. *Journal of Fluid Mechanics*, **223**, 135-163.

DALZIEL, S.B. (1992) Maximal exchange in channels with nonrectangular cross sections. *Journal of Phyusical Oceanography*, **22**, 1188-1206.

DEACON, M. (1971) *Scientists and the Sea, 1650-1900: A Study of Marine Science*. Academic Press, New York, 445pp.

FARMER, D.M. and L. ARMI (1986) Maximal two-layer exchange over a sill and through the combination of a sill and contraction with barotropic flow. *Journal of Fluid Mechanics*, **164**, 53-76.

FOFONOFF, N.P. and R.C. MILLARD JR (1983) Algorithms for computation of fundamental properties of sea water. *UNESCO Technical Papers in Marine Science*, **44**, 53pp.

GARRETT, C., M. BORMANS and K. THOMPSON (1990) Is the exchange through the Strait of Gibraltar maximal or submaximal? In: *The Physical Oceanography of Sea Straits*, L.J. PRATT, editor, Kluwer Boston, 271-294.

GARRETT, C., R. OUTERBRIDGE and K. THOMPSON (1993) Interannual variability in Mediterranean heat and buoyancy fluxes. *Journal of Climate*, **6**, 900-910.

GEYER, W.R. and G.A. CANNON (1982) Sill processes related to deep-water renewal in a fjord. *Journal of Geophysical Research*, **87**, 7985-7996.

HARZALLAH, A., D.L. CADET and M. CREPON (1993) Possible forcing effects of net evaporation, atmospheric pressure, and transients on water transports in the Mediterranean Sea. *Journal of Geophysical Research*, **98**, 12341-12350.

HELFRICH, K.R. (1994) Time-dependent two-layer hydraulic exchange flows. *Journal of Physical Oceanography*, **24**, (in press).

HOPKINS, T.S. (1978) Physical processes in the Mediterranean basins. In: *Estuarine Transport Processes*, B. KJERVE, editor, University of South Carolina Press, Columbia, 269-310.

KINDER, T.H. and H.L. BRYDEN (1987) The 1985-1986 Gibraltar Experiment. *EOS*, **68**, 786-787 and 793-795.

KINDER, T.H. and H.L. BRYDEN (1988) Gibraltar Experiment: Summary of the field program and initial results of the Gibraltar Experiment. *Woods Hole Oceanographic Institution Technical Report*, **WHOI-88-30**, 118pp.

KINDER, T.H. and H.L. BRYDEN (1990) The aspiration of deep waters through Straits. In: *The Physical Oceanography of Sea Straits*, L.J. PRATT, editor, Kluwer, Boston, 295-319.

KINDER, T.H., D.A. BURNS and R.D. BROOME (1986) Hydrographic measurements in the Strait of Gibraltar, November 1985. *Naval Ocean Research Development Activity (NORDA) Report*, **141**, 332pp.

KINDER, T.H., D.A. BURNS and M.R. WILCOX (1987)Hydrographic measurements in the Strait of Gibraltar, June 1986. *Naval Ocean Research Development Activity (NORDA) Technical Note*, **378-1**, 355pp.

LACOMBE, H. (1961) Année Géophysique Internationale 1957-1958, Participation francaise: Contribution à l'étude du régime du Détroit de Gibraltar, Etude dynamique. *Cahiers Océanographiques*, **13**, 73-107.

LACOMBE, H. (1971) Le Détroit de Gibraltar, océanographie physique. *Notes et Mémoires du Service Géologique du Maroc*, **222**, 111-146.

LACOMBE, H. and C. RICHEZ (1982) The regime of the Strait of Gibraltar. In: *Hydrodynamics of Semi-Enclosed Seas*, J.C.J. NIHOUL, editor, Elsevier, Amsterdam, 13-73.

LACOMBE, H. and P. TCHERNIA (1972) Caractères hydrologiques et circulation des eaux en Méditerrannée. In: *The Mediterranean Sea: A Natural Sedimentation Laboratory*. D.J. STANLEY, editor, Dowden, Hutchinson and Ross, Stroudsburg, Pennsylvania. 765pp.

LAVIOLETTE, P.E. and H. LACOMBE (1988) Tidal-induced pulses in the flow through the Strait of Gibraltar. *Oceanologica Acta*, **SP**, 13-27.

MACDONALD, A.M., J. CANDELA and H.L. BRYDEN (1994) Net heat transport through the Strait of Gibraltar. In: *Seasonal and Interannual Variability of the Western Mediterranean*, P. LAVIOLETTE, editor, American Geophysical Union, (in press).

MARSIGLI, L.F. (1681) Internal observations on the Thracian Bosphorus, or true channel of Constantinople, represented in letters to her majesty, Queen Christina of Sweden. Translated by E. HUDSON, in *Oceanography: Concepts and History*, M.B. DEACON, editor, Dowden, Hutchinson and Ross, Stroudsburg, Pennsylvania, 33-44.

NIELSEN, J.N. (1912) Hydrography of the Mediterranean and adjacent waters. *Report of the Danish Oceanographical Expedition 1908-1910, Copenhagen*, **1**, 77-191.

PILLSBURY, R.D., D. BARSTOW, J.S. BOTTERO, C. MILLEIRO, B. MOORE, G. PITTOCK, D.C. ROOT, J. SIMPKINS III, R.E. STILL and H.L. BRYDEN (1987) Gibraltar Experiment: Current measurements in the Strait of Gibraltar. *Oregon State University Technical Report*. **87-29**, 284pp.

PRICE, J.F. and M. O'NEIL-BARINGER (1994) Outflows and deep water production by marginal seas. *Progress in Oceanography*, **33**, 157-196.

PRICE, J.F., M. O'NEIL-BARINGER, R.G. LUECK, G.C. JOHNSON, I. AMBAR, G. PARRILLA, A. CANTOS, M.A. KENNELLY and T.B. SANFORD (1993) Mediterranean outflow mixing and dynamics. *Science*, **259**, 1277-1282.

REID, J.L. (1979) On the contribution of the Mediterranean Sea outflow to the Norwegian-Greenland Sea. *Deep-Sea Research*, **26**, 1199-1223.

SCHOTT, G. (1915) Die Gewasser des Mittelmeeres. *Annalen der Hydrographie und Maritimen Meteorologie*, **43**, 63-79.

SHULL, S. and N.A. BRAY (1989) Gibraltar Experiment CTD Data Report II: September-October 1986, USNS *Lynch. Scripps Institution of Oceanography Reference Series*, **89-23**, 258pp.

STOMMEL, H., H. BRYDEN and P. MANGELSDORF (1973) Does some of the Mediterranean outflow come from great depth? *Pure and Applied Geophysics*, **105**, 879-889.

SVERDRUP, H.U., M.W. JOHNSON and R.H. FLEMMING (1942) *The Oceans: Their Physics, Chemistry and General Biology*, Prentice-Hall, New York, 1087pp.

TIXERONT, F. (1970) Le bilan hydrologique de la Mer Noire et de la Méditerranée. *Cahiers Océanographiques*, **22**, 227-237.

WATSON, G. and I.S. ROBINSON 91990) A study of internal wave propagation in the Strait of Gibraltar using shore-based marine radar images. *Journal of Physical Oceanography*, **20**, 374-395.

WESSON, J.C. and M.C. GREGG (1994) Mixing at Camarinal Sill in the Strait of Gibraltar. *Journal of Geophysical Research*, **99**, (in press).

WÜST, G. (1952) Der Wasserhaushalt des Mittellandischen Meeres und der Ostsee in vergleichender Betrachtung, *Revista Geofisica Pura e Applicata*, **21**, 1-14.

of V

Classification of flow variability though the Strait of Gibraltar.

	Type of Flow	Forcing
mainly barotropic	**Tidal** (hrs. --> day) O(1m/s) r.m.s. transport 2.1 Sv	North Atlantic tide
mainly barotropic	**Subinertial** (days --> few months) O(0.3m/s) r.m.s. transport 0.4 Sv	Meteorological - specifically the atmospheric pressure fluctuations over the Mediterranean Sea. [*Crepon, 1965, Garrett, 1983 & Gacia La Fuente, 1984*]
baroclinic	**Long-Term** (Seasonal --> interannual) O(0.5m/s) transport O(1 Sv, each way)	- (E-P) and Mass-Salt balance. [*Nielsen, 1912 & Defant, 1961*] - Overmixing in the Mediterranean. [*Bryden and Stommel, 1984*] - Interface depth fluctuations, deep water formation, seasonal wind cycle, etc. [*Bormans et al., 1986*] - Hydraulic control and maximal exch [*Armi and Farmer, 1986, 1987 & 1988*] - TIME SCALE OF MET. FORCING & SYSTEM TIME RESPONSE (LASCARATOS, 1997)

Subinertial Principal Axis Currents at the Sill of the Strait of Gibraltar

so without tides

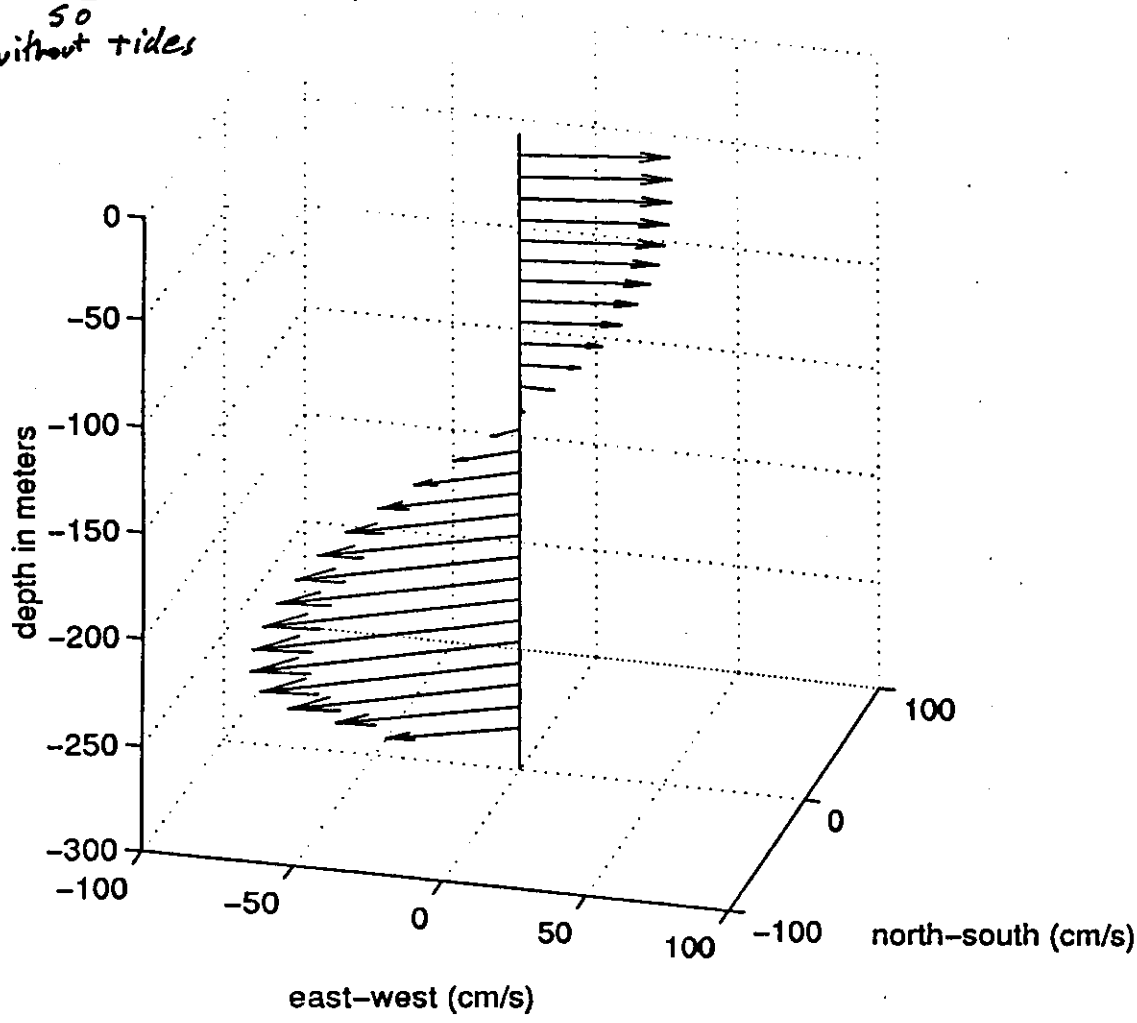

EOF mode # 1 of currents at sill from ADCP mooring. (wmean=1).

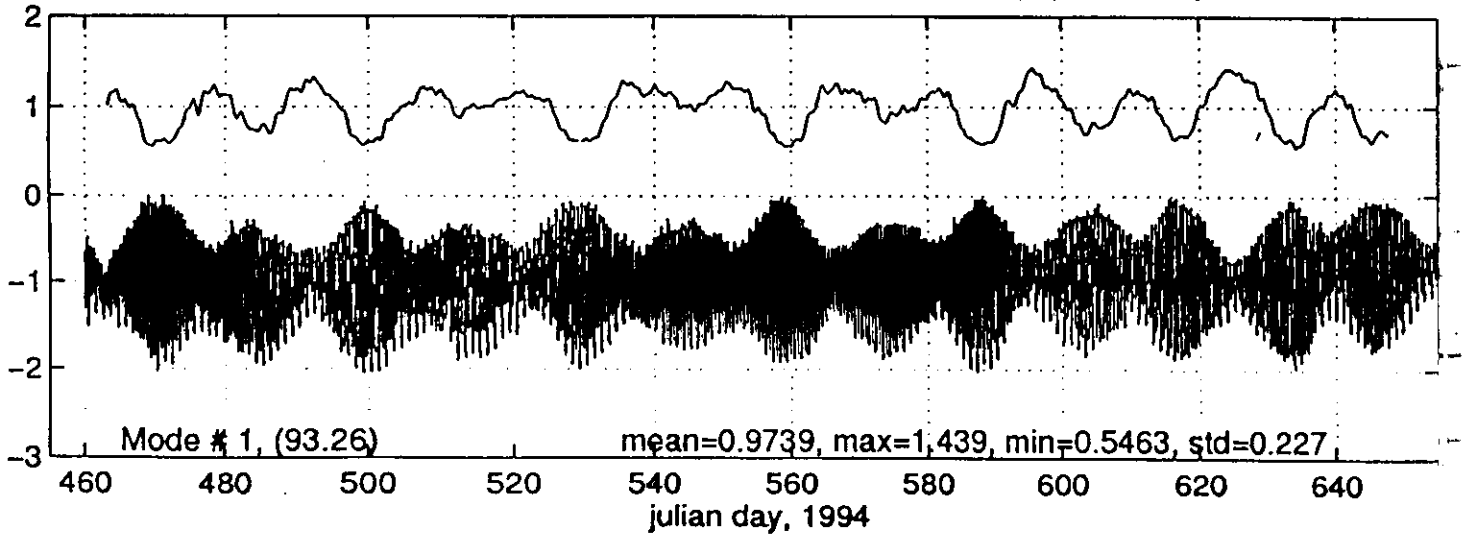

WAYS TO CALCULATE Q_M OUTFLOW TRANSPORT

$$\overline{Q_M} = \int dy \int_{\text{BOTTOM}}^{z(\bar{u}=0)} \bar{u}(z)\, dz \qquad (1)$$

$$Q_M(t) = \int dy \int_{\text{BOTTOM}}^{h(t)} u(z,t)\, dz$$

AND THEN AVERAGING; $\overline{Q_M(t)}$ (2)

(1) GIVES -0.38 Sv

(2) GIVES -0.68 Sv

$\therefore \int \overline{u' h'}\, dy$ CONTRIBUTES ~ 1/2 OF THE TOTAL TRANSPORT

$$(\bar{u}+u')(\bar{h}+h') = \bar{u}\bar{h} + \cancel{\overline{u'}\,\bar{h}}^{\,0} + \cancel{\bar{u}\,\overline{h'}}^{\,0} + \overline{u'h'}$$

$\overline{u'} = \overline{h'} = C$

$\neq C$ IF u' & h' ARE CORRELATED

J

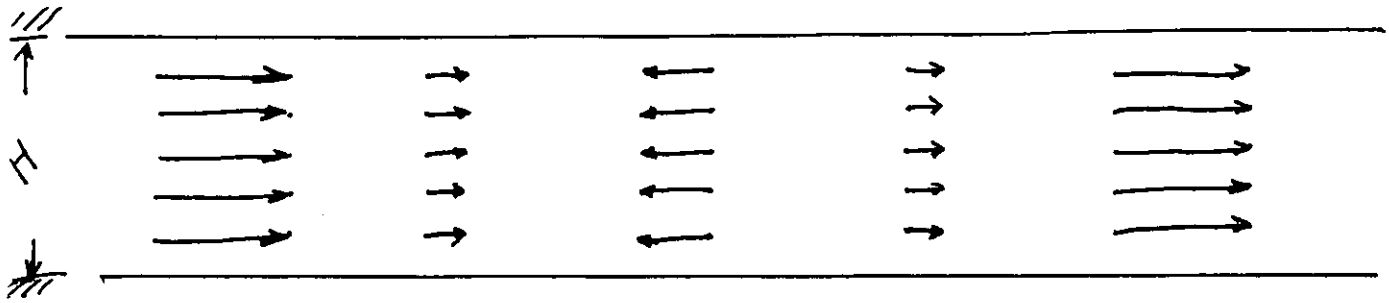

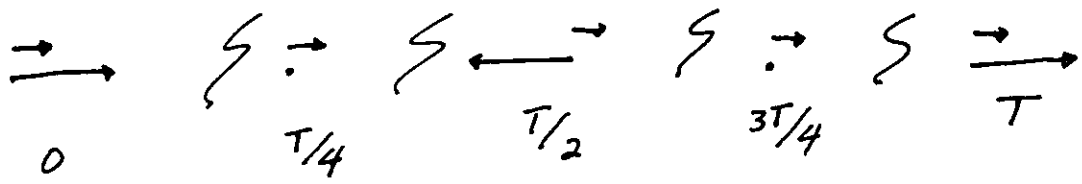

$H = \bar{H}$, $U = \bar{U} + \delta u$, $\langle U \rangle = \bar{U}$

$\langle \text{Transport} \equiv UH \rangle = \bar{U}\bar{H}$

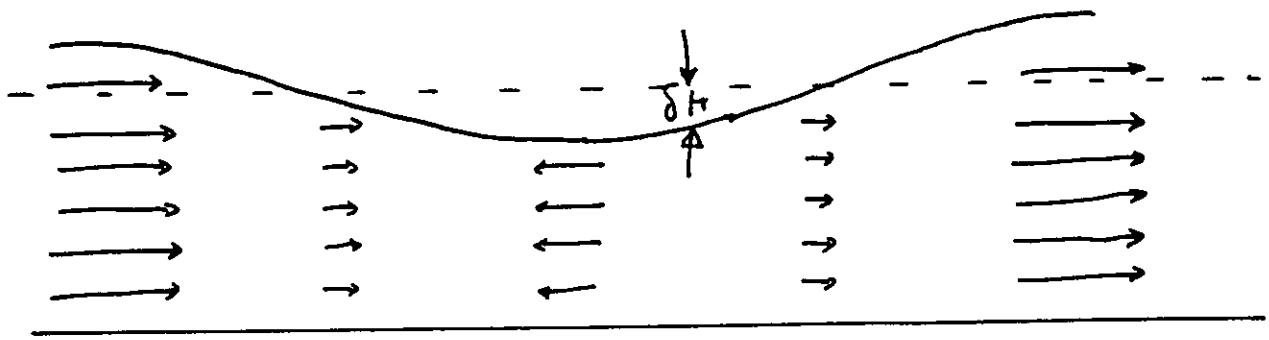

$H = \bar{H} + \delta h$, same U

$\langle \text{Transport} \rangle = \bar{U}\bar{H} + \langle \delta u \, \delta h \rangle$

$\bar{H} = 1$ $\qquad$ $\bar{U} = .2$

$\delta h = 0.2 \cos \omega t$ $\qquad$ $\delta u = \cos \omega t$

$H = \bar{H} + \delta h$, $\qquad$ $U = \bar{U} + \delta u$

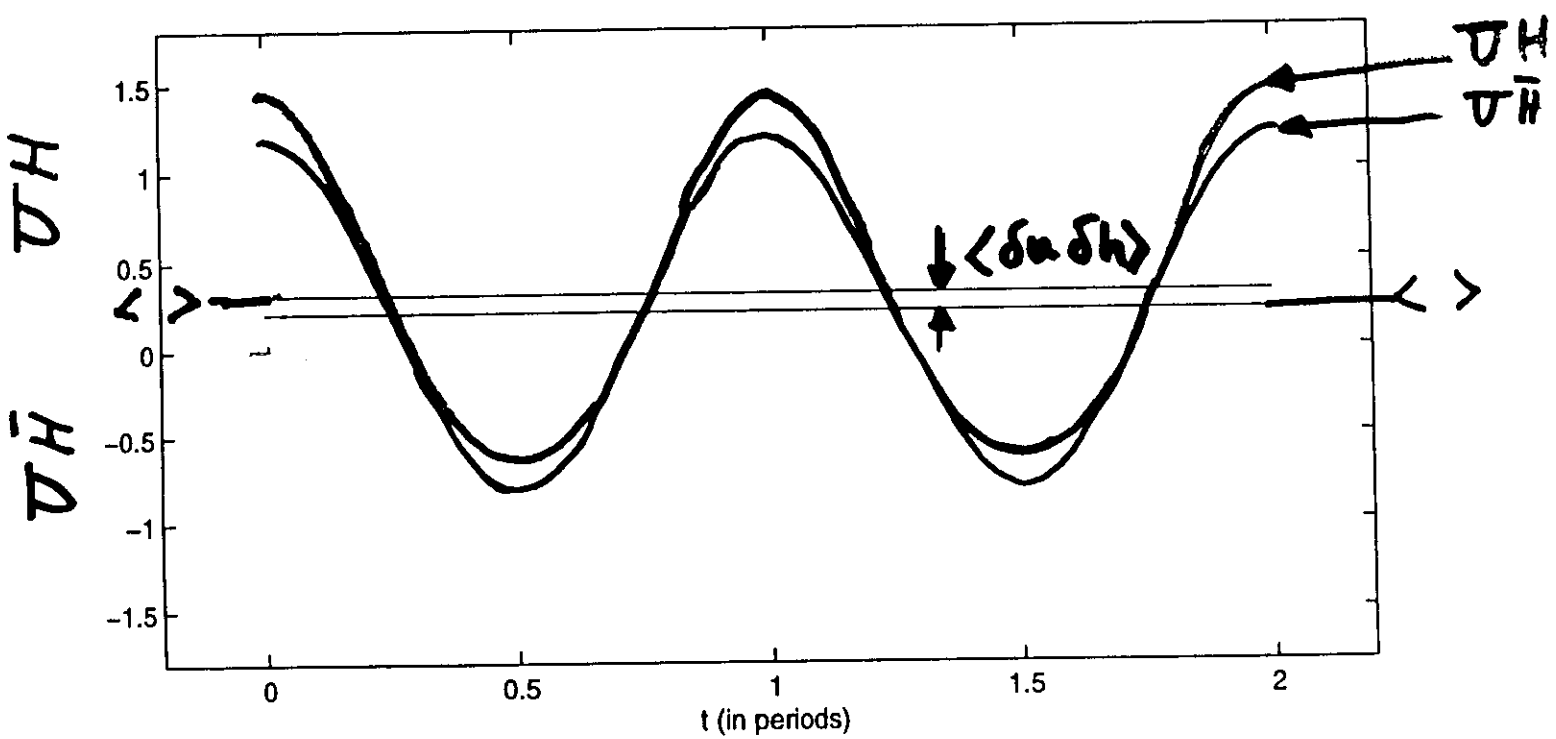

I-41

EOFs is the same thing as SVD (NOV 20 | 30)

Empirical Orthogonal Eigenfunctions — Singular Value Decomposition

$$\begin{pmatrix} d_{11} & d_{12} & \cdots & d_{1m} \\ d_{21} & d_{22} & \cdots & d_{2m} \\ d_{31} & d_{32} & & \\ \vdots & \vdots & & \\ d_{n1} & d_{n2} & & d_{nm} \end{pmatrix} = \begin{pmatrix} a_1 \\ a_2 \\ \vdots \\ a_n \end{pmatrix} \underbrace{\begin{matrix} b_1 & b_2 & \cdots & b_m \end{matrix}} + \begin{pmatrix} \varepsilon_{11} & \varepsilon_{12} & & \varepsilon_{1m} \\ & & & \\ & & & \end{pmatrix}$$

$n \times m \quad = \quad n \times 1 \times m$

1st EOF

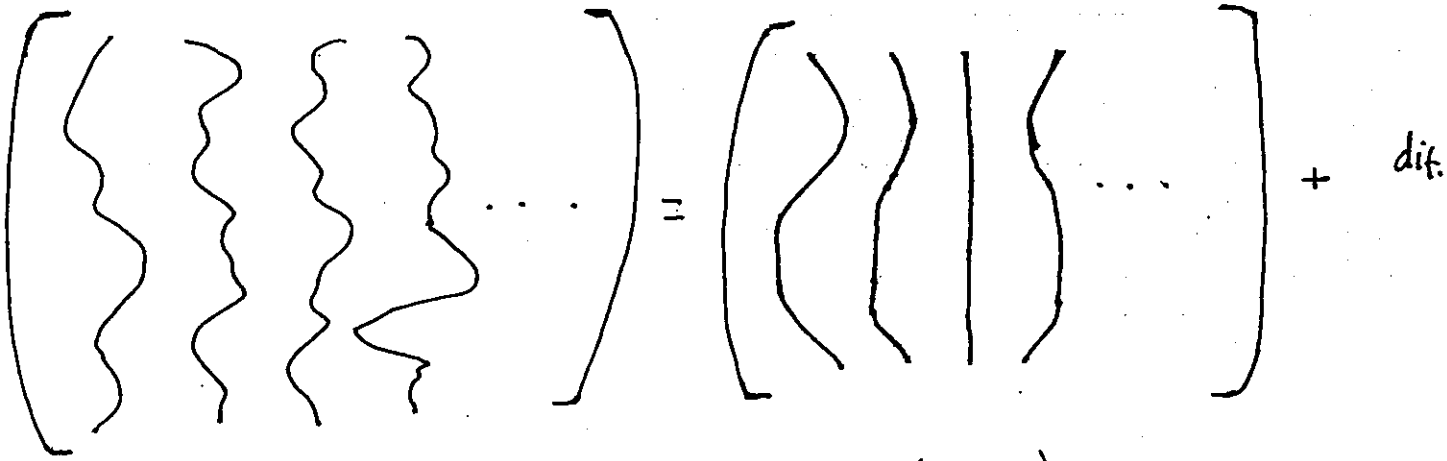

Set of profiles = Same profile (= shape) each time multiplied by its amplitude + differ

$n \times m$ = data values $\qquad n + m$ = descriptors

1st EOF of $\underline{\underline{d}}$ is the pair $\underline{a}$ (of dim. n)

$\underline{b}$ (of dim. m)

Such that $\sum_{j=1}^{m} \sum_{i=1}^{n} \varepsilon_{ij}^2 =$ minimum

$$\underline{\underline{d}} = \begin{pmatrix} a_1 \\ \vdots \\ a_n \end{pmatrix}_1 (b_1 \cdots b_m)_1 + \begin{pmatrix} a \\ \vdots \\ a \end{pmatrix}_2 (b \cdots b)_2 + \cdots \begin{pmatrix} a \\ \vdots \\ a \end{pmatrix}_{\text{Last}} (\ b\ )_{\text{last}}$$

orthogonal to — & orthogonal to each — (in space of dim. n)

Last = min of $(n, m$

$\underline{b}$'s are also orthogonal in their space

2 of

$$d_{ij} = a_i b_j + \varepsilon_{ij}$$

10

$$SS = \text{Sum of squares} = \sum_j \sum_i \varepsilon_{ij}^2 = \sum\sum (d_{ij} - a_i b_j)^2$$

(I am assuming NO gaps, i.e. all data points are known this can be relaxed since the correlation matrices can be constructed w/out all the data points, care should be taken for non-positive defined matrices = not all eigenvalues positive)

SS only depends on a_i, $i = 1, \ldots, n$ & b_j, $j = 1, \ldots, m$ because the data $\underline{\underline{d}}$ is given.

$$SS = \sum_i (d_{i1} - a_i b_1)^2 + \sum_i (d_{i2} - a_i b_2)^2 + \cdots + \sum_{i=1}^{n} (d_{im} - a_i b_m)^2$$

then $\frac{\partial SS}{\partial a_\ell} = 0$ (to find the extremal, gives)

$$0 = 2(d_{\ell 1} - a_\ell b_1)(-b_1) + 2(d_{\ell 2} - a_\ell b_2)(-b_2) + \cdots + 2(d_{\ell m} - a_\ell b_m)(-b_m)$$

or $$\sum_{i=1}^{m} (d_{\ell i} - a_\ell b_i) b_i = 0$$ or $$\boxed{\sum_i^m \varepsilon_{\ell j} b_j = 0}$$

This is an orthogonality condition (for $\ell = 1, 2, \ldots$)
(typical result of 'least square optimization')

Using 'column' vectors (notation)

$$\underset{n \times m}{d} = \underset{n \times 1 \times m}{a\, b^T} + \underset{m \times m}{\varepsilon} \; ; \quad a = \underset{m \times 1}{a} \; , \; b = \underset{m \times 1}{b}$$

The conditions to get the extremal of SS are:

$$\underset{n \times m \times 1}{\varepsilon\, b} = 0 \qquad (n \text{ equations})$$

& $$\underset{1 \times m \times m}{a^T \varepsilon} = 0$$ (m equations from $\frac{\partial SS}{\partial b_k} = 0$; $k = 1, \ldots, m$ (good homework))

Hence:

$$a^T d = \underbrace{a^T a}_{\text{scalar}} b^T + a^T \overrightarrow{\varepsilon}^{\,0}$$

& $$d\, b = a \underbrace{b^T b}_{\text{scalar}} + \varepsilon \overrightarrow{b}^{\,0}$$

$$\Rightarrow \quad \boxed{\begin{aligned} \underset{n \times n}{d d^T}\, a &= \lambda^2 a \\ \underset{m \times m}{d^T d}\, b &= \lambda^2 b \end{aligned}} \quad \text{w/ } \lambda^2 = \xi a^T a \xi \xi b^T b \xi$$

First EOF is the pair of eigenvectors corresponding to largest eigenvalue
Second " " " " next.
See SVD in any linear Algebra textbook

Nov 98, J

For complex data, say $\zeta = u + iv$

$\zeta = \zeta(z,t)$, u = east comp. of velocity, v = north...

use dd^{*T}. where d^* is the complex conjugate

For ζ = vert. displacement use

$d(z,t) = N(z)\,\zeta(z,t)$ as data

since Pot. energy is $\left\langle \frac{1}{2}\int_{\text{bottom}}^{\text{surface}} N^2 \zeta^2 \, dz \right\rangle$

---

if $n < m$ get eigenvectors & eigenvalues

from $dd^T a = \lambda^2 a$ &

construct b's from $a^T d \propto b^T$

if $n > m$ get b's & eigenvalues from

$d^T d$, then compute $a \propto d\,b$

Matlab constructs directly the SVD

I use normalized a's & b's (in corresponding spaces) & show a table of λ^2's (or $\lambda^2/SS\phi \times 100$ since $\Sigma \lambda^2$'s $= SS\phi$). $\left(SS\phi = \sum_j \sum_i d_{ij}^2\right)$.

INTERPRETATION is more important than algebra, so the choice of $\underline{\underline{d}}$ must be precise

Deep-Sea Research, Vol. 38, Suppl. 1, pp. S465–S503, 1991.
Printed in Great Britain.

0198-0149/91 $3.00 + 0.00

Water mass exchange in the Gulf of Cadiz

J. OCHOA*† and N. A. BRAY†

(*Received* 9 *November* 1988; *in revised form* 15 *April* 1990; *accepted* 21 *May* 1990)

Abstract—Velocities inferred from several closed hydrographic sections in the Gulf of Cadiz are used to estimate the volume transport and the heat and freshwater fluxes associated with the exchange of Atlantic and Mediterranean waters through the Strait of Gibraltar. Five different sets of constraints are imposed to obtain absolute flow fields from the baroclinic shear determined by the thermal wind equation. The resultant transports and fluxes through a given section are similar for all five cases. Transports and fluxes from sections near the strait underestimate the actual exchange. This is attributed to ageostrophic effects associated with the gravity-driven downslope flow that is characteristic of the deep Mediterranean outflow near the strait. West of 7°W, the estimated fluxes are larger, comparable to those deduced from climatological observations over the Mediterranean. In this region, the outflow appears to have no significant downslope component, so that transports calculated from closed sections are independent of the orientation relative to the direction of the outflow.

Exchange between the Atlantic and Mediterranean can be characterized in several ways. A common measure used is volume transport, usually that of the outflow, observed somewhere near the sill. This is not an adequate definition of exchange, as transport may be altered by recirculation or entrainment without changing the net flux of properties. Thus, volume transport is a function of position; fluxes of freshwater, salt and heat, on the other hand, should be independent of position in the absence of local sources and sinks. In these observations, the total volume transport exchanged through each section increases from 1 Sv at 6°30′W to nearly 7 Sv at 8°W. The part of the total exchange that does not recirculate along density surfaces increases from 0.5 Sv near the strait to 2.2 Sv through sections at 7°30′W and 8°W. Part of this increase is due to entrainment, and part to the ageostrophic character of the outflow near the strait. Freshwater flux is estimated to be the equivalent of 0.53 m y^{-1} of evaporation excess over the Mediterranean. Heat flux was higher in the autumn of 1986 than in the spring (6.0 W m^{-2} vs 2.2 W m^{-2}), due to warmer surface temperatures in the autumn. For comparison with earlier estimates, the observed outflow transport may be converted to an equivalent transport of "pure" Mediterranean water of 0.7 Sv, assuming salinities of 38.4 and 35.6 for Mediterranean and Atlantic waters. This implicit flux, while useful for comparisons with observations where true fluxes cannot be estimated, involves several approximations, and should not, in general, be used to characterize the exchange if fluxes can be calculated directly.

1. INTRODUCTION

CIRCULATION in the Gulf of Cadiz is dominated by the exchange of Atlantic and Mediterranean waters through the Strait of Gibraltar. The exchange is driven by an excess of evaporation over precipitation and runoff in the Mediterranean Basin, and by an

*CICESE, Ensenada, B.C., Mexico.
†Scripps Institution of Oceanography, La Jolla, CA 92093, U.S.A.

accompanying loss of heat to the atmosphere. Atlantic waters flow into the Mediterranean at the surface, are transformed by air–sea fluxes into colder, saltier and therefore denser waters, and eventually leave the Mediterranean as a deep current with unique temperature and salinity characteristics that may be traced far from the source. REID (1979) implicated Mediterranean Waters in the formation of deep waters of the Norwegian Sea and, through the circulation of those bottom waters, in the characteristics of the deep waters throughout the world oecan (REID and LYNN, 1971).

The question addressed here is whether it is possible to make reliable estimates of the exchange of water masses through the Strait of Gibraltar using only hydrographic observations that form closed sections in the Gulf of Cadiz (Fig 1). There are several reasons why such estimates might not be valid. In addition to the usual ambiguity of many possible absolute flow fields that satisfy the inferred vertical shear, Mediterranean waters leave the strait as a density current: a bottom-intensified, very dense flow that crosses isobaths in its progress into the Gulf of Cadiz. Near the strait, it is unlikely that the flow will be in geostrophic balance, at least in the direction of flow. Other ageostrophic effects such as friction, mixing through entrainment, and unsteadiness of the flow also may be important near the strait.

On the other hand, the interface between Atlantic and Mediterranean waters is well-defined by its salinity structure, and makes a natural choice for a reference level. Far enough from the strait that the flow is in nearly geostrophic balance, it should be possible to exploit this structure to determine the absolute flow field with reasonable accuracy and thereby to make estimates of the heat, salt and freshwater fluxes associated with the exchange. These estimates will be "snapshots" of the flow, and many realizations would be needed to average out temporal variability to identify a mean exchange or seasonal and interannual fluctuations.

Why not simply measure the exchange directly in the strait, where geographic restrictions make the region to be observed much smaller? That approach has certain obvious advantages as well as several subtle disadvantages. In fact, the Gibraltar Experiment, of which this work was a part, was designed to make just those direct measurements in the strait, over the period of a year. The experiment was successful in providing lower layer transport estimates, as well as a description of the behavior of the interface. However, ship traffic prevented any moored measurements shallower than about 80 m, or the top third of the water column over the sill. Thus, any estimates of exchange or flux from these measurements must involve extrapolation through the upper layer (BRYDEN *et al.*, 1989).

The temporal variability of the flow is also much stronger in the strait, due to those same bathymetric and geographic constraints, and a dynamical correlation between tidal currents and interface depth requires that interface depth, as well as current, measured in order to estimate the effective transport in either layer (BRYDEN and PILLSBURY, 1989). Intense mixing and entrainment occur on very short scales within the strait, and are responsible for cross-isopycnal exchange comparable in magnitude to the layer transports (BRAY and LACOMBE, in preparation). Interpretation of the exchange in terms of volume transport then becomes dependent upon position in the strait.

Until this point in the discussion, exchange has remained a rather vague quantity that somehow characterizes the interaction between the Mediterranean Sea and the North Atlantic Ocean. A few definitions are in order. The inter-basin exchange consists of relatively large transports of fresh, warm surface waters into the Mediterranean, and of denser waters into the Atlantic. The net transport of mass is small: only that required to

balance the evaporative loss of moisture over the Mediterranean. The net transport of salt is presumed to be zero and the net transport of heat is only that required to balance the small net loss of heat from the surface of the Mediterranean. In this paper, the term "exchange" will be used to describe the large transports that are nearly equal but opposite in direction; the term "flux" will refer to the net transports. The adjective "baroclinic", rather than geostrophic, is used here to describe flow fields inferred by integration of the thermal wind equation, simply to emphasize that the total pressure field is not known.

It should be noted that volume transport is an ambiguous measure of exchange, as it increases with distance from the strait due to entrainment and recirculation. It is not sufficient to say that the exchange is 1 Sv (10^6 m^3 s^{-1}), for instance, either the location or the characteristics of the flow must also be specified. Fluxes, on the other hand, should be independent of position, as there are no sources or sinks of heat or salt near the strait. However, specifying only the flux omits the oceanographically interesting information of how much volume is involved in the exchange. Both quantities are identified in the present work.

2. BACKGROUND

2.1. *Structure of the Mediterranean outflow*

The distribution of Mediterranean water in the Gulf of Cadiz has been the focus of a number of studies in the past. MADELAIN (1970), using observations from 1958 to 1967, described the path of the outflow from the strait to Cape St Vincent, the southwestern corner of the Iberian Peninsula. The topography of the gulf is uneven, with numerous ridges and canyons tending west and south out of the shallower regions of the strait. As the outflow exits the strait, it flows across isobaths as a density current, though under the influence of the earth's rotation. Within about 50 km west of Tarifa, the outflow makes an abrupt turn to the north as the result of blockage by a north–south ridge. The outflow then generally follows the curve of the coastline around to the west, though there are several branches that flow down smaller canyons, eventually rejoining the main branch about 150 km downstream from the strait, or half-way to Cape St Vincent. The depth of the outflow increases from about 300 m at the sill in the strait to about 1200 m at Cape St Vincent. Two distinct Mediterranean water types appear in profiles from the open northeast Atlantic (ZENK, 1975b). There is also a separate, shallower layer of the outflow apparent west of about 7°W. This layer is found at 400–600 m depth, is warmer than the deeper outflow, and maintains its identity in potential temperature vs salinity (θ/S) characteristics even after the outflow turns northward along the west coast of Portugal (AMBAR and HOWE, 1979a; AMBAR, 1983). It is not clear what causes this vertical separation of the outflow, though ZENK (1975b) argues that the structure is caused by tidal currents within the strait, rather than by topographic effects in the Gulf of Cadiz. HOWE (1982), in his review of the Mediterranean water outflow, concurs that some type of mixing in the strait is probably responsible for creating distinct sub-species of outflow water types.

The behavior of the outflow near the strait, where it appears to act like a density-driven current under the influence of rotation, is of particular interest in the present work. The premise of the calculations is that, if the flow is geostrophically balanced and an appropriate reference level can be found, closed sections will identify the transports, regardless of the orientation of the flow relative to the section. However, if the flow is still density-driven, this is not necessarily true, as only the cross-stream component of velocity

is geostrophic. It is therefore important to identify those regions of the outflow where ageostrophic effects may be important.

SMITH (1975) describes a model of density-driven flow in the presence of rotation, in which the cross-stream balance is geostrophic except for a curvature term, but the along-stream balance is not, so long as there is a component of the flow crossing isobaths. One way to look at the effect of this type of flow on a baroclinic calculation is to consider what the apparent transport would be if a hypothetical section crossed the flow at an arbitrary angle. If it is perpendicular to the flow, the correct transport would be resolved. However, if it crosses at some oblique angle, then a part of the downslope density gradient would appear in the observed density field. Depending upon the relative orientations of flow, topography and section, this could result in either an over- or underestimate of the vertical shear, and thereby of the transport. The effect disappears when the downslope component of the flow vanishes, as there is no longer an along-flow density gradient. Combined with MADELAIN's (1970) observations of the outflow, SMITH's (1975) model predicts that this transition to geostrophic balance in the along-stream direction occurs west of about 7°W, 130 km downstream of the source. At this point, entrainment, rather than friction, dominates the model outflow in the along-stream direction.

Entrainment of Atlantic water modifies the characteristics as well as the volume of the outflow. Similarly, the inflow is modified through contact with the outflow, increasing the minimum salinity of Atlantic water from 35.6‰ in the Gulf of Cadiz to 36.2‰ near the strait. While entrainment does change the structure of the water masses, it does not alter the property fluxes. Entrainment increases the observed volume of outflow from about 1 Sv near the strait to about 3 Sv at Cape St Vincent (AMBAR and HOWE, 1979b). In addition to the vertical recirculation implied by entrainment, horizontal recirculations or eddies also may contribute to the observed exchange. Using neutrally buoyant floats, SWALLOW (1969) identified an eddy off Cape St Vincent at the depth of the outflow, with recirculating velocities on the order of 10–20 cm s^{-1} and a diameter of roughly 20 km. The volume exchange through a section containing an eddy will be augmented by the recirculation of the eddy. Calculations of the exchange transport should be made in such a way as to eliminate these recirculations.

2.2. *Temporal variability*

Large fluctuations of the outflow transport occur within the strait as a result of forcing by the tides and by atmospheric fluctuations over the Mediterranean (LACOMBE and LIZERAY, 1959a,b; CREPON, 1965; CANDELA *et al.*, 1989). Smaller, but still possibly significant, variations occur seasonally and interannually (LACOMBE *et al.*, 1981; BORMANS *et al.*, 1986). Tidal and atmospheric effects are most pronounced within the strait, though possible downstream influence has been noted as far as 50 km away (BOYUM, 1963, 1967; GRUNDLINGH, 1981). These fluctuations are nearly barotropic and only contribute to the exchange because the depth of the interface changes in phase with the velocity. Periods of westward barotropic flow are associated with a deep lower layer and, conversely, eastward flow with a deep upper layer, resulting in a net exchange (CANDELA *et al.*, 1989). The volume exchange, as estimated from time mean current meter observations, is about 0.4 Sv (1 Sv = 10^6 m^3 s^{-1}) (BRYDEN and PILLSBURY, 1989; CANDELA *et al.*, 1989). Superimposed on the mean currents, rectification of tidal and atmospherically forced barotropic currents adds approximately 0.4 Sv to the exchange in the strait (CANDELA *et al.*, 1989).

Seasonal and interannual fluctuations have not been measured directly in the strait, but rather have been inferred from examination of tide gauge records along and across the strait (BORMANS *et al.*, 1986) and from changes in evaporation and surface heat flux over the Mediterranean (BUNKER, 1972; BETHOUX, 1979; LACOMBE *et al.*, 1981). BORMANS *et al.* (1986) suggest a seasonal cycle in the inflow of about 6%, with maximum transport in spring. They attribute the increase to changes in interface depth and argue that winter water mass formation processes raise the interface level within the Mediterranean, while draining of the Levantine Intermediate Water (LIW) reservoir occurs during the rest of the year, effectively lowering the interface. Evaporation and heat loss from the Mediterranean have seasonal cycles, with maximum loss of both heat and moisture during winter; heat is actually gained from the atmosphere by the Mediterranean during April–August (BUNKER, 1972). The effect of seasonal air–sea forcing over the Mediterranean on the instantaneous transport through the strait, however, may be quite small, as the residence time involved in the transformation of Atlantic water to Mediterranean water is of the order of decades (LACOMBE *et al.*, 1981). It is more likely that seasonal fluctuations of transport result from dynamic effects local to the strait, or from a mechanism of draining and filling of the LIW reservoir, as suggested by BORMANS *et al.* (1986).

At interannual time scales, the formation of Mediterranean water masses may occur under varying conditions in different years, changing the characteristic temperatures and salinities (LACOMBE *et al.*, 1985). As a result, different volume transports of outflow in different years might accomplish the same flux of properties. This is generally thought to be a small effect, but investigators have noted a wide range in the maximum salinity observed west of the sill: SCHOTT (1928) found a maximum of 37.25‰ over several years of observations, BOYUM (1963) a maximum of 38.2‰, and KINDER and PARRILLA (1987) a maximum of 38.44, as defined by the 1978 Practical Salinity Scale (PSS) (FOFONOFF and MILLARD, 1983). By convention, this salinity has no units, though it is nearly equivalent to the older salinity designation of parts per thousand (‰). In this paper, historical salinities will be given the units ‰, to distinguish them from the newer PSS values, given without units.

2.3. *Transport*

Historically, exchange through the strait has been identified as a volume transport, occasionally converted to an equivalent flow of "pure" Mediterranean water for comparison with other estimates. If pure Mediterranean water has a salinity S_m and pure Atlantic a salinity S_a, then the volume of pure Mediterranean water in a two-layer system is given by:

$$V_m = V_t(S_t - S_a)/(S_m - S_a), \tag{1}$$

where V indicates transport and subscript t indicates observed outflow. This provides a rough measure E' of the actual evaporation excess E:

$$E' = V_a - V_t$$

or

$$E' = V_m(S_m - S_a)/S_a \tag{2}$$

in which integral salt transports have been approximated by the product of pure Mediterranean water transport and the assumed salinities S_m and S_a. Table 1 lists some of

the historical estimates of transport, and estimates of V_m and E'. For consistency, values of S_m and S_a of 38.4‰ and 35.6‰ have been used throughout. This follows ZENK (1975a), though other investigators have used lower values for S_m (BOYUM, 1963) and higher values for S_a (LACOMBE *et al.*, 1981; BRYDEN *et al.*, 1989).

2.4. *Fluxes*

Although there are as yet no direct measurements of heat and freshwater fluxes through the strait, there have been several investigations of climatological fluxes over the Mediterranean (TIXERONT, 1970; BETHOUX, 1979, 1980; BUNKER *et al.*, 1982), and recent direct measurements in the strait were used to estimate the outflow transport of salt (BRYDEN *et al.*, 1989). From the climatological air–sea flux studies, an evaporation excess rate of about 1 m y^{-1} is expected over the Mediterranean Sea. This implies, for a two-layer flow, a volume exchange of about 1.5 Sv through the Strait of Gibraltar, depending upon the salinities chosen to characterize the inflow and outflow. In contrast, the outflow salt transport estimated by BRYDEN *et al.* (1989) corresponds to an evaporation excess of 0.55 m y^{-1} (a freshwater flux of 0.044 Sv), assuming an inflow salinity of 36.2. Their calculation relied upon extrapolating the structure of the upper 100 m of the inflow layer, which was not resolved by the instrumentation.

The evaporative loss of moisture from the surface of the Mediterranean is accompanied by a small net heat loss, based on the colder temperature of the outflow relative to the inflow. However, BUNKER *et al.* (1982) found that their best estimate of sea–air heat flux components over the Mediterranean resulted in a net heat gain, rather than the loss implied by outflow colder than inflow, as is observed. They argued that either inadequate sampling or their computational methods caused the evaporation rate to be too low. Heat fluxes estimated from advection (heat content difference between inflow and outflow) would improve the accuracy of the net heat flux estimate.

Table 1. *Historical transport and evaporation estimates*

	Volume transport (Sv)			Evaporation excess (m y^{-1})		Average S of outflow
	Inflow	Outflow	V_m*	Air–Sea† E	Med Water‡ E'	S_i
NIELSEN (1912)	1.87	1.78	1.34	1.26	1.40	37.75§
SCHOTT (1915)	1.75	1.65	1.27	1.40	1.26	37.75§
SVERDRUP *et al.* (1942)	1.75	1.68	1.29	0.98	1.26	37.75§
CARTER (1956)	0.96	0.92	0.71	0.56	0.70	37.75§
BOYUM (1963)		0.96	0.74		0.70	37.75§
TIXERONT (1970)				0.70		
LACOMBE and TCHERNIA (1972)	1.20	1.15	0.94	0.70	0.98	37.90
BRYDEN *et al.* (1989)	1.04	0.76	0.57		0.55	37.70

*V_m is volume of "pure" Mediterranean water calculated according to equation (1).
†Evaporation excess estimated from meteorological observations over the Mediterranean.
‡Evaporation excess estimated from equation (2).
§Value given by SVERDRUP *et al.* (1942).

Fluxes calculated from hydrographic observations were not found in the literature, although BOYUM (1963) used baroclinic calculations to estimate outflow just west of the strait. Unfortunately, the data he used did not extend into the inflow layer. AMBAR and HOWE (1979b) also made baroclinic estimates of the outflow through several sections west of the strait, though none were closed sections in the sense of extending from Europe to Africa. Despite the many intensive studies of the outflow over the period 1958–1967, there are few synoptic closed sections available, and no flux calculations were published from those few.

3. OBSERVATIONS

As part of the Gibraltar Experiment, hydrographic sections were occupied in the Gulf of Cadiz and the Alboran Sea during both spring and autumn of 1986. The station pattern in the Gulf of Cadiz, shown in Fig. 1, was designed to allow baroclinic calculations of the flow field through closed, north–south sections, labeled VI to IX (BRAY, 1986; SHULL and BRAY, 1989). In all of these sections, the interface between Mediterranean water and the overlying Atlantic water is identifiable by a high gradient of salinity separating the salinity minimum of the Atlantic water and the salinity maximum of the Mediterranean water (Figs 2 and 3).

All data used were taken with one of two Neil Brown Mark III CTDs, calibrated in the laboratory before and after each cruise, and at sea with water samples and reversing thermometers. The raw data were processed as described in BRAY (1986). Stations were made to within a few meters of the bottom, to resolve the bottom-intensified outflow, and the final profiles consisted of 2 decibar bin averages (a decibar is 10^{-4} Pa, and is nearly equivalent to 1 m of water depth). The accuracy of the observations is ±0.005°C, ±0.005 and ±5 db, for temperature, salinity and pressure, respectively.

Data for each section were objectively mapped onto a regular grid, using a procedure described in BRAY (1988) and ROEMMICH (1983). Objective mapping is a technique for optimal estimation of data at a given position, based on the values of neighboring measurements and on an assumed correlation function of the field. It is often desirable to interpolate unevenly spaced data onto a regular grid for calculations of first differences, integrations and fluxes.

Following ROEMMICH (1983), the data are mapped twice, once with large correlation scales, to represent the background stratification, and again with the large-scale field removed, using correlation scales appropriate to the variations of properties about the large-scale field. A further parameter is involved in both calculations: the error variance. This parameter is an r.m.s. measure of the agreement between the observations and the estimate values at the observation points. A variance of 0.001, for example, requires that the data and observations agree to within an average of 3% of the observed values. Imposing a small error variance, then, prevents the data from being smoothed, even with large correlation scales. Rather, the correlation scales determine the smoothness of the interpolation between observations. The error variance imposed for the large-scale field was 0.1, while that for the small-scale field was 0.001.

Two different methods of determining appropriate correlation scales were employed. The first, and perhaps most appropriate, requires that the resulting vertical sections appear to the eye as they would if contoured by hand. Alternatively, the observations may be used to calculate the scales directly as e-folding or zero-crossing lengths of the observed

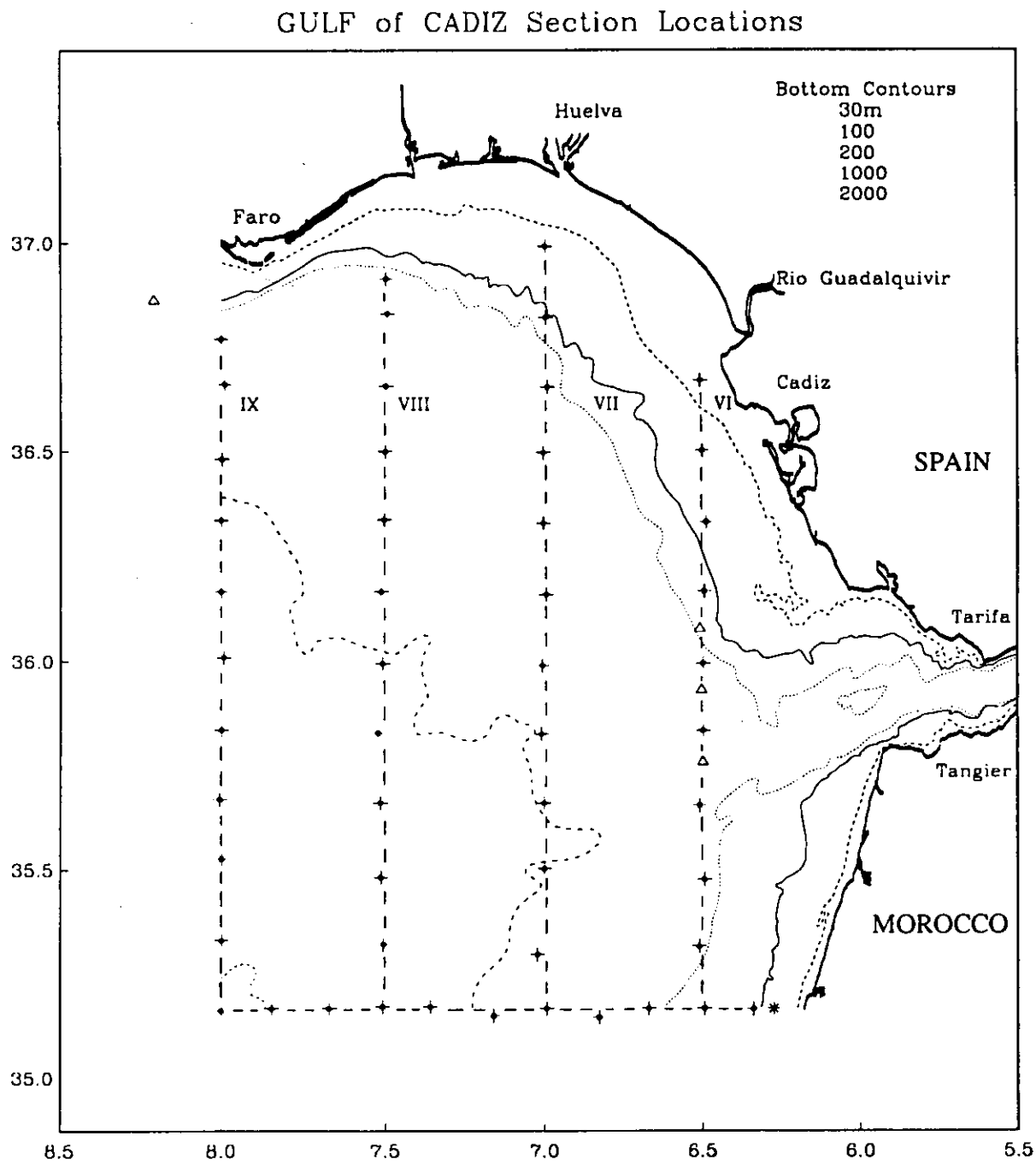

Fig. 1. Large-scale survey pattern in the Gulf of Cadiz for cruises in March–April and September–October 1986. The station marked with an asterisk marks the "southern" end of all four L-shaped section (VI–IX). All section maps will have this station as the leftmost station. The corner of the L is denoted by a vertical dashed line in all contour maps. Section labels are noted at the northern end on this map. Stations marked with a triangle were occupied in autumn but not in spring.

correlation function. This latter requires some care, in that the large-scale field will contribute to enhanced correlation at long lags. Therefore, two steps were used: first the large-scale field correlations were calculated by removing the arithmetic mean from the observations, and separate correlation functions derived for vertical and horizontal scales. The objectively mapped large-scale field was then removed from the observations, and the

residual observations were used to calculate the small-scale field correlation scales. Correlation calculations suggested, for the large-scale field, a horizontal scale greater than 200 km and a vertical scale greater than 200 m. For the small-scale field (having removed large-scale correlations of 250 km and 500 m) the correlation scales were about 20 km and 50 m. The scales actually used, though not dissimilar from these, were determined by the first method (Table 2).

Other parameters used in the objective mapping procedure included the extent of vertical averaging of the observations before gridding, and the grid sizes (Table 2). Velocity fields were calculated by simple first difference of the gridded specific volume

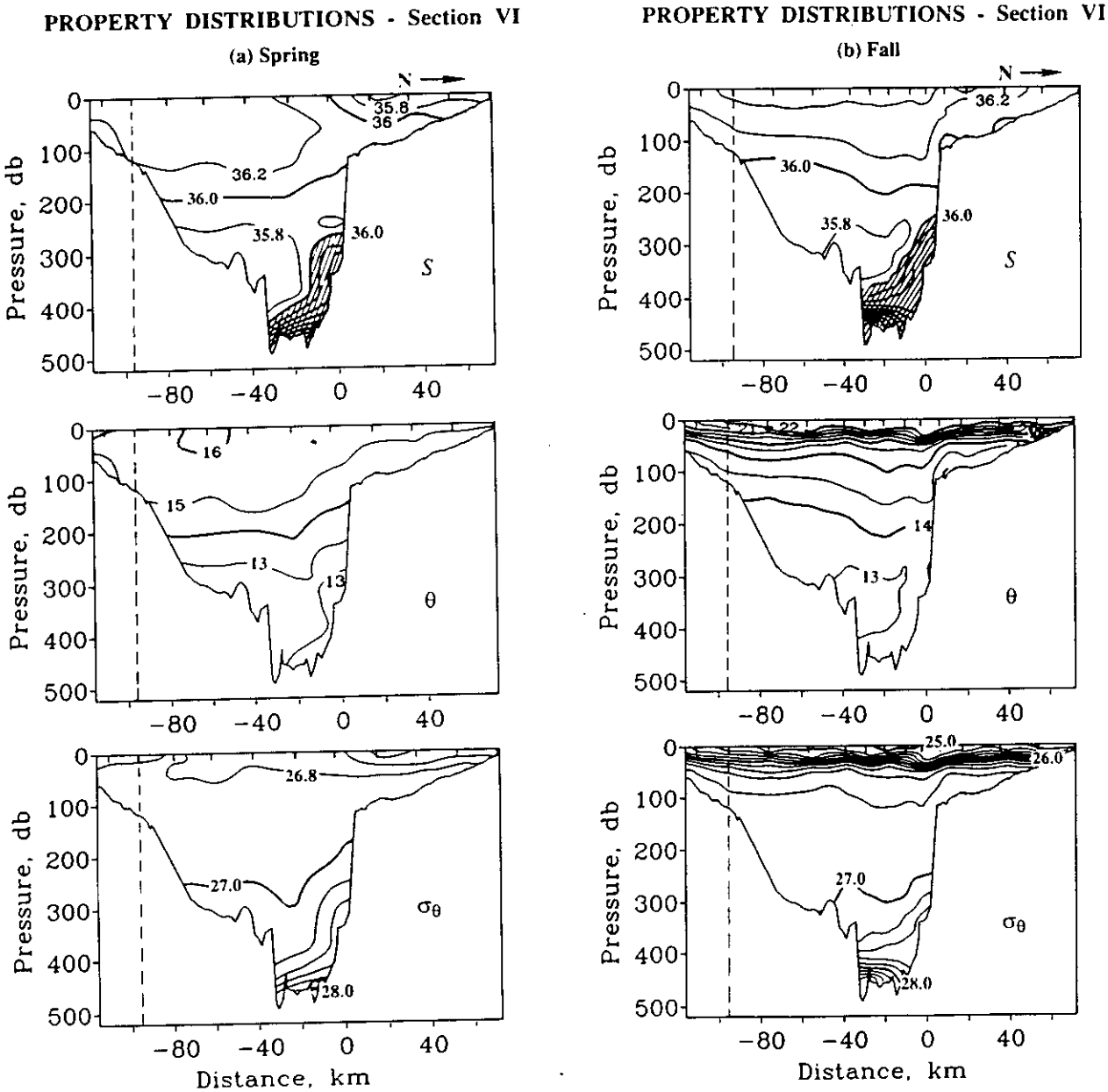

Fig. 2. Salinity, potential temperature, and potential density for section VI in (a) spring and (b) autumn. Station locations are noted by tick marks along the top of each plot. The vertical dashed line indicates the southwest corner of the section. The zero in distance along track corresponds to 36°N.

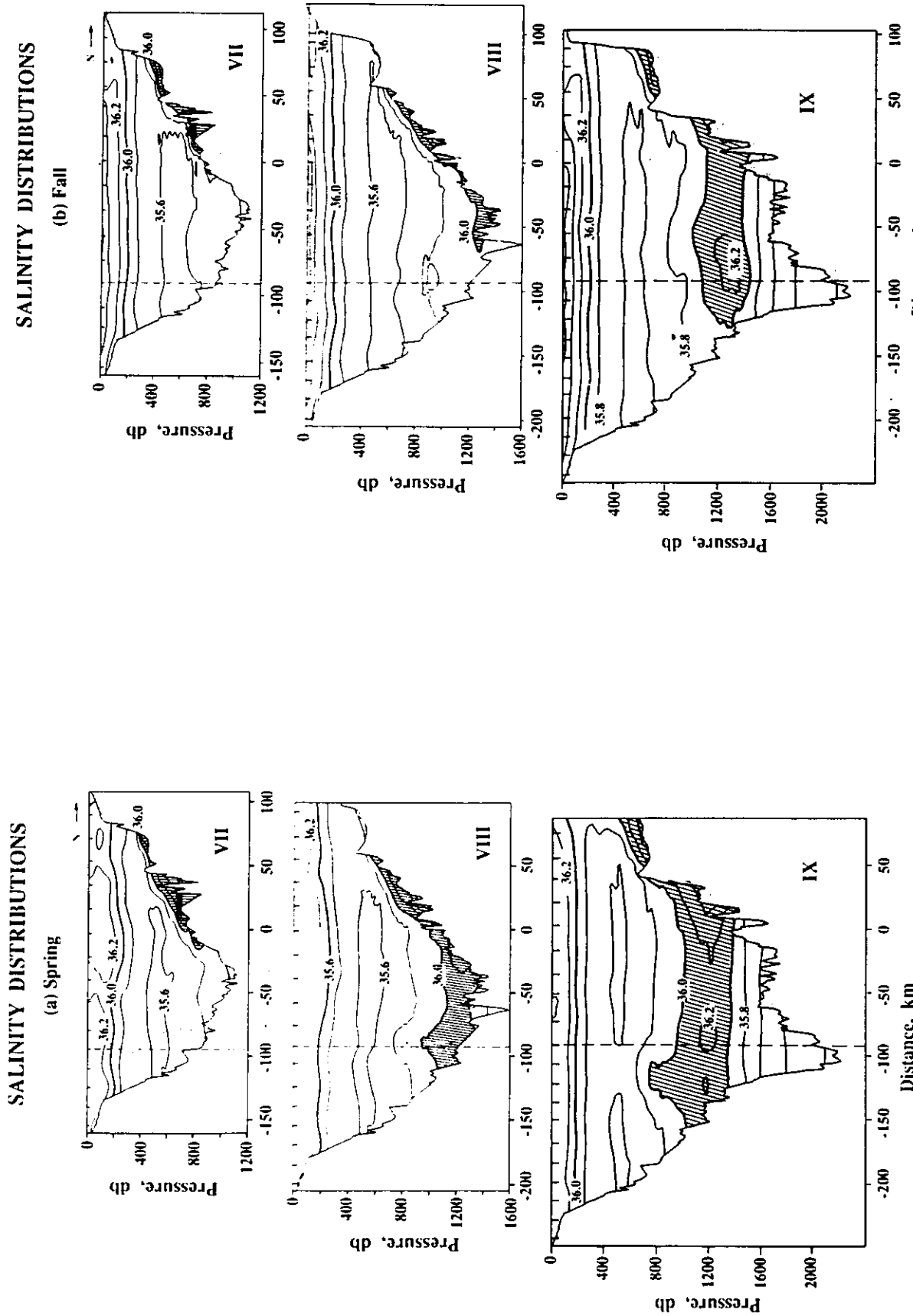

Fig. 3. Salinity for sections VII, VIII and IX in (a) spring and (b) autumn. Cross-hatching denotes salinity greater than 36‰, with density greater than 27 σ_θ. The vertical dashed line indicates the southwest corner of the section. The zero in distance along track corresponds to 36°N.

fields, subject to constraints, as described in the following section. The depth of the bottom was recorded at 5 min intervals while the ship was underway; this corresponds to two to four measurements per grid in the along-track direction. All calculations involving areas utilize this high-resolution bottom contour, with the depth at a given grid point taken to be the average of the depths observed. The distance along-track is adjusted so that the zero point lies at 36°N, even though the starting point of each section is the same station, marked by an asterisk in Fig. 1, at the coast of Africa. In all figures, sections run from south to north, as though the observer were looking toward the Atlantic from the Strait of Gibraltar.

4. VELOCITY FIELD ESTIMATES

4.1. *Formulation*

Five baroclinic estimates of the flow field in the Gulf of Cadiz are presented and compared in this paper. The different estimates will be labeled E0 to E4 for convenience of reference. By flow field we mean the component of the velocity field perpendicular to the vertical sections labeled VI–IX in Fig. 1. Note that some of the inflow across any of these sections may be outflowing through the same section without necessarily transiting the Strait of Gibraltar. Given the density field $\rho = \rho(y,z)$ inferred from the measured temperature and salinity fields (y and z north and upwards) and assuming hydrostatic and geostrophic balance in the direction perpendicular to the section, the vertical shear of the east component of the flow $u(y,z)$ is determined. This component can be expressed as

$$u(y,z) = v_{ref}(y) + u_b(y,z), \tag{3}$$

where v_{ref} may vary along a prescribed level defined by $z_{ref} = z_{ref}(y)$ and u_b is defined as

$$u_b(y,z) = \frac{g}{\rho_o f}\int_{z_{ref}}^{z} \frac{\partial \rho}{\partial y}\,dz. \tag{4}$$

Therefore,

$$\frac{\partial u}{\partial z} = \frac{g}{\rho_o f}\frac{\partial \rho}{\partial y}$$

and

$$v_{ref}(y) = u(y,z_{ref}). \tag{5}$$

Table 2. Objective mapping parameters

Section	Correlation length y/z		Error variance		Grid size		Vertical averaging interval (m)
	Large-scale (km m^{-1})	Small-scale (km m^{-1})	Large-scale	Small-scale	y (km)	z (db)	
VI	250/500	16/40	0.1	0.001	4	10	10
VII	500/500	16/40	0.1	0.001	4	10	30
VIII	500/500	16/40	0.1	0.001	4	10	40
IX	500/500	16/40	0.1	0.001	4	12	80

Here f is the Coriolis parameter and g is the gravitational acceleration. Equation (4) is the integrated version of the thermal wind equation and is the contribution derived directly from the observations. The lower limit of integration, z_{ref}, is called the level of no motion when $v_{ref} = 0$, and, in the more general case, simply the reference level.

All flow estimates satisfy the thermal wind equation and have zero instantaneous salt flux. It is assumed that there is a large exchange of salt with a negligibly small loss or gain. The constraint on the salt flux, $SF = 0$, is an integral constraint on the function v_{ref} because

$$SF \equiv \int_{y=0}^{y=L} \int_{z=-h(y)}^{z=0} \rho S u dz dy = 0 \tag{6}$$

with $h(y)$ the bottom contour. The mass flux (MF) is left unconstrained

$$MF \equiv \int_{y=0}^{y=L} \int_{z=-h(y)}^{z=0} \rho u dz dy. \tag{7}$$

Application of the integral constraint of zero net salt transport to the baroclinic or thermal wind calculation reduces the potentially large error in transport estimates which results from integrating a small error in the reference velocity over a large area. Sources of error in these estimates are discussed in Section 6.

4.2. *Flow fields and transports*

The problem of deducing the velocity field from hydrographic data has been addressed in a variety of ways over the past several decades. WUST's (1961) core method utilized the assumption that property tongues indicate the direction of low frequency flow. More recently, estimates by WORTHINGTON (1976) and by REID (1965) exploited more detailed water mass and nutrient distributions to deduce flow direction and hence the depth of z_{ref} and the magnitude of v_{ref}. Over the last decade, inverse theory formalism has been used, imposing extra constraints in order to choose a solution (ROEMMICH, 1980; RINTOUL, 1988; and others). While the techniques used here are inverse calculations, they are distinguished from more complex inverse problems by the very simple constraints used.

Typically, baroclinic calculations use z_{ref} as deep a reference level as is possible with a given set of observations, and assign a zero value to v_{ref}. Usually, this method results in near-surface velocities which are reasonable and often in good agreement with actual measured velocities. The Gulf of Cadiz data extend to the bottom, which would allow us to use the bottom as the reference level; however, that choice of z_{ref} results in net salt and mass transports into the Mediterranean Sea (3.5 Sv in section VI).

Another possible choice of reference level, other than the bottom, is the level corresponding to the interface between Mediterranean and Atlantic waters (BOYUM, 1963; AMBAR and HOWE, 1979b). Isolines of specific volume anomaly are used to define z_{ref}. Specific volume anomaly δ is defined as $[\alpha(S,T,p) - \alpha(35,0,p)] \times 10^5$, where α is specific volume, or $1/\rho$. Because potential density varies differently with pressure than does specific volume, the relationship between the two is a function of the distribution of temperature and salinity with depth. In Fig. 4 the relationship between δ and σ_θ for the deepest station from section VI is shown. In Fig. 5, σ_θ is plotted as a function of depth for the deepest station in each section. As an isoline of interest may well intersect the bottom (or the surface) at some sections, a computational scheme for extending z_{ref} beyond those

intersections is needed. The scheme used here simply sets z_{ref} to be the bottom in the first case and the surface in the second case. In section VI, $\delta = 100$ ($\sigma_\theta \sim 27.2$) defines the interface of the Mediterranean and Atlantic waters fairly accurately. The first flow field estimate, E0, is illustrated in Fig. 6, for section VI. The constraint of zero salt transport may be satisfied readily by choosing a constant value for v_{ref}:

$$v_{ref} = -\frac{\int\int \rho S u_b \mathrm{d}z\mathrm{d}y}{\int\int \rho S \mathrm{d}z\mathrm{d}y}; \tag{8}$$

this holds for arbitrary z_{ref} (see equations 3 and 6). Note in Fig. 2 the well-defined bottom layer of Mediterranean outflow, apparent in all property fields. The structure of the flow is similar in both cruises, although the second cruise has better spatial resolution in the region of the outflow. Transports through section VI are listed in Table 3.

The procedure of defining z_{ref} by δ guarantees the existence of a z_{ref} for which zero salt flux can be satisfied with $v_{ref} = 0$, i.e. a level of no motion. For the flow estimate E1, that level of no motion is found for each section. In Figs 7 and 8 the flow estimates E1–E4 through section VI are illustrated for spring and autumn, respectively. Transports are listed in Tables 4 and 5.

For the E2 flow estimate, consider the following definition of mass (ME) and (SE) exchanges:

$$(ME,SE) = \int\int \rho(1,S) u H(u) \mathrm{d}z\mathrm{d}y, \tag{9}$$

where $H(x) = 1$ if $x > 0$ and 0 if $x < 0$ (i.e. the step function) and the integral limits are the same as equation (6). ME and SE are the positive contributions of MF and SF, respectively. MF is very small compared with ME since a nearly equal but negative

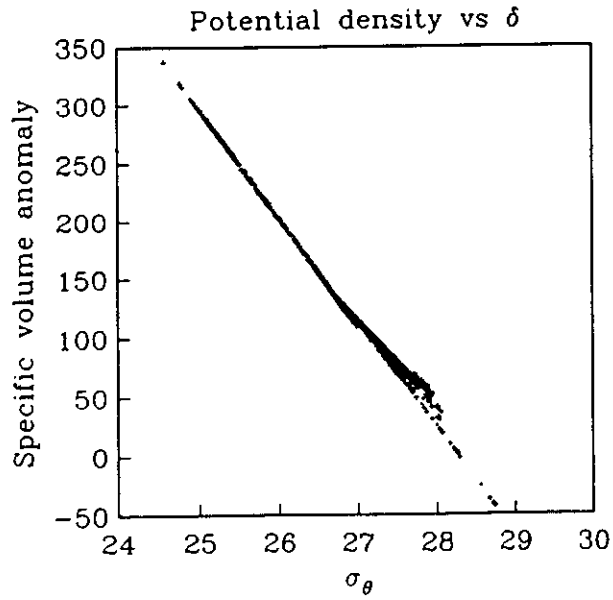

Fig. 4. Observed relationship between specific volume anomaly δ and potential density (σ_θ) for section VI. Dots correspond to spring cruise data and plus signs to autumn data.

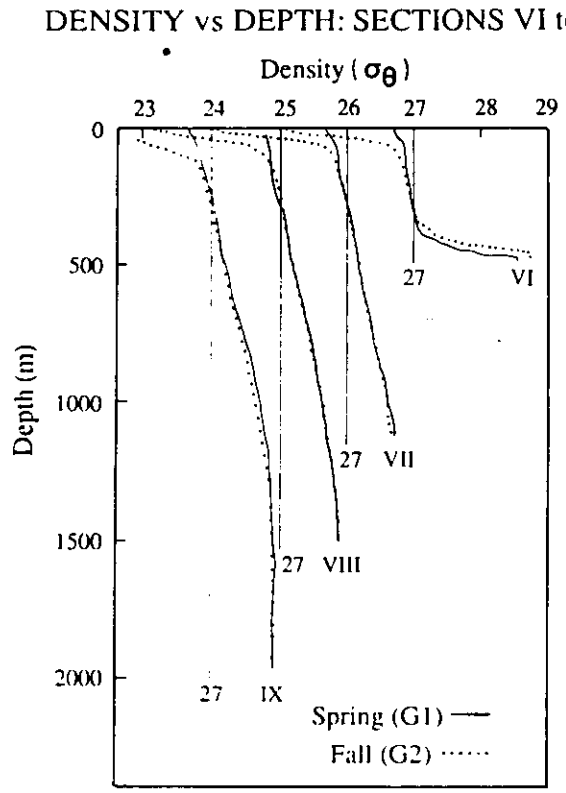

Fig. 5. Variation of σ_θ with depth for the deepest station in all four sections.

contribution is outflowing. The salt flux, SF, has been set to zero for all estimates. The following relationships can be written:

$$SE = \int\int \rho S(-u)H(-u)\mathrm{d}z\mathrm{d}y = \int\int \rho S|u|H(-u)\mathrm{d}z\mathrm{d}y = \tfrac{1}{2}\int\int \rho S|u|\mathrm{d}z\mathrm{d}y.$$

For each member of the z_{ref} family, v_{ref}, as defined in equation (8) is chosen, so that $SF = 0$, and a corresponding SE is calculated. Therefore, v_{ref} and SE vary as functions of z_{ref} (Fig. 9). E1 and E2 correspond to the cases when $v_{ref} = 0$, and when the minimum of SE are found, respectively.

The SE minima that define E2 are found with a prescribed set of levels, and do not necessarily represent the absolute minimum in SE possible within the given salinity and density structure. The fourth set of estimates, E3, represents the flow field consistent with equations (3)–(6), subject to the further requirement that SE is the absolute minimum (Fig. 10). Details of the mathematical procedure used to determine this minimum are given in Appendix A. Notice that estimates E2 and E3 are very similar (Tables 4 and 5).

Finally, estimates E4 are made subject to minimization of lateral roughness. This type of estimate is similar to various smoothing schemes used by other authors (ROEMMICH, 1980; PROVOST, 1986; RINTOUL, 1988). The roughness measure (RM) is a digital version of

$$RM = \int\int \left(\frac{\partial u}{\partial y}\right)^2 \mathrm{d}y\mathrm{d}z. \tag{10}$$

E4 is then the estimate with minimum horizontal recirculation. This minimization was chosen for its simplicity, as the inversion of a matrix needed to compute the solution can be

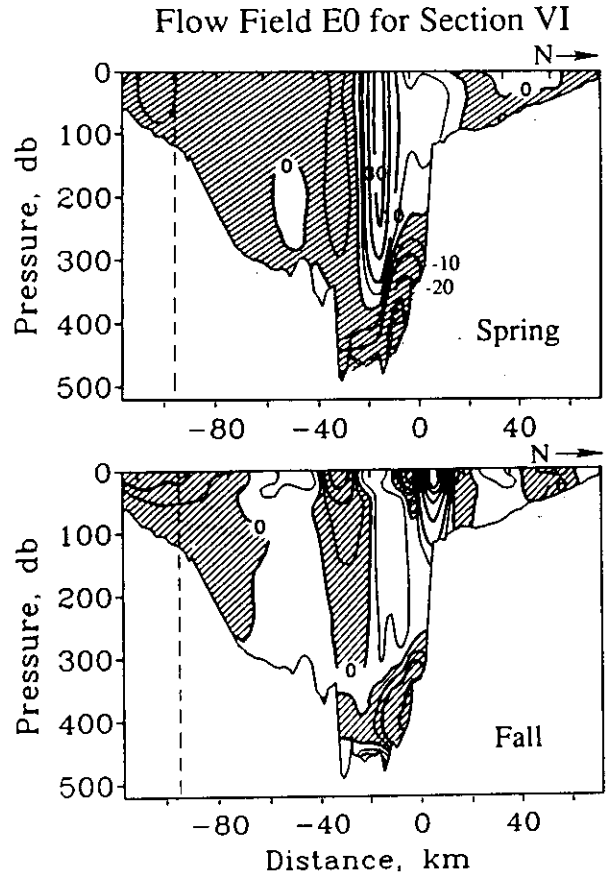

Fig. 6. The E0 estimate of the flow for section VI. In this estimate, the interface is used as a reference level and assumed to lie approximately along $\sigma_\theta = 27.2$ ($\delta = 100$ and $\delta = 110$ for spring and autumn, respectively). Cross-hatched areas in all flow maps represent outflowing regions (westward or southward flow). The vertical dashed line indicates the southwest corner of the section. The zero in distance along track corresponds to 36°N. Velocity units are cm s^{-1}.

Table 3. *Section* VI: *transport estimates from flow field* E0

	Spring	Autumn
δ_{ref}	100	110
v_{ref}	−1.6	+0.4
ME	1.2	0.9
MF	0.006	0.002
SE	42	34

MF and *ME* are the mass analogs to *SF* and *SE*, respectively (equations 6, 7 and 9). The units of *MF* and *ME* are 10^9 kg s^{-1} (the mass equivalent of Sverdrups = 10^3 kg $m^{-3} \times 10^6$ m^3 s^{-1}). Units of v_{ref} are cm s^{-1} and units of *SE* are 10^6 kg s^{-1} (assuming that salinity is essentially g of solutes per kg of seawater).

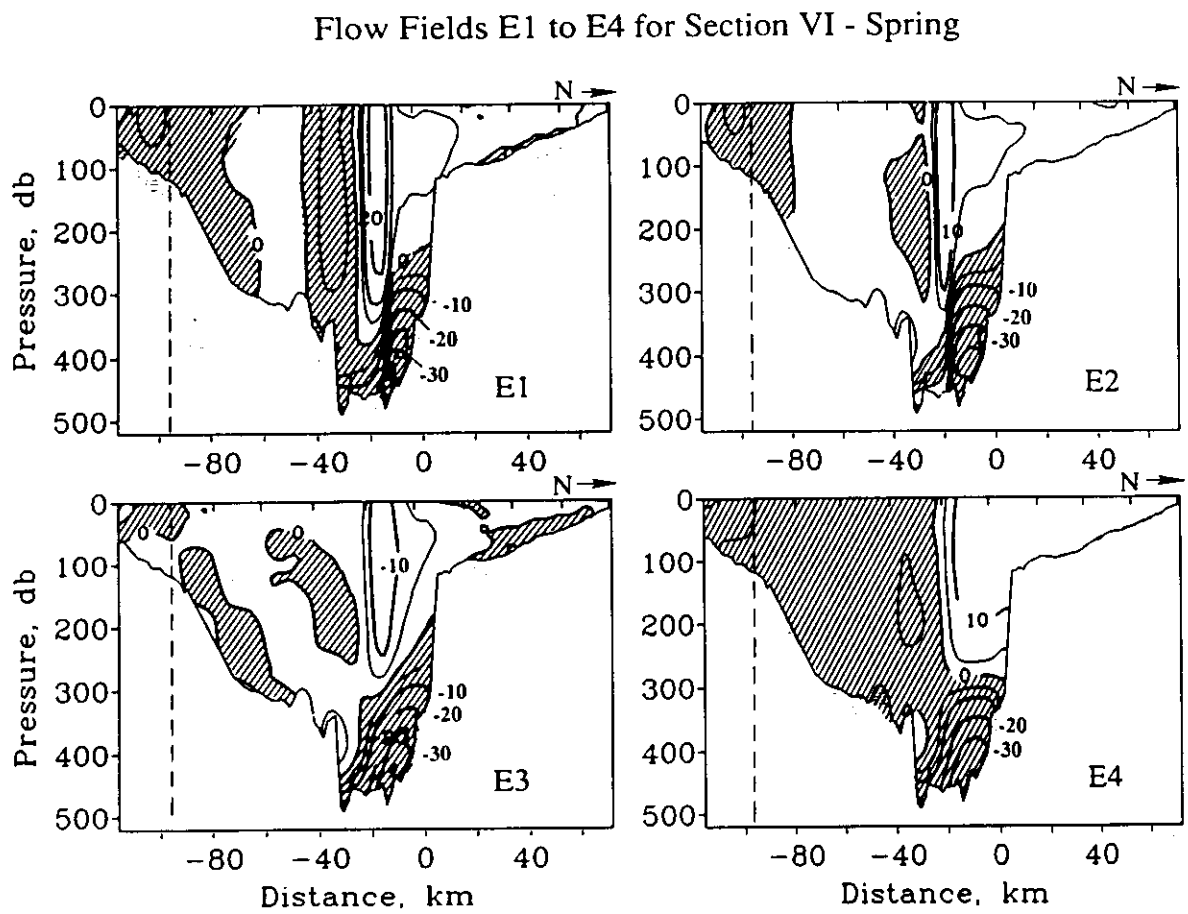

Fig. 7. Comparison of four flow estimates for section VI, in spring. Cross-hatched areas in all flow maps represent outflowing regions (westward or southward flow). The vertical dashed line indicates the southeast corner of the section. The zero in distance along track corresponds to 36°N. Velocity units are cm s^{-1}.

carried out recursively. It is also a close analog to the minimum kinetic energy, i.e. u instead of $\partial u/\partial y$ in equation (10), for a flat bottom, differing only by an arbitrary additive constant (RIPA, personal communication). The corresponding flow fields are illustrated in Fig. 11.

4.3. *Discussion of flow field estimates*

All estimates show the most intense westward flow coinciding with the most saline water for all sections, as expected for the Mediterranean outflow. The most intense inflow occurs above the saline outflow. This similarity in structure between different types of estimates is an indication of the robustness of the system. That is, the different extra constraints used do not change the result by much, even though, for instance, E3 is a lower bound on the possible salt exchange. Once the thermal wind equation and the conservation of salt are satisfied, the extra requirement imposed to choose a solution does not give very different results.

The constraint of zero salt flux results in a small mass flux (MF) for all estimates. This is positive in nearly all cases, and agrees in sign and magnitude with the excess of evaporation over precipitation inside the Mediterranean Sea, as discussed further in Section 5. The

observed increase in SE and ME away from the strait is consistent with the presence of both horizontal recirculation and entrainment or vertical recirculation (SMITH, 1975; AMBAR and HOWE, 1979b). As discussed in Section 2, ageostrophic effects near the strait may introduce errors in the baroclinically determined transport, and some of the observed increase in SE and ME will be attributed to that effect. In Section 5, it is argued that the observed flux of freshwater should not change as a function of distance from the strait if the outflow transport is accurately resolved. As will be seen, that flux does increase between sections VI and VIII, suggesting that the baroclinic transports through sections VI and VII underestimate the actual transport.

A significant difference between estimates E3 and E4 and the other estimates is that they are independent of the choice of z_{ref}. E0, E1 and E2 depend directly on a pre-established family of reference levels z_{ref}. The inclusion of z_{ref} in the formulation is based on the concept of a special surface: the level of no motion. The justification for a level of no motion as the interface between oppositely flowing water masses in E0 is fairly evident, but there is no simple way to establish the reference velocity in regions where the interface of Mediterranean and Atlantic waters has intersected the bottom of the ocean, and thus does not exist. The continuation through the bottom or the surface of δ isolines to define z_{ref} and the use of a constant v_{ref} is an implicit acceptance of the existence of special levels of motion. These notions are used in E0, E1 and E2 but not in E3 or E4.

For these baroclinic calculations, the minimization of SE makes sense only if SF is fixed. If SF were not constrained to be constant, the minimum SE defined by equation (9) would

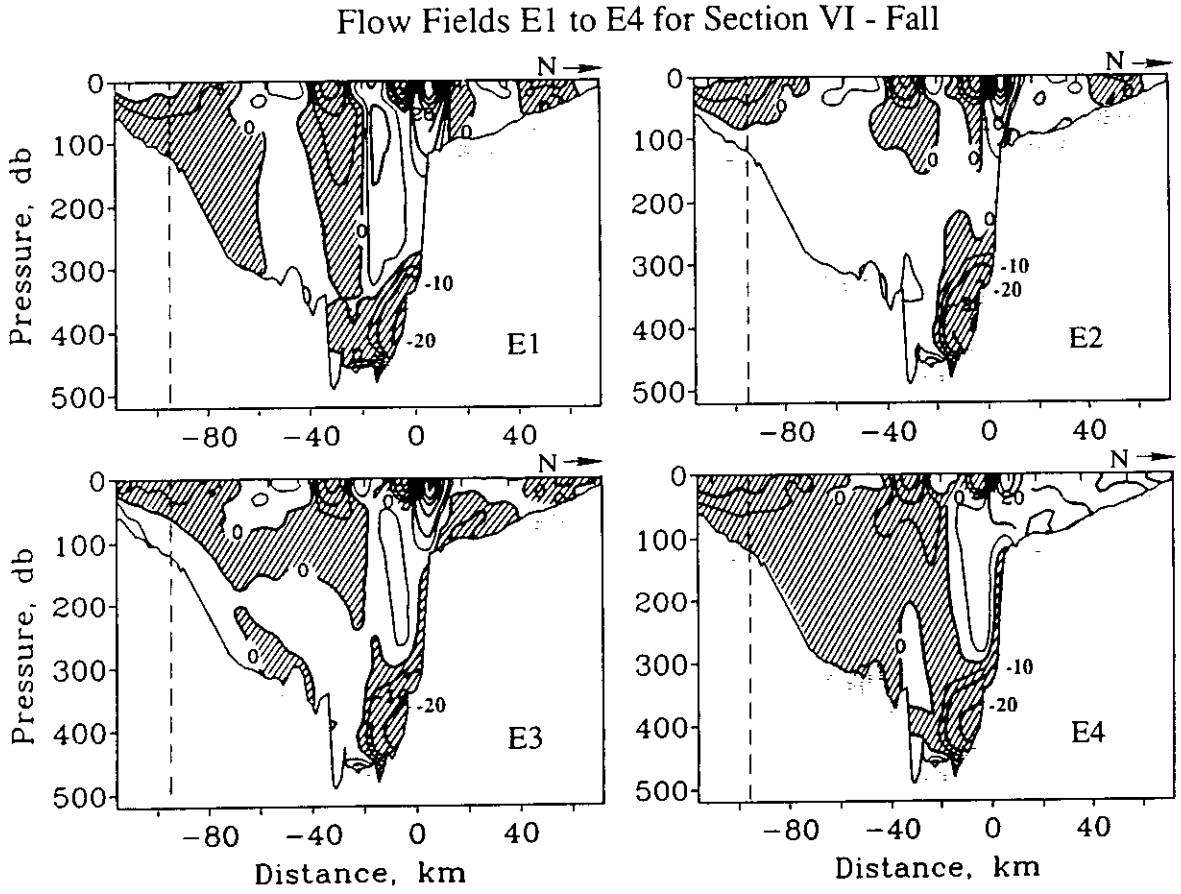

Fig. 8. Comparison of four flow estimates for section VI, in autumn (refer to caption of Fig. 7).

be zero and would not determine the flow field. The lower bound on SE represented by E3 offers a good reference to compare against other estimates.

5. FLUXES OF MASS, HEAT AND FRESHWATER

The flow fields presented in the previous section provide an estimate of the total transport in each direction through a given hydrographic section. Heat and freshwater fluxes may be calculated in integral form from the combination of temperature or salinity fields and the total velocity fields. The mass or volume transport associated with the outflow of Mediterranean water, however, is less than the mass exchange through a given section because of horizontal recirculation and entrainment. Before calculating the integral fluxes, a brief discussion of recirculation and entrainment is presented.

5.1. *Outflow transport, recirculation and entrainment*

The outflow transport of Mediterranean water is augmented by entrainment of Atlantic water into the outflow and by horizontal or along-isopycnal recirculations. In order to estimate the horizontally non-recirculating part of the total transport, the velocity within a density layer is integrated across the entire section. Potential density layers are used rather than depth surfaces because the interface changes depth significantly along a section, but the density defining the interface does not. The resultant transport is plotted as a function

Table 4. Spring cruise transports

		Section			
		VI	VII	VIII	IX
E1	δ_{ref}	106.8	91.2	85.8	93.5
	ME	1.04	4.2	6.3	7.75
	MF	0.007	0.009	0.029	0.06
	SE	37.5	152	225	278
E2	δ_{ref}	112	112.4	103	92
	v_{ref}	0.97	0.63	−0.09	0.62
	ME	0.88	3.47	5.06	7.72
	MF	0.008	0.020	0.037	0.06
	SE	32	125	182	277
E3	L^*	0.64	0.63	0.62	0.57
	ME	0.78	3.13	4.84	6.43
	MF	0.009	0.020	0.040	0.046
	SE	28	112	174	231
E4	ME	1.52	5.61	7.89	7.43
	MF	0.012	−0.0011	0.023	0.031
	SE	54.7	202	283	267

Refer to explanation of Table 3.
*L is the Lagrange multiplier (see Appendix A).

of layer density in Fig. 12. For comparison with the structure of potential temperature and salinity, those properties are averaged along density surfaces and plotted in Fig. 13. Transports in each layer are then summed into negative and positive bins over the water column, giving estimates of that part of the exchange that does not recirculate along density surfaces, designated U_ρ (Table 6). The difference between U_ρ and the total transport U (the volume equivalent to the mass exchange, ME) through each section is a measure of the horizontally recirculating transport U_H (Table 7). Through the outer sections VIII and IX, U_ρ is nearly constant at about 2 Sv, and much smaller than the total transport U.

That part of the total transport U contributed by entrainment, or cross-isopycnal recirculation, is more difficult to ascertain. One approach is to convert the observed outflow volume transport into an equivalent volume of "pure" Mediterranean water. The difference between the observed and pure outflow transports is then an estimate of the entrainment that has occurred in the distance from the source. As was done for the historical estimates, the salinity of Mediterranean waters is taken to be 38.4, and that of Atlantic water 35.6 for this calculation. The observed outflow transport of salt $(u_o S_o)$, integrated along isopycnals, is converted to a corresponding volume of pure Mediterranean water according to a variation of equation (1),

$$U_{med} = \frac{(\langle u_o S_o \rangle - U_\rho \times 35.6)}{(38.4 - 35.6)},$$

Table 5. Autumn cruise transports

		Section			
		VI	VII	VIII	IX
E1	δ_{ref}	106	97	91.6	90.3
	ME	0.96	3.0	5.9	6.7
	MF	0.001	0.002	0.02	0.004
	SE	34.7	106	215	241
E2	δ_{ref}	122	108	105	94
	v_{ref}	0.78	0.89	0.95	0.23
	ME	0.83	2.8	5.8	6.7
	MF	0.002	0.005	0.02	0.005
	SE	30.0	100	208	240
E3	L	0.59	0.62	0.58	0.54
	ME	0.75	2.60	5.2	6.0
	MF	0.002	0.007	0.03	0.01
	SE	27.3	93.2	189	215
E4	ME	1.40	4.2	7.4	7.25
	MF	0.0003	−0.011	0.008	0.001
	SE	32.8	151	266	260

Refer to explanation of Tables 3 and 4.

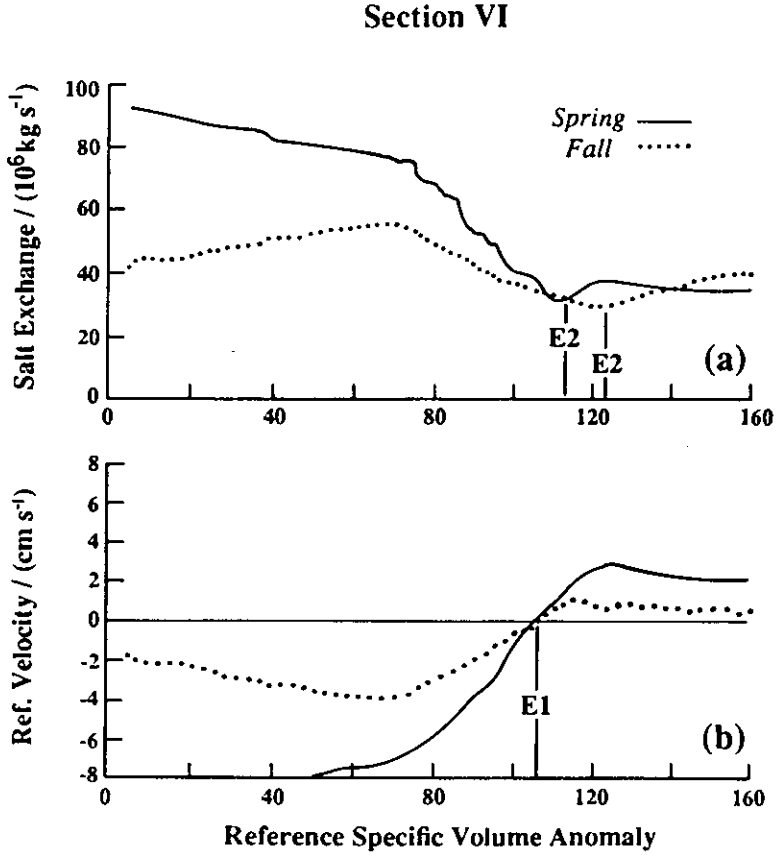

Fig. 9. (a) Salt exchange (SE) and (b) reference velocity (V_{ref}) computed as a function of specific volume anomaly δ for section VI, for both cruises. These curves illustrate the choices of reference level δ for estimates E1 and E2, as noted.

where $\langle\ \rangle$ indicate integration along density surfaces. The equivalent salinity of the observed outflow is taken to be:

$$S_{eq} = \frac{\langle u_o S_o \rangle}{U_p}.$$

U_{med} and S_{eq} are listed in Table 6. The difference between U_p and U_{med} is a measure of entrainment, U_{ent}, occurring between the source and a given hydrographic section. The change in U_{ent} from one section to the next is a measure of the entrainment occurring between those two sections (Table 7). In the outer sections, U_{ent} is fairly constant at 1.4–1.8 Sv, suggesting that most of the entrainment occurs east of section VIII (7°30′W). U_{ent} increases substantially between the source, section VI and section VII. For the inner sections entrainment is comparable to recirculation; for the outer sections recirculation along isopycnals is larger.

5.2. *Evaporation and freshwater fluxes*

The freshwater flux through the Strait of Gibraltar is equivalent to the difference in mass transported into the Mediterranean Sea and that transported out. This net transport of mass into the Mediterranean occurs in response to a net loss of moisture (water of zero salinity, hence "freshwater" flux) through evaporation. Freshwater flux may be formulated in terms of the difference between inflow and outflow transports, for a salt-

conserving flow field, or, equivalently, in terms of salinity difference between inflow and outflow for a volume-conserving velocity field. To illustrate the equivalence of these two formulations, consider the integral conservation equations

$$\int_A us\mathrm{d}A = 0 \tag{11}$$

and

$$\int_A u\mathrm{d}A = E. \tag{12}$$

These equations are often expressed in two-layer form as

$$V_i S_i - V_o S_o = 0$$
$$V_i - V_o = E,$$

with subscripts i and o representing inflow and outflow, respectively. Let average quantities $\bar{u}$ and $\bar{s}$ be defined by

$$\bar{u} = \frac{1}{A}\int_A u\mathrm{d}A = \frac{E}{A}$$

$$\bar{s} = \frac{1}{A}\int_s s\mathrm{d}A.$$

Then u is a salt-conserving flow field, satisfying equation (11), while $u' = u - \bar{u}$ is a volume-conserving field, satisfying $\int_A u'\mathrm{d}A = 0$. Rewriting equation in terms of $\bar{u}$ and $\bar{s}$:

$$\int_A (\bar{u} + u')(\bar{s} + s')\mathrm{d}A = 0$$

or

$$E = -\frac{1}{\bar{s}}\int_A u's'\mathrm{d}A. \tag{13}$$

Evaporation excess calculated using equation (12) is designated E_{MF} (Table 6), because it is actually the value of MF normalized by the area of the Mediterranean, and expressed in units of m y^{-1}. As can be seen in Tables 3–5, all but one of the observed estimates of MF are positive, and of the right amplitude to reflect the actual excess of evaporation over precipitation and runoff in the Mediterranean.

Evaporation excess calculated according to equation (13) is designated E and also listed in Table 6. The horizontally averaged salinity anomaly s' for each section is plotted as a function of depth in Fig. 14. New flow fields conserving volume rather than salt were used to calculate E, though with the same parameters and interface definition as estimate E0. (The interface is defined by $\delta = 100$ for sections VI and VII, and by $\delta = 110$ for sections VIII and IX.) It should be noted that these calculations utilize the total flow field; no averaging along isopycnals is involved. The maximum evaporation excess was that of section VIII during spring: 0.57 m y^{-1}. This value is lower than expected from climatological values of evaporation, but consistent with estimates by Bryden *et al.* (1989) using recent current measurements within the strait over the same time period. The low values of

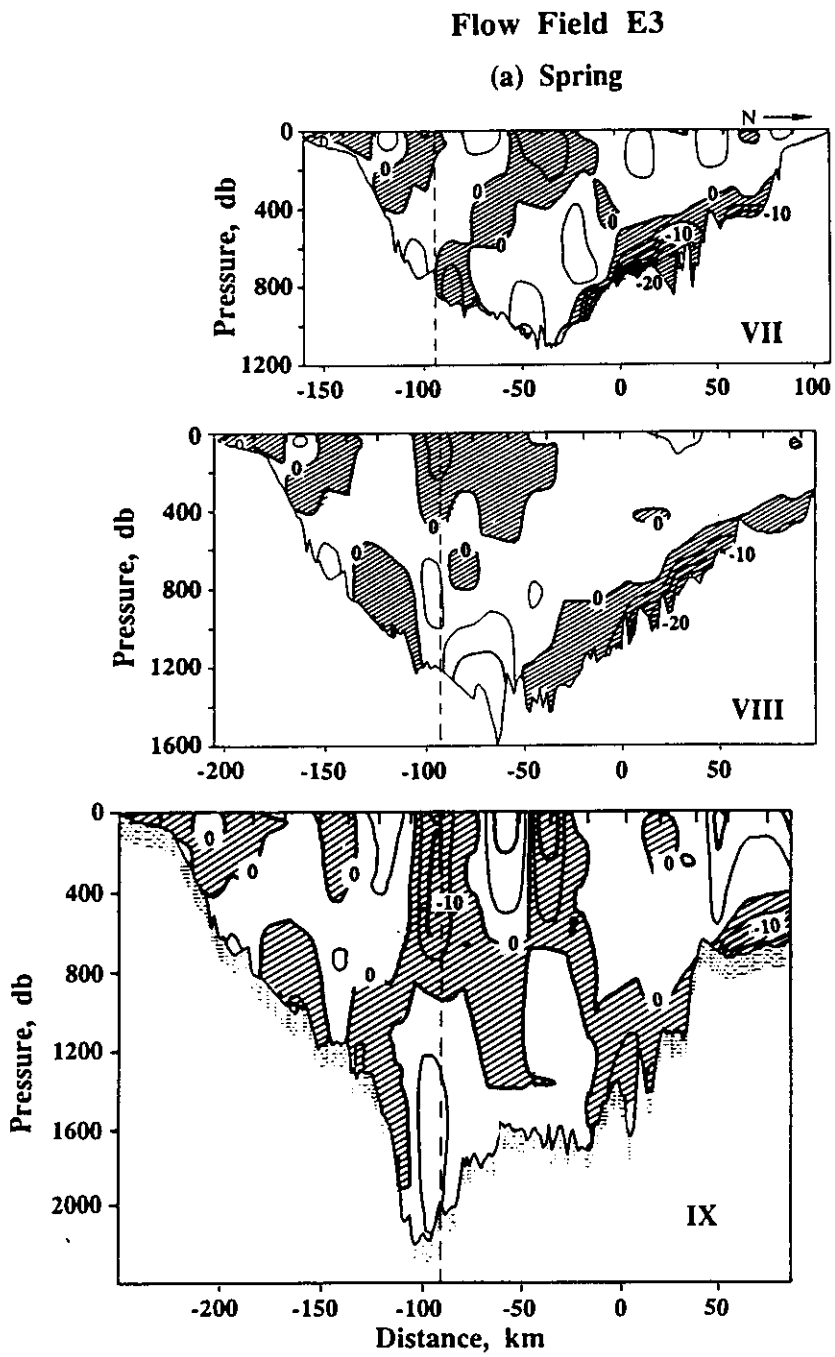

Fig. 10. The E3 flow estimate for sections VII, VIII and IX in (a) spring and (b) autumn. No other flow can satisfy the thermal wind equation, have $SF = 0$ and have a lower value of SE for the given salinity and density structure. Cross-hatched areas in all flow maps represent outflowing regions (westward or southward flow). The vertical dashed line indicates the southwest corner of the section. The zero in distance along track corresponds to 36°N. Velocity units are cm s^{-1}.

E from the inner sections VI and VII are consistent with the conclusion that transports through those sections are underestimated due to ageostrophic effects.

5.3. *Heat flux*

The heat balance of the Mediterranean interacts with the salt balance through evaporation, which contributes to both. Evaporation causes a heat loss from the surface of the

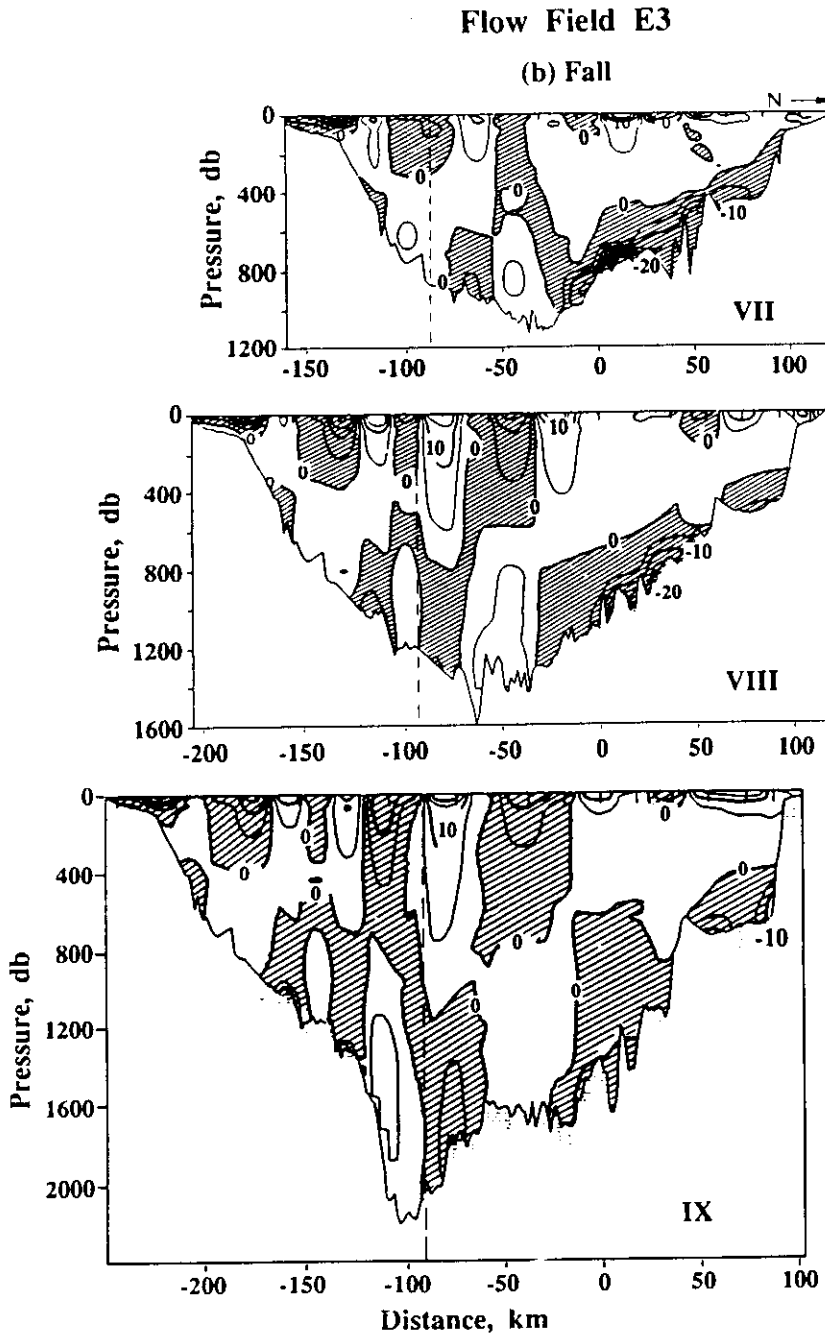

Fig. 10. *Continued.*

ocean, that may be balanced by other air–sea heat flux terms or by advection in the ocean. Attempts to infer the advective contribution to the heat balance by examining the residual of the air–sea fluxes has met with little success (BUNKER *et al.*, 1982) because the errors in the known flux terms are larger than the net air–sea flux. A direct estimate of advective flux (which should be equal and opposite to the net air–sea flux) from oceanic observations, while subject to errors, is still likely to be more accurate than the residual atmospheric calculation. In much the same way as the freshwater flux is calculated by integration over the area of each section, heat flux is given by:

$$Q_T = \int_A \rho C_p u' \theta' \mathrm{d}A.$$

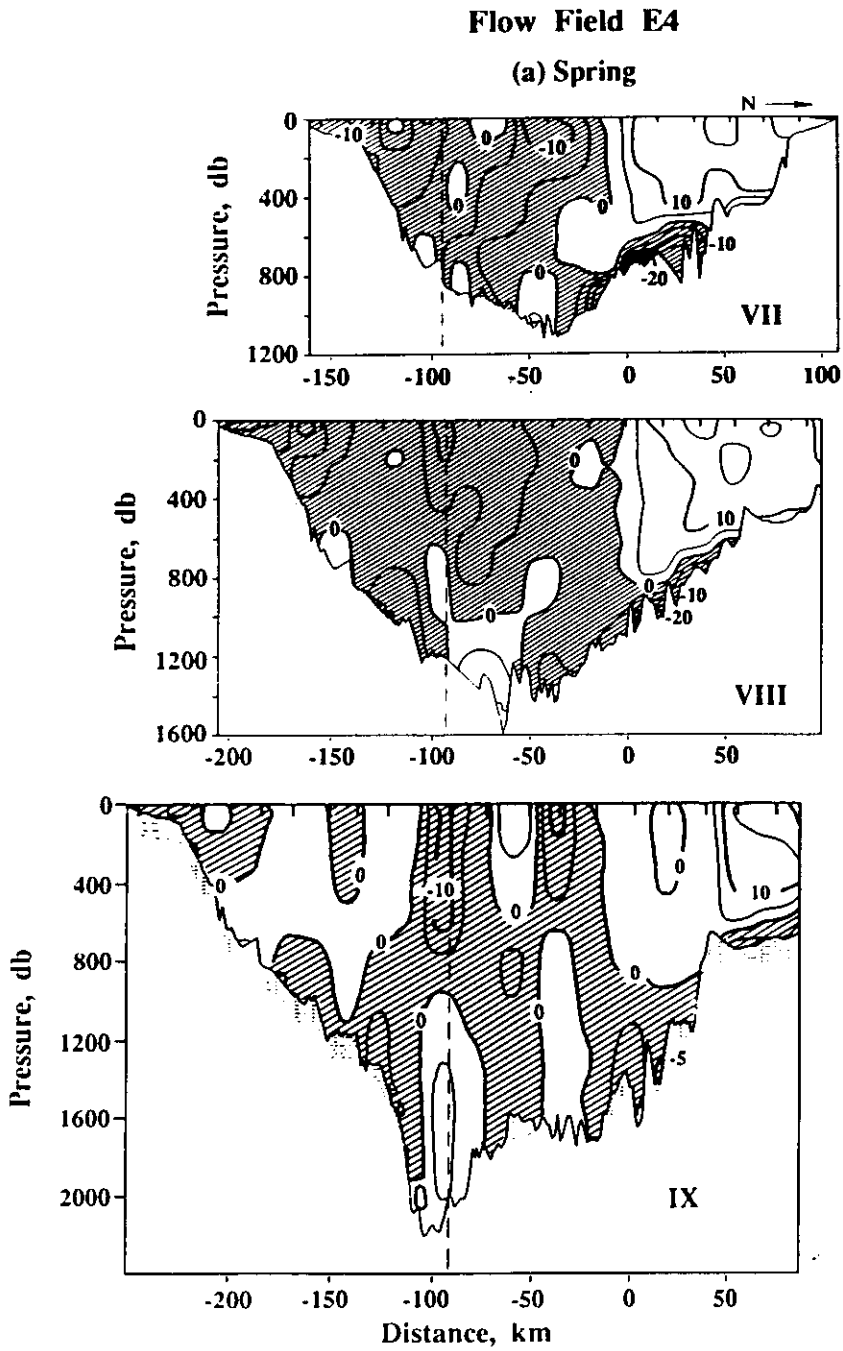

Fig. 11. The E4 flow estimate for sections VII, VIII and IX in (a) spring and (b) autumn. This estimate minimizes a measure of the horizontal shear, thereby smoothing the field laterally. Cross-hatched areas in all flow maps represent outflowing regions (westward or southward flow). The vertical dashed line indicates the southwest corner of the section. The zero in distance along track corresponds to 36°N. Velocity units are cm s^{-1}.

Again, flow fields conserving volume rather than salt were used to calculate heat flux (Table 6). The average potential temperature anomaly θ' is plotted in Fig. 14 as a function of depth, along with the average θ vs S relationship. Heat fluxes were larger in the autumn cruise sections than during spring, due primarily to surface warming. Again, fluxes calculated from the inner sections should be interpreted with caution. The average spring value for the outer sections was 2.2 W m^{-2}, and for autumn 6.0 W m^{-2}. These are within the range expected from climatological values.

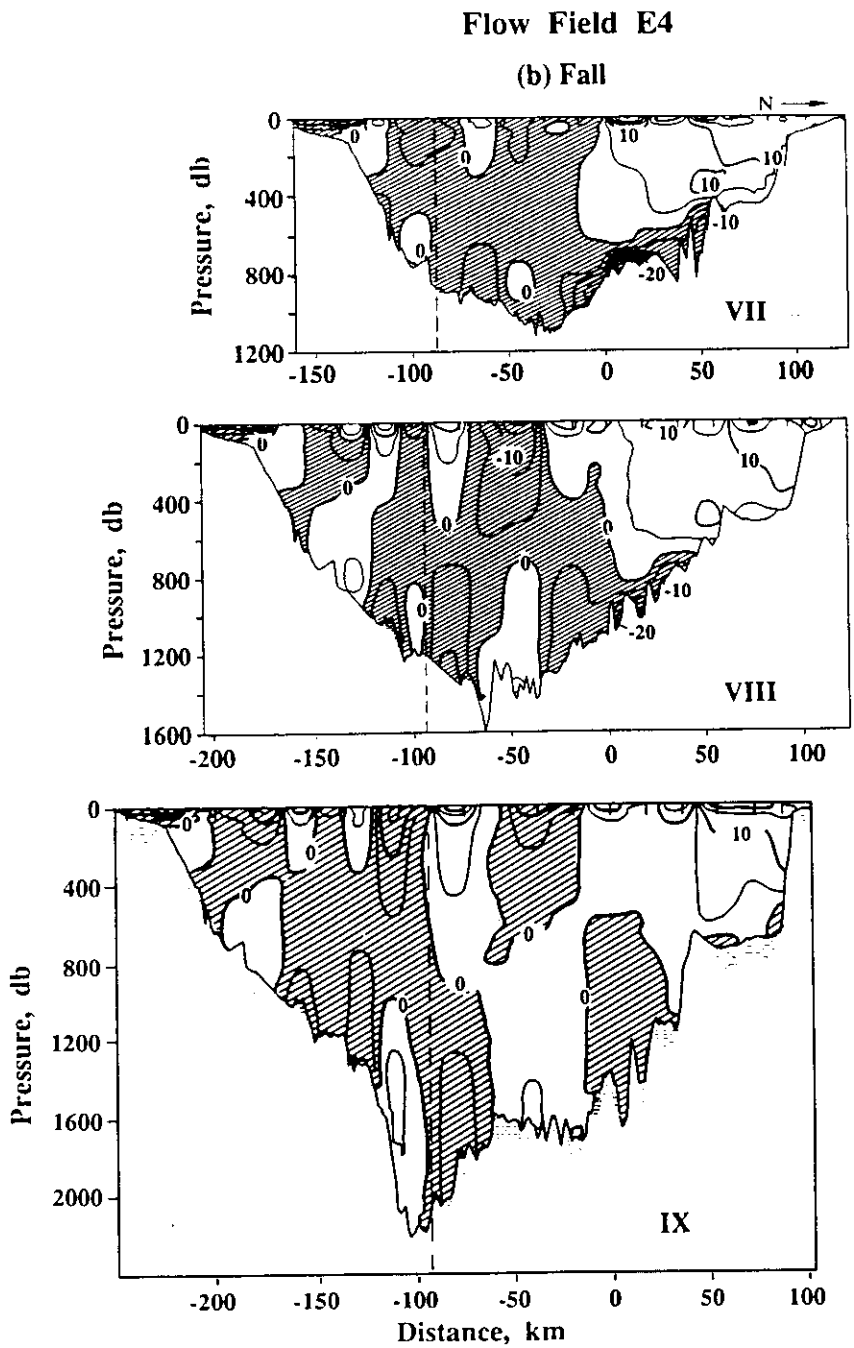

Fig. 11. *Continued.*

The contributions to volume transport, freshwater flux and heat flux at a given depth are illustrated in Fig. 15. Here the quantities u, $u's'$ and $u'\theta'$ are averaged along depth surfaces across the entire section. As expected, outflow is associated with a negative (out of the Mediterranean) salt transport and positive heat transport. While there is little contribution to the freshwater flux near the surface, a significant fraction of the heat flux is associated with the large temperature anomalies in the upper water column.

6. ERRORS

Errors in transport estimates made from hydrographic data are often difficult to assess, in good part because of the uncertainty in identifying the main causes of error. Errors in

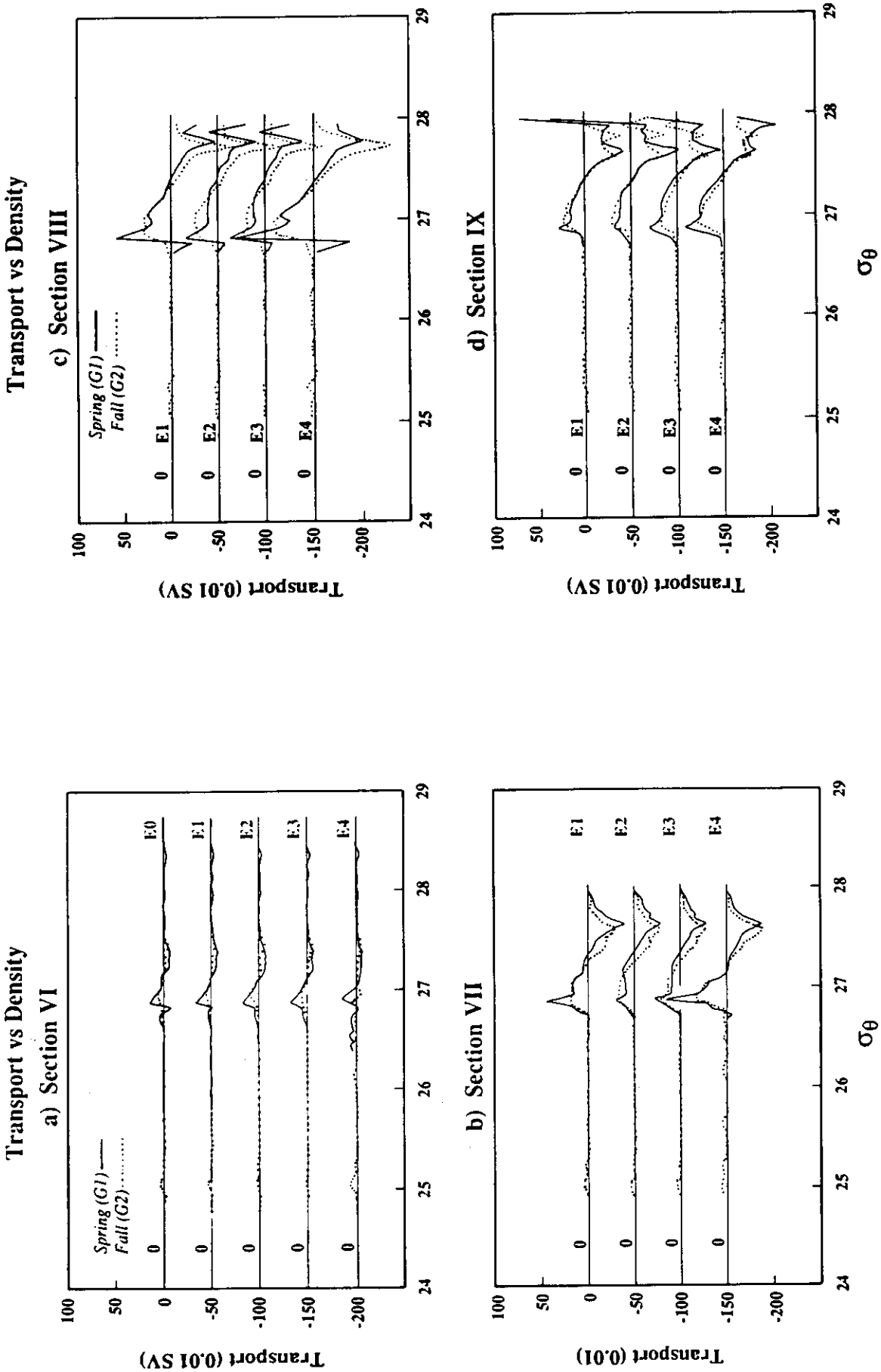

Fig. 12. Contributions to the non-recirculating transport U_ρ as a function of density: (a) section VI, estimates E0–E4; (b) section VII, estimates E1–E4; (c) section VIII, estimates E1–E4 and (d) section IX, estimates E1–E4. For all plots, the solid line corresponds to the spring cruise and the dashed line to the autumn cruise.

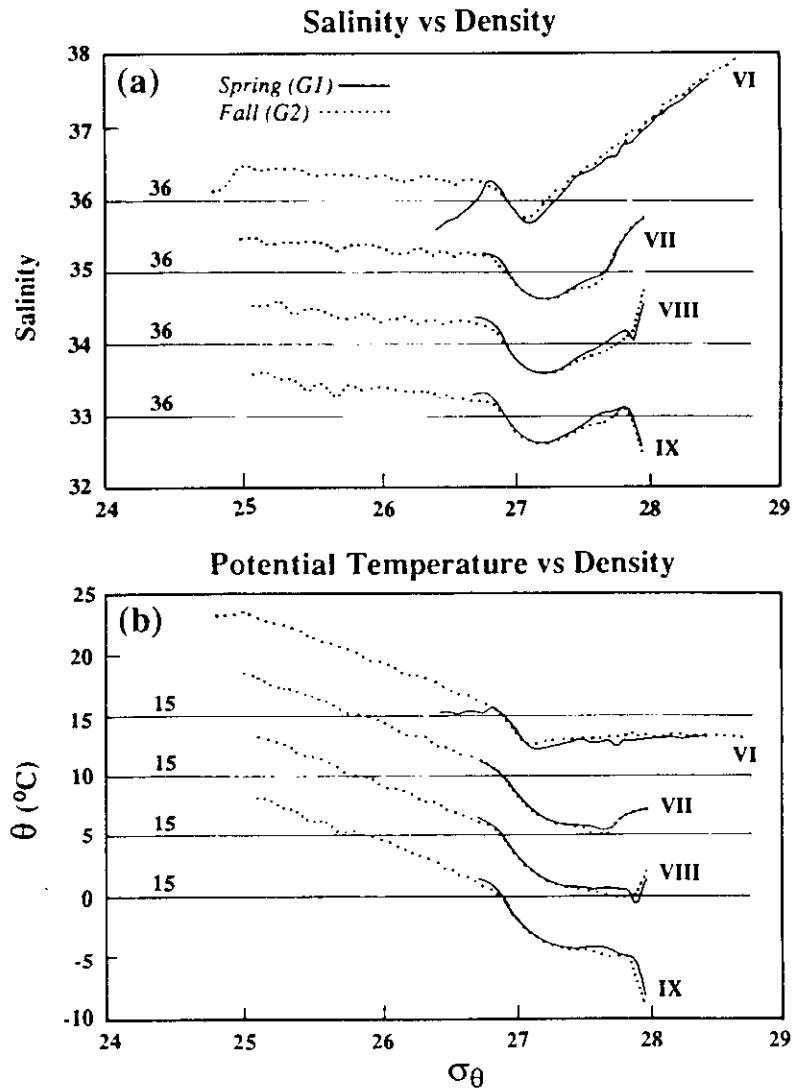

Fig. 13. Density-averaged (a) salinity and (b) potential temperature for sections VI–IX. Solid line is spring cruise, dashed is autumn cruise.

Table 6. Evaporation, heat flux and outflow transport

Season	Section	E (cm y^{-1})	E_{MF} (cm y^{-1})	Q (W m^{-2})	U (Sv)	U_p (Sv)	U_{med} (Sv)	S_{eq}
Spring	VI	15	11	1.4	1.01	0.67	0.21	36.537
	VII	28	20	−3.6	3.60	1.37	0.38	36.460
	VIII	57	41	3.0	5.32	2.00	0.62	36.564
	IX	48	62	1.5	7.09	2.09	0.70	36.553
Autumn	VI	−1	2	−0.2	0.91	0.44	0.10	36.466
	VII	10	6	9.2	2.78	1.53	0.28	36.129
	VIII	39	25	6.3	5.71	2.18	0.55	36.323
	IX	21	8	5.7	6.41	2.18	0.32	36.093

Evaporation and heat flux estimates assume an area of 2.5×10^6 km^2 for the Mediterranean Sea.

the instantaneous transport may be divided into two categories: those associated with the actual calculation of velocity from baroclinic shear and those associated with assuming that geostrophy holds. Whether a given instantaneous transport is representative of a longer term average is a separate issue, depending upon the natural variability of the system. Temporal variability is an "error" only if one wishes to claim that the results may be extended beyond the measurement period, or if significant variability occurs during the period of observation. Estimates of all three types of errors are presented in this discussion.

6.1. *Errors in converting shear to velocity*

The different flow field estimates use different constraints to convert vertical shear to absolute velocity. One measure of this error is then the variance of the different estimates. That variance is function of section as well as component of flow: the errors in the total flow through each section are larger than those for the density-averaged component U_ρ, and smaller for the pure Mediterranean water component U_{med} (Table 8). For the outer sections, VIII and IX, the error in the exchange U is about 0.5 Sv, in U_ρ about 0.25 Sv and in U_{med} about 0.15 Sv.

These errors ignore any barotropic component of the flow. While there are almost certainly barotropic flows in this region on time scales of a few days (CANDELA *et al.*, 1989), the mass balance of the Mediterranean Sea requires such flows not to persist for long, and eventually to reverse sign. Within the strait, correlations between the interface height and the direction of the barotropic flow result in a net contribution to the exchange. This interaction is unlikely to occur outside the geographically confined strait, and it is assumed that barotropic flows in the Gulf of Cadiz do not contribute to the exchange.

Table 7. Entrainment and horizontal recirculation transports

Season	Section	U_H $(U - U_\rho)$ (Sv)	U_{ent} $(U_\rho - U_{med})$ (Sv)	ΔU_H (Sv)	ΔU_{ent} (Sv)
Spring	VI	0.34	0.46		
				2.20	0.45
	VII	2.56	0.91		
				0.76	0.47
	VIII	3.32	1.38		
				1.68	0.01
	IX	5.00	1.39		
Autumn	VI	0.47	0.34		
				0.78	0.91
	VII	1.25	1.25		
				2.28	0.38
	VIII	3.53	1.63		
				0.70	0.23
	IX	4.23	1.86		

6.2. *Errors from assuming geostrophic balance*

In assuming that the velocity field is in geostrophic balance, a number of effects have been ignored, including friction, mixing and downslope flow. Of these the most significant is probably the latter, as discussed earlier in the paper.

Appendix B shows what is expected in the idealized model of a stream-tube flowing over a sloping bottom. Given the characteristics of the tube, including its shape, and the vertical section involved, the errors introduced for not having the section lie in the cross-stream

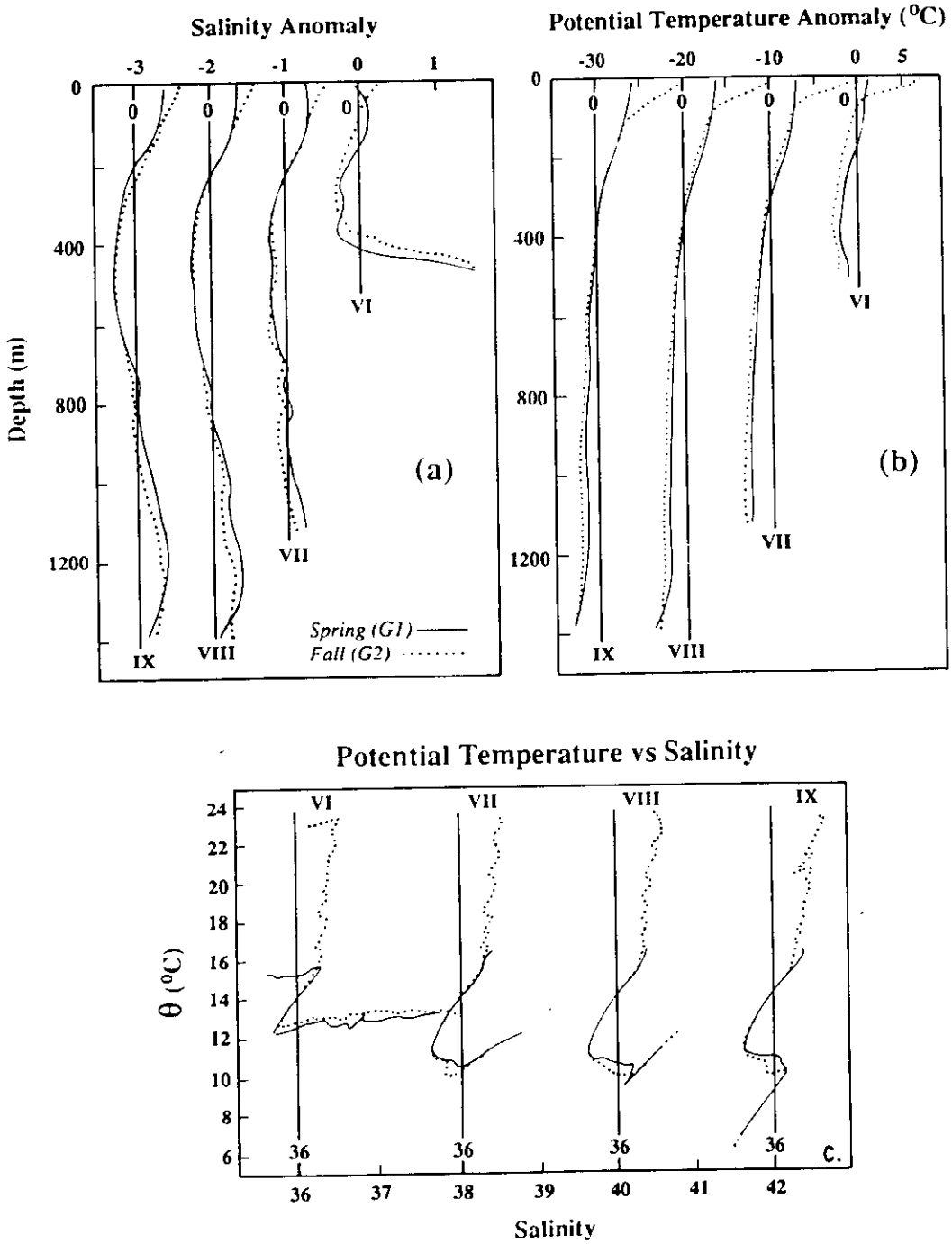

Fig. 14. Depth-averaged (a) salinity anomaly $(S - \bar{S})$, (b) potential temperature anomaly $(\theta - \bar{\theta})$, and (c) θ vs S for all four sections. Solid line corresponds to the spring cruise, dashed line to the autumn cruise.

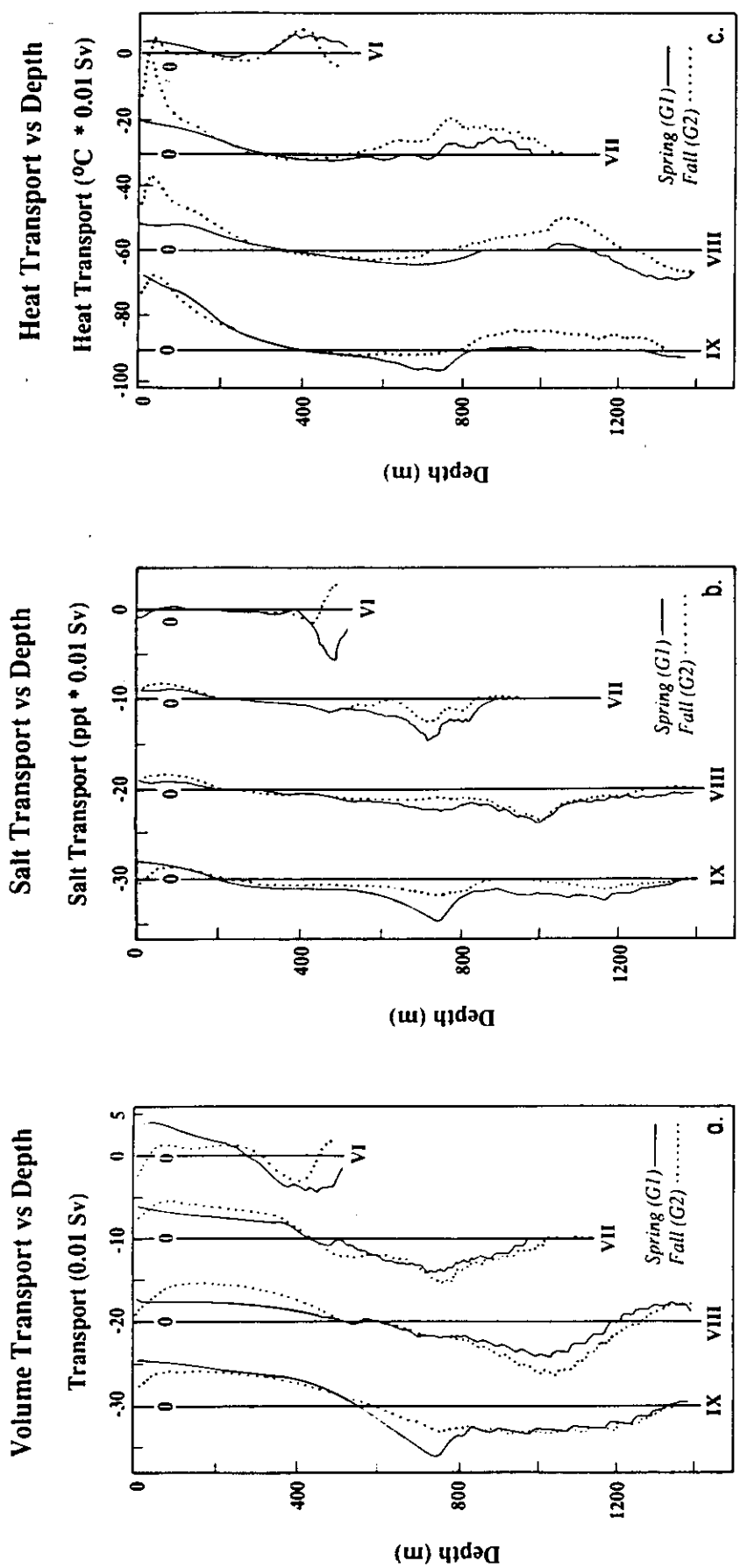

Fig. 15. Contributions to (a) volume transport, (b) salt transport and (c) heat transport (given in 0.001°C Sv), as a function of depth for all four sections. With $\rho = 10^3$ kg m^{-3} and $C_p = 4 \times 10^3$ J kg^{-1}, the heat transport implied by 1°C Sv is 4×10^{12} W. Solid line corresponds to the spring cruise, dashed line to the autumn cruise.

direction can be calculated analytically. These results cannot be applied straightforwardly to the measurements: if they could, they would become "corrections" rather than "errors." This because the model is very limited. Nevertheless, the model explains the cause and gives a good idea of the amplitude and sign of the error. This error is large in section VI: the actual values of *ME* and *SE* should be between two and four times larger than the values given in Tables 3 and 4, depending upon the values chosen for model parameters.

Another indication of the error in assuming geostrophic balance can be found in comparisons of direct current measurements with baroclinic shear from historical data. Observations taken in 1967 (MUSEUM, 1970), along 6°20'W and along 8°W, through the outflow, included hydrographic sections as well as short-term moored current measurements. Neither section was closed, and both were oriented north–south. Using the same parameters and reference levels as in the recent work, baroclinic velocities were calculated for these two sections, and compared with the current measurements corresponding to the time at which the closest station to the mooring was occupied. For the section closer to the strait, the deepest station was occupied four times during the current meter deployment; the comparison is the average of the four realizations. Near the strait, the average current meter velocity at 360 m was 0.80 ms^{-1}, while the average baroclinic velocity relative to the interface ($\delta = 100$) was 0.25 m s^{-1}, or an average of 0.55 m s^{-1} low. Far away from the strait, near the longitude of section IX of the present work, the baroclinic velocity at 850 m (in the outflow) was 0.10 m s^{-1}, while the current meter velocities varied between 0.10 and 0.25 m s^{-1}. Thus, near the strait, baroclinic transports may underestimate actual transports by something like 0.5 m s^{-1} times the area of the outflow, or as much as 1 Sv. However, observations sufficiently far from the strait indicate that the baroclinic transports accurately reflect the directly measured transports.

6.3. *Temporal variability in the outflow*

How representative of the climatological average exchange are these transports from two seasons of a single year? The temporal variability of the outflow near the strait is large, with maximum variance at M_2 tidal frequencies, and significant variance on synoptic

Table 8. Errors in flow fields: standard deviation over all estimates

Season	Section	$\langle U \rangle$ (Sv)	$\langle U_p \rangle$ (Sv)	$\langle U_{med} \rangle$ (Sv)
Spring	VI	0.29	0.07	0.03
	VII	0.98	0.32	0.07
	VIII	1.27	0.70	0.02
	IX	0.55	0.27	0.02
Autumn	VI	0.27	0.09	0.01
	VII	0.65	0.30	0.06
	VIII	0.81	0.65	0.03
	IX	0.48	0.23	0.04

weather time-scales of days to weeks (CANDELA *et al.*, 1989). Little is known about the seasonal and interannual variability (BORMANS *et al.*, 1986). How much of the high frequency variability is transmitted downstream into the Gulf of Cadiz is not known, though GRUNDLINGH (1981) reports tidal and 2–4 day variability in current meter records east of about 7°W (corresponding to section VII). He found that the tidal variations in current were smaller than those of isolated events of a few days' duration, when the current increased by 20–30 cm s^{-1} in the outflow. The increase in transport implied by these currents is in the order of 0.2–0.5 Sv, depending on the actual area of the outflow. A resonable estimate of the uncertainty in transport from a given section is, then, about 0.5 Sv due to temporal variability of the outflow.

6.4 *Errors in heat and freshwater fluxes*

Flux errors, like those in transport, can be estimated from the standard deviation over all formulations, including, for freshwater fluxes, all the E_{MF} estimates as well as E. For sections VI–IX, in spring, the error in evaporation excess is: 7, 12, 12 and 14 cm y^{-1}, and for autumn: 6, 10, 6 and 5 cm y^{-1}. The corresponding errors for heat flux are, for spring: 0.2, 2.0, 3.5 and 1.7 W m^{-2}, and for autumn: 0.2, 0.5, 2.0 and 1.0 W m^{-2}. These errors are very small compared to errors in meterological air–sea fluxes, probably unrealistically so.

An upper limit might be better estimated from the expected error in the exchange through each section multiplied by the observed salinity or temperature difference between the inflow and outflow. Given an exchange error of 0.5 Sv, a salinity difference of 1‰ and temperature differences of 2°C in spring and 4°C in autumn, this error would be 22 cm y^{-1} for evaporation excess, 3 W m^{-2} for flux in spring and about 6 W m^{-2}in autumn. These errors are probably more realistic than those estimated from the standard deviation over all estimates made. If they are correct, then the observed differences in evaporation and heat flux between the spring and autumn cruises are only marginally resolved. However, the consistency of heat flux estimates from these observations is encouraging, as air–sea fluxes derived from meterological data have proven less than satisfactory, even when calculated with the best available formulae for drag coefficients (BUNKER *et al.*, 1982). Because of the large uncertainties in air–sea estimates, it was not previously possible to identify seasonal variations in advective, or residual, heat flux.

7. DISCUSSION

Hydrographic data from four closed, north–south sections in the Gulf of Cadiz were used to estimate outflow transports from the Mediterranean, as well as advective heat and freshwater fluxes associated with the exchange of Atlantic and Mediterranean waters through the Strait of Gibraltar. Because there are an infinite number of absolute velocity fields that satisfy the thermal wind equation, additional constraints must be imposed in order to obtain an estimate of the velocity through a given section. Five different estimates of the flow field, utilizing three classes of constraints, were used to examine the sensitivity of the solution to the specific constraints chosen. Common to all five estimates are the thermal wind equation balance and zero salt flux through the section. The classes of additional constraints used were: (1) reference level chosen to coincide with the interface between Atlantic and Mediterranean water; (2) reference level chosen corresponding to observed minima in derived quantities, such as the minimum (in absolute value) of

uniform velocity required to satisfy the zero salt flux, or the level which results in the minimum observed one-way salt transport (salt exchange); and (3) generalized integral minimization of quantities such as $(\partial u/\partial y)^2$ (lateral roughness) or one-way salt transport, without specification of reference level. The velocity fields were calculated separately for each section. While it would be logical to incorporate all the sections into a single, three-dimensional calculation, the apparently ageostrophic character of the outflow near the strait argues against that approach.

Despite the physical and computational differences between the five estimates presented, the resultant flow fields, property fluxes and transports are remarkably similar. The authors interpret this consistency to mean that the geophysical system of water mass exchange between the Atlantic and Mediterranean is sufficiently well-defined and has a strong enough density signal associated with it that estimation of the absolute velocity field is relatively independent of the constraints imposed, so long as the basic requirements of geostrophic balance and zero salt flux are met.

This result is very encouraging for calculations of exchange through straits and, by implication, of air–sea fluxes over semi-enclosed seas from hydrographic observations. While current meter measurement of the low frequency exchange can be made, logistics are often difficult, precluding long-term measurements and measurements near the surface. Furthermore, the tidal frequency modulation of exchange, at least in the Strait of Gibraltar, is not resolved by direct observation of the current alone: the behavior of the interface at tidal frequencies must also be measured. Geostrophically determined transports outside the strait provide an alternate approach to making estimates of exchange and fluxes. Similarly, net air–sea fluxes deduced from meterological observations have larger errors than those estimated here for advective fluxes. This suggests that, for many semi-enclosed regions, the best seasonal or annual estimates of evaporation excess over precipitation and of net air–sea heat flux would be those made from correctly designed hydrographic surveys. The sections used must be far enough from the bathymetric constriction (strait or sill) that the flow is in geostrophic balance, and be occupied frequently enough to average out expected fluctuations in the observed exchange with periods of days to weeks.

Variations in transport, heat and freshwater fluxes with distance from the strait and with season were also examined. Integral property fluxes, as well as transport, increase with distance from the strait as far west as 7°30′. West of that section, fluxes are constant, though the total transport exchanged continues to increase. While transport is expected to increase downstream of the sill due to entrainment and recirculation, fluxes should be constant, as there are no significant sources or sinks of heat or salt in this region. Nevertheless, heat and freshwater fluxes from sections near the strait are much lower than expected from air–sea fluxes over the Mediterranean. Further west, the hydrographic estimates are comparable to climatological values, though somewhat lower. This apparent downstream increase in property fluxes is interpreted as resulting from the gradual adjustment of initially ageostrophic components of the outflow. Adjustment appears to occur as the outflow reaches its ambient density and begins to separate from the bottom: somewhere between 120 and 160 km from the strait. Fluxes estimated from sections at 160 and 200 km downstream are comparable, as would be expected if the flow had adjusted fully at 160 km. Thus, under the criteria outlined above for a well-designed survey to identify exchange, only the outer two sections would satisfy the constraint of geostrophic balance.

The non-recirculating transport through the westernmost two sections was the same for both cruises: 2.2 (±0.2) Sv. The estimated transport of "pure" Mediterranean water was 0.77 (±0.1) Sv in spring and 0.43 (±0.1) in autumn. The errors noted reflect the standard deviation of different transport estimates for a given realization. Natural variability of the outflow contributes at least a further 0.5 Sv to the uncertainty of the mean. Evaporation inferred from freshwater fluxes through those same sections was 0.53 (±0.2) m y^{-1} in spring and 0.30 (±0.2) m y^{-1} in autumn. Heat fluxes, on the other hand, were higher in autumn 6 (±6) W m^{-2}, as opposed to 2.2 (±3) W m^{-2} in spring, due to summertime surface warming that increases the temperature difference between inflow and outflow.

Acknowledgements—This work was supported under ONR contract N00014-85-C-0407. José Ochoa was supported on sabbatical leave from CICESE during the preparation of the manuscript and was supported under N00014-85-C during the revision of the paper. Special thanks are due to Mike Clark for his careful and artistic preparation of the figures, to Joan Semler for typing the manuscript, and to Clinton Winant, Julio Candela, and Dean Roemmich for discussion and criticism which materially improved the paper. The detailed and constructive comments on the original manuscript from Henri Lacombe, Walter Zenk and an anonymous reviewer are gratefully acknowledged. We also acknowledge the discussions, comments and ideas given by participants in two meetings; the Seminario Sobre la Oceanografía Física del Estrecho de Gibraltar (October 1988, Madrid) organized by J. L. Almazán, H. Bryden, T. Kinder and G. Parilla; and the workshop on the Gulf of Cadiz (October 1989, WHOI) organized by M. Kennelly, T. Sanford and J. Price.

REFERENCES

AMBAR I. (1983) A shallow core of Mediterranean Water off western Portugal. *Deep-Sea Research*, **30**, 677–680.

AMBAR I. and M. R. HOWE (1979a) Observations of the Mediterranean outflow—I. Mixing in the Mediterranean outflow. *Deep-Sea Research*, **26**, 535–554.

AMBAR I. and M. R. HOWE (1979b) Observations of the Mediterranean outflow—II. The deep circulation in the vicinity of the Gulf of Cadiz. *Deep-Sea Research*, **26**, 555–568.

BETHOUX J. P. (1979) Budgets of the Mediterranean Sea. Their dependence on the local climate and on the characteristics of the Atlantic waters. *Oceanologica Acta*, **2**, 157–163.

BETHOUX J. P. (1980) Mean water fluxes across sections in the Mediterranean Sea, evaluated on the basis of water and salt budgets and of observed salinities. *Oceanologica Acta*, **3**, 79–88.

BORMANS M., C. GARRETT and K. TOHMPSON (1986) Seasonal variability of the surface inflow through the Strait of Gibraltar. *Oceanologica Acta*, **9**, 403–414.

BOYUM G. (1963) Hydrology and currents in the area west of Gibraltar. Results from the "Helland-Hansen" Expedition, May–June 1961, NATO no. 7. Geophysical Institute, Bergen.

BOYUM G. (1967) Hydrology and currents in the area west of Gibraltar. Results from the "Helland-Hansen" Expedition, May 1965, NATO no. 36, Geophysical Institute, Bergen.

BRAY N. A. (1986) Gibraltar experiment CTD data report: March–April 1986, U.S.N.S. *Lynch*, Scripps Institution of Oceanography Reference Series no. 86-21, 212 pp.

BRAY N. A. (1988) Thermohaline circulation in the Gulf of California. *Journal of Geophysical Research*, **93**, 4993–5020.

BRAY N. A. and H. LACOMBE (in preparation) Tidal modulation of water mass exchange in the Strait of Gibraltar.

BRYDEN H. L., E. C. BRADY and R. D. PILLSBURY (1989) Flow through the Strait of Gibraltar. In: *Seminario sobre la oceanografia fisica del estrecho de Gibraltar, Madrid, 24–28 Octubre* 1988, J. L. ALMAZAN, H. BRYDEN, T. KINDER and G. PARRILLA, editors, SECEG, pp. 166–194.

BRYDEN H. L. and R. D. PILLSBURY (1989) Measurement of the flow through the Strait of Gibraltar. *Advances in Water Resources*, **13**, 64–69.

BUNKER A. F. (1976) Wintertime interactions of the atmosphere with the Mediterranean Sea. *Journal of Physical Oceanography*, **2**, 225–238.

BUNKER A. F., H. CHARNOCK and R. A. GOLDSMITH (1982) A note on the heat balance of the Mediterranean and Red Seas. *Journal of Marine Research*, **40**, supplement, 73–84.

CANDELA J., C. D. WINANT and H. L. BRYDEN (1989) Meteorologically forced subinertial flows through the Strait of Gibraltar. *Journal of Geophysical Research*, **94**, 12,667–12,679.

CARTER D. B. (1956) The water balance of the Mediterranean and Black Seas. Publication in Climatology, Centerton, New Jersey, Dresel Institute of Technology, Laboratory of Climatology, **9**, 123–175.

CRÉPON M. (1965) Influence de la pression atmospherique sur le niveau moyen de la Méditerranée Occidentale et sur le flux à travers le détroit de Gibraltar. *Cahiers Oceanographiques*, **1**, 15–32.

FOFONOFF N. P. and R. C. MILLARD (1983) Algorithms for computation of fundamental properties of sea-water, *UNESCO Technical Papers in Marine Science*, **44**, 53.

GELFAND I. M. and S. V. FOMIN (1963) *Calculus of Variations*. Prentice-Hall, Englewood Cliffs, New Jersey, 232 pp.

GRUNDLINGH M. L. (1981) On the observation of a solitary event in the Mediterranean outflow west of Gibraltar, *Meteor Forsch.-Ergebnisse A/B*, No. 23, 15–46.

HOWE M. R. (1982) The Mediterranean water outflow in the Gulf of Cadiz. *Oceanography Marine Biology Annual Review*, **20**, 37–64.

KINDER T. H. and G. PARRILLA (1987) Yes, some of the Mediterranean outflow does come from great depth. *Journal of Geophysical Research*, **92**, 2901–2906.

LACOMBE H. and J.-C. LIZERAY (1959a) Sur le regime des courants dans le detroit de Gibraltar, Extrait des *Comptes rendus des séance de l'Academie des Sciences*, **248**, 2502–2504.

LACOMBE H. and J.-C. LIZERAY (1959b) Sur une cause des variations du niveau moyen de la Mediterranee et du regime du detroit de Gibraltar, Extrait des *Comptes rendus des séance de l'Academie des Sciences*, **249**, 734–736.

LACOMBE H. and P. TCHERNIA (1972) Caracteres hydrologiques et circulation des eaux en Mediterranee. In: *The Mediterranean Sea: a natural sedimentation laboratory*, D. J. STANLEY, editor, Dowden, Hutchinson and Ross, Standsburg, PA, pp. 25–30.

LACOMBE H., J. C. GASCARD, J. GONELLA and J. P. BETHOUX (1981) Response of the Mediterranean to the water and energy fluxes across its surface, on seasonal and interannual scales. *Oceanologica Acta*, **4**, 247–255.

LACOMBE H., P. TCHERNIA and L. GAMBERONI (1985) Variable bottom water in the western Mediterranean basin. *Progress in Oceanography*, **14**, 319–338.

MADELAIN F. (1970) Influence de la topographie du fond sur l'ecoulement Mediterraneen entre le detroit de Gibraltar et le cap Saint-Vincent. Extrait des *Cahiers Oceanographiques*, **22**, 43–61.

MUSEUM (1970) Bulletin d'information du Comite Central d'Oceanographie et d'Etude des Cotes. *Cahiers Oceanographiques*, supplement **1**, 90 pp.

NIELSON J. N. (1912) Hydrography of the Mediterranean and adjacent waters. Report on the Danish Oceanographic Expedition 1908–1910, vol. 1, 77–191.

PROVOST C. (1986) The variational inverse method for the general circulation in the ocean. In: *Variational methods in geosciences*, Y. K. SASAKI, editor, Elsevier, Amsterdam, pp. 55–70.

REID J. L. Jr (1965) Intermediate waters of the Pacific Ocean. The Johns Hopkins Oceanographic Studies, **2**, 85 pp.

REID J. L. (1979) On the contribution of the Mediterranean Sea outflow to the Norwegian–Greenland Sea. *Deep-Sea Research*, **26**, 1119–1223.

REID J. L. and R. J. LYNN (1971) On the influence of the Norwegian–Greenland and Weddell seas upon the bottom waters of the Indian and Pacific oceans. *Deep-Sea Research*, **13**, 1063–1088.

RINTOUL S. (1988) Mass heat and nutrient fluxes in the Atlantic Ocean determined by inverse methods. WHOI–MIT Joint Program, Ph.D. Thesis, 287 pp.

ROEMMICH D. H. (1980) The application of inverse methods to problems in ocean circulation. Ph.D Thesis MIT/WHOI, WHOI-80-6, 193 pp.

ROEMMICH D. (1983) Optimal estimation of hydrographic station data and derived fields. *Journal of Physical Oceanography*, **13**, 1544–1549.

SCHOTT G. (1915) Die Geswasser des Mittelmeeres. *Annalen der Hydrographie und Maritimen Meteorologie*. Deutsche Seewarte, 63–79.

SCHOTT G. (1928) Die Wasserbewegungen im Gebiete der Gibraltarstrasse. *Journal du Conseil International pour l'Exploration de la mer*. Vol. III, No. 2, Copenhagen, September.

SHULL S. and N. A. BRAY (1989) Gibraltar Experiment CTD Data Report II. Scripps Institution of Oceanography Reference Series no. 89-23, 258 pp.

SMITH P. C. (1975) A streamtube model for bottom boundary currents in the ocean. *Deep-Sea Research*, **22**, 853–873.

SVERDRUP H. U., M. W. JOHNSON and R. H. FLEMING (1942) *The oceans, their physics, chemistry and general biology*. Prentice-Hall, Englewood Cliffs, New Jersey, 1087 pp.

SWALLOW J. C. (1969) A deep eddy off Cape St Vincent. *Deep-Sea Research*, Supplement to **16**, 285–295.

TIXERONT F. (1970) Le bilan hydrologique de la Mer Noire et de la Méditerranée. *Cahiers Oceanographiques*, **22**, 227–237.

WORTHINGTON L. V. (1976) On the North Atlantic Circulation. *The Johns Hopkins Oceanographic Studies*, **6**, 110 pp.

WUST G. (1961) On the vertical circulation of the Mediterranean Sea. *Journal of Geophysical Research*, **66**, 3261–3271.

ZENK W. (1975a) On the Mediterranean outflow west of Gibraltar, *Meteor Forsch.-Ergebenisse*, *A* (16), 23–34.

ZENK W. (1975b) On the origin of the intermediate double-maxima in T/S profiles from the North Atlantic. *Meteor Forsch.-Ergebnisse*, *A* (16), 35–43.

APPENDIX A: DETERMINATION OF THE MINIMUM SALT EXCHANGE

Given the data u_b, regardless of the z_{ref} used, the determination of a function $v_{ref}(y)$ for which the constraint $SF = 0$ is imposed has an infinite set of solutions. To find the solution that minimizes

$$SE = \int_{y=0}^{y=L} \int_{z=h(y)}^{z} \rho S u H(u) \mathrm{d}z\mathrm{d}y, \tag{A1}$$

where $u = v_{ref} + u_b$ and

$$H(u_b + v_{ref}) = \begin{cases} 1 \text{ if } (u_b + v_{ref}) > 0 \\ 0 \text{ if } (u_b + v_{ref}) \leq 0 \end{cases} \tag{A2}$$

is a variational problem (u_b, S, and ρ are known functions). $SF = 0$ is an isoperimetric constraint (GELFAND and FOMIN, 1963) and can be dealt with using Lagrange multipliers. In fact, other constraints like zero mass flux can easily be accommodated in this approach. The problem is formulated so that the functional

$$SE' = SE - L \times SF \tag{A3}$$

of v_{ref} has a stationary value, i.e. find a function $v_{ref}(y)$ such that for any arbitrary but small function $\delta v = \delta v(y)$

$$\Delta SE' \equiv SE'(v_{ref} + \delta v) - SE'(v_{ref}) = \text{order}(\delta v^2). \tag{A4}$$

Here L is the Lagrange multiplier. Due to the properties of the functions involved

$$\Delta SE' = \int_y \delta v \int_{z=h(y)}^{z=0} [\rho s H(u) - L\rho s + 0(\delta v)] \mathrm{d}z\mathrm{d}y \tag{A5}$$

where H is evaluated as in equation (A2). The solution is

$$\int_{-h}^{0} \rho s H(u) \mathrm{d}z = L \int_{-h}^{0} \rho s \mathrm{d}z. \tag{A6}$$

In other words, for $0 < L < 1$, $v_{ref}(y)$ must accommodate the same fraction (L) of ρs with $u_b + v_{ref}$ positive for all values of y. As in most variational problems, in order to satisfy $SF = 0$, the solution is found by an iterative process. Very few (less than seven) iterations for L were required. This was accomplished by taking into account previous guesses for L and linearly interpolating the new guess of L ($L = 0$ gives $SF < 0$ and $L = 1$ gives $SF > 0$) until the absolute value of SF is less than $SE \times 10^{-4}$. For the first cruise and in sections VI, VII, VIII and IX, the corresponding Lagrange multipliers (L) are 0.64, 0.63, 0.62 and 0.57, respectively.

APPENDIX B: STREAMTUBE MODEL OF THE OUTFLOW

For an inviscid, rotating fluid in turbulent motion but with its mean current such that $\langle \rho v \rangle \equiv 0$ (i.e. zero mean momentum in the y direction), its mean momentum equation in the x direction reads:

$$f\langle \rho u \rangle = -\frac{\partial \langle p \rangle}{\partial y} \nabla - \langle (\rho v)' \underline{u}' \rangle, \tag{B1}$$

where the brackets ($\langle\ \rangle$) mean averages and the rest of the notation is standard. This equation is valid independent of time and length scales. Assuming that the cross-stream momentum equation is in geostrophic balance requires the neglect of Reynolds stress. Equation (B1) simply points out the strength of the geostrophic approximation for the cross-stream momentum balance.

In order to use hydrographic data to infer veolcities, one must either neglect (or maybe model) the Reynolds stress, as can be done by simplifying the momentum equation (B1) to:

$$f\rho u = -\frac{\partial p}{\partial y}, \tag{B2}$$

where the brackets have been removed for simplicity. Assuming the approximation is valid, the cross-stream direction has to be determined. Application of (B2) in another direction results in errors when the along-stream momentum equation is not in geostrophic balance.

In this appendix it is shown that for a downsloping "streamtube" current, bounded above by an inert layer and below by a uniform sloping bottom, the use of equation (B2) underestimates (overestimates) the mass flux when the vertical section is upslope (downslope) of the appropriate cross-stream section. To begin with, the pressure gradient above the tube chosen is zero i.e. no "inflow."

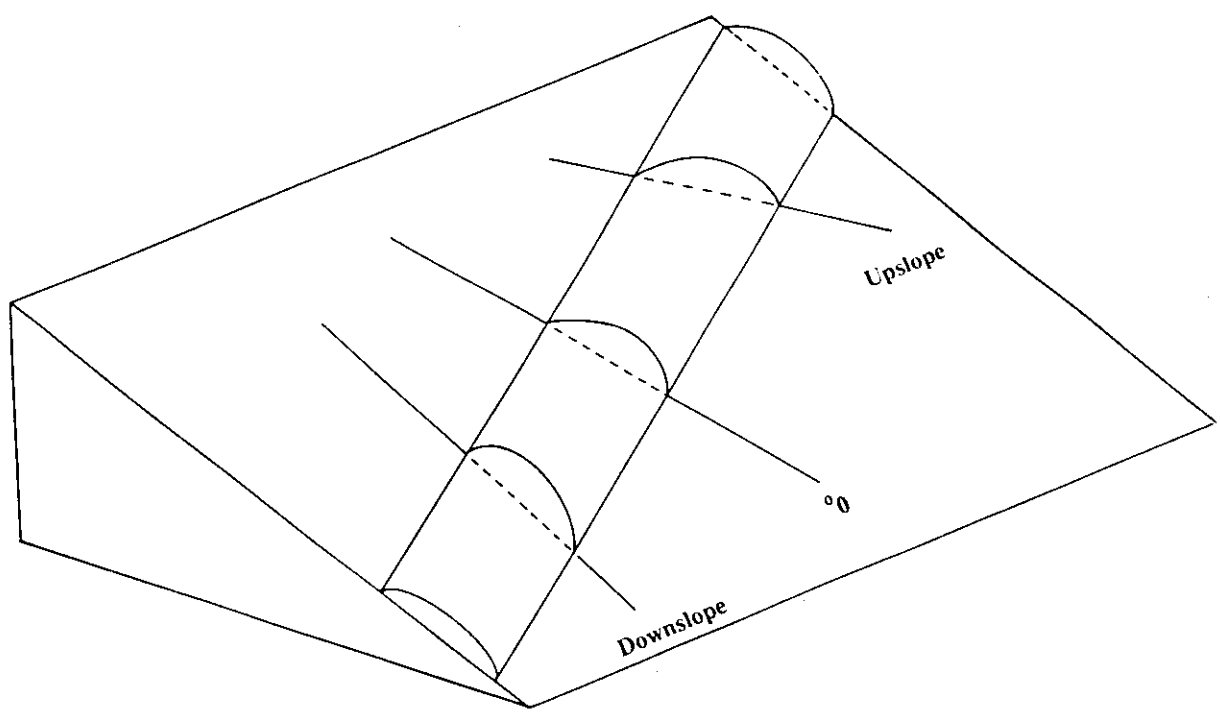

Fig. B1. Schematic of a sloping "tube" flowing over the bottom with vertical sections crossing in different directions. The interface of the tube separates slightly heavier water from the surrounding water. The geostrophic balance is (assumed to be) correct for the horizontal momentum equation in the direction perpendicular to the horizontal projection of the tube axis. This is the direction marked by 0°. Velocities and fluxes derived by utilizing the geostrophic relation in other directions than 0° are in error. This error is positive for downslope directions and negative for upslope directions.

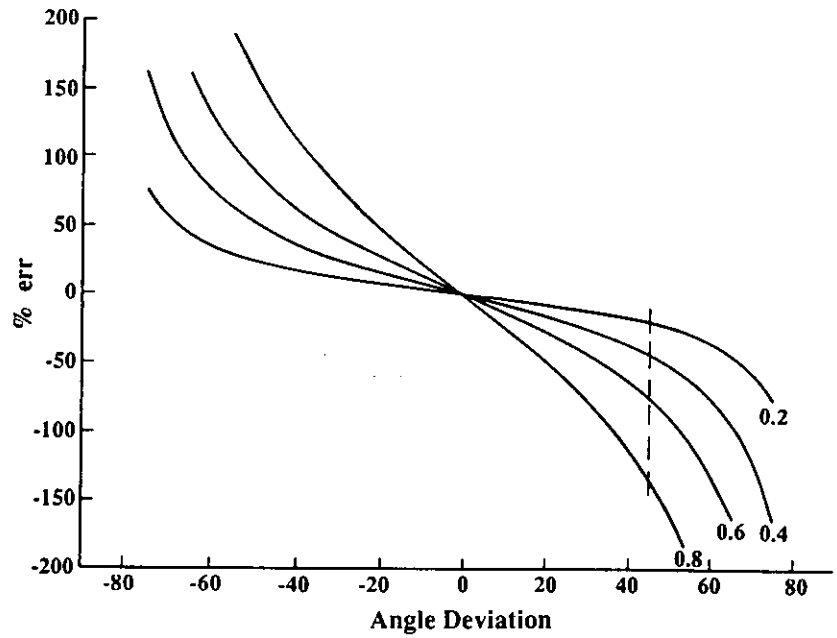

Fig. B2. The abscissa is the mass flux percentage error (equation B3) for utilizing the geostrophic relation in a sloping tube as shown in Fig. B1. This figure is for weak bottom slopes, less than 0.05. There is no error for the appropriate direction marked as 0°. The angle deviation is positive for upslope vertical sections and negative for downslope. The error is a function of the tube to bottom slope ratio, as shown by the label of each curve. The topography of the Gulf of Cadiz and the sections used in this work are consistent with a 45° angle deviation and a tube to bottom slope ratio between 0.4 and 0.6.

Figure B1 shows a schematic of the geometry of a circular tube. The tube is such that its tangent in the cross-stream direction is horizontal at the shallow intersection with the bottom i.e. $u = 0$ at the shallow edge.

We compute by using (B2) and the hydrostatic equation the apparent mass flux for any vertical cut as:

$$ME = \int_y \int_{z=-H}^{z=-h} \rho u \mathrm{d}z\mathrm{d}y = \frac{g\Delta\rho}{f} \int_y \left[H(y) - h(y)\right] \frac{\partial h}{\partial y} \mathrm{d}y,$$

where $z = -H(y)$ is the bottom, $z = -h(y)$ is the interface and the integral along y covers the whole tube. This apparent mass flux is different from the actual mass flux if the section is not in the appropriate direction. The percentage error in the mass flux is independent of the density constrast ($\Delta\rho$), latitude (f) and the actual size of the tube. This percentage error is a function of the angle deviation from the cross-stream direction. It is also a function of the bottom slope and, the actual tilt of the tube, which can go from horizontal or minimum (in which case there is no error no matter what the angle deviation and bottom slope are) to a maximum of the bottom slope. Figure B2 shows the percentage error in mass flux, explicitly:

$$\%\mathrm{err} \equiv \frac{ME(\theta) - ME(0°)}{ME(0°)} \times 100, \tag{B3}$$

where θ is the angle deviation (positive upslope). For weak (less than 0.05) bottom slopes the percentage error is essentially a function of the deviation angle and the tube to bottom slope ratio.

The purpose of this calculation is to show that, for sections VI and VII and, according to this simplified model, the error due to crossing the streamtube at an oblique angle is one of underestimation. For both sections, a bottom slope in the order of 0.01, an angle deviation in the order of 45°, and a tilt of the tube in the order of 0.006 are assumed. These parameters are taken from examination of MADELAIN's (1970) map of the outflow and topography, although accurate parameters are difficult to ascertain. This results in a mass flux error of −75%, or $ME_{real} = 4\, ME_{computed}$. For a smaller tilt of the streamtube, 0.004, the error would be −43%.

The model can be extended to include inflow maintaining the same velocity jump across the interface. Modeling it in such a way as to conserve mass in any column, i.e.

$$\int_{-H}^{0} \rho u \mathrm{d}z = 0 \text{ (for any } y)$$

produces some changes and adds dependency of the percentage error to the actual depths of the bottom and interface. Qualitatively, there are no changes and these become zero asymptotically as the maximum value of $(H - h) \rightarrow 0$. For typical values of H and h in the Gulf of Cadiz, the changes in Fig. B2 are small.

JOURNAL OF GEOPHYSICAL RESEARCH, VOL. 100, NO. C6, PAGES 10,755–10,776, JUNE 15, 1995

The role of the interface in exchange through the Strait of Gibraltar

N. A. Bray, J. Ochoa, and T. H. Kinder

Abstract. Five cross-strait hydrographic sections repeated several times during the Gibraltar Experiment in 1985–1986 are used to examine the structure of the interface layer between the inflowing Atlantic waters and outflowing Mediterranean waters in the Strait of Gibraltar. The interface is 60–100 m thick, with a strong vertical salinity gradient identified by fitting individual salinity profiles to a piecewise-linear, three-layer model. The interface is deeper, thicker, fresher, and colder on the west end of the strait than in the Narrows, where there is a minimum in thickness and a maximum in salinity gradient. Farther east, the interface thickens again and continues to get saltier, warmer, and shallower. Property variations in all three layers are also cast in terms of the three principal water types involved in the exchange. The traditional Knudsen model of exchange is extended to three layers, assuming that the interface is a transport-carrying third layer with uniform vertical shear. As much as half of the inflowing or outflowing transport occurs in the interface layer. Transport converges in both the upper and lower layers, implying, over the length of the strait, vertical exchange between layers that is comparable to about half the horizontal exchange. The richness of structure and complexity of interaction between the interface and the upper and lower layers argues against the use of two-layer models to characterize exchange through the Strait of Gibraltar.

1. Introduction

The structure of water mass exchange through the Strait of Gibraltar (Figure 1) is traditionally characterized as a two-layer system. Atlantic waters, which are fresh and warm, flow into the Mediterranean in the upper layer, while a compensating flow of colder and more saline water exits through the strait in a lower layer [*Lacombe and Richez*, 1982]. While this image of the exchange is useful in a qualitative sense, it ignores aspects of the structure of velocity and physical properties that are significant to a quantitative description of the exchange. First, the interface is of finite thickness, so that forcing the description into a two-layer model means incorporating the interface structure artificially into one or both layers. Second, the structure of the interface and the hydrographic characteristics of the different layers change with position along the strait, in response to vertical exchange between the layers. Third, the vertically sheared velocity within the interface may carry a significant fraction of the horizontal exchange.

In this paper, recent hydrographic observations in the strait are used to expand the description of exchange to include a more realistic structure: one that incorporates an interface layer of finite thickness, defined by the halocline. Because there is a seasonal thermocline in the upper layer, the halocline, rather than the pycnocline, best identifies the interface between Atlantic and Mediterranean waters (Figure 2). Using that definition of the interface, variations in the properties and structure of the three layers are examined within the strait and, to a limited extent, with time. The interface is an active layer, in the sense that net horizontal transport can and does occur there, and it also serves as a buffer for vertical exchange between the upper and lower layers.

Equations relating transport through a channel connecting two basins to the difference in evaporation excess between the basins were developed by *Knudsen* [1899] in studies of fjords. The Knudsen relations, as those equations have come to be called, provide transport estimates that are independent of the geostrophic or thermal wind balance more commonly used in oceanographic contexts. Knudsen relations are valid even for unsteady flow, provided that appropriate averages can be constructed.

In an evaporative basin like the Mediterranean, the net salt flux to an adjoining ocean is zero if the salt content in the Mediterranean basin is assumed to be constant. The evaporative loss is water of zero salinity, so evaporation does not change the salt content but can change the salinity by changing the volume of water in the basin. Excess of evaporation over precipitation and runoff for the basin as a whole should be balanced by a small net inflow of fresh water through the strait (hence the term often used: freshwater flux). However, since both inflow and outflow have substantial salinities, a much larger volume must be exchanged in order to maintain the balance of salt. The integral equations describing this system are

$$\left\{\int\int \rho u \, dy \, dz\right\} = E \tag{1a}$$

$$\left\{\int\int \rho u S \, dy \, dz\right\} = 0 \tag{1b}$$

where u is the eastward (x direction) component of velocity, ρ is the mass density, y is the northward coordinate, and z is

Paper number 95JC00381.
0148-0227/95/95JC-00381$05.00

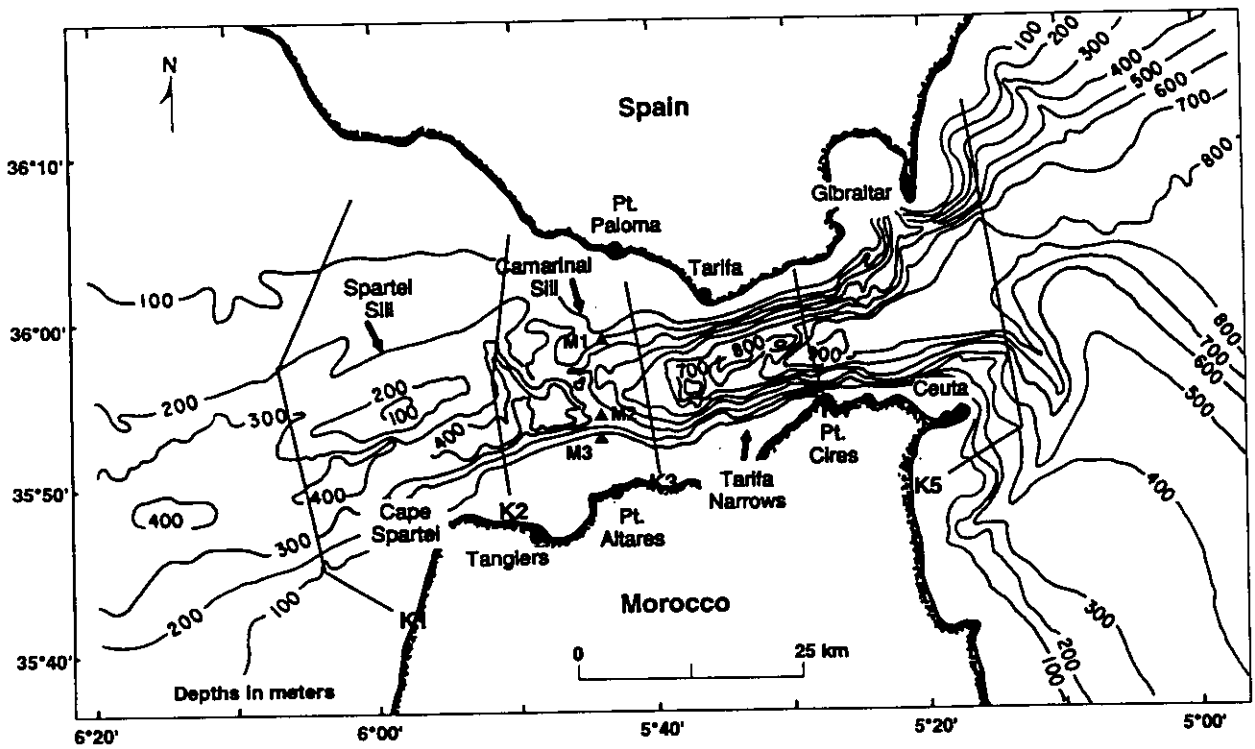

Figure 1. Bathymetry and location of principal geographic features in the Strait of Gibraltar. Conductivity-temperature-depth (CTD) sections were occupied repeatedly along the five cross-strait sections noted as K1 to K5 during the yearlong Gibraltar Experiment. Moorings M1, M2, and M3 were also part of the Gibraltar Experiment and are used for comparison with the calculations presented here.

the vertical coordinate, taken to be positive upward, E is evaporation excess, and S is salinity. The area of integration corresponds to a cross section of the channel, from the surface to the bottom. Braces denote a time average, unnecessary for steady flow. However, regardless of the steadiness of the flow, the system (1) may always be written in terms of "equivalent" quantities. Consider, for instance, the following definitions of mass and salt transports:

$$\bar{V}_1 \equiv \left\{ \int \int \rho u H(u)\, dy\, dz \right\} \tag{2a}$$

$$\bar{V}_2 \equiv -\left\{ \int \int \rho u H(-u)\, dy\, dz \right\} \tag{2b}$$

$$\bar{S}_1 \equiv \left\{ \frac{1}{V_1} \int \int \rho u S H(u)\, dy\, dz \right\} \tag{2c}$$

$$\bar{S}_2 \equiv -\left\{ \frac{1}{V_2} \int \int \rho u S H(-u)\, dy\, dz \right\} \tag{2d}$$

where $H(x) = 1$ if $x > 0$ and $H(x) = 0$ if $x \leq 0$ is the step function. Notice that $H(x) + H(-x) = 1$, so in terms of these definitions or equivalent quantities, the system (1) can be rewritten as:

$$\bar{V}_1 - \bar{V}_2 = E \tag{3a}$$

$$\bar{V}_1 \bar{S}_1 - \bar{V}_2 \bar{S}_2 = 0. \tag{3b}$$

These relationships were published by *Knudsen* [1899, 1900] and have been used frequently to model transports in the Strait of Gibraltar. An additional equation for the heat balance can be included in the form:

$$\bar{V}_1 \bar{T}_1 - \bar{V}_2 \bar{T}_2 = F. \tag{3c}$$

Here the term "heat balance" is used rather freely to mean that temperature is used as a conservative tracer within the strait itself, that is, that no gain or loss of heat is expected from one section to the next. This system of equations ((3a), (3b), and (3c)) allows simple calculations to be made. For example, horizontal transports as a function of section along the channel may be estimated by rewriting (1a) and (1b) as

$$\bar{V}_1 = \frac{\bar{S}_2}{\bar{S}_2 - \bar{S}_1} E \tag{4a}$$

$$\bar{V}_2 = \frac{\bar{S}_1}{\bar{S}_2 - \bar{S}_1} E \tag{4b}$$

and considering that E cannot change from section to section.

A three-layer modification of these traditional Knudsen conservation equations is used in this paper to identify the transport within each layer and also to examine along-strait variations in the horizontal transports: by implication, a measure of the vertical exchange between layers. The first step in the analysis is to identify, using a simple model, the three layers within any observed salinity profile in the strait. This identification is done by a least squares minimization, fitting each observed salinity profile to a continuous model profile consisting of three linear sections. Using the fitted profiles, the depth, thickness, and property characteristics of

upper or lower layer. Definition of the interface in terms of a single value of salinity has been common in past work. Although this might be accurate enough for estimates of vertical excursions of the interface depth, it is not appropriate for examining exchanges between layers. The mean shear in the strait should correspond in vertical extent with the halocline, rather than with any particular salinity, since the shear results from waters of differing salinities flowing in opposite directions through the strait. In the instantaneous flow, shear and halocline do not always, or necessarily, correspond (see, e.g., *Pettigrew and Hyde* [1990]). This is due to the interaction of the internal tide with the mean flow. The average salinity of the halocline, as well as of the upper and lower layers, changes with distance along the strait due to vertical exchange.

The finite thickness of the halocline is important, both kinematically and dynamically. For example, since there is a salinity change of ~2 psu across the interface, if half of the interface layer is incorporated into the upper layer, the salinity contribution from that interface layer constitutes a major bias in the upper layer average. This reduces the apparent salinity difference between layers to values like 1.5 psu. The volume and type of water within the halocline region changes with distance along the strait, as does the structure (depth, thickness, vertical gradient) of the halocline. The interface is not a passive, if permeable, surface that separates the inflow from the outflow. Rather, it is an active third layer with a structure that is determined by the interaction of strait dynamics and the kinematic structure imposed by large-scale variations in water mass composition. For the analysis that follows, the interface is defined in terms of the halocline. Once the halocline is identified from a given profile, the interface structure and layer properties may be determined readily. A quantitative method for dividing any salinity profile into upper, interface (halocline), and lower layers follows.

Taking an actual salinity profile $S = S(z)$, a model salinity profile $\hat{S}$ is fitted by least squares. The model salinity profile has the following four free parameters: the upper interface boundary height and salinity (Z_1 and S_1) and the lower interface boundary height and salinity (Z_2 and S_2). The surface salinity is fixed at the observed value, and the lower layer is assumed to be homogeneous (Figure 3). This model profile then consists of the following three linear sections: the upper layer from the surface to Z_1, the interface from Z_1 to Z_2, and a homogeneous lower layer from Z_2 to the bottom or 400 m, whichever is less. Other model possibilities were explored, including one with a salinity gradient in the lower layer and one with the number of free parameters increased to six by allowing the surface and deepest salinities as parameters. Judging subjectively, in both of those models, part of the halocline is apparently included in the lower layer; the simpler four-parameter system avoids that difficulty. To exclude profiles that do not have a definite interface layer, profiles with a salinity minimum >37 psu, a salinity maximum <37 psu, or an average salinity difference between upper and lower layers <0.85 psu were rejected from the analysis. Most of the rejected profiles violated the salinity maximum criterion, thus did not extend into the lower layer. These profiles were located near the coast on either side of the strait (Figure 4). It should be noted that the fitting procedure introduces some bias into the interface structure by excluding profiles with only a partial interface

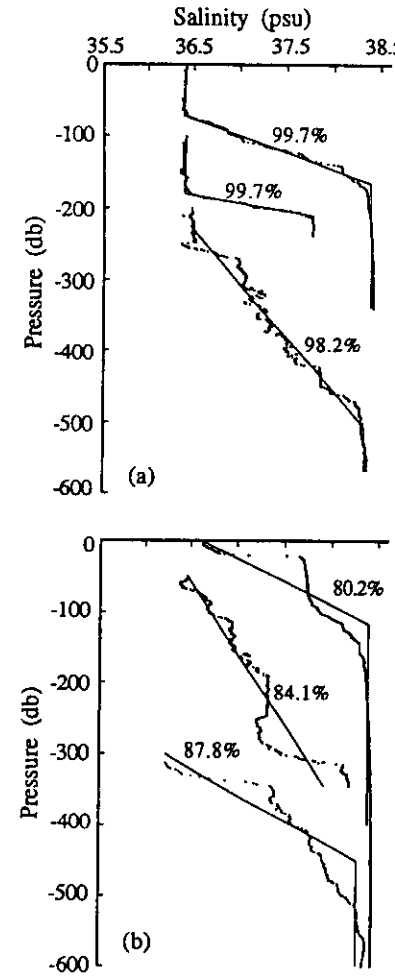

Figure 3. Comparison of observed with fitted profiles. (a) Two profiles with the lowest value of fq as defined by (5), or those best fit, and one with a thick interface. Percentages are $(1 - fq) \times 100$. (b) Three profiles with the highest values of fq, or those with the worst fit quality.

(i.e., where the interface has surfaced and the minimum salinity is >37 psu as a result), which happens principally on the north side of the strait.

There is a wide variety of vertical structure observed in the strait, and the fitting procedure approximates the real profiles with varying success that is measured quantitatively by the fit quality fq:

$$fq \equiv \sum_i (S_i - \hat{S}_i)^2 \Big/ \sum_i (S_i - \bar{S})^2 \qquad (5)$$

where the index i labels the equally spaced depths of CTD processed data, each with salinity S_i and modeled salinity $\hat{S}_i$, and $\bar{S}$ is the arithmetic mean of the profile. The quantity fq is a measure of the amount of variance that is explained by the model. Variability in the fit quality (Figure 3) indicates which profiles are well or poorly estimated by the four-parameter, three-layer model. Even those profiles most poorly fit (those without a surface layer) explain at least 80% of the total variance in the profile. Profiles with the best fit explain 99% of the total variance.

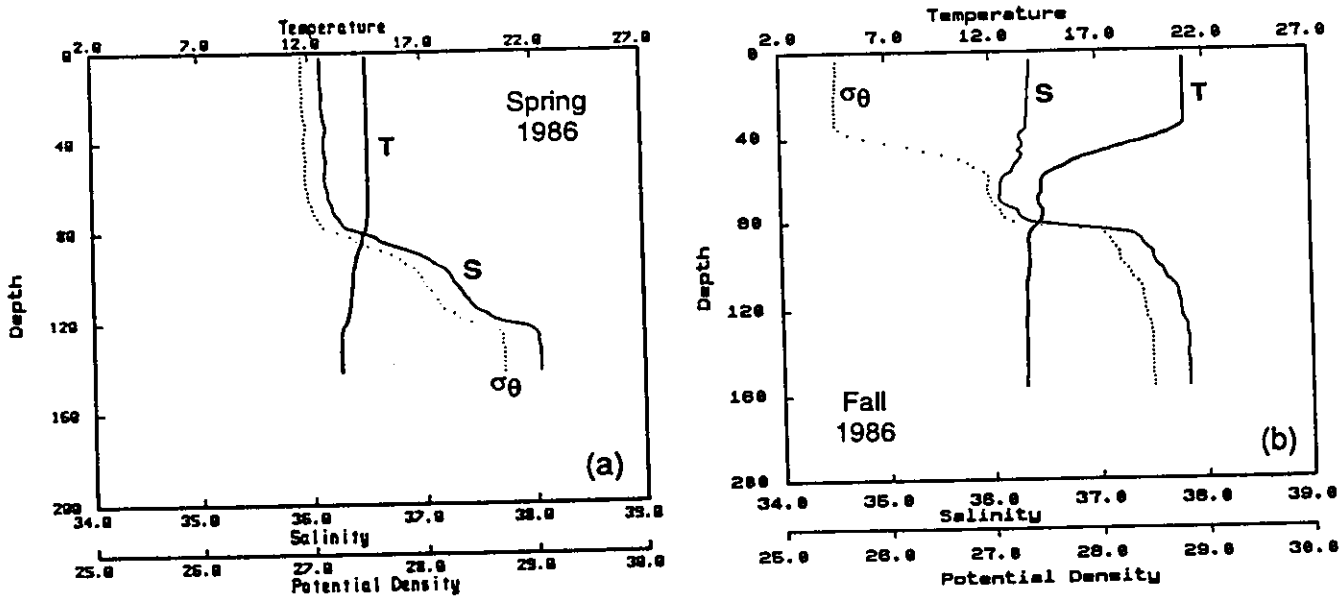

Figure 2. Typical profile of temperature (thick solid line), salinity (thin solid line), and density (dots) from a station near the Camarinal Sill for (a) spring of 1986, where there is no seasonal thermocline and the small change in temperature across the halocline is evident, and (b) fall of 1986, where there is a strong seasonal thermocline in the upper layer.

the interface, upper, and lower layers are described throughout the strait.

Water mass characteristics at any point in the strait can be readily described in terms of a mixture of three principal sources. Relative contributions of Surface Atlantic, North Atlantic Central, and Mediterranean water types are calculated in the different layers for sections across the strait at various positions. Finally, assuming a value for evaporative loss over the Mediterranean, the vertical structure of the horizontal exchange is estimated through each section using a modification of the classical Knudsen relationships that takes into account the vertical shear through an active interface. Convergences observed from section to section within the upper and lower layers, found to be somewhat larger than the estimated errors in horizontal transport, are interpreted as vertical exchange between those layers and the interface.

The analysis presented here does not take explicit account of tidal variability in exchange through the strait. Most of the energy for fluctuations in the strait derives from tidal forcing of currents [*Candela et al.*, 1990; *Bray et al.*, 1990]. This energy, together with the mean shear, apparently provides much of the impetus for mixing and cross-halocline exchange [*Wesson and Gregg*, 1988, 1994; *Ambar and Howe*, 1979].

2. Interface Definition and Property Distributions Within the Strait

2.1. Observations Used

During the Gibraltar Experiment conducted in 1985 and 1986 [*Kinder and Bryden*, 1987], over a thousand conductivity-temperature-depth (CTD) profiles were taken in and near the strait [*Kinder et al.*, 1986, 1987; *Bray*, 1986; *Shull and Bray*, 1989]. Five cross-strait sections (labeled K1 to K5) were occupied repeatedly during the experiment (Figure 1). Observations were made with Neil Brown Instrument Systems Mark III profilers, calibrated under laboratory conditions for accuracy of temperature and pressure before and after each cruise; salinity samples taken in situ and calibrated against standard seawater were used to correct the profiles of conductivity and thereby of salinity. The overall accuracy of the measurements is ±0.005 practical salinity units (psu), ±0.005°C, and ±5 dbar for salinity, temperature, and pressure, respectively. Stations were taken to within a few meters of the bottom, except when excessive velocity shear prevented lowering of the instrument. Observations from four cruises are used in this paper: November of 1985, March of 1986, June of 1986, and October of 1986, although in June of 1986, diplomatic clearance difficulties prevented completion of the easternmost two sections. A total of 416 profiles are contained in the multiple occupations of standard lines. Of these, 313 were used in this analysis. The remaining 103 had only a partial interface (for the most part, located near the coast and depth limited to the upper layer) and were therefore not included.

2.2. Interface Definition

The transition between Atlantic and Mediterranean waters in the strait is clearly denoted by a sharp halocline, with a change in salinity of ~2 psu occurring over a depth range of 50 to 100 m. This halocline does not typically coincide with the primary thermocline, as there is a strong seasonal thermocline within the Surface Atlantic Water for much of the year. As a result, density profiles may have two pycnoclines: one for the seasonal thermocline and one for the interface, which is principally defined by the halocline (see Figure 2b). In the following analysis, the halocline will be used to define the interface, to avoid the confusion engendered by the seasonal thermocline. The thickness and property characterization of the halocline varies along the strait, though it is consistently distinguishable from either the

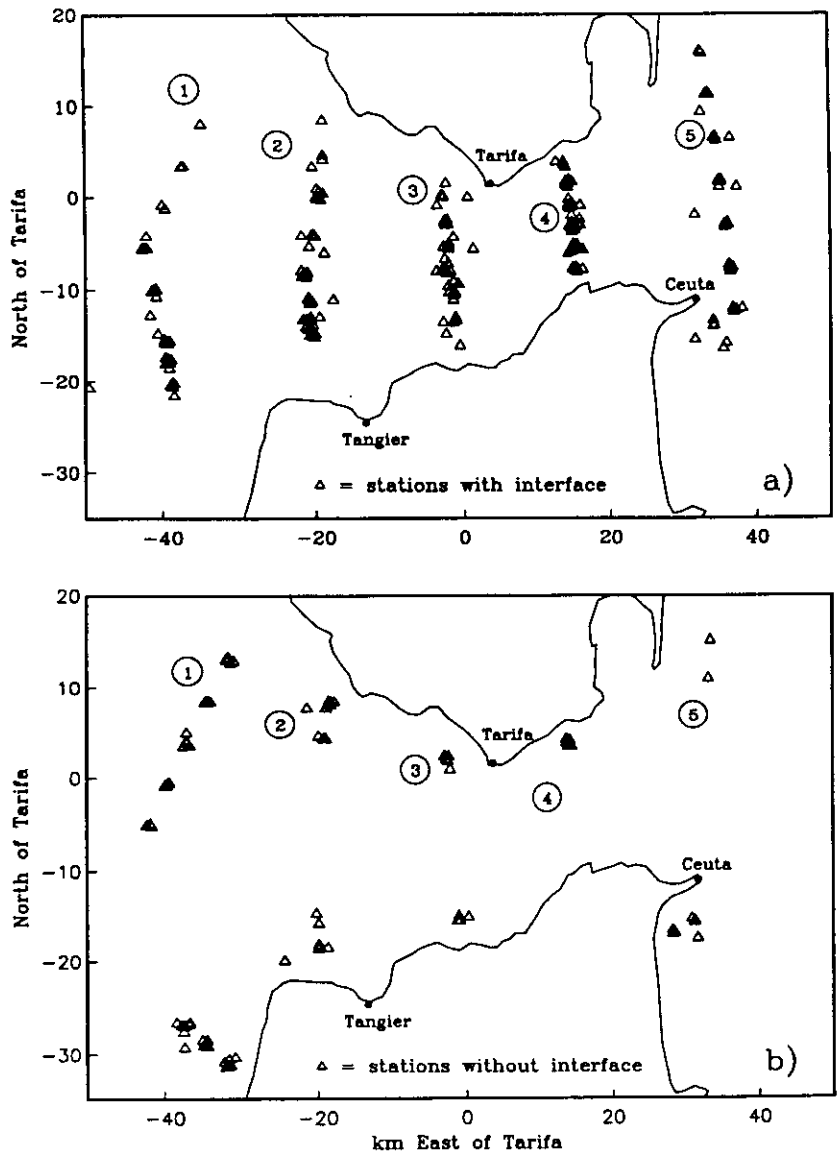

Figure 4. Station locations in the strait (a) with an identifiable interface layer and (b) without an identifiable interface layer.

Interface depth and thickness, averaged across the strait, vary considerably with distance along the strait (Figure 5 and Table 1). The interface depth is taken to be $(Z_1 + Z_2)/2$; its thickness is $(Z_2 - Z_1)$. The interface is deepest and thickest on the west end of the strait, with a minimum between Camarinal Sill and Tarifa Narrows. There is surprisingly little seasonal variability evident in either depth or thickness of the interface from the different cruises. Standard deviations over the four cruises (Table 1) are 5 to 25 m for the depth and 5 to 21 m for the thickness. The smaller standard deviations are found on the eastern end. Note that for many of the calculations presented in this and succeeding sections, two different estimates are given: the first involves using all of the data, regardless of cruise, in a single calculation; in the second, each cruise is calculated separately and the results averaged. The standard deviation given is from the second calculation. In general, the two estimates are in good agreement.

In plan view (Figures 6–8) the interface layer is found at an average depth of 75–100 m throughout the eastern half of the strait, deepening rapidly to 250 m on the southwestern side (Figure 6a). While the interface is, on average, somewhat deeper on the south side of the strait, the cross-strait gradient in interface depth is much less apparent than that in the along-strait direction on the western end. Interface thickness (Figures 5 and 6c) has a minimum between Camarinal Sill and Tarifa Narrows and increases from a value of 60 m there to maximum thicknesses of 110 m on either end of the strait. The average salinity of the interface layer (Figure 6b) increases monotonically eastward along the strait, with a significant cross-strait gradient present everywhere, except at the eastern end. Higher interface salinities are found on the south side of the strait. Interface temperature (Figure 6d) is relatively uniform in the along-strait direction; the principal variation is across the strait, with warmer temperatures (consistent with a shallower depth) on the north side.

The density gradient across the interface may be interpreted in terms of a buoyancy frequency N (Figure 7), with the usual oceanographic definition:

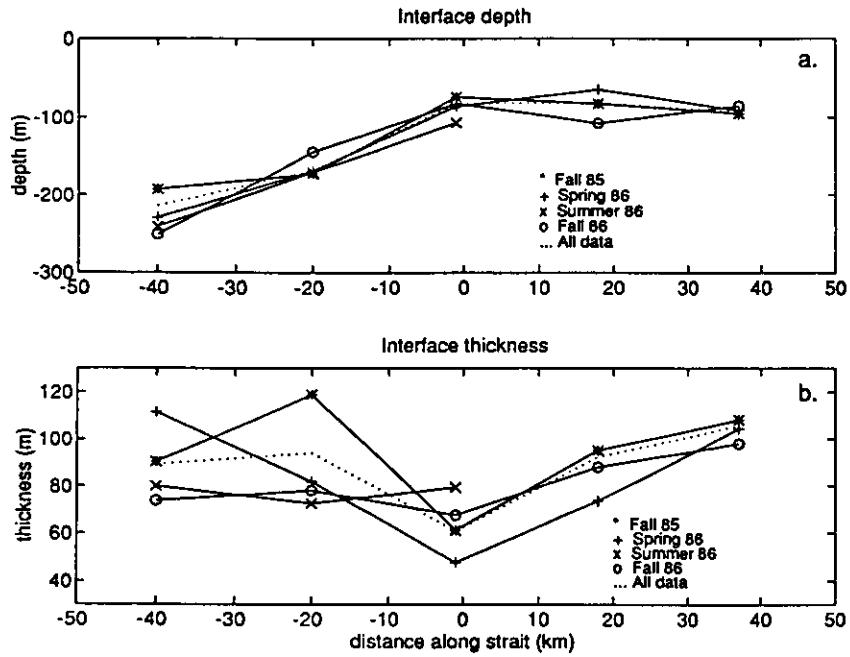

Figure 5. (a) Interface depth and (b) thickness as a function of distance along the strait, for each cruise and for the single calculation involving all of the data. The origin is at Tarifa.

$$N^2 = -\frac{g}{\rho}\frac{\partial \rho}{\partial z}$$

and where the derivative on the right-hand side has been approximated by the density difference across the interface divided by the thickness of the interface. There is a pronounced maximum in N^2 on the south side of the strait between Camarinal Sill and the Tarifa Narrows, corresponding to the minimum interface thickness seen in Figure 6c.

Throughout most of the strait the difference in average salinity between the upper and lower layers (i.e., excluding the interface layer) is between 2 and 2.2 psu (Figure 8). This is in good agreement with the value inferred from moored conductivity and velocity measurements during the Gibraltar

Table 1. Interface Structure

	Depth, m	Thickness, m	S_1	S_2	Cross-Strait Slope, m km^{-1}	Geostrophic Shear, s^{-1}	Knudsen Shear, s^{-1}
				K1			
All data	214	89	36.028	37.889	−6.94	0.018	0.007
Average	229	89	35.970	37.913	−4.35	0.011	0.008
Standard deviation	26	17	0.125	0.044	2.30	0.006	0.002
				K2			
All data	168	94	36.160	38.082	−3.71	0.010	0.006
Average	165	88	36.141	38.106	−4.00	0.013	0.007
Standard deviation	13	21	0.066	0.067	2.85	0.009	0.001
				K3			
All data	83	61	36.227	38.295	0.72	−0.003	0.013
Average	88	64	36.222	38.281	−0.77	0.002	0.013
Standard deviation	14	13	0.035	0.101	3.72	0.017	0.003
				K4			
All data	83	92	36.395	38.330	−3.30	0.010	0.014
Average	86	86	36.244	38.343	−3.26	0.010	0.014
Standard deviation	22	11	0.070	0.017	3.44	0.011	0.004
				K5			
All data	93	106	36.395	38.318	−2.31	0.006	0.004
Average	91	104	36.370	38.314	−2.57	0.006	0.004
Standard deviation	5	5	0.061	0.020	1.92	0.004	0.001

S_1 is salinity at the top of the interface. S_2 is salinity at the bottom of the interface. Geostrophic shear assumes cross-strait slope is balanced geostrophically. Knudsen shear anticipates the three-layer calculation of section 3.2. "All data" is a calculation using all of the available profiles in a given section. "Average" and "standard deviation" are statistics over the four cruises, each done as an individual calculation.

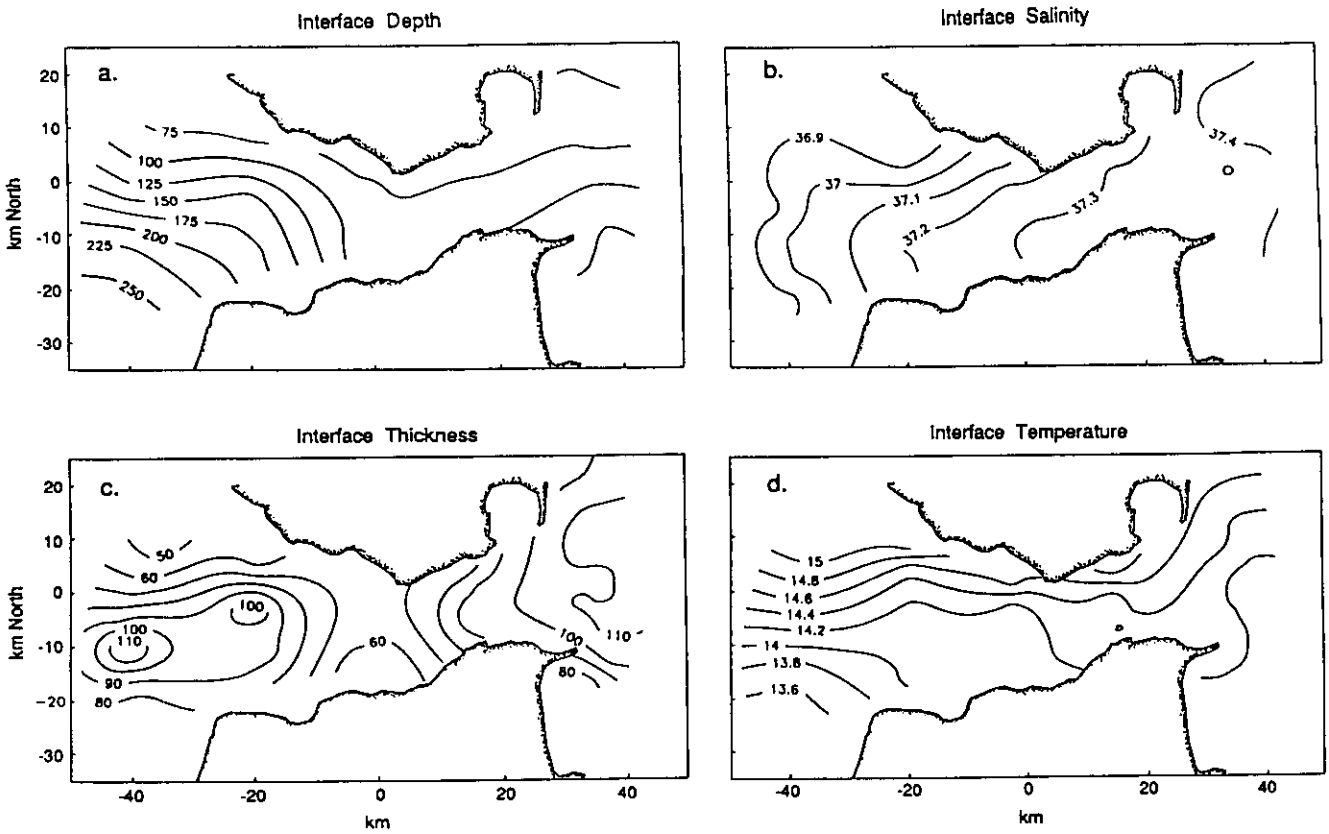

Figure 6. Interface layer structure, using data from all cruises, with the origin at Tarifa. (a) Depth of the midpoint of the interface layer. (b) Salinity averaged vertically over the interface layer. (c) Thickness of the interface layer. (d) Temperature averaged vertically over the interface layer.

Experiment [*Bryden et al.*, 1989]. The temperature difference between layers (Figure 9) varies principally with distance along the strait, from a minimum of 2.25°C on the western end to a maximum of 4.5°C on the eastern end.

2.3. Average Property Differences Across the Interface

Another way to look at the results described above is to consider averages over the five cross-strait sections and the four cruises. This provides information about variations in the structure along the strait and with season. Averaged over all the observations (Table 2), the differences in salinity, temperature, and density between the upper and lower layers (excluding the interface layer) are as follows: 1.99 (±0.12) psu, 3.01 (±0.88)°C, and 2.20 (±0.22) σ_t units, respectively. The errors are standard deviations over all four cruises and five cross-strait sections. The relatively large temperature error value reflects seasonal changes of ~2° in upper layer average temperatures, associated with opposing changes of ~0.1 psu in salinity, resulting in seasonal density variations of 0.3 σ_t in the upper layer (Figure 10).

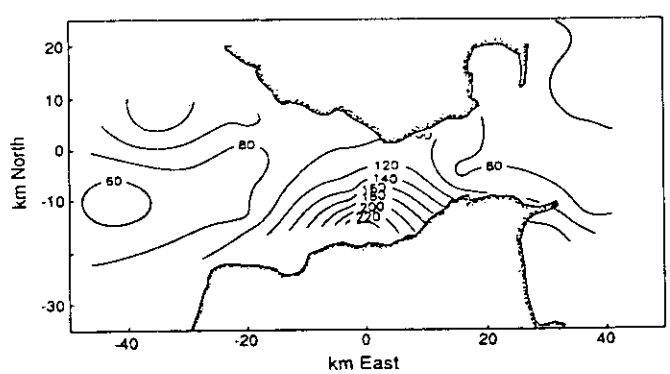

Figure 7. Buoyancy frequency N^2 (cycles per hour squared) across the interface layer. The origin is at Tarifa.

Averaged by sections, salinity and density differences are largest at sections K3 and K4, between Camarinal Sill and Gibraltar itself (Figure 11). Temperature difference increases to the east, with the largest value of 3.45°C at the Gibraltar section. Quantitative differences between a two-layer and a three-layer description (Figure 11) are seen in all three variables: the two-layer salinity difference underestimates the three-layer value by 0.3 psu throughout the strait, the temperature difference is underestimated by 0.4 to 0.8°C, and the density by ~0.4 σ_t. (The two-layer system is defined using the middle of the interface layer as the division between upper and lower layers.)

The agreement between the average salinity difference from these data and that inferred from moored observations by *Bryden et al.* [1989] is in some sense surprising, as the moored estimate includes effects of correlations between the velocity and salinity fields in the lower layer. Because the subsequent agreement between transports of volume, salt, and heat between the two estimates hinges on the parity of

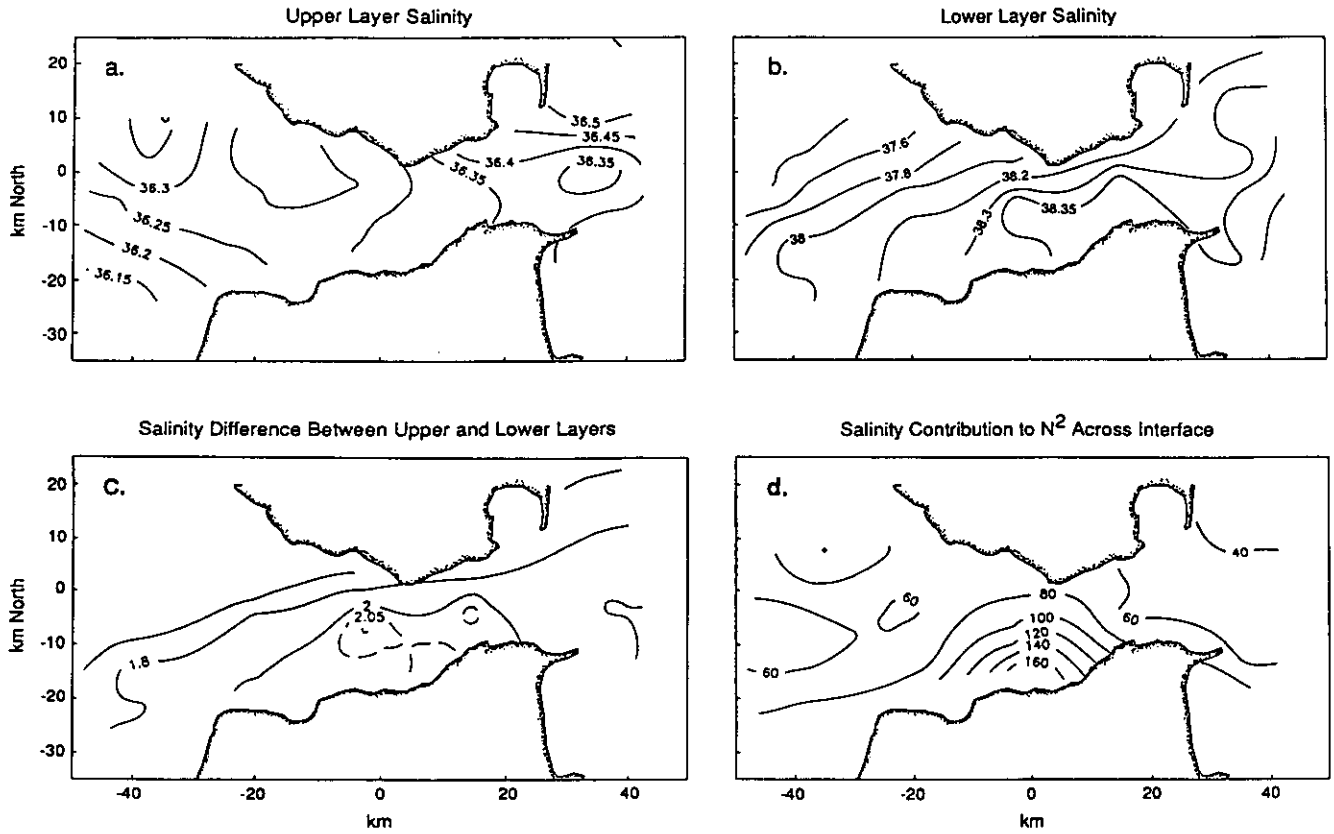

Figure 8. Salinity contrast between the upper and lower layers using data from all cruises, with the origin at Tarifa. (a) Salinity averaged vertically over the upper layer. (b) Salinity averaged vertically over the lower layer. (c) Salinity difference (lower-upper) between layers. (d) Salinity contribution to N^2 (cycles per hour squared) across the interface layer.

the two salinity difference estimates, it is worth discussing why the two estimates agree. *Bryden et al.* [1989] estimate the salinity difference between inflow and outflow as:

$$\Delta S = \frac{\left\langle \int_{h_B}^{h_i(t)} u(z,\, t)[S(z,\, t) - S_{\text{ref}}]W(z)\, dz \right\rangle}{\left\langle \int_{h_B}^{h_i(t)} u(z,\, t)W(z)\, dz \right\rangle}$$

where $h_i(t)$ is the (time-dependent) depth of the interface, h_B is the bottom depth, $W(z)$ is the width of the strait, u and S are the velocity and salinity of the outflow layer, and S_{ref} is the salinity of the inflow, taken to be a constant 36.2 psu. Angle brackets signify a time average. The value of ΔS given by *Bryden et al.* [1989] for the M2 mooring is 2.2 psu (see Figure 1 for mooring locations). Using the results from CTD section K3, the salinity difference excluding the interface layer is 2.1 psu and the upper layer average salinity is 36.25 psu. Since the upper layer salinities are nearly equal in the two estimates and are taken to be a constant in both, it becomes apparent that:

$$\left\langle \int_{h_B}^{h_i(t)} u(z,\, t)S(z,\, t)W(z)\, dz \right\rangle \approx S_{\text{CTD}}U,$$

where

$$U = \left\langle \int_{h_B}^{h_i(t)} u(z,\, t)W(z)\, dz \right\rangle.$$

In other words, when the interface is defined with precision in the hydrographic data, the salt transport of the lower layer is well represented by the product of the average salinity times the transport. The interface h_i used for the moored data was defined as the 37 psu isoline; while this is a different definition than that used for the CTD analysis, the crucial element in the time series calculation is that the time dependence of interface depth be incorporated in the transports. With the CTD analysis it is crucial that the interface structure be resolved precisely. Note that the moored estimate could be further refined by a more careful definition of the interface in the moored observations and by measurements of salinity variability in the upper layer from moored current meters, as the latter were not available from the Gibraltar Experiment moorings.

Bryden et al. [1989] go on to estimate the evaporation excess E to be 0.55 m yr^{-1}, by applying the Knudsen equations to their values of ΔS and U. Therefore, since ΔS agrees between the two entirely different estimates (CTD and moored observations), if we here use the value of E

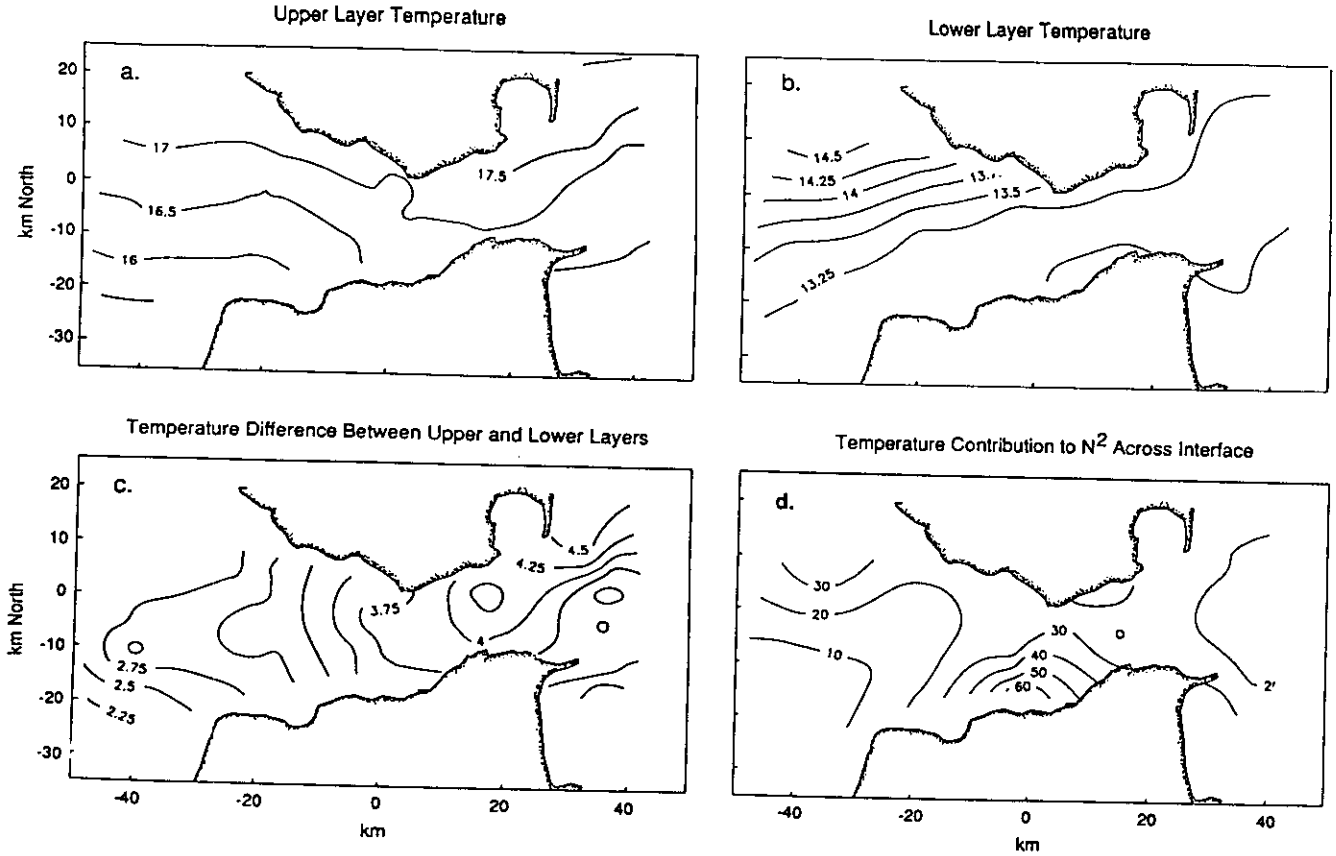

Figure 9. Temperature contrast between the upper and lower layers using data from all cruises, with the origin at Tarifa. (a) Temperature averaged vertically over the upper layer. (b) Temperature averaged vertically over the lower layer. (c) Temperature difference (upper-lower) between layers. (d) Temperature contribution to N^2 (cycles per hour squared) across the interface layer.

inferred from the moored ΔS, we will get the same transports as did *Bryden et al.* [1989]. What is surprising, at least initially, is that the product of the average salinity and the average transport is a good representation of the average of the time-dependent product of the two in the lower layer. One reason that this is true is that the average transport has been defined carefully in the time series estimate to include fluctuations in the interface depth. The second reason is that the salinity in the lower layer, when the interface is excluded, has relatively little vertical structure, so that it is, in fact, nearly a constant in the integrand.

2.4. Water Mass Distributions Within the Strait

The relationship between temperature and salinity is a result of the water mass origin of parcels of water. Throughout the North Atlantic, North Atlantic Central Water (NACW) is ubiquitous in the range of ~8 to 19°C. NACW is a water mass defined to lie along the line in TS space connecting the points 8°C, 35.1 parts per thousand (ppt) and 13°C, 36.7 ppt [*Sverdrup et al.*, 1942]. In the strait, NACW is found below the surface during all cruises; near the surface a modified form of NACW, warmer at the same salinity, is also found. For the purposes of this discussion, the latter will be referred to as Surface Atlantic Water (SAW). The observed temperature and salinity distributions within the strait can be described as a mixture of three principal water types: SAW, NACW, and Mediterranean Water (MW). SAW is warm and fresh, NACW is colder and fresher than SAW, and MW is cold and saline. Each of these principal water types is itself a mixture; MW, for instance, is composed principally of Levantine Intermediate Water and Western Mediterranean Deep Water (LIW and WMDW) types [*Parrilla et al.*, 1989; *Pettigrew*, 1989]. Similarly, Spanish Shelf Water (SSW) and other constituents influence the composition of SAW [*van Geen and Boyle*, 1989]. These more specific water masses are not included explicitly in the analysis presented here. In the case of LIW and WMDW, the contrast is slight, and in the case of SAW, SSW is a minor contributor.

The TS composition within the different layers with distance along the strait (Figure 12) indicates that the upper layer is composed mostly of SAW and NACW on the western end of the strait; as the upper layer flows eastward, the lower part of the upper layer, containing NACW, is eroded away, leaving a layer that is both thinner (Figure 13) and more saline, due mostly to the loss of fresher NACW from the layer and not to a gain of saline MW. Within the interface layer, composition varies rapidly from Atlantic to Mediterranean over the depth of the layer. Progressively more SAW influence is found at the top of the interface layer as NACW disappears. In the lower layer the TS distribution becomes more diffuse on the Atlantic end of the strait, although there is some indication of NACW even at the section farthest east.

The composition of water masses at a particular location

Table 2. Property Differences Between Upper and Lower of Three Layers

	Salinity, psu	Temperature, °C	Density, σ_θ
	K1		
All data	1.809	2.585	1.967
Average	1.837	2.415	1.949
Standard deviation	0.102	0.692	0.082
	K2		
All data	1.988	2.825	2.158
Average	1.995	2.797	2.158
Standard deviation	0.017	0.585	0.138
	K3		
All data	2.109	3.363	2.373
Average	2.118	3.264	2.359
Standard deviation	0.049	0.806	0.159
	K4		
All data	2.022	4.187	2.504
Average	2.074	3.370	2.353
Standard deviation	0.072	1.178	0.219
	K5		
All data	1.942	3.771	2.342
Average	1.955	3.404	2.269
Standard deviation	0.029	1.270	0.272
	All Sections		
All data	1.974	3.346	2.269
Average	1.994	3.013	2.207
Standard deviation	0.118	0.879	0.222

All data is a calculation using all of the available profiles in a given section. Average and standard deviation are statistics over the four cruises, each done as an individual calculation.

in the strait can be quantified by a straightforward division into three components, point values in TS space that are taken to represent SAW, NACW, and MW (Figure 14). Seasonal variations in surface temperature change the apparent end point for SAW from one cruise to the next, so composition triangles are defined individually by cruise. In order for the decomposition to work sensibly, the point considered must lie within the triangle defined by the end points. Although more than three sources can be used in the analysis [e.g., *van Geen and Boyle*, 1989], limiting the number to three assures that the solution is unique.

Points representing SAW near the surface, NACW at the salinity minimum, and MW are used to define the triangle, where MW is taken to be an average of the different sources of Mediterranean water masses found in the strait. A triangle is formed for each cruise (Figure 14 and Table 3), with the requirement that it is the triangle of minimum area (in units of degrees Celsius and practical salinity units) containing the four extreme TS points in all individual profiles considered from a given cruise. These four extreme points correspond to the maximum and minimum temperatures (with associated salinities) and maximum and minimum salinities (with associated temperatures) (Table 4).

Within each of the three layers, temperature and salinity are averaged over each cross-strait section (Figure 14). The progression of TS characterization from one section to the next in each layer indicates changes in composition as a function of distance along the strait. Averaged over all cruises and all sections (Figure 15a), the upper layer is roughly half SAW, less than half NACW, and ~10% MW. The interface layer is half MW, a third NACW, and a fifth SAW. The lower layer is mostly MW, with minor contributions from SAW (2%) and NACW (7%).

As a function of distance along the strait (Figures 15b and 15c), there is actually an increase, from the westernmost to the easternmost section, of 12% in the percentage of SAW in the upper layer, accompanied by a decrease in NACW of 20%. MW in the upper layer also increases, from 5% to 10%, from west to east. Along-strait changes in the interface layer are similar to those in the upper layer. MW in the lower layer decreases from 95% to 83%, going from east to west, while SAW and NACW increase from 1% and 4% to 4% and 13%, respectively. The actual transport, as opposed to fractional composition, of water types within the different layers is discussed in section 3.2.

Variations in water mass composition in the upper layer between cruises are as large as those from one end of the strait to the other (Figures 15d and 15e). SAW in the upper layer was a maximum of 73% during the fall 1985 cruise and a minimum of 39% in spring of 1986. Some of that difference is made up by an increase in MW (8% versus 2% in fall 1985), though most is compensated by an increase in NACW (52% from 26%). Similar differences are seen in the interface layer between those two cruises, although there is little variation in MW. No significant differences occur in the lower layer compositions between the two cruises.

3. Horizontal Transports

3.1. Two-Layer Calculation of Horizontal Transports

Using the simplified Knudsen relations of (4a) and (4b), an estimate of the transport through any section can be made by

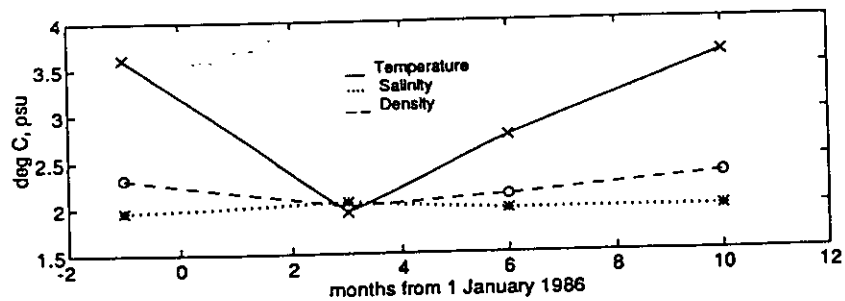

Figure 10. Seasonal changes in property differences between the upper and lower layers of the three-layer system.

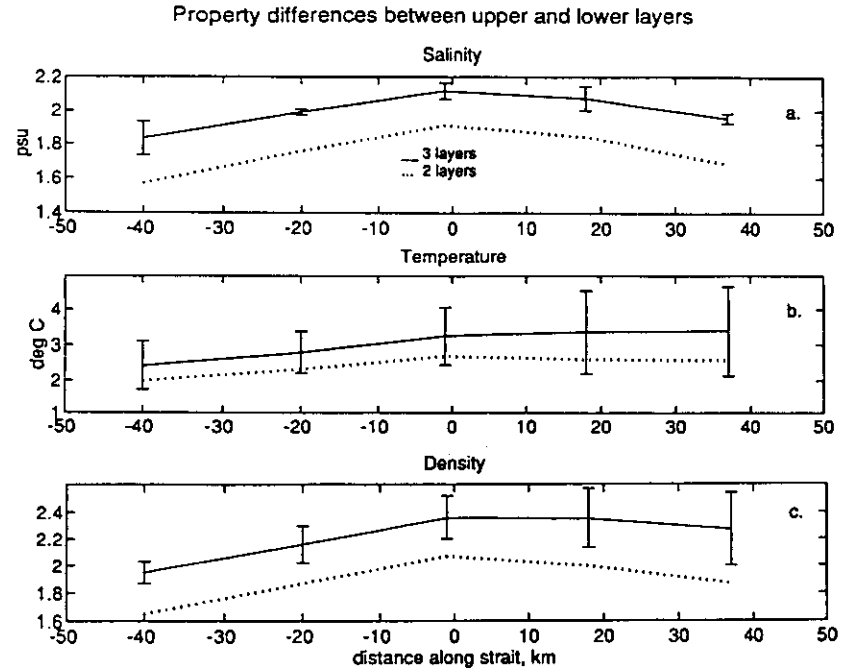

Figure 11. Along-strait variations in property differences between the upper and lower layers: comparison between two- and three-layer systems, showing (a) salinity, (b) temperature, and (c) density. Error bars represent standard deviations over the four cruises for the three-layer system.

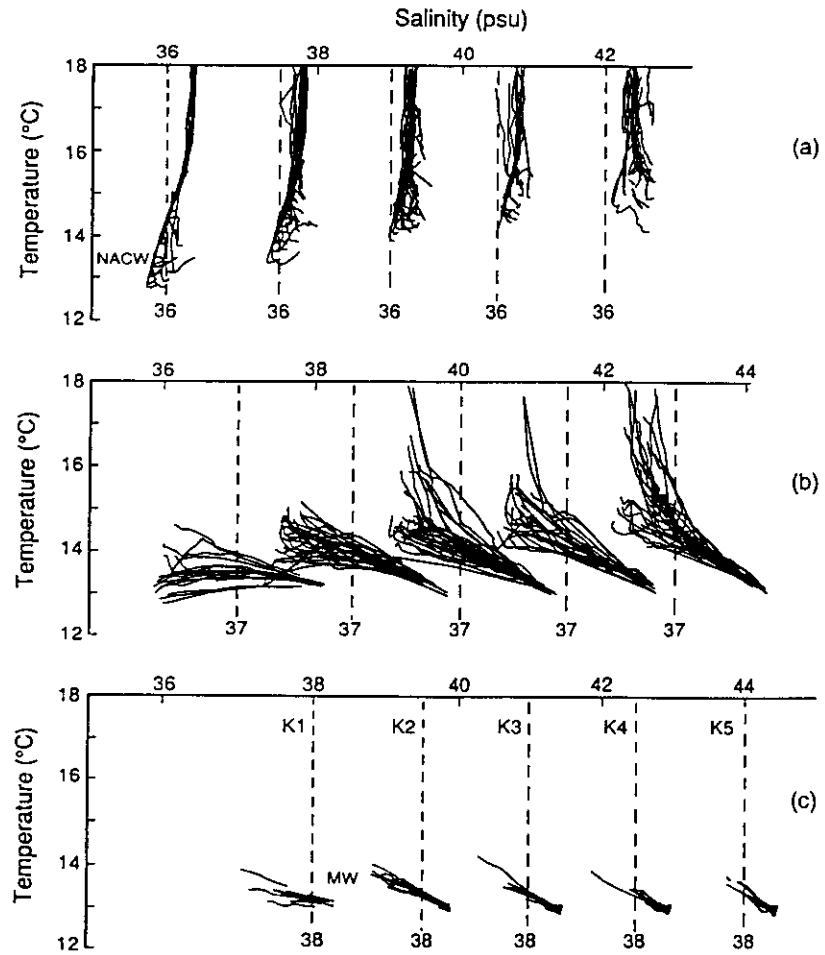

Figure 12. Temperature versus salinity structure as a function of distance along the strait. (a) Upper layer TS characteristics for all occupations of each standard cross-strait section. (b) Same as in Figure 12a, but for the interface layer. (c) Same as in Figure 12a, but for the lower layer.

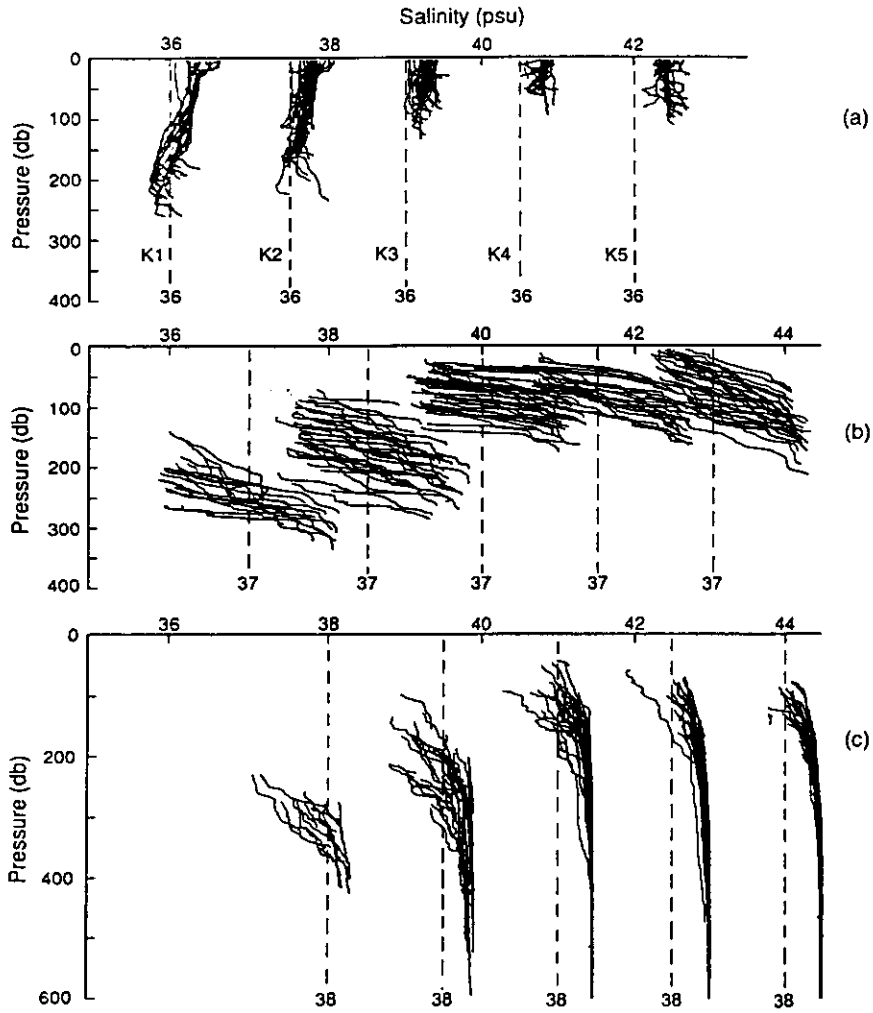

Figure 13. Salinity structure as a function of depth and distance along the strait. (a) Upper layer. (b) Interface layer. (c) Lower layer.

simply dividing the interface layer at its middepth and incorporating the upper part of the interface into the upper layer and the lower part into the lower layer. The values of S and T are determined from the observations: $\bar{S}_1$ and $\bar{T}_1$, the respective averages from $\bar{Z}$ to the surface; and S_2 and T_2, the averages from $\bar{Z}$ to the bottom, where $\bar{Z}$ is the midpoint of the interface, defined by $(Z_1 + Z_2)/2$. The evaporation excess is taken to be 0.55 m yr^{-1}, on average, over the entire Mediterranean Sea, equivalent to a transport of 0.08 Sv [*Bryden and Kinder*, 1991]. This estimate is based on recent moored observations, though it is comparable to historical estimates (*Bethoux* [1979] gives a value of 1 m yr^{-1}). The objective here is to examine along-strait variations in horizontal transport, not to determine the actual transport or evaporation values (see *Ochoa and Bray* [1991] for a discussion of those quantities). Since transports are directly proportional to E ((4a) and (4b)), a value of 1 m yr^{-1} is convenient for estimating the transport associated with any value of E. The horizontal transports that result from this simple, two-layer calculation are instructive for comparison with the three-layer, active interface calculation that follows. Note that the two-layer transports exhibit substantial variation along the channel (Figure 16). If it is assumed that those transport estimates are correct, then vertical exchanges between the layers are required in order to balance mass within each layer. Errors in the horizontal transports are examined in section 4.

3.2. Horizontal Exchange With Three Active Layers

A more realistic estimate of horizontal exchange in the strait incorporates an interface layer of finite thickness and vertical salinity gradient and with vertical shear through the layer as a transition between the inflowing upper and outflowing lower layers (Figure 17). In order to identify that vertical shear, it is further necessary to take into account the actual cross-sectional areas of each layer for each section. The areas are determined from the average position of the halocline and the local bathymetry in each section, from the profiles collected during the cruises (Table 5). Then, (1a) and (1b) are solved, subject to the requirement that the velocity through the interface is a linear function of depth and matches the upper and lower layer velocities at the top and bottom of the interface layer.

The formulas for the horizontal velocities in the upper and

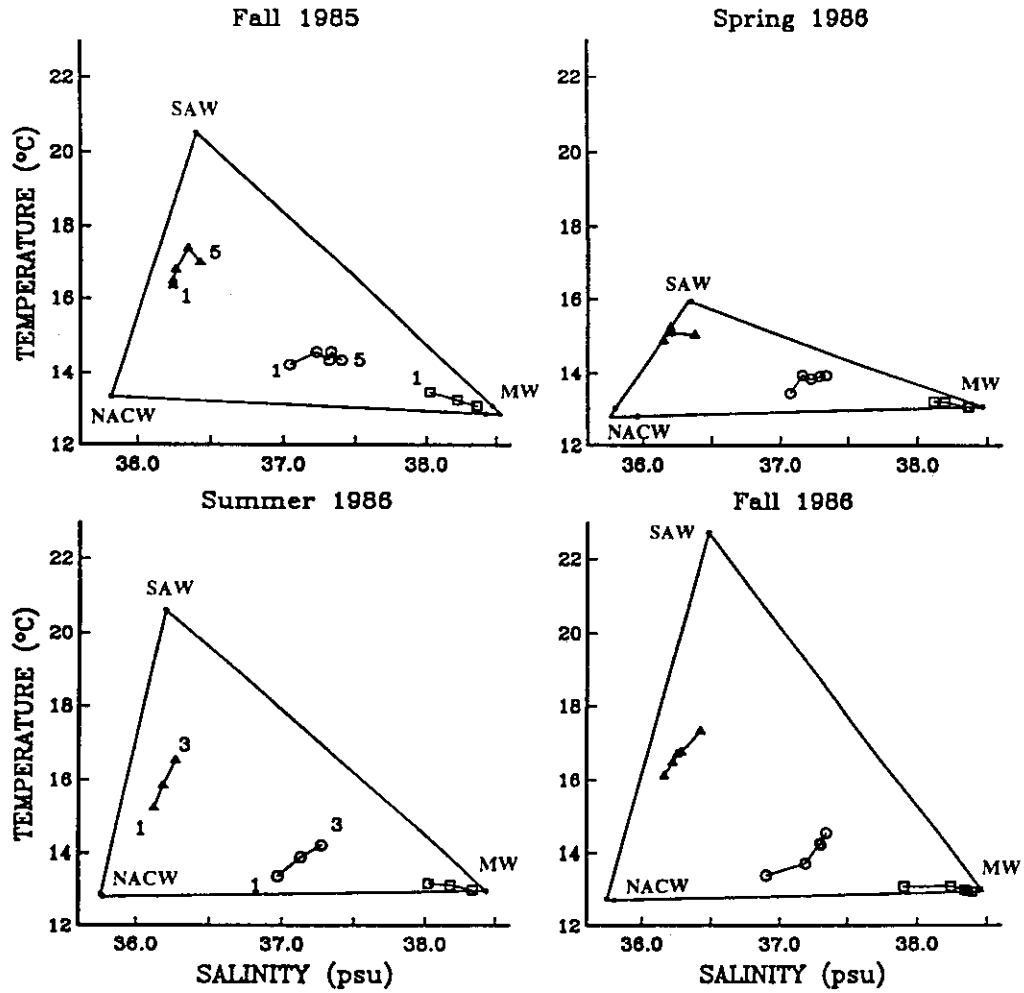

Figure 14. Water mass composition triangles for each cruise. The apexes of each triangle are taken to be the values of Surface Atlantic Water (SAW) (top), North Atlantic Central Water (NACW) (left), and Mediterranean Water (MW) (right). Solid triangles denote upper layer; circles, the interface layer; and squares, the lower layer. Each symbol denotes the average for a given section, with section K1 on the western end of the strait.

Table 3. Composition Triangle Apex Points

	Salinity, psu	Temperature, °C
	Fall 1985	
SAW	36.404	20.536
NACW	35.815	13.314
MW	38.537	12.825
	Spring 1986	
SAW	36.330	15.962
NACW	35.758	12.766
MW	38.473	13.057
	Summer 1986	
SAW	36.201	20.624
NACW	35.751	12.835
MW	38.437	12.999
	Fall 1986	
SAW	36.480	22.726
NACW	35.745	12.738
MW	38.471	12.974

SAW is Surface Atlantic Water, NACW is North Atlantic Central Water, and MW is Mediterranean Water.

Table 4. Extreme Values of Temperature and Salinity

Temperature Extrema			Salinity Extrema		
T	*Z*	*S*	*S*	*Z*	*T*
		Fall 1985			
12.788	208.	35.961	35.799	176.	12.997
15.936	28.	36.349	38.464	386.	13.070
		Spring 1986			
12.743	224.	35.801	35.747	218.	12.769
22.726	18.	36.480	38.455	382.	13.050
		Summer 1986			
12.845	213.	38.424	35.815	202.	13.314
20.536	4.	36.404	38.470	331.	13.067
		Fall 1986			
12.836	203.	35.770	35.755	199.	12.897
20.624	4.	36.201	38.437	377.	12.999
		All Cruises			
12.743	224.	35.801	35.747	218.	12.769
22.726	18.	36.480	38.470	331.	13.067

T is temperature (in degrees Celsius), *Z* is midpoint of the interface, and *S* is salinity (in practical salinity units).

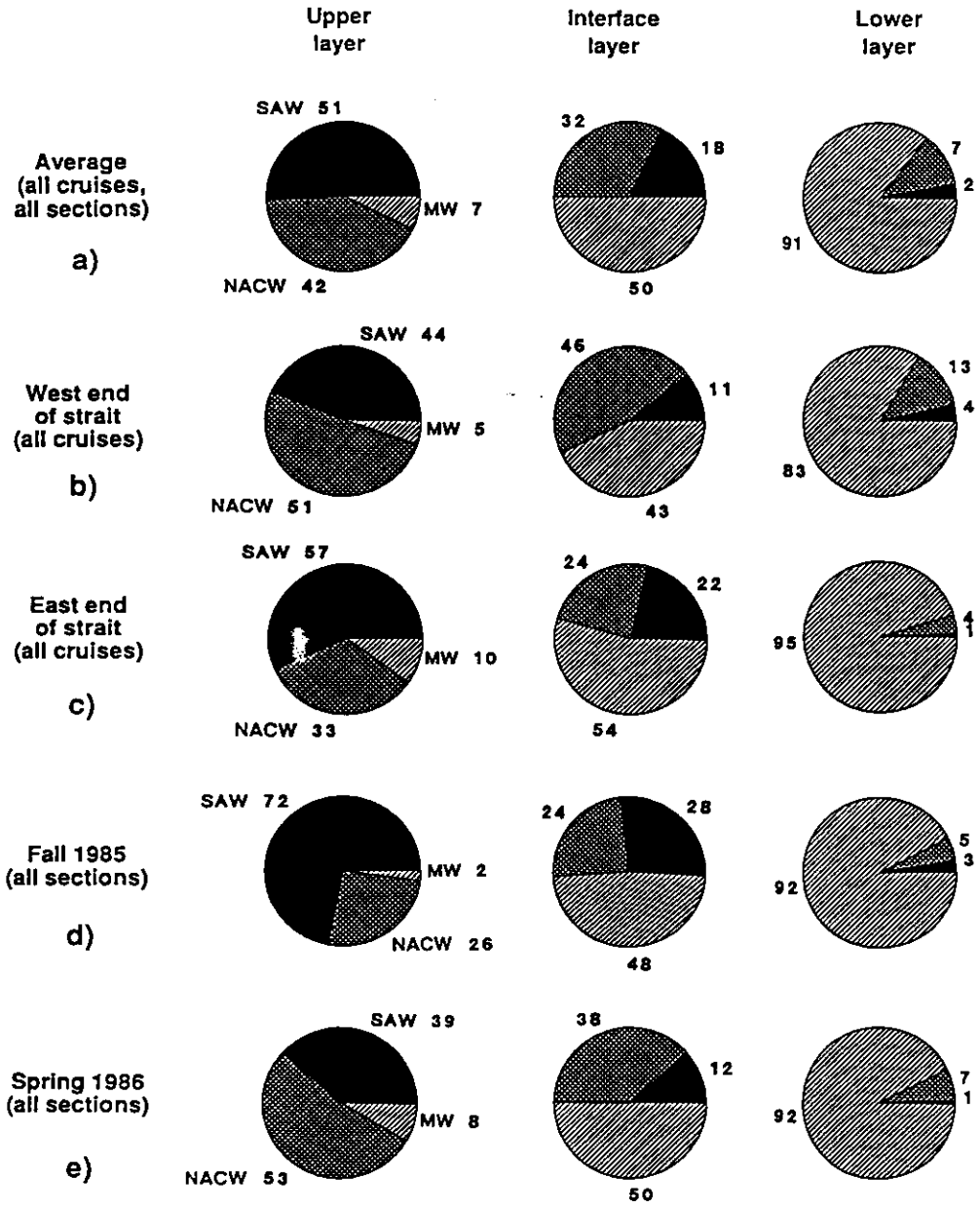

Figure 15. Water mass compositions of the three layers. (a) Average over all sections and cruises. (b) Average over all cruises for section 1 at the western end of the strait. (c) Average over all cruises for section 5 at the eastern end of the strait. (d) Average over all sections for the fall 1985 cruise. (e) Average over all sections for the spring 1986 cruise.

lower layers, in agreement with the equations of system (1) and the model drawn schematically in Figure 17 are

$$v_1\left[A_1 + \frac{A_{in}}{2}\right] + v_2\left[A_2 + \frac{A_{in}}{2}\right] = E$$

$$v_1\left[\bar{S}_1 A_1 + \frac{(2s_1 + s_2)A_{in}}{6}\right] + v_2\left[\bar{S}_2 A_2 + \frac{(s_1 + 2s_2)A_{in}}{6}\right] = 0$$

where v_1 is the horizontal velocity (not transport) in the upper layer, uniform throughout the upper layer of area A_1, v_2 is the horizontal velocity in the lower layer of cross-sectional area A_2. A_{in} is the area of the interface layer. $\bar{S}_1$ and $\bar{S}_2$ are the average salinities in the upper and lower layers, respectively, and s_1 and s_2 are salinity values at the top and bottom of the interface. As with the two-layer system, these formulas are applied to each section along the strait. Convergences in horizontal transports between sections are interpreted in terms of vertical exchange between layers, including the interface layer. The calculated vertical shear from this Knudsen formulation is compared to the geostrophic shear associated with the interface cross-strait slope in Table 1. While the shear magnitudes are comparable in the two calculations on the east and west ends of the strait, the geostrophic shears for the midstrait sections K3 and K4 are smaller than expected and highly variable (even of the opposite sign at times). Instantaneous velocity profiles [e.g., *Pettigrew*, 1989] show that not only does the flow in both layers reverse,

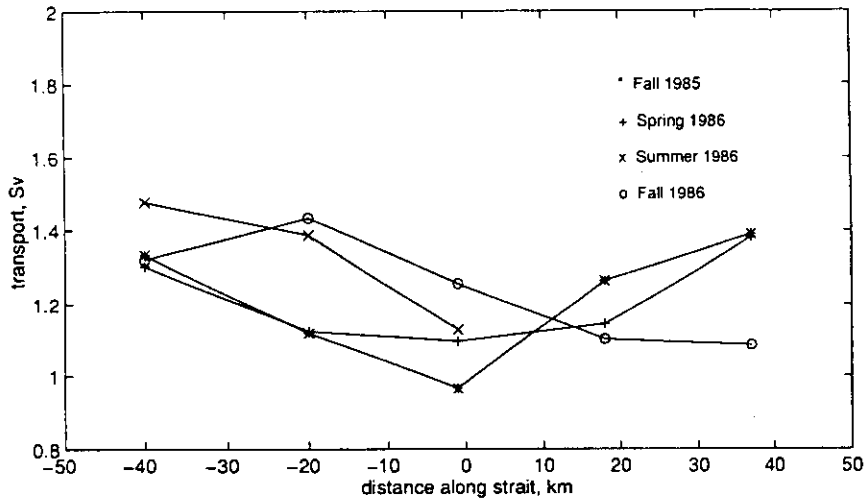

Figure 16. Two-layer horizontal transport as a function of distance along the strait, for the four different cruises, with the origin at Tarifa. Evaporation excess is assumed to be 0.55 m yr^{-1} for the purposes of this calculation.

but also, even the vertical shear reverses direction with the tides in The Narrows.

The Knudsen-derived transports through each layer in each cross-strait section, using all of the profiles available (Tables 6–8 and Figure 18), exhibit several interesting characteristics. First, a substantial fraction of the total transport, more than half in the eastern sections, occurs in the interface layer. On the western end of the strait the interface transport is to the west (in the same direction as the high-speed lower layer), and on the eastern end the interface transport is to the east (in the same direction as the high-speed upper layer). There are also significant convergences in horizontal transports in the upper and lower layers along the strait. The implied vertical exchanges (Table 9) into and out of the interface layer are roughly 20% of the horizontal transport between K1, K2, K3, and K4 and are into the interface layer from both the upper and lower layers. Overall, there is no vertical exchange implied between K4 and K5. The statistical confidence of the implied vertical exchange transports can be estimated in two different ways. First, the error is estimated simply as a standard deviation over all cruises (Table 9). Alternatively, since the vertical exchange is calculated as a convergence of horizontal transports, the errors in those transports may be used. During one of the four cruises, 16 occupations of the K4 section were made; those repeated realizations are used in section 3.4 to estimate sampling errors in the horizontal transports. As it turns out, those errors are about the same as the standard deviations given in Table 9. Thus the implied vertical exchanges between sections (0.07 to 0.19 Sv) are somewhat larger than the errors (0.03 to 0.08 Sv). Taken over the length of the strait, from K1 to K5, the vertical exchange is surprisingly large, 0.5 Sv out of the upper layer into the interface and 0.45 Sv out of the lower layer.

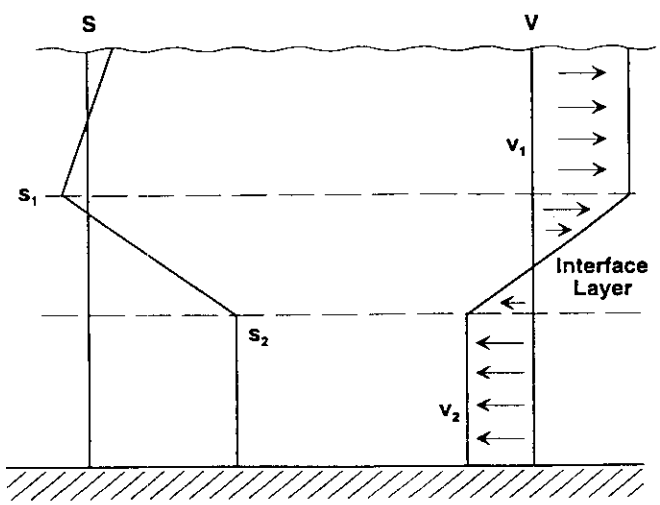

Figure 17. Schematic of the three-layer model of exchange.

Given the horizontal volume transports in each layer, it is possible to estimate the transports of the different water types (SAW, NACW, MW) that are involved in the exchange (Figure 19), since the composition is known. Within the upper layer (Figure 19, top row) the eastward transport of NACW decreases markedly toward the east end of the strait, reflecting the erosion of the upper layer into the interface and the decrease of upper layer volume transport as more and more of that transport is incorporated into the interface layer. Correspondingly, the eastward transport of NACW in the interface layer increases toward the east (Figure 19, second row, middle panel). Similarly, the eastward transport of MW increases toward the east end of the strait within the interface layer, again reflecting the increased eastward volume transport in that layer. To compensate for the eastward flow of MW in the interface layer, the westward transport of MW in the lower layer is largest on the east end, nearly twice the amplitude found in the lower layer on the west end (Figure 19, third row, right panel). On the west end of the strait the transport of all three water types is westward, as expected. Without errors in the determination of water types, the total water type transports (Figure 19, bottom row) should be independent of position in the strait; the

Table 5. Cross-Sectional Areas

	Total	Upper Layer	Interface	Lower Layer	Interface/ Total
		K1			
All data	9.24	5.22	2.72	1.30	0.29
Average		5.66	2.48	1.10	0.27
Standard deviation		0.69	0.57	0.24	
		K2			
All data	7.34	2.94	1.90	2.50	0.26
Average		2.92	1.75	2.67	0.24
Standard deviation		0.12	0.33	0.40	
		K3			
All data	6.73	0.96	1.00	4.78	0.15
Average		1.02	1.07	4.64	0.16
Standard deviation		0.21	0.23	0.33	
		K4			
All data	7.81	0.42	1.07	6.32	0.14
Average		0.49	1.01	6.32	0.13
Standard deviation		0.20	0.11	0.27	
		K5			
All data	22.33	1.42	3.97	16.94	0.18
Average		1.30	3.77	17.27	0.17
Standard deviation		0.30	0.32	0.61	

All values are in square kilometers. All data is a single calculation using all available profiles for each section. Average and standard deviation are statistics over the four cruises, each done as an individual calculation.

small deviations from a constant value are indicative of relatively small errors in the water type determinations from the available observations.

3.3. Comparison With Moored Velocity and Density

As part of the Gibraltar Experiment, several long-term moorings were deployed in the strait [*Candela et al.*, 1989, 1990]. The only comprehensive cross-strait array was composed of three moorings, M1, M2, and M3, located roughly halfway between K2 and K3 (see Figure 1). The vertical extent of the moorings was limited by navigational constraints, so the shallowest instrument was located deeper than 100 m (thereby not consistently in the upper layer). However, the instruments measured temperature and salinity, as well as current, so it is possible to determine, for instance, the average relationship between velocity and

Table 6. Property and Transport Statistics (Upper Layer)

	Temperature, °C	Salinity, psu	Density, σ_θ	Velocity, m s^{-1}	Transport, Sv
		K1			
All data	15.941	36.194	26.681	0.18	0.96
Average	15.668	36.166	26.720	0.17	0.92
Standard deviation	0.750	0.054	0.136	0.02	0.06
		K2			
All data	16.017	36.215	26.679	0.26	0.77
Average	15.975	36.211	26.685	0.26	0.77
Standard deviation	0.570	0.024	0.118	0.01	0.01
		K3			
All data	16.402	36.248	26.616	0.64	0.62
Average	16.285	36.242	26.636	0.61	0.61
Standard deviation	0.790	0.039	0.153	0.10	0.03
		K4			
All data	17.261	36.336	26.478	1.11	0.47
Average	16.422	36.279	26.631	1.07	0.48
Standard deviation	1.175	0.068	0.222	0.25	0.08
		K5			
All data	16.822	36.421	26.649	0.33	0.47
Average	16.446	36.407	26.723	0.36	0.45
Standard deviation	1.231	0.030	0.264	0.05	0.04

All data is a single calculation using all available profiles for each section. Average and standard deviation are statistics over the four cruises, each done as an individual calculation.

Table 7. Property and Transport Statistics (Interface Layer)

	Temperature, °C	Salinity, psu	Density, σ_θ	Velocity, m s^{-1}	Transport, Sv
		K1			
All data	13.957	37.000	27.744	−0.13	−0.34
Average	13.655	36.968	27.783	−0.17	−0.39
Standard deviation	0.397	0.060	0.059	0.05	0.05
		K2			
All data	14.300	37.186	27.814	−0.01	−0.02
Average	14.040	37.170	27.857	−0.01	−0.01
Standard deviation	0.368	0.039	0.066	0.02	0.03
		K3			
All data	14.293	37.279	27.887	0.24	0.24
Average	14.213	37.259	27.889	0.22	0.23
Standard deviation	0.259	0.054	0.061	0.05	0.06
		K4			
All data	14.542	37.326	27.869	0.48	0.52
Average	14.240	37.307	27.920	0.46	0.46
Standard deviation	0.335	0.020	0.058	0.13	0.10
		K5			
All data	14.331	37.386	27.962	0.14	0.54
Average	14.277	37.359	27.952	0.15	0.56
Standard deviation	0.304	0.034	0.064	0.03	0.05

All data is a single calculation using all available profiles for each section. Average and standard deviation are statistics over the four cruises, each done as an individual calculation.

density across the mooring array, for comparison with the averages calculated here using only property information and an assumed value of evaporative loss. Density is used as the property variable because it is monotonic with depth; water mass characteristics in the upper layer include a local minimum of salinity along some sections, implying a potential ambiguity in the u versus S relationship. Unfiltered time series (including the tidal signal) were used to construct the average u versus density relationship (Figure 20) for all instruments on the three moorings. By including the tidal frequencies, correlations between tidal currents and interface depth that are important to the total property transport [*Bryden et al.*, 1989] are resolved. Velocity at a given density compares surprisingly well between the two calculations, certainly within the errors of either calculation. Note that the velocity from the modified Knudsen calculation is an average over the entire layer in each case, whereas the velocity derived from the moorings is not. An average over the

Table 8. Property and Transport Statistics (Lower Layer)

	Temperature, °C	Salinity, psu	Density, σ_θ	Velocity, m s^{-1}	Transport, Sv
		K1			
All data	13.355	38.002	28.648	−0.43	−0.57
Average	13.252	38.003	28.670	−0.50	−0.54
Standard deviation	0.153	0.075	0.059	0.09	0.08
		K2			
All data	13.192	38.202	28.837	−0.28	−0.70
Average	13.178	38.207	28.843	−0.27	−0.72
Standard deviation	0.046	0.027	0.026	0.03	0.03
		K3			
All data	13.039	38.357	28.989	−0.17	−0.81
Average	13.021	38.360	28.995	−0.17	−0.80
Standard deviation	0.038	0.023	0.024	0.02	0.03
		K4			
All data	13.074	38.358	28.983	−0.15	−0.94
Average	13.052	38.353	28.983	−0.14	−0.90
Standard deviation	0.033	0.013	0.004	0.01	0.04
		K5			
All data	13.050	38.363	28.992	−0.06	−0.97
Average	13.042	38.361	28.992	−0.06	−0.97
Standard deviation	0.047	0.002	0.009	0.00	0.01

All data is a single calculation using all available profiles for each section. Average and standard deviation are statistics over the four cruises, each done as an individual calculation.

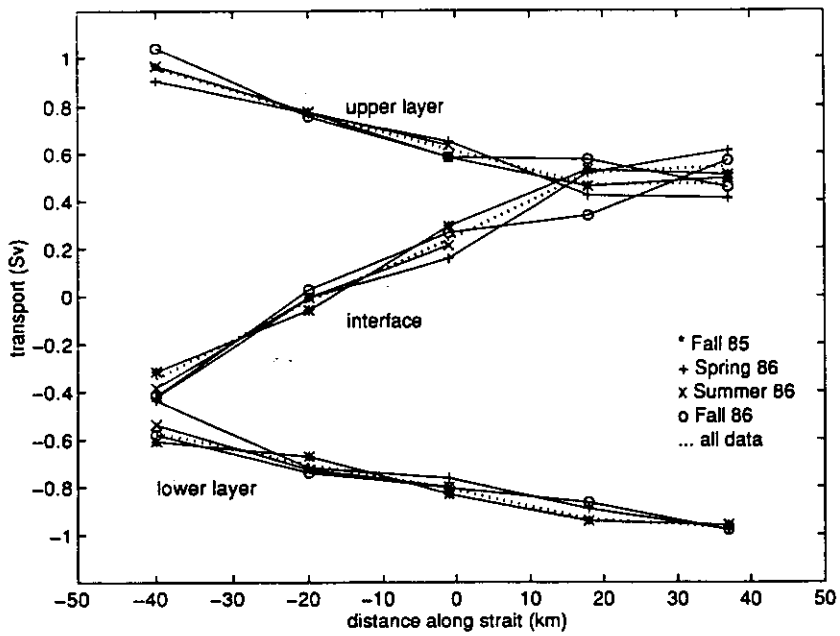

Figure 18. Horizontal transports in three active layers as a function of distance along the strait. Evaporation excess is assumed to be 0.55 m yr^{-1} for the purposes of this calculation.

moored velocities would result in a lower total transport than that implied by the Knudsen calculation, as expected from the difference in evaporation excess between the two calculations. This is done explicitly in section 3.4.

3.4. Estimation of Transport Errors

Errors in horizontal transports calculated by the methods of the previous sections may result from at least two sources: insufficient sampling of the fields and the assumption of equivalence between velocity-weighted salinities and spatially averaged quantities. The cross-strait section K4 near Point Cires was repeated 16 times during the November 1985 cruise. That collection of sections is used to estimate the errors due to sampling variability. To examine the validity of assuming that spatial averages may replace velocity-weighted averages, a comparison of the present calculation and that of *Bryden et al.* [1989] for the outflow salt transport from moored observations is made.

To estimate the sampling error associated with a single realization of the section at K4, horizontal transport is calculated from each of the 16 occupations. Since it is the same vertical section in each calculation, sampling without errors would result in identical values of horizontal transport. Standard deviations in the horizontal transports of the upper and lower layers are 0.09 and 0.08 Sv, respectively (Table 10), comparable to the standard deviations over the four cruises (Tables 6 and 8). In the interface layer the standard deviation for this error calculation is somewhat larger, 0.17 Sv, than that over the cruises (0.10 Sv) or the upper and lower layers. Presumably, this larger sampling error in the interface layer

Table 9. Implied Vertical Exchange Between Sections

	K1–K2	K2–K3	K3–K4	K4–K5	K1–K5
		Upper Layer Into Interface Layer			
Fall 1985	0.19	0.19	0.12	−0.03	0.47
Spring 1986	0.13	0.12	0.23	0.01	0.50
Summer 1986	0.19	0.14	...	...	...
Fall 1986	0.29	0.18	0.01	0.12	0.59
All data	0.19	0.15	0.15	−0.01	0.48
Average	0.20	0.16	0.12	0.03	0.51
Standard deviation	0.06	0.03	0.11	0.08	0.06
		Lower Layer Into Interface Layer			
Fall 1985	0.07	0.16	0.12	0.02	0.36
Spring 1986	0.28	0.04	0.13	0.09	0.54
Summer 1986	0.19	0.07	...	...	...
Fall 1986	0.16	0.07	0.06	0.12	0.40
All data	0.14	0.10	0.13	0.03	0.40
Average	0.17	0.09	0.10	0.07	0.42
Standard deviation	0.08	0.04	0.03	0.05	0.09

All values are in sverdrups. All data is a single calculation using all available profiles for each section. Average and standard deviation are statistics over the four cruises, each done as an individual calculation.

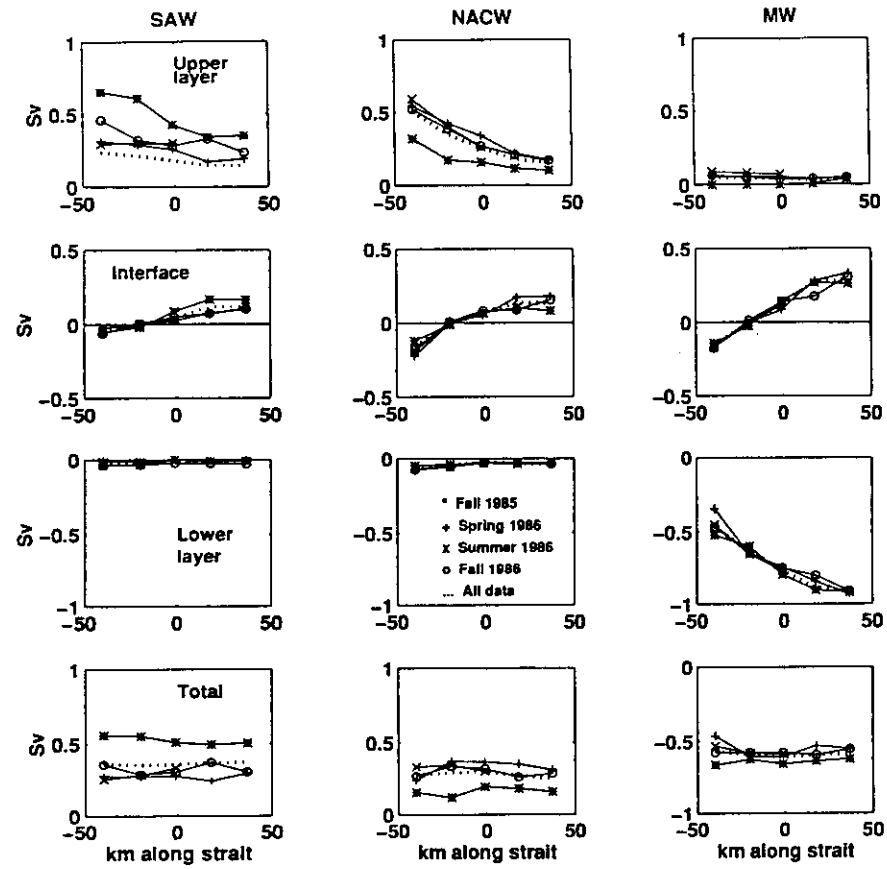

Figure 19. Variations in water type transports along the strait, based on the three-layer horizontal transports of Figure 18 and the water type compositions described in text (section 2.4). Evaporation excess is assumed to be 0.55 m yr^{-1} for the purposes of this calculation.

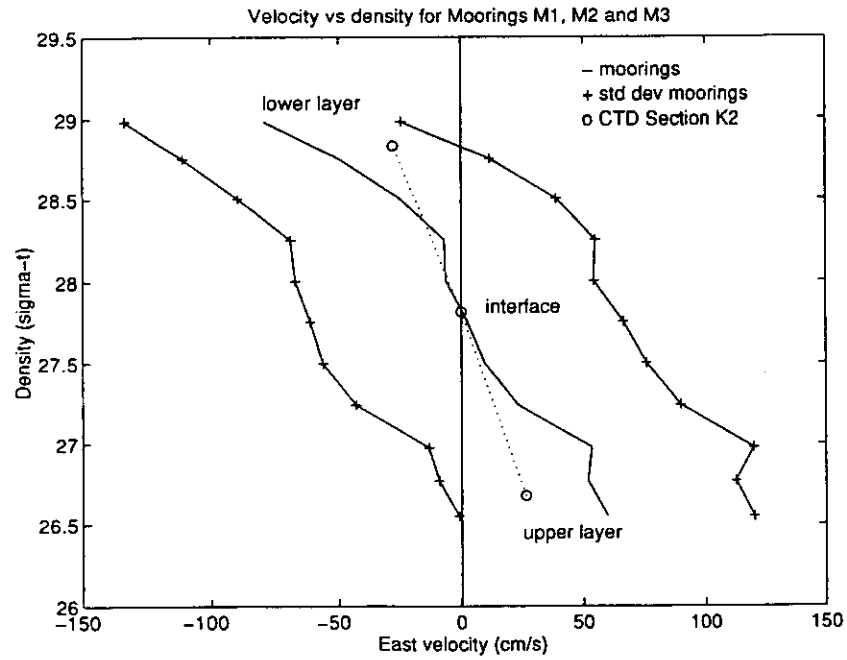

Figure 20. Comparison of the structure of velocity versus density from the moored current, temperature, and salinity data and from the CTD sections.

Table 10. Transports and Errors From Repeated K4 Sections

	Temperature, °C	Salinity, psu	Density, σ_θ	Velocity, m s^{-1}	Transport, Sv
		Upper Layer			
All data	17.261	36.336	26.487	1.11	0.47
Average	17.462	36.366	26.451	1.18	0.45
Standard deviation	0.548	0.070	0.106	0.35	0.09
		Interface Layer			
All data	14.542	37.326	27.869	0.48	0.52
Average	14.542	37.329	27.870	0.51	0.55
Standard deviation	0.413	0.043	0.073	0.17	0.17
		Lower Layer			
All data	13.074	38.358	28.983	−0.15	−0.94
Average	13.075	38.355	15.980	−0.28	−0.96
Standard deviation	0.029	0.030	0.029	0.02	0.08

All data is a calculation using all available profiles from section K4, 16 repetitions during fall 1985. Average and standard deviation are statistics from the 16 individual occupations of section K4, each calculated separately.

results from real variability in the interface structure due to tides and to interfacial tidal bores found preferentially in this section of the strait [*Pettigrew and Hyde*, 1990].

In an analogous fashion, sampling errors in the implied vertical exchange can be estimated by considering pairs of the repeated sections and examining the differences in horizontal transport of the different layers between the two realizations. Again, sampling without errors would imply no vertical exchange. The average vertical exchange over 15 pairs of K4 sections is 0.01 (±0.08) Sv and 0.01 (±0.06) Sv for the upper and lower layers, respectively. Within the interface layer both the average and standard deviations are somewhat larger, −0.02 (±0.13) Sv. From this analysis it is argued that error in the implied vertical exchange between the upper and interface layers is 0.08 Sv and between the lower and interface layers is 0.06 Sv, comparable to the standard deviations found over the four cruises (Table 9).

Turning to the question of velocity-weighted versus spatial averaging, *Bryden et al.* [1989] used salinity and velocity data from mooring M2 to estimate the velocity-weighted outflow salt transport to be 1.6 Sv psu, relative to the "Atlantic" inflow salinity of 36.2 psu, as discussed in section 2. From that salt transport, Bryden et al. estimate the evaporation excess, using Knudsen's relations, to be 0.55 m yr^{-1}. Comparable estimates of the spatially averaged outflow salt transport from the present calculation can be made for sections K2 and K3, on either side of mooring M2. Using the transports in Table 8, the outflow salt transport relative to 36.2 psu for K2 is 1.43 Sv psu and 1.74 Sv psu for K3. The average of the two sections is 1.58 Sv psu, very close to the 1.6 Sv psu found by *Bryden et al.* [1989] for the velocity-weighted outflow salt transport. As noted in section 2, it is the fact that the salinity difference between inflow and outflow is the same as in the two estimates that makes the transports, when scaled to the same evaporation excess, so nearly equal. The implication is that, under these circumstances, spatial averages of salinity can replace velocity-weighted averages.

A similar comparison of heat flux calculated from the two data sources can also be made. In order to calculate a meaningful heat flux, we have assumed that inflow and outflow are equal in magnitude. Using the observed temperature differences between the upper and lower layers, together with the implied horizontal transport using 0.55 m yr^{-1} as the excess evaporation rate, the average heat flux for sections K2 and K3 is 2.7 (±1) W m^{-2}, where the error is a standard deviation over the four cruises. Although *Bryden et al.* [1989] did not estimate heat fluxes, *Macdonald et al.* [1994] found a value of 5.2 (±1) W m^{-2} from the Gibraltar moored data.

4. Discussion

4.1. Implications of an Interface With Finite Thickness

That the interface between Atlantic and Mediterranean waters is of significant vertical extent has several important implications for the exchange of properties between the two ocean basins. First, a simple two-layer model of the structure of the exchange will result in underestimates of the property differences between the two layers based on observations within the strait, by as much as 30%. This is because the high-gradient region of the interface takes up 60 to 110 m of the water column; a two-layer system divided by a single isohaline denoting the middle of the interface will produce an average upper layer salinity substantially higher and lower layer salinity substantially lower than the actual values in those layers exclusive of the interface. The three-layer system introduced here circumvents that difficulty by identifying the interface layer with the region of high-salinity gradient that is observed in actual profiles from the strait. Salinity differences between the upper and lower layers of the three-layer system (2 psu versus 1.5 for the two-layer model) are only slightly lower than values inferred from moored current and salinity data [*Bryden et al.*, 1989, 1994].

Second, because the interface takes up a substantial fraction of the water column and because there is no constraint that the vertical integral of transport over the interface vanish, an important contribution to the exchange can and does occur within the interface layer. On the eastern end of the strait, roughly half of the transport into the Mediterranean is found in the interface layer, while on the west end an equivalent outflowing transport occurs in the interface layer. Near Camarinal Sill there is little net transport within the interface layer. The interface layer, then, is an active participant in the process of exchange, carrying a substantial fraction of the transport and

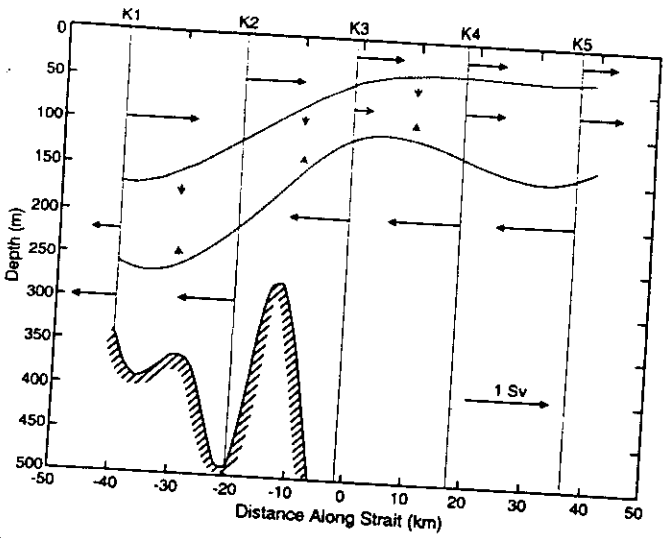

Figure 21. Summary of along-strait variations in transports nd interface structure. Dotted contours outline the average nterface layer along the strait. Arrows are scaled to indicate ie magnitude of horizontal transport in each layer at the arious sections along the strait. Vertical transports implied / the convergence of horizontal transports from one section the next are represented by vertical arrows, with the same aling as the horizontal transports. Evaporation excess is sumed to be 0.55 m yr^{-1} for the purposes of this calcula- n, and the origin is at Tarifa.

periencing large variations (in sign and magnitude) of trans- t with position along the strait.

Third, the interface acts as a buffer layer for property hange between the upper and lower layers. Thus, as the perties and horizontal transports in the upper and lower rs change along the strait as a result of mixing, entrain- t, and vertical advection, the interface layer absorbs e changes and is altered accordingly. For example, the ity of the interface layer changes by nearly 0.4 psu from east to the west end of the strait, as both somewhat er NACW and much saltier MW are incorporated into interface (Table 7). Temperature and density of the face layer also change, by 0.6°C and 0.2 σ_t. Horizontal port within the layer changes dramatically with distance the strait, implying substantial vertical exchange be- n the interface and the upper and lower layers, as ibed below.

Estimation of Horizontal Transport Using dified Version of Knudsen's Relations

en an observationally well-defined three-layer system, ntforward modification of the classical Knudsen calcu- of transport as a function of evaporation excess provides tes of horizontal transport in each of the three layers 18). As the property distributions change with position he strait, so does the calculated transport (Figure 21): on st end of the strait all of the inflow occurs in the upper while the outflow is split roughly equally between the e and lower layers. Over the Camarinal Sill there is no nsport in the interface layer, and on the east end the is all in the lower layer, while the inflow is again split equally between the upper and the interface layers. nsformation is associated with the depth of the layers: vest end the outflow layer is thin, with high velocities; on the east end the same can be said of the upper layer. The pronounced along-strait variation in horizontal transport within different layers has important implications, both for vertical exchange between the layers and for the transport of properties in the strait.

4.3. Implied Vertical Exchange Between Layers

The large differences in horizontal transport that are observed as a function of position along the strait can be interpreted as implying convergence or divergence in those layers and hence vertical exchange between layers. Over the length of the strait the property distributions imply that roughly one half of the inflowing transport is exchanged between the upper and interface layers and slightly less of the outflow is exchanged between the interface and the lower layer. The propriety of interpreting convergences in the horizontal transports as vertical exchange depends on the relative size of the errors associated with those estimates and also on the physical interpretation of how the observed lateral changes in property distributions within a layer, the heart of the entire calculation, are actually accomplished. In section 3.4 the errors in estimating horizontal transports were shown to be somewhat less than the magnitudes of the convergences: sampling errors are of the order of 0.06 Sv, as compared with convergences of the order of 0.3 Sv.

4.4. Water Type Distributions

Another way of looking at the exchange between the Atlantic and Mediterranean is to cast the problem into transport of water types, rather than transport of heat and salt. The principal water types involved in the exchange can be identified as SAW, NACW, and MW (surface Atlantic, North Atlantic Central, and Mediterranean water types). By defining a triangle in TS space with these three water types as apexes, it is possible to quantify the fraction and hence the volume transport of each type as a function of position along the strait and layer. The upper layer is composed of roughly half SAW, 40% NACW, and 10% MW, on average, over the strait and the four cruises (Figure 15). A similar average for the interface layer is 20% SAW, 30% NACW, and 50% MW, while the lower layer is dominated by MW (90%), with only 2% SAW and 8% NACW. The principal changes with position along the strait occur in the upper and interface layers: the upper layer fraction of NACW decreases rather dramatically eastward, as the lower part of the upper layer is eroded into the interface layer. With season the largest change is, not surprisingly, in the upper layer: NACW comprises twice the fraction in spring as it does in the fall.

Transport of water types, calculated simply as the product of water type fraction and the three-layer horizontal transports, is most variable in the interface layer, for all three types, in the Atlantic types of the upper layer and the Mediterranean types of the lower layer (Figure 19). This reflects the remarkable spatial shifts in the exchange transports over the length of the strait: inflow occurs predominantly in the upper layer on the west end of the strait, while it is split equally between the upper and interface layers by the time it reaches the eastern end of the strait. Similarly, outflow occurs principally in the lower layer in the east and is split between the lower and interface layers at the western end of the strait.

4.5. Implications for Future Work

Although two-layer models, including those that utilize hydraulic flow principles [e.g., *Stommel et al.*, 1973; *Farmer*

and Armi, 1986; *Bryden and Kinder*, 1991], have provided insight into the basic dynamics of flow in the strait, some expansion of that theoretical approach is suggested by the results of this analysis. Given the considerable vertical interchange between layers and the failure of two-layer kinematic descriptions to adequately describe the physical characteristics of the horizontal exchange, a model that incorporates both an interface of finite thickness and exchange of properties and momentum between the layers would be a useful addition to the study of strait dynamics in general and of the Strait of Gibraltar in particular.

Acknowledgments. We are indebted to the many professionals who made it possible to collect the CTD stations used in this analysis. Particular thanks go to Suzanne Shull, Don Burns, Walt Waldorf, Jerry Wanetick, and Steve Rintoul for their technical support at sea. Gregorio Parrilla and Henri Lacombe provided both intellectual inspiration and steadfast assistance with the mundane work of 24-hour watches. The comments of two anonymous reviewers led to substantial revision and improvement of the manuscript; we deeply appreciate the care they took in reviewing. Comments by Pedro Ripa, Greg Johnson, and Bill Schmitz are also appreciated. Illustration credits go to Mike Clark. Joan Semler prepared the manuscript. This work was supported by the ONR Coastal Sciences Program, grants N00014-85-C-0497 and N00014-89-J-1914. N.A.B. was supported by ONR Coastal Sciences grant N00014-90-J-1127, J.L.O. was supported by CICESE, and T.H.K. was supported by the ONR Scientific Officer Research Program during the final preparation of the manuscript.

References

Ambar, I., and M. R. Howe, Observations of the Mediterranean outflow, I, Mixing in the Mediterranean outflow, *Deep Sea Res., Part A*, *26*, 535–554, 1979.

Bethoux, J. P., Budgets of the Mediterranean Sea. Their dependance on the local climate and on the characteristics of the Atlantic Waters, *Oceanol. Acta*, *2*(2), 157–163, 1979.

Bray, N. A., Gibraltar experiment CTD data report: March–April 1986, USNS *Lynch*, *SIO Ref. 86-21*, 212 pp., Scripps Inst. of Oceanogr., La Jolla, Calif., 1986.

Bray, N. A., C. D. Winant, T. H. Kinder, and J. Candela, Generation and kinematics of the internal tide in the Strait of Gibraltar, in *The Physical Oceanography of Sea Straits*, edited by L. J. Pratt, pp. 477–491, Kluwer Academic, Norwell, Mass., 1990.

Bryden, H. L., and T. H. Kinder, Steady two-layer exchange through the Strait of Gibraltar, *Deep Sea Res., Part A*, *38*, suppl. 1, S445–S463, 1991.

Bryden, H. L., E. C. Brady, and R. D. Pillsbury, Flow through the Strait of Gibraltar, in *Seminario Sobre la Oceanografía Física del Estrecho de Gibraltar*, edited by J. L. Almazán, H. Bryden, T. Kinder, and G. Parrilla, pp. 95–121, Sociedad Espanola de Estudios Para la Comunicacion Fija a Traves del Estrecho de Gibraltar, Madrid, 1989.

Bryden, H. L., J. Candela, and T. H. Kinder, Exchange through the Strait of Gibraltar, *Progr. Oceanogr.*, *33*, 201–248, 1994.

Candela, J., C. D. Winant, and H. L. Bryden, Meteorologically forced subinertial flows through the Strait of Gibraltar, *J. Geophys. Res.*, *94*(C9), 12,667–12,679, 1989.

Candela, J., C. D. Winant, and A. Ruiz, Tides in the Strait of Gibraltar, *J. Geophys. Res.*, *95*(C5), 7313–7335, 1990.

Farmer, D. M., and L. Armi, Maximal two-layer exchange over a sill and through the combination of a sill and contraction with barotropic flow, *J. Fluid Mech.*, *164*, 53–76, 1986.

Kinder, T. H., and H. L. Bryden, The 1985–1986 Gibraltar Experiment: Data collection and preliminary results, *Eos Trans. AGU*, *68*, 786–787, 793–795, 1987.

Kinder, T. H., D. A. Burns, and R. D. Broome, Hydrographic measurements in the Strait of Gibraltar, November 1985, *NORDA Rep. 141*, 332 pp., Nav. Ocean Res. and Dev. Activ., Stennis Space Center, Miss., 1986.

Kinder, T. H., D. A. Burns, and M. R. Wilcox, Hydrographic measurements in the Strait of Gibraltar, June 1986, *NORDA Tech. Note 378-1* (appendix), 355 pp., Nav. Ocean Res. and Dev. Activ., Stennis Space Center, Miss., 1987.

Knudsen, M., De hydrografiske forhold i de danske farvande indenfor Skagen i 1894–98, *Komm. Vidensk. Unders. Dan. Farvande*, *2*(2), 19–79, 1899.

Knudsen, M., Ein hydrographischer Lehrsats, *Ann. Hydrogr.*, *28*, 316–320, 1900.

Lacombe, H., and C. Richez, The regime of the Strait of Gibraltar, in *Hydrodynamics of Semi-enclosed Seas*, edited by J. C. J. Nihoul, pp. 13–74, Elsevier, New York, 1982.

Macdonald, A. M., J. Candela, and H. L. Bryden, An estimate of the net heat transport through the Strait of Gibraltar, in *Seasonal and Interannual Variability of the Western Mediterranean Sea*, *Coastal and Estuarine Stud. Ser.*, vol. 46, edited by P. E. LaViolette, pp. 13–32, AGU, Washington, D. C., 1994.

Ochoa, J., and N. A. Bray, Water mass exchange in the Gulf of Cadiz, *Deep Sea Res., Part A*, *38*, suppl. 1, S465–S503, 1991.

Parrilla, G., T. H. Kinder, and N. A. Bray, Hidrología del Agua Mediterránea en el Estrecho de Gibraltar Durante el Experimento Gibraltar (Octobre, 1985–Octobre, 1986), in *Seminario Sobre la Oceanografía Física del Estrecho de Gibraltar*, edited by J. L. Almazán, H. Bryden, T. Kinder, and G. Parrilla, pp. 95–121, Sociedad Espanola de Estudios Para la Comunicacion Fija a Traves del Estrecho de Gibraltar, Madrid, 1989.

Pettigrew, N. R., Direct measurements of the flow of Mediterranean Deep Water over the Gibraltar sill, *J. Geophys. Res.*, *94*(C12), 18,089–18,093, 1989.

Pettigrew, N. R., and R. A. Hyde, The structure of the internal bore in the Strait of Gibraltar and its influence on the Atlantic inflow, in *The Physical Oceanography of Sea Straits*, edited by L. J. Pratt, pp. 493–508, Kluwer Academic, Norwell, Mass., 1990.

Shull, S., and N. A. Bray, Gibraltar experiment CTD data report, II, September–October 1989, USNS *Lynch*, *SIO Ref. 89-23*, 258 pp., Scripps Inst. of Oceanogr., La Jolla, Calif., 1989.

Stommel, H., H. Bryden, and P. Mangelsdorf, Does some of the Mediterranean outflow come from great depth? *Pure Appl. Geophys.*, *105*, 879–889, 1973.

Sverdrup, H. U., M. W. Johnson, and R. H. Fleming, *The Oceans*, Prentice-Hall, Englewood Cliffs, N. J., 1942.

van Geen, A., and E. A. Boyle, Atlantic water masses in the Strait of Gibraltar: Inversion of trace metal data, in *Seminario Sobre la Oceanografía Física del Estrecho de Gibraltar*, edited by J. L. Almazán, H. Bryden, T. Kinder, and G. Parrilla, pp. 68–81, Sociedad Espanola de Estudios Para la Comunicacion Fija a Traves del Estrecho de Gibraltar, Madrid, 1989.

Wesson, J. C., and M. C. Gregg, Turbulent dissipation in the Strait of Gibraltar and associated mixing, in *Small-Scale Turbulence and Mixing in the Ocean*, Proceedings of the 19th International Liege Colloquium on Ocean Hydrodynamics, edited by J. C. H. Nihoul and B. M. Jamart, pp. 201–222, Elsevier, New York, 1988.

Wesson, J. C., and M. C. Gregg, Mixing at Camarinal Sill in the Strait of Gibraltar, *J. Geophys. Res.*, *99*(C5), 9847–9878, 1994.

N. A. Bray, Center for Coastal Studies, Scripps Institution of Oceanography, University of California, San Diego, 9500 Gilman Drive, La Jolla, CA 92093. (e-mail: nbray@ucsd.edu)

T. H. Kinder, Department of Oceanography, United States Naval Academy, Annapolis, MD 21402.

J. Ochoa, Centro de Investigación y de Educación Superior de Ensenada, Apartado Postal 2732, Ensenada, B. C. Mexico.

(Received February 5, 1993; revised July 20, 1994; accepted September 17, 1994.)